FUNCTIONALIZED RENEWABLE POLYMERS TO TOUGHEN POLYLACTIDE

A DISSERTATION
SUBMITTED TO THE FACULTY OF THE GRADUATE SCHOOL
OF THE UNIVERSITY OF MINNESOTA
BY

William Mike Gramlich

IN PARTIAL FULFILLMENT OF THE REQUIREMENTS
FOR THE DEGREE OF
DOCTOR OF PHILOSOPHY

Marc A. Hillmyer, Adviser

February 2012

Acknowledgments

During my graduate studies I have had the opportunity to work closely with many talented individuals at the University of Minnesota. Not only did these people enrich my research experience, but I also learned a great deal from them. Most notably, my advisor Marc Hillmyer has been a great mentor and as a result I have become an improved scientist. His guidance throughout the years has been invaluable.

Helpful direction from Kwanho Chang got me started with polylactide blends, while David Olson and Nate Lynd helped me with the more general laboratory practices as a young graduate student. Additionally, I collaborated with several researchers over my graduate career that have been directly associated with the toughening polylactide goal: Megan Robertson, Grayce Theryo, Jessica Paxton, and Sinéad Murphy. With their assistance in the lab and discussions, many of the breakthroughs set forth in this document were made. I would also like to thank Feng Jing, Eric Todd, Myung Seo, Justin Kennemur, Josh Speros, Jennifer Lowe, Liz Jackson, Ligeng Yin, Adam Moughton, and Louis Pitet for helpful discussions.

I would like to thank my family and friends for supporting me throughout my graduate studies; in particular, my mother and father for giving me encouragement and support. Finally, I thank my fiancée Sara for always being there and continuing to be there in the future.

Abstract

Sustainable polymers can overcome the limitations of petroleum sourced materials due to their renewable feedstocks, biodegradability, recyclability, and nontoxic nature. The renewably sourced polymer polylactide is commercially produced, but its use is limited by its brittle nature. Consequently, reactive melt blends of end-functionalized polylactide and renewably sourced conjugated soybean oil were investigated. End-functionalized polylactide and conjugated soybean oil reacted in the melt to produce compatibilizers that reduced the droplet diameter, yielding blended materials with improved elongation to break over the parent polylactide homopolymer. Additionally, polyisoprene, a potentially sustainable polymer, was investigated as a macroinitiator for tough polylactide graft polymers. Two methods were investigated to synthesize the polyisoprene macroinitiator: post-polymerization functionalization and isoprene copolymerization with a hydroxyl functionalized monomer. To this end, Conjugated polyisoprene was synthesized by a ruthenium hydride catalyst post-polymerization and subsequently functionalized with a hydroxyl containing maleimide through a facile Diels–Alder reaction. The post-polymerization functionalized conjugated polyisoprene produced well defined polylactide graft copolymers. Furthermore, the hydroxyl containing monomer 2-methylenebut-3-en-1-ol was copolymerized with isoprene in both reversible addition-fragmentation transfer controlled radical and emulsion polymerization schemes. In spite of Diels–Alder side reactions, the copolymerizations produced macroinitiators for polylactide graft polymer synthesis. Polylactide graft polymers made from polyisoprene macroinitiators gave microphase separated, potentially tough materials.

Table of Contents

List of Tables

List of Figures

Chapter 1

Introduction

As polymers are an integral part of our lives, recent efforts have focused on their continued production in a sustainable manner. In Chapter 1, we introduce the concept of sustainable polymers and set forth criteria for materials to be considered sustainable. Two potential sustainable polymers are introduced: polylactide and polyisoprene. As one of the limitations of polylactide is its brittle nature, the discussion focuses on methods to rubber toughen it through melt blending with special attention to reactive compatibilization while blending. We propose that our research will focus on incorporating fully renewable materials into a reactively compatibilized melt blend. Evidence in the literature indicates that polylactide materials with complex architectures can be tough, so the discussion shifts to methods to functionalize polyisoprene to create such polymers. Both post-polymerization functionalization and copolymerization are discussed as methods to create functionalized polyisoprene.

1.1 Sustainable Polymers

1.1.1 What is sustainability?

Sustainability is a perhaps overused term that conveys a sense of environmental responsibility and oftentimes erroneously ascribed (e.g. sustainable coal).[1] If one wants to truly understand the sustainability of a process or material, sustainability must be defined accurately first. A typical dictionary definition of sustainability's root sustain includes "to keep going"[2] which translates to an environmental definition of sustainability that includes "the property of not being harmful to the environment or depleting natural resources."[3] Though these definitions are a good starting point, they can be a bit simplistic for complex systems such as the production and use of polymeric materials.

Chemical sustainability is not only the ability to continue synthesizing chemicals over time, but it includes the 12 principles of "green chemistry."[4] Chemical/chemistry safety, pollution prevention, and renewable feed stocks (i.e. raw materials) are the major areas of focus for green chemistry and likewise apply to sustainability.[5] Renewable feed stocks are perhaps the most recited principle in the sustainable chemistry literature as it is the most tangible factor and immediately knowable for chemists justifying their research in this field. One could argue that it is also the most important for sustainability as chemistry would not be able to continue if the feed stocks were depleted. Not to be overlooked, though tend to be afterthoughts, are safety and pollution. By creating processes that are safe and limit pollution, the continued existence of raw materials and workers is ensured. Additionally, for a molecule or chemical process to be truly sustainable, ethics and sociological consequences need to be considered as well.[6,7] By considering the larger societal implications, the scientist prevents public mistrust and allows for wider acceptance of the chemistry. These ethical and sociological concerns are perhaps the most difficult for chemists to grasp as they are not necessarily measurable quantities. As discussed, the concept of sustainability in chemistry is complex and typically one researcher cannot account for all its factors alone. For this reason, to truly consider all aspects of sustainability for a particular molecule or chemical process, there need to be dialogue between scientists and authority figures in many disciplines.

The general aspects of sustainable chemistry can be applied to the specific disciplines that fall under it. Currently, a majority of the polymers (e.g. plastics, rubber) ubiquitous throughout everyone's life are derived from petroleum sources. Petroleum is an unsustainable source for polymer raw materials (monomers) as it is finite (produced over millions of years).[8] Furthermore, the use of petroleum for monomers faces competition from its use as fuels.[9] With the predicted peak in oil production in the near future, such competition is set to increase, leading to higher prices of polymer starting materials and a lower availability.[10] Other unsustainable factors are present with the synthesis of the current polymers from petroleum. As with nearly every chemical process on the industrial scale, polymer synthesis releases net carbon dioxide into the atmosphere that can attribute to global climate change. Furthermore, the commodity polymers are notorious for their inability to break down.[11] This property has directly attributed to the Northern Pacific Gyre "garbage patch" and even some communities to ban the use of non-degradable plastic bags.[12,13] Lately, health concerns have arisen towards some of the additives and residual monomers leading to countrywide bans of chemicals in consumer products.[14] Fortunately, current research is undergoing to address these concerns and develop sustainable polymers.

The atoms of a sustainable polymer are derived from renewable sources and follow a cyclic path (Figure 1.1).[15] Plant materials are the renewable source of atoms. Water and carbon dioxide are combined by photosynthesis to ultimately produce all plant materials, whether the materials are complex sugars such as starch or other derivatives like terpenes and aromatics. These chemicals from plants can then be refined into their useful parts – raw materials for polymer production. Naturally occurring polymers like starch and cellulose can be used as is, with modification, or broken down into their base sugars (e.g. glucose) and fermented into other chemicals.[16] Additionally, terpenes, oils, aromatics, and alcohols present in plant materials can be collected and chemically modified to produce monomers for polymer production.[17,18] The monomers are combined into polymers and the polymers (synthetics and natural) are made into resins for product production. These products are used by consumers until they reach the end of their useful lives at which point they must be disposed. Instead of placing the renewably sourced

materials in the landfill, they would be disposed in such a way to bring the raw materials (carbon dioxide, monomers, etc.) back into the polymer synthesis stream. Methods of disposal include industrial composting, hydrolytic degradation, recycling, and combustion.[19,20]
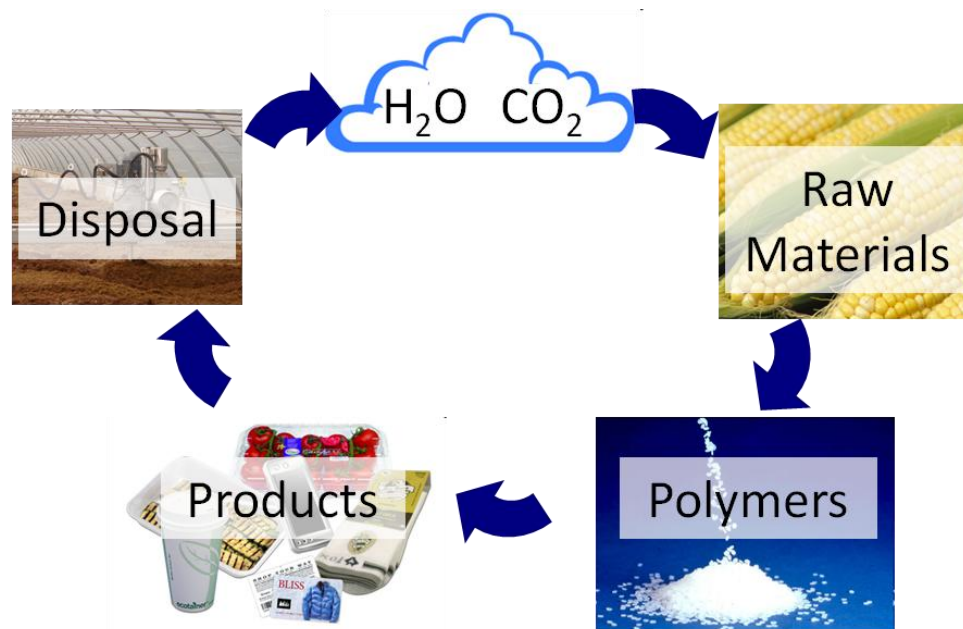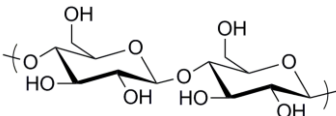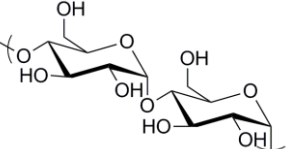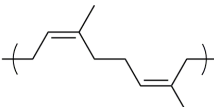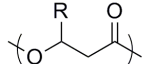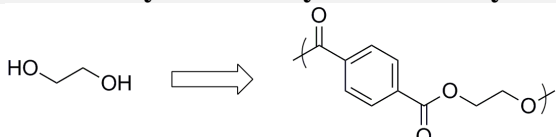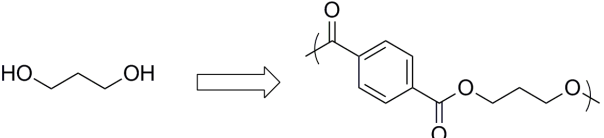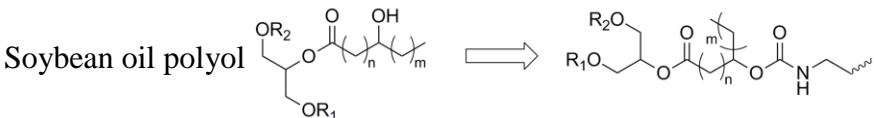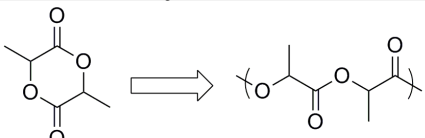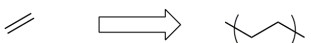
Figure 1.1. Sustainable polymer life cycle. Carbon dioxide and water are transformed by photosynthesis to give plants as the polymer raw materials. The plant material is transformed into polymers through refining and polymerization processes. The polymers are then processed into products for use. At the end of the products life the polymer products are disposed in a manner to regenerate the plan raw materials or recycled back into the polymer stream.

Though extensive research has been performed, commercial acceptance of sustainable polymers could be argued to be in its infancy. Many of the commercial or soon to be commercial renewably sourced polymers (Table 1.1) have yet to achieve all the criteria for sustainability. Three types of renewably sourced polymers exist: natural polymers, partially renewably sourced polymers, and polymers from renewably sourced monomers.[21] Natural polymers such as cellulose (wood, rayon, cellophane, etc.) and starch are nearly sustainable as they degrade in the environment and their toxicity is known.[22,23] Deforestation and fertilizer use are concerns that could potentially limit the sustainable nature of not only these materials, but also all renewably sourced polymers in general.

Table 1.1. Repeat units and structures of some of the currently or soon to be commercially available renewable polymers. Three classes of renewable polymers are given: natural polymers, partially renewable polymers, and polymers made from renewably sourced monomers.

Renewable Repeat Unit	Monomer/Polymer Structure	Polymer Name
Natural Polymers		
Glucose		Cellulose
Glucose		Starch
Isoprene		Natural Rubber (NR)
Hydroxyalkanoic acids		Poly(hydroxyalkanoic acid) (PHA)
Partially Renewably Sourced Polymers		
1,2-ethane diol		Polyethylene terephthalate (PET)
1,3-propane diol		Polytrimethylene terephthalate (PTT)
Soybean oil polyol		Polyurethanes (PU)
Renewably Sourced Monomers		
Lactide (lactic acid)		Polylactide (PLA)
Isoprene		Polyisoprene (PI)
Ethylene		Polyethylene (PE)

Partially renewable sourced polymers aim to replace petroleum chemicals with renewably sourced chemicals in currently used polymers.[24] Typically, one component (e.g. diol) of the structure unit is substituted with the same compound derived from a renewable source. This substitution approach allows for rapid assimilation of renewably sourced materials into commercial products. The polymers (e.g. polyethylene terephthalate) are typically already in use and the partially renewably sourced resin can be dropped right in to production. Other efforts aim to replace petroleum based components with slightly different renewably sourced materials. Consequently, more effort is required to design the partially renewably sourced material with the same properties as the petroleum sourced materials. The use of soy polyols to partially replace petroleum polyols in polyurethane foams is one example.[25]

Of particular interest are renewably sourced monomers that ultimately give renewably sourced polymers. The monomers can be fermentation products of sugars or chemical modifications of such fermentation products. Additionally, chemical modification of natural products can also lead to new renewable monomers.[26,27,28,29] New polymers from renewable monomers are perhaps the most difficult to commercialize as polylactide (PLA) is the only current example. Other soon to be commercial renewably sourced monomers ethylene and isoprene already have respective petroleum sourced polymers that are widely used and understood, guaranteeing their acceptance as long as they are cost competitive.[30] Moreover, the availability of these monomers allows for not only the synthesis of the homopolymer but also the inclusion of them in more complex architectures such as block polymers, copolymers, and graft copolymers. Particularly, PLA and polyisoprene (PI) are interesting materials as they are not only renewable, but also have the ability to be sustainable.

1.1.2 Polylactide

To produce PLA, bacteria ferment sugars, giving lactic acid. The lactic acid is then dimerized through a series of reactions to produce the cyclic dimer lactide.[31] As lactic acid is a chiral molecule, three isomers of lactide are made: L-lactide, D-lactide, and meso-lactide of which L-lactide is the most common (Figure 1.2). Distillation gives the

pure lactide isomers that are available for subsequent polymerization with a host of catalysts.[31] The PLA polymer is a glassy material with a glass transition temperature (T_g) between 60 and 70 °C.[32] As a consequence of the availability and abundance of pure L-lactide, commercial materials typically are poly(L-lactide) (PLLA). The PLLA materials tend to be semicrystalline due to the isotactic nature of the polymer with a melting temperature around 160 °C.[32] If a copolymer of L-lactide and D-lactide is synthesized, the material does not crystallize, giving an amorphous polymer.

L-lactide   D-lactide   meso-lactide   poly(L-lactide) (PLLA)   poly(L-lactide-*co*-D-lactide) (PLA)
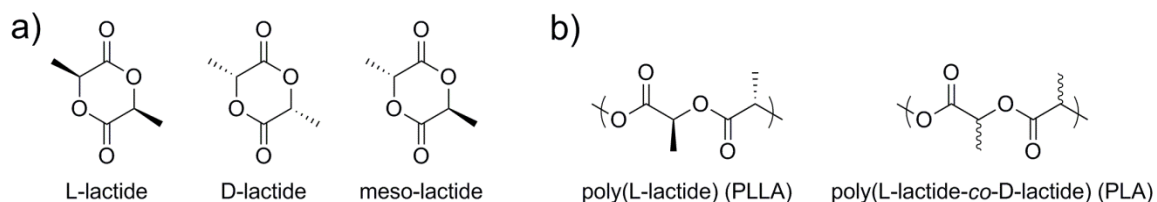
Figure 1.2. Chemical structures for (a) lactide monomers and (b) the L-lactide homopolymer (PLLA) and L-lactide/D-lactide copolymer (PLA). The PLLA is semicrystalline while PLA is amorphous.

As PLA is an aliphatic polyester, it is readily degradable through hydrolysis under both basic and acid conditions. PLA is industrially compostable as well. Hydrolysis breaks PLA polymer chains down to molecular weights small enough for microorganisms to consume the material.[32] Eventually, given sufficient conditions, PLA breaks down into carbon dioxide and water. Additional sustainable degradation mechanisms of PLA include hydrolytic depolymerization, recycling, and combustion. All disposal methods provide the starting materials to make more PLA. Natureworks, a commercial producer of PLA, has also taken steps to reduce the carbon dioxide emissions of the production process by offsetting with renewable sources of energy and process efficiency.[33] On a cradle to gate basis, a pound of PLA has less carbon dioxide emissions than a pound of PET.[33] With the above attributes, PLA is the polymer closest to be considered sustainable. Some issues that put this position in doubt are the use of corn for raw materials and its extensive water usage, but efforts are underway to address these concerns.[33] Generally, PLA is accepted as the first success in the mass production of sustainable polymers.

Like any polymer, PLA is not suitable for all applications. The mechanical properties of PLA are similar to those of polystyrene (PS) – a commodity petroleum based polymer (Table 1.2). Unfortunately, the T_g is low enough that it cannot be used for applications that require temperatures much warmer than 50 °C. Consequently, PLA has been used in disposable packaging and clothing fibers as it has fiber properties similar to other polyesters (e.g. PET).[32] Like PS, PLA has a high entanglement molecular weight and is a brittle material. Both PLA and PS have low values for their elongation to break and Izod impact toughness, while PET (a ductile polymer) has high values for these properties. The brittle nature of PLA currently limits its uses, but significant research has been undertaken to improve its mechanical properties. Such toughening efforts are reviewed in Section 1.2 and are the subject of the research described in Chapter 2.

Table 1.2. Physical and mechanical properties of PLLA, PS, and PET.[34,35,36,37]

	PLLA	PS	PET
Density (kg/m^3)	1.26	1.05	1.40
Entanglement molecular weight (g/mol)	10000	13000	1200
Tensile strength (MPa)	59	45	57
Elastic modulus (GPa)	3.8	3.2	3.4
Elongation to break (%)	5	3	300
Izod impact toughness (J/m)	26	21	59
Heat deflection (°C)	55	75	67

1.1.3 Polyisoprene

Another interesting, potentially sustainable material is renewably sourced polyisoprene (PI). Natural rubber (NR) is primarily *cis*-1,4-polyisoprene along with proteins and fatty acids and is generated by many types of plants (Figure 1.3).[38] The largest sources of NR are trees of the *Hevea brasiliensis* species that are cultivated in tropical locations. The average molecular weight (M_n) of NR is high (10^6 g/mol) and set by the biosynthesis in trees.[39] Until recently, NR was the only renewable source of PI, but advancements in genetic engineering have allowed for the monomer isoprene to be

directly produced by bacteria from the fermentation of sugars. Sugars from sources such as corn are fed to genetically engineered *E. coli* which consume the sugars, producing isoprene.[40] Isoprene gas bubbles out of the fermentation baths and is collected as a nearly pure product. The renewable isoprene (BioIsoprene®) can then be used as a drop in replacement for isoprene derived from petroleum sources.

Isoprene   poly(*cis*-1,4-isoprene) (NR)   polyisoprene (PI)

Isomers of PI repeat units

cis-1,4-isoprene   *trans*-1,4-isoprene   1,2-isoprene   3,4-isoprene
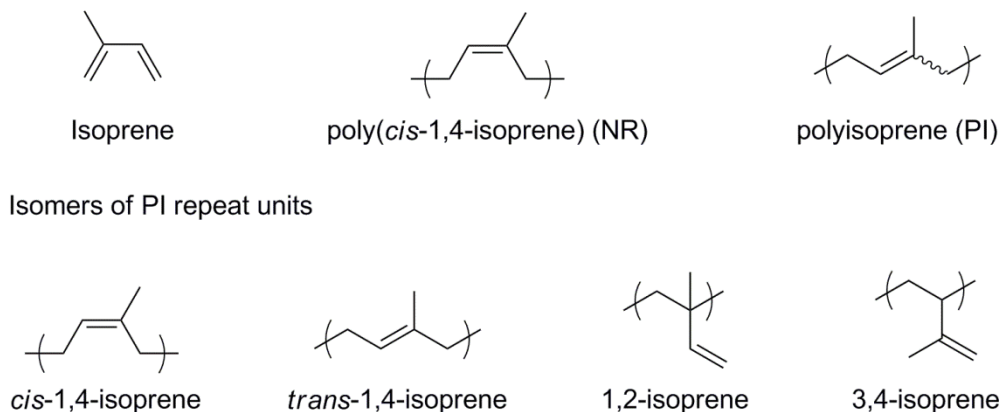
Figure 1.3. Chemical structures of isoprene, natural rubber (NR), and polyisoprene (PI). Includes the possible PI repeat unit isomers.

In order for renewably sourced PI to be considered a sustainable material, it has to have a mechanism to return to its starting materials. Several methods exist to break down PI. Perhaps the least elegant method to close the sustainable cycle is the combustion of PI, producing carbon dioxide and water as the byproducts. Of course with the combustion of any material other oxidative products are present in a complex mixture, some of which could be toxic (e.g. carbon monoxide). Furthermore, formation of tar byproducts that would have to be land filled is another concern.[41] Nevertheless, the heat of combustion for PI is similar to polyolefins and studies have shown that the gasification of PI containing tires can be profitable and generate electricity.[41,42,43] Incineration of rubber tires that contain a large amount of NR and PI serves as a method to produce electricity and regenerate the starting materials of renewably sourced PI.[44] Photo-oxidation of PI, essentially a lower energy analogous process to combustion, breaks down the PI into smaller chain lengths under ambient conditions or accelerated UV processes, but is far from being commercialized.[45,46]

PI is also biodegradable. Both bacteria and fungi will grow on PI (both NR and synthetic), decreasing the molecular weight and eventually completely consuming the material.[47,48,49,50] The mechanism appears to proceed with enzymes that oxidize the double bonds of PI with subsequent cleavage of the adjacent carbon-carbon bonds.[47,50] With the cleavage of the bonds, bacteria are able to use PI as their only carbon source to create biomass. Bacteria can consume PI in either a suspension of latex particles or directly on the rubber material. Latex gloves incubated with PI consuming bacteria in media completely were consumed in three months.[48] In a controlled environment such as an industrial compost setting, PI consuming bacteria could be introduced into the system to increase the rate of its consumption. Even vulcanized PI and NR are consumed by bacteria, just at a slower rate than the unvulcanized material.[47] Other additives also decrease the ability of microorganisms to consume PI.[50] Currently, more research is required to provide a microbial option that will consume PI under a variety of conditions in industrially relevant time frames.[51]

Renewably sourced PI holds significant sustainable advantage over other synthetic rubbers (e.g. butadiene, styrene-butadiene rubber) as its starting material can be renewably produced. Furthermore, of the synthetically produced rubbers, PI is the only material that has been show to undergo microbial degradation.[50] Even the compositionally similar polybutadiene has not been found to degrade by microbial consumption.[50] PI has the ability to close the sustainable polymer cycle for its raw materials as it can be both renewably sourced and biodegradable. In doing so, numerous current materials would become sustainable or at least partially renewable.

Most interestingly, new renewably sourced/sustainable materials could be created due to renewable PI. The low T_g of PI (ca. -60 °C) allows for its use in materials that require flexibility and stickiness. Block copolymers containing PI (Kraton) are thermoplastic elastomers and adhesives.[52] Fully renewable analogs can be synthesized by combining PI and a glassy renewable polymer such as PLA. Furthermore, and most relevant to the work presented in this thesis, are the availability of chemically active double bonds along the PI backbone. The double bonds can undergo reactions to create functionalized rubbery polymers. Furthermore, the ability of isoprene to undergo radical

polymerization, allows for the copolymerization of isoprene and functional monomers. Further discussion of the post-polymerization functionalization of PI will be given in Post-polymerization Functionalization of PI1.3.2 and Chapter 3. Copolymerization of isoprene and functional monomers will be discussed in Section 1.3.3 and Chapter 4.

1.2 Toughening Polylactide

1.2.1 Introduction to toughening

Two widely used methods can determine the "toughness" of a material: tensile and impact tests. Tensile testing (uniaxial extension at a constant rate) generates a curve with the stress (force divided by cross-sectional area) on the y-axis and strain (displacement divided by original length) on the x-axis.[53] The "tensile toughness" of a material can be calculated by integrating the area under this stress-strain curve.[54] Often used as a surrogate for the tensile toughness is the elongation (strain) at break. Brittle materials have low elongations at break ($< 10\%$), while ductile materials have higher elongations at break. Other data such as the elastic modulus and stress at break also are calculated from tensile testing. Impact testing measures the energy required to break a notched or un-notched sample of material.[55] In an Izod impact test, one end of a vertical sample is clamped leaving a free end. A pendulum swings into the free end, breaking the sample. The energy to break the sample is divided by either the linear thickness or cross-sectional area of the sample to give the "Izod impact toughness."

As discussed in Section 1.1.2 PLA is considered a brittle material due to its low values of both elongation at break and impact toughness. Consequently, significant research has been undertaken to improve the toughness of PLA. PLA statistical copolymerization, stereochemistry, crystallinity, processing and the addition of plasticizers or rigid fillers affects the mechanical properties of PLA. These techniques offer their own advantages and disadvantages. Thorough reviews of the aforementioned toughening techniques can be found by Anderson et al.[56] and Lui and Zhang.[57] Incorporation of small amount of a low T_g, rubbery, immiscible material is another method to improve the mechanical properties of PLA. So called rubber toughening can be

achieved by two methods: physical blending and chemically linking PLA with a rubbery material.

1.2.2 Rubber toughening phenomena

When a stress is applied to a bulk material, defects present in the sample serve as the starting point for microcracks. The cracks propagate throughout the material to release the energy being applied in the form of stress.[58,59] Once a crack becomes macroscopic the sample fails and breaks. In brittle material such as PLA cracks propagate easier than in a ductile material (e.g. polyethylene). Rubber toughening changes the deformation behavior of the material under stress, allowing for energy dissipation through mechanisms other than crack propagation.[60] In glassy polymers, crazes can dissipate the strain energy.[60,61] Crazes form from microvoids in the material opening up due to the applied stress (Figure 1.4a). The craze formation draws polymer chains into fibrils that span the void, dissipating energy. Only once the fibrils break does the craze propagate to form a crack. The inclusion of micron size or smaller domains of rubbery or glassy materials or small voids can serve as craze initiators, providing more locations to dissipate energy.[62,63] Thus, crazing allows the material to undergo more applied stress before failing – the material becomes more ductile.
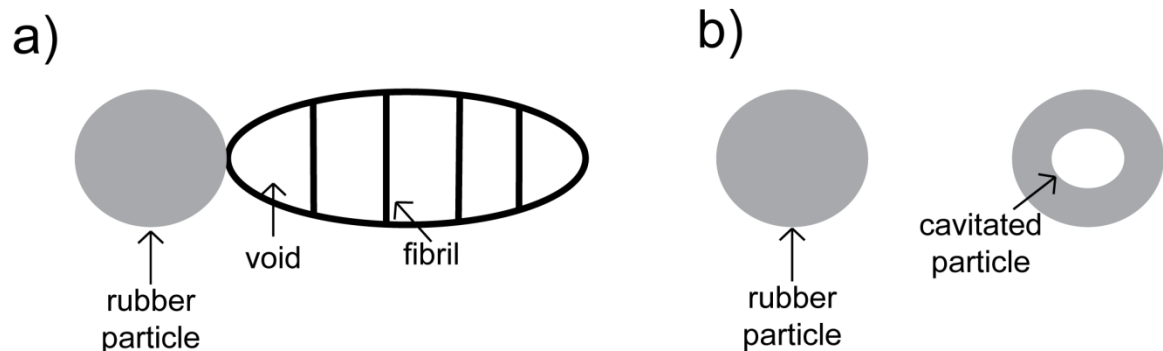
Figure 1.4. Schematic images of (a) crazing and (b) cavitation. Crazing produces a void that originates from the rubber particle where polymer fibrils span the void. Cavitation creates a void inside the rubber particle due to the hydrostatic pressure created by the applied stress.

Cavitation of the rubber particle also releases energy (Figure 1.4b). When a particle cavitates it promotes the material around it to shear yield, causing local flow of

the polymer near the particle.[64] If the particles are sufficiently close together, the shear yielding effects of each particle combine, leading to the entire sample to shear yield on the macroscopic level. Typically, for a rubber toughened, glassy material, both crazing and shear yielding occur to some degree.[65] The relative magnitude of each mechanism determines the ultimate toughness of the material. Shear yielding allows the sample to elongate further before break. Thus, the toughest materials dissipate energy by shear yielding.

1.2.3 Melt blending process

The most industrially relevant method to mix two immiscible polymers is melt blending. During melt blending, the bulk polymers liquefy and the applied shear from the compounding process generates instabilities in a sheet of the liquid polymer.[66,67] The instabilities cause the sheet to break up, forming particles of the minor phase (i.e. minority component) in the matrix phase (i.e. majority component).[68] A number of factors influence the ultimate particle diameter: the interfacial tension between the two phases, the shear rate, and the ratio of the viscosities of the two components.[69,70,71] Materials with similar viscosities and a low interfacial tension give the smallest droplets in the dispersed phase.[71] Intuitively, a higher shear rate gives smaller particles as well.

Droplet diameter has a significant effect on the final material properties of the blend. For a set volume of material, as the particle diameter is decreased the number of particles increases. With more droplets dispersed throughout the matrix, the interparticle distance goes down. A measure of the interparticle distance is the matrix ligament thickness (MLT). Numerous studies have concluded that a critical MLT exists for a material, at which there is a brittle to ductile transition.[72,73] At the critical MLT, the shear yielding effects (shear fields) from individual particles overlap sufficiently to allow for bulk shear yielding.[74]

For a material toughened primarily through crazing, an optimum particle diameter exists as opposed to a critical one.[75] Additional particles lead to more crazing sites, providing added energy dissipation as the particle diameter drops. However, the smaller

particles are less efficient at initiating the crazes which counteracts the additional sites. The disparaging behaviors lead to the optimal particle diameter observed.

As the particle diameter affects the final material properties, methods have been devised to control it. The addition of block polymer surfactants to polymer blends has been successful at decreasing the particle diameter.[76,77,78,79] In these tertiary blends, the block polymer contains a block that preferentially dissolves in the matrix phase polymer and another block that preferentially dissolves in the minor phase polymer. As the system is blended some of the surfactant diffuses to the interface of the two phases, while other surfactant remains as micelles.[80,81] At the interface, the block polymer reduces the interfacial tension, promoting drop break up into smaller domains.[76,77,78,79] The block polymers also inhibit droplet coalescence during mixing and can act as a stitch between the two phases, allowing for improved transfer of stress.[82,83,84] An alternative to adding the preformed block polymer compatibilizer is the synthesis of compatibilizer at the droplet interface while blending. This reactive blending scheme has added benefits over the preformed block polymer because compatibilizer is not wasted forming micelles. Both procedures have proved to be highly effective at creating tough materials and have found commercial use (e.g. high impact polystyrene).

1.2.4 Renewable blends of PLA

Tough block copolymer compatibilized blends of PLLA have been synthesized, but they use 10 to 20 wt % non-renewable materials as toughening agents.[85,86,87,88] The presence of non-renewable materials decreases the sustainability of these blends. Consequently, research has targeted the incorporation of renewable materials into PLA blends. PHAs have been blended with PLA and typically result in materials without significant improvement of the blend toughness.[89,90,91,92,93,94,95,96,97,98] The lack of improvement stems from the stiff nature of the PHAs investigated and the poor interfacial adhesion between PLA and the PHAs. The toughest PHA/PLA blends used the ductile PHA poly(3-hydroxybutyrate-*co*-3-hydroxyhexanoate) (PHBHx) as the blending partner.[96,97,98] Research by Schreck and Hillmyer[98] and Gao et al.[97] produced blends of 15 and 33 wt % PHBHx, respectively, that gave elongations to break with only a 2-fold

increase over neat PLA. These results contrast the work of Noda et al.[96] where they observed an 8-fold increase in elongation to break with 10 wt % PHBHx. The discrepancy may be due to the different bacterial syntheses of PHBHx providing blending materials with different bulk properties and interfacial adhesions.

Potentially sustainable succinic acid polyesters have been blended with PLA to produce tough materials. Blends of poly(butylene succinate-*co*-L-lactate) (PBSL) and PLA have given 14 to 25-fold increases in elongation to break over the parent PLA with only 10 to 20 wt % PBSL.[99,100] Poly(butylene succinate) (PBS) also proves to be effective at toughening PLA a similar loadings.[100] Poly(ethylene succinate) (PES), which has a similar structure to PBS, can be blended with PLA to improve the toughness of the material as well.[101,102] The ability of PES, PBS, and PBSL to toughen PLA appears at first to be at odds with rubber toughening theory as they are semicrystalline materials with melting temperatures around 100 °C.[100,102] However, at low loadings of PES, PBS, and PBSL (ca. 20 wt %) the confinement of the material to small domains suppresses crystallization.[100,102] PES, PBS, and PBSL have T_g values of -9, -16, and -20 °C respectively, so without crystallization the polymers behave as rubbery materials at room temperature, allowing for rubber toughening mechanisms to operate.[100,102]

PI and natural rubber (NR) have been blended with PLLA, giving mixed results. PI blends led to a decrease in the overall toughness of the material due to the poor interfacial adhesion between it and PLA.[103,104] Conversely, blends of 10 wt % NR and PLA gave materials with a 60-fold increase in elongation to break over neat PLA when tested as thin films.[105] Interestingly, very similar blends of PLA and NR give significantly worse properties in the work of Zhang et al.[106] With 10 wt % NR, the impact strength was only twice that of neat PLA and the elongation to break was unchanged. The blending of a NR-*g*-poly(butyl acrylate) (NR-*g*-PBA) graft copolymer into PLA led to a 6-fold improvement in the elongation to break as the NR-*g*-PBA had lower interfacial tension and better adhesion than the NR homopolymer. However, the improvement did compromise the sustainability of the material as PBA is non-renewable. The material properties of the NR/PI blends with PLA are strongly dependent upon processing,

suggesting that radical reactions and decomposition of NR/PI may cause the differing results reported.

Besides NR, other natural products and their derivatives have been blended with PLA. Natural fillers lead to materials with higher moduli, but not improved toughness.[107,108,109] Thermoplastic starch (TPS) blends with PLA only doubled the elongation to break over neat PLA.[110] More successful blends have been synthesized using natural oils as the minor component. Robertson et al. demonstrated a 4-fold increase in elongation to break with blends of 15 wt % polymerized soybean oil (polySOY).[111] The degree of toughening was found to be dependent upon the amount of cross linking present in the polySOY samples as it affected the ultimate droplet diameter. Blends of 5 wt % castor oil and PLA gave further improvement in mechanical properties with an 8-fold increase in elongation to break as compared to neat PLA.[112] Further improvement was realized (12-fold increase in elongation to break over neat PLA) by the addition of 5 wt % of a PLA/poly(ricinoleic acid) block polymer as a compatibilizer. The improvement underscores the compatibilizer requirement to produce the toughest melt blends.

1.2.5 Reactive blends of PLA

Instead of adding preformed block copolymers to compatibilize blends, reactive blending schemes create the compatibilizer as the system is mixed. Reactive blends of PLA and rubbery minor component have received a lot attention over the last two to three years as the commercial use of PLA has increased. Five major chemistries for the reactive compatibilization of PLA have emerged: transesterification, radical coupling, maleic anhydride grafting, isocyanate coupling, and epoxide coupling. Blending partners tend to be other degradable polyesters or non-degradable rubbery materials. Few examples exist of completely renewably sourced blending partners. The following is a review of the reactive blending techniques used to toughen PLA. A summary of the mechanical properties of the blends discussed is given in Table 1.3.

Table 1.3. Formulation and improvements over PLA homopolymer physical properties for literature examples of PLA reactive blends targeting tough materials.

Minor Component[a]	Wt % MC[b]	F_σ[c]	F_ε[d]	F_{IT}[e]	Reaction Type[f]	Notes[g]	Ref.
PETG	20	0.6	13		TE		113
PCL	20	0.7	42		TE		114
PCL	30	0.7	36	3	Radical	0.2 wt % DCP	117,118
PBAT/PC	58	1	13	1	Radical	18/40 PBAT/PC, 0.3 wt % DCP	119
PBAT	25		12		Radical	0.2 wt % Trigonox 101	120
PBS	20	0.7	60	12	Radical	0.1 wt % DCP	121
TPS	25	0.7	40		MA		124
TPS	50		3		MA		125
POE	20	0.6	30		MA	2.5 wt % POE-*g*-MA	129
PP	10	1	1	1	MA		130
PCL	20	0.8	12	1	CN	0.5 wt % LTI	133
PBS	10	0.6	40	3	CN	0.3 wt % LTI	134
PBSL	20			4[h]	CN	2 wt % LTI	135
PP	10	0.7	1	1	Epoxide	PP-*g*-GMA	130
EBA-GMA	15			34	Epoxide	5 wt % zinc ionomer	140,141
EGMA	20	0.6	40	50	Epoxide	3 wt % GMA	142
POE	30	0.5	10	12	Epoxide	POE-*g*-GMA	143
ABS	30		16	27	Epoxide	GMA grafted off ABS particles	144
PBAT	30	0.2	36	6	Epoxide	5 wt % EGMA	145
SEBS	20		61	30	Epoxide	10 wt % EGMA	146
PE	20		12		Epoxide	5 wt % EGMA	147
ABS	30	0.7	6	2	Epoxide	10 wt % SAN-GMA	148
CS	5	0.6	17		DA	HEMI-PLLA matrix	149

[a]PETG = poly(ethelene glutaric-*co*-terephthalate), PCL = polycaprolactone, PBAT = poly(butylene adipate-*co*-terephthalate), PC = polycarbonate, PBS = polybutylene

succinate, TPS = thermoplastic starch, POE = poly(ethylene-*co*-octene), PP = polypropylene, PBSL = poly(butylene succinate-*co*-L-lactate), EBA-GMA = ethylene-*n*-butyl acrylate- glycidyl methacrylate copolymer , EGMA = poly(ethylene-*co*-glycidyl methacrylate), ABS = acrylonitrile-butadine-styrene copolymer, SEBS = styrene-ethylene butadiene-styrene block polymer, PE = polyethylene, CS = conjugated soybean oil. [b]Wt % minor component in blend, does not include compatibilizer. [c]x-fold increase in stress at break compared to PLA homopolymer. [d]x-fold increase in elongation at break compared to PLA homopolymer. [e]x-fold increase in impact toughness compared to PLA homopolymer. [f]TE = transesterification, MA = maleic anhydride, CN = Isocyanate, DA = Diels–Alder. [g]DCP = dicumyl peroxide, LTI = lysine triisocyanate, SAN-GMA = styrene-acrylonitrile-glycidyl methacrylate copolymer, HEMI-PLLA = PLLA end-functionalized with *N*-2-hydroxyethyl maleimide. [h]x-fold increase in fracture toughness.

Transesterification Reactions

Transesterification reactions proceed between two polyesters. The terminal alcohol of one polymer reacts with the esters along the backbone of another (Figure 1.5). If the reaction occurs between two different types of polymers, a block polymer compatibilizer is formed. Either a catalyst or the heat during melt blending can promote transesterification reactions with PLA and other polyesters. Yeh et al.[113] reported the transesterification between PLA and poly(ethylene glutarate-*co*-terephthalate) (PETG) (20 wt %) while melt blending to give a material with a 13-fold increase in elongation to break. Similar results have been observed for the transesterification of PLA and polycaprolactone (PCL) catalyzed by triphenyl phosphate.[114] Blends of PLA and cellulose fibers have been compatibilized by the simultaneous lactide polymerization off cellulose and transesterification of PLA with the cellulose-PLA material.[115] Tough materials were not synthesized, but the system improved the adhesion of the cellulose in the system. Similar to transesterification, liquid crystal polymer (LCP) and PLLA blends with polycarbodiimide (PCD) formed compatibilized systems through polymer-polymer reactions.[116] Carboxylic acids from the LCP and PLLA reacted with the PCD, forming compatibilizers between the immiscible components and giving stiffer materials. Though transesterification is a novel approach to tough materials, its use is limited in reactive blending schemes.
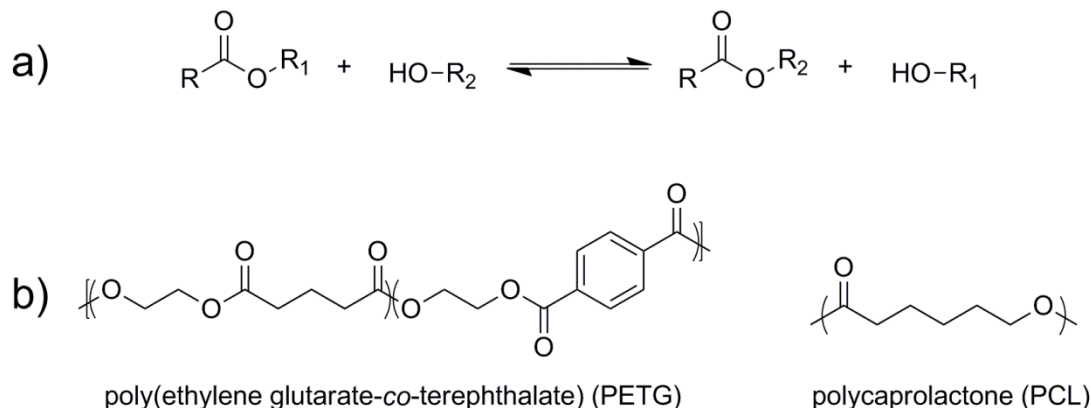
Figure 1.5. Chemical structures for (a) transesterification reaction scheme and (b) polyesters that have been transesterified with PLA to yield tough materials. Transesterification swaps the R_1 group of the original ester with the R_2 group of the alcohol. Between two different polymers this results in the formation of block polymers.

Radical Coupling

PLA and aliphatic polyesters can be linked through a radical mechanism to form compatibilizers. Radicals are generated by the decomposition of peroxides in the blend, which abstract protons from PLA and the aliphatic polyester. The aliphatic polyester undergoes β-scission to give a terminal alkene. Polymeric radicals from PLA then react with the terminal alkene to give a block polymer compatibilizer. Using this reaction scheme, Semba et al.[117,118] investigated melt blends of degradable PCL and PLLA using dicumyl peroxide (DCP) as the radical generator. With 30 wt % PCL and 0.2 wt % DCP a 36-fold increase in elongation to break was realized over the homopolymer. Impact strength of the reactive blend improved modestly over the PLLA homopolymer (3-fold increase). The reactive blend also represented a significant improvement in the mechanical properties over the binary blend of PCL and PLLA. Kanzawa et al.[119] investigated blends of 30 wt % poly(butylene adipate-*co*-terephthalate) (PBAT) with PLA and DCP (0.3 wt %) that gave a similar improvement to the elongation to break (24-fold increase) with no observed change in impact properties. With the replacement of some of the PLA with polycarbonate (PC), the reactive system (18/40/42 PBAT/PC/PLLA) still had improved elongation to break (13-fold) in addition to improved thermal properties. Binary blends of 25 wt % PBAT and PLA with 0.2 wt %

Trigonox 101 (organic peroxide) gave a 12-fold increase in elongation to break.[120] Similar improvement in mechanical properties were observed in blends of another degradable polymer poly(butylene succinate) (PBS) and PLLA.[121] With 20 wt % PBS and 0.1 wt % DCP, the elongation to break of the materials increased 60-fold over the parent PLLA. Additionally, the impact toughness improved by a factor of 12. For all the DCP initiated reactive blends, the concentration of DCP had an optimal value. Increasing the DCP concentration above this value resulted in a decline of the mechanical properties, possibly due to the embrittlement of the matrix from an increased crosslink density.
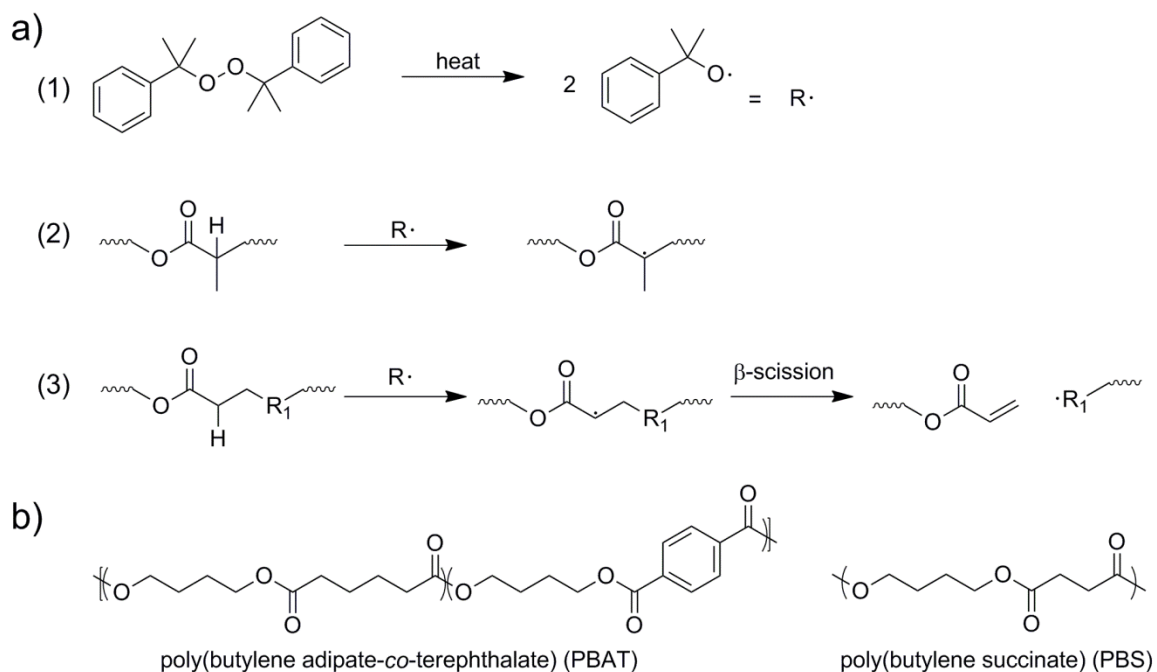
Figure 1.6. Reaction scheme of (a) radical reactive blending and (b) structures of polymers radically compatibilized with PLA. For the radical formation of compatibilizer, (1) dicumyl peroxide (DCP) decomposes to give free radical species, (2) radicals abstract the methine proton from PLA to give a polymeric radical, and (3) radicals abstract the α-hydrogen from the aliphatic polyesters which is followed by β-scission to give a terminal alkene. The terminal alkene and PLA radical react to give compatibilizer.

Maleic anhydride functionalization

The use of maleic anhydride (MA) in the formation of compatibilized blends is accomplished through the radical functionalization of one of the blending components with MA. Hydroxyl groups then react with the anhydride functionalized material to form

compatibilizer. One use of maleated PLA is to react with starch filler to improve its adhesion (Figure 1.7).[122,123] Reactions of maleated PLA with thermoplastic starch (TPS), starch that has been heated with plasticizers such as glycerol to break up its crystalline structure, can lead to tough materials. Huneault and Li[124] investigated blends of 25 wt % TPS with maleated PLA that gave materials with a 40-fold increase in elongation to break. The properties of the material depended heavily on the processing of the material during extrusion. A similar blend of TPS and PLA by Leadprathom et al.[125] had a more modest increase in toughness (2.5-fold increase in elongation to break). Additionally, maleated PLA has been reacted with poly(ethylene oxide) (PEO) to give a plasticized material.[126]
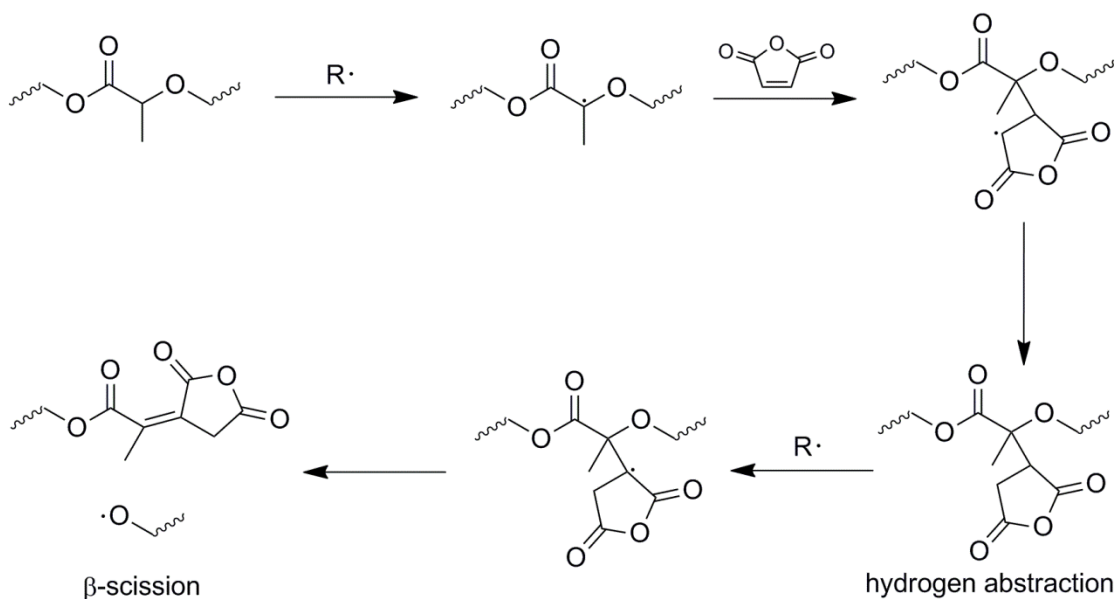
Figure 1.7. Reaction scheme for maleic anhydride (MA) grafting to PLA. A radical generating species abstracts the methine hydrogen from PLA which subsequently reacts with MA. The resultant radical then abstracts a hydrogen from another source to give MA grafted off the PLA backbone. Further radical reactions can lead to β-scission, yielding MA end-functionalized PLA. The pendent anhydride group can react with hydroxyl groups while blending to give compatibilizer and improve adhesion.

Polyolefins have been maleated and used as blending partners with PLA to make tough materials.[127,128] Ho et al.[129] synthesized a blend with 20 wt % poly(ethylene-*co*-octene) (POE) that was compatibilized with POE-*g*-PLA. The POE-*g*-PLA was

synthesized when PLA reacted with maleated POE, catalyzed by 4-dimethylaminopyridine (DMAP). The blends consisted of a few percent of the graft copolymer in addition to the POE and gave a 30-fold increase in the elongation to break. Maleated polyolefins do not always give improved mechanical properties. Maleated polypropylene (PP) blends with PLA (10 wt %) did not give a significant improvement in mechanical properties.[130] The maleation process tends to decrease the molecular weight of polymer (e.g. PLA) as the radicals cut up the polymer chains when adding MA to them (Figure 1.7). The lower molecular weights can lead to decreased mechanical properties if they become sufficiency low.

Isocyanate coupling

In blends, small molecule isocyanates react with the terminal hydroxyl groups of PLA and its blending partner, linking the two polymers and forming compatibilizer (Figure 1.8). The isocyanates are multifunctional and consequently can lead to cross-linking. Blends of PLA and PCL with lysine triisocyanate (LTI) have led to compatibilized systems with a 12-fold increase in elongation to break and improved fracture properties, but no observed improvement in impact behavior.[131,132,133] Similar blends with 10 wt % PBS and 0.5 wt % LTI gave a significantly higher increase in elongation to break (40-fold) and a modest increase in impact toughness (3-fold).[134] Likewise, a fourfold increase in fracture resistance was realized with a 20 wt % blend of poly(butylene succinate-*co*-L-lactate) and 2 wt % LTI.[135] In general, the addition of the isocyanates leads to better interfacial addition between the immiscible phases whether they are rubbery polymers or stiff starches.[136,137] The toughness of the blends was a function of the concentration of the isocyanate. Too little isocyanate caused insufficient compatibilization, but too much isocyanate lead to a more cross-linked material that tended to be brittle. Optimal values of isocyanate were found to be on the order of 0.3 to 1 wt %.
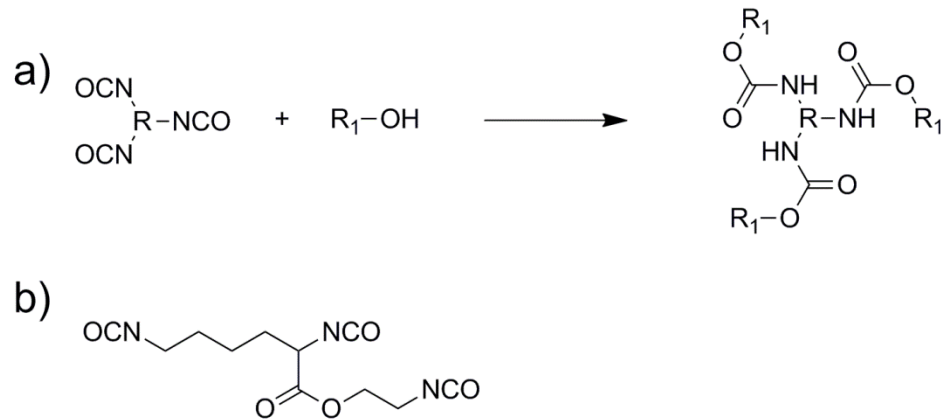
Figure 1.8. Chemical structures for (a) general reaction scheme between polymeric alcohol and multifunctional isocyanate and (b) lysine triisocyanate (LTI). Alcohols react with the isocyanates to form urethane bonds, linking polymeric chains to give compatibilizers and cross-linking.

Epoxide Reactions

Perhaps the most common chemistry employed to reactively compatibilize blends of PLA involves the epoxide group. Typically a rubbery material with pendent epoxy groups is mixed with PLA. The terminal hydroxyl groups of PLA react with the epoxide forming compatibilizer (Figure 1.9). Stiff epoxy containing materials also have been blended with PLA to improve its thermal properties, following the same reaction scheme.[138,139] For most applications, glycidyl methacrylate (GMA) is either used to post-polymerization functionalize a rubbery material or it is copolymerized with the appropriate monomers to give a functionalized copolymer.

poly(ethylene-*co*-*n*-butyl acrylate-*co*-glycidyl methacrylate) (EBA-GMA)
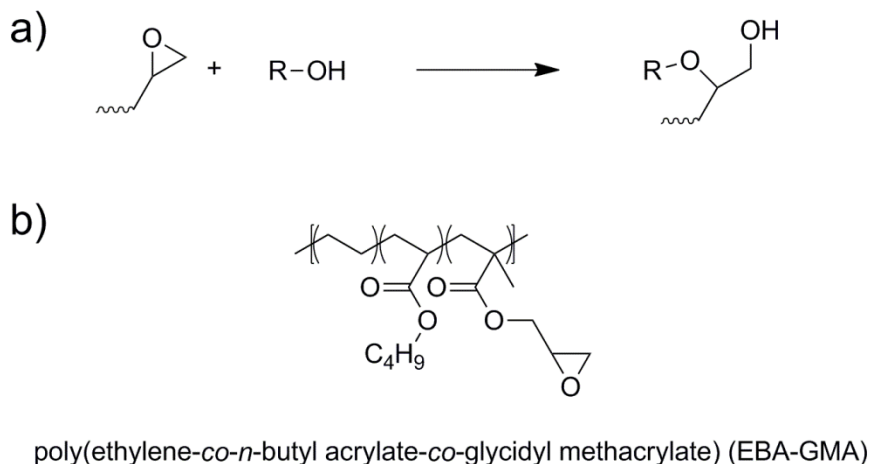
Figure 1.9. Chemical structures for (a) the general reaction between a pendent epoxy group and polymeric alcohol and (b) the EBA-GMA copolymer. The terminal alcohol of PLA reacts with pendent hydroxyl groups of the rubbery phase to form compatibilizer.

Blends of the pure GMA functionalized materials have resulted in extremely tough materials. Liu et al.[140,141] synthesized blends of an ethylene/*n*-butyl acrylate/glycidyl methacrylate terpolymer (EBA-GMA) with an ethylene/methacrylic acid zinc ionomer (EMAA-Zn) and PLLA. The EMAA-Zn catalyzed not only the coupling between EBA-GMA and PLLA, but also the simultaneous cross-linking of the rubber minor components. The resulting blend of 20 wt % rubber components in PLLA had an impact toughness 34 times that of the original PLLA. Similar results were observed with a 20 wt % blend of poly(ethylene-*co*-glycidyl methacrylate) (EGMA) and PLLA.[142] The blending partners do not need to be copolymers with GMA. POE post-polymerization functionalized with GMA was blended with PLLA to afford tough materials with a 12-fold increase in impact toughness with 30 wt % of rubber.[143] Additionally, acrylonitrile/butadiene/styrene (ABS) emulsion particles were functionalized post-polymerization with GMA to give reactive particles. The ABS-GMA particles were blended with PLLA at a 30 wt % loading to give materials with a 16-fold increase in elongation to break and a 27-fold increase in impact toughness.[144]

Tertiary blends of PLLA, a rubbery polymer, and a GMA containing compatibilizer also have been synthesized. The GMA compatibilizer is the minor component (5–10 wt %) of the system that is preferentially soluble in the rubber phase

and reacts with PLLA to form the compatibilizer. PBAT, styrene-ethylene-butadiene-styrene block copolymers (SEBS), and PE have been blended with PLLA using EGMA as the reactive agent. The PLLA and EGMA react to form a compatibilizer at the interface of the two phases. Zhang et al.[145] obtained at 36-fold increase in the elongation to break for a 30 wt % PBAT blend with PLLA and 5 wt % EGMA compatibilizer, but suffered significant decrease in the tensile strength (20 % of the PLLA value). Tougher materials were synthesized with SEBS polymer (20 wt %) and 10 wt % EGMA as not only the elongation to break increased significantly (60-fold), but also the impact toughness increased 30-fold over PLLA homopolymer.[146] More modest increases in physical properties were observed in blends of 20 wt % PE (5 wt % EGMA)[147] and 30 wt % ABS with a styrene-acrylonitrile copolymer containing grafted GMA (5 wt %).[148] The greatest improvements in mechanical properties for the ternary systems were achieved when the formed compatibilizer was efficient at decreasing the minor phase particle diameter.

As the discussed reactive blends of PLA illustrate, tough PLA blends have been synthesized. However, examples of tough, reactive compatibilized PLA blends with a renewable minor phase are few. When 10–20 wt % of the blend is made of non-renewable material, the sustainability and degradability of the system are questionable. Some of the above examples do contain degradable polymers, but room exists for the investigation of a fully renewable reactive blend. Hence, we undertook research to develop a completely renewable, reactively compatibilized blend, which is discussed in Chapter 2.[149]

1.2.6 Block and graft polymer toughened PLA

Block and graft polymers can serve as compatibilizers for melt blends as discussed above. In these blends, the compatibilizer, whether preformed or formed while blending, is a fraction of the total material. Several groups have investigated the ability of these block and graft polymers to be tough materials alone. In these tough materials, the block or graft polymers have PLA as the major block and the rubbery component as the minor block. Grijpma et al.[150] synthesized block polymers with a PLLA-Poly(L-lactate-

co-caprolactone) (PLLA-PLACL) structure (Figure 1.10), where the copolymer block was a 50/50 molar blend. The PLACL block behaves as a low T_g material, allowing for rubber toughening to occur. Interestingly, the toughness of the PLLA-PLACL block polymers was dependent upon the polymerization temperature. With similar PLACL content (30–34 wt %), copolymers made at 100 °C had lower elongations to break (90%) as compared to those synthesized at 140 °C (1500%). The variation may be due to changes in copolymerization kinetics affecting the copolymer microstructure. Similar improvement in mechanical properties were observed in tri-block copolymers of PLA-*b*-poly(trimethylene carbonate)-*b*-PLA (PLA-PTMC-PLA) (Figure 1.10), which gave tough materials (135% elongation to break) with 11 wt % TMC.[151] Analogously, tri-block copolymers of PLA and a polycyclooctadiene (PCOD) mid-block gave a 40% elongation to break with 8 wt % of PCOD (Figure 1.10).[152]
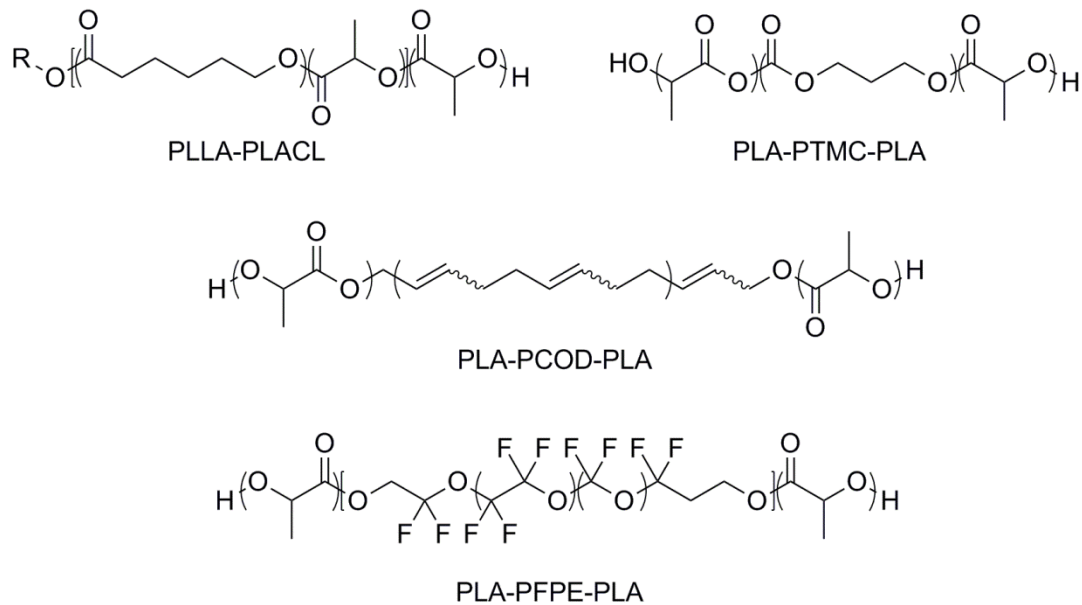
Figure 1.10. Chemical structures of tough PLA block copolymers.

Other tri-block polymers have lead to tough materials. The bis-functional poly(tetrafluoroethylene oxide-*co*-difluoromethylene oxide) PFPE was used as a macroinitiator for the synthesis of PLLA-PFPE-PLLA tri-block polymer (Figure 1.10).[153] With 1 wt % and greater than 10 wt % PFPE in the block polymer, the materials were

brittle. However, polymers with 5 wt % PFPE were tough materials. Interestingly, the achieved improvement in elongation to break was dependent upon the molecular weight of the PFPE. With a 4 kg/mol PFPE mid-block and 5 wt % PFPE, a 5-fold increase in elongation to break was observed. When the molecular weight of the PFPE mid-block was decreased to 2 kg/mol the elongation to break increased to around 300% (30-fold increase). The differences in properties were attributed to variations in the molecular weight of the PLLA blocks.

Block polymers with more complex architectures also have led to tough materials. Star block polymers of PLA and a rubbery component were synthesized by Grijpma et al.[154] Four arm stars of TMC and TMC/CL (50/50 mole ratio) copolymers were used as macroinitiators for the ring opening polymerization of lactide. The star-PLA-TMC and star-PLA-TMC-co-CL polymers lead to tough materials (ca. 250% elongation to break) with around 20 wt % rubbery material in the polymers. When the rubbery material content was reduced to 6 wt % TMC the star polymers were no longer tough (4% elongation to break). Graft polymers of PLA attached to a rubbery backbone also lead to tough materials. Jing and Hillmyer[155] synthesized a bifunctional lactide monomer containing norbornene functionality. Ring opening metathesis copolymerization of the norbornene-lactide with cyclooctadiene gave a rubbery macroinitiator for the polymerization of lactide. Polymerization of racemic lactide off the macroinitiator gave graft copolymers (PCN-*g*-2PLA) (Figure 1.11) containing 20 wt % rubbery content and with a 13-fold increased elongation to break. In a similar system, Theryo et al.[156] copolymerized cyclooctadiene with norbornene-methanol (PCN) to give a macroinitiator with pendent hydroxyl groups. Using only 5 wt % of the macroinitiator, racemic lactide was polymerized off the PCN to give a PCN-*g*-PLA polymer (Figure 1.11). Interestingly, with this low loading of rubbery content extremely tough materials were synthesized with a 17-fold increase in elongation to break (elongation to break = 240 %).

PCN-*g*-2PLA   PCN-*g*-PLA
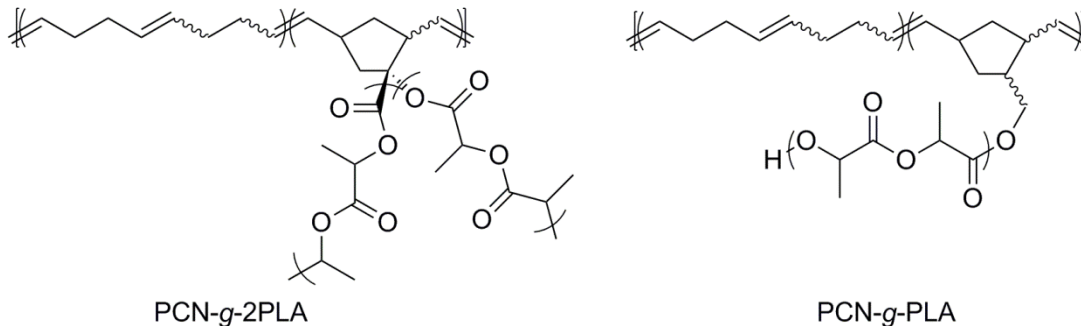
Figure 1.11. Chemical structures of tough PLA graft polymers.

None of the tough graft and block polymers of PLA are completely derived from potentially sustainable materials. Efforts have been made to reduce the amount of non-renewable content, but in many cases 20 wt % of the polymers are non-renewable. Some of the minor components are not degradable either. With these deficiencies, an opportunity exists to develop potentially sustainable, rubbery materials to act as macroinitiators for the synthesis of PLAs with complex architectures. As discussed, PI is a potentially sustainable rubbery material. With the subsequent functionalization of PI, it could potentially be used as a replacement macroinitiator for tough PLA graft polymers.

1.3 Functionalized PI

1.3.1 Introduction to functional polymers

The functionalization of polymer chains is a widely used technique to create specialty polymers.[157,158] New properties and complex architectures (star, branched, graft, etc.) are produced from these macroinitiators. For example, the properties of the tough graft copolymers discussed above are due to their complex architecture. The polymer chain functionality may be incorporated by copolymerization or post-polymerization functionalization. In both cases, the functional group must be amenable to all subsequent reactions. The chemical handle can be used either for direct initiation of polymerization (e.g. hydroxyl group for lactide polymerization) or further functionalized to give a suitable initiation system. Many options exist for the synthesis of functionalized PI as isoprene can be polymerized by several techniques and PI contains reactive carbon-carbon double bonds. A discussion follows that outlines the synthetic techniques

amenable to the post-polymerization functionalization of PI and isoprene copolymerizations. The chemistries discussed will focus on methods specifically suited to produce PLA graft copolymers as it has been shown that they can be tough materials. However, many of the techniques to be discussed could be adapted to produce other complex materials.

1.3.2 Post-polymerization Functionalization of PI

Numerous functional monomers exist, but not all of them can be copolymerized with isoprene due to their functionality interacting with the polymerization chemistry. The other option is to impart the desired functionality to PI after polymerization. Post-polymerization functionalization of polymers allows for one parent polymer chain to undergo many different reactions, produce an array of new functional materials from one parent polymer. Numerous methods exist to impart new chemical functionality onto the backbone of PI post-polymerization.[159,160,161,162] The schemes take advantage of the carbon-carbon double bonds along the polymer backbone. Reactions that can be performed on small molecule alkenes typically will work on PI. Using these analogous reactions PI has been fluorinated,[163] chlorinated,[164] brominated,[164,165] iodated,[164] hydrosilylated,[166] hydrochlorinated,[167] hydrobrominated,[165] and sulfonated.[164] Additions of chlorosulfonyl isocyanate and trichloromethylsilane have led to the formation of cycles along the polymer chain.[160] Beyond these transformations, other reactions exist that allow for functionalized PI to be used as a scaffold for more complex architectures.

Addition reactions to a carbon-carbon double bond

In several reactions, small molecules add across the double bonds of PI to impart the additional functionality that they carry. Small molecule carbenes can react with PI (Figure 1.12),[168] forming cyclopropane moieties along the polymer backbone with the other end of the carbene free to undergo subsequent reactions. Thiol-ene chemistry can also be used to functionalize PI (Figure 1.12).[169] In this reaction, the thiol adds across the double bond though a UV or radical catalyzed process. The other end of the thiol (e.g. alcohol) can be reacted further such as functionalization with a reversible addition-fragmentation transfer (RAFT) agent or atom transfer polymerization (ATRP) initiator.[169]

These groups can be used for controlled radical polymerization. Maleic anhydride (MA) can either be added to PI through a radical mechanism or the thermally induced ene reaction to give maleated PI that can be used for further reactions (Figure 1.12).[159,160,170]
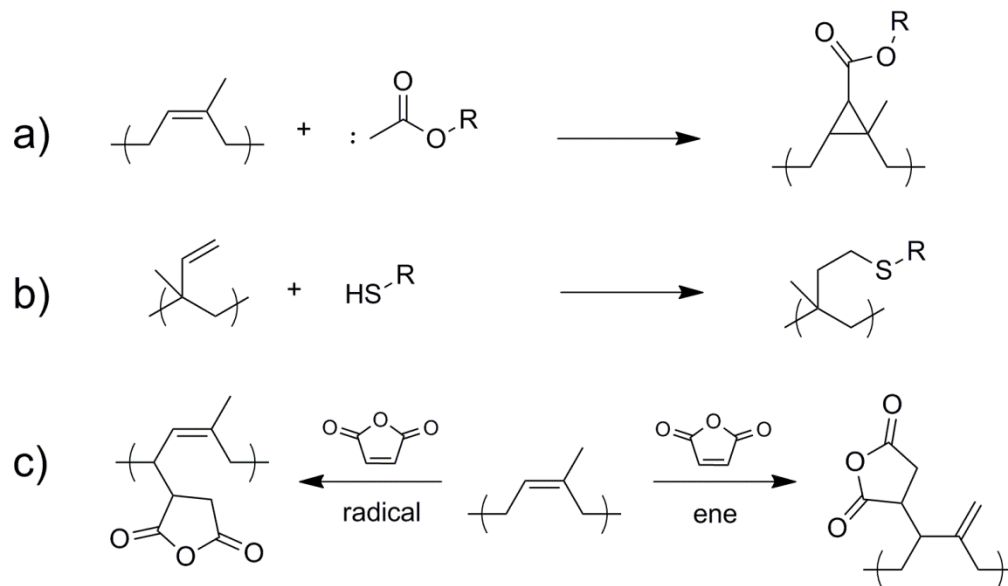
Figure 1.12. Addition reaction schemes for (a) carbene reaction, (b) thiol-ene reaction, and (c) maleic anhydride reaction with PI. The major products for both the ene and radical addition of maleic anhydride to PI are shown.

Reactions with maleated PI

Maleated PI can react in methods similar to those used for small molecule anhydrides. Under protic conditions with available water, the anhydride can be converted to carboxylic acids (Figure 1.13).[171] Analogously, alcohols will ring open the anhydride under heating.[172] Using this method, the alcohols can impart additional functionality to the polymer chain. For example, Derouet et al.[172,173] reacted maleated PI with 2-hydroxyethyl acrylate (HEA) and 2-hydroxylethyl cinnamate to give PI with pendent double bonds (Figure 1.13). Hydroxyl cinnamate esters with longer alkyl chains also underwent similar alcohol ring opening reactions with maleated PI.[174] The pendent double bonds allowed for subsequent photo cross linking reactions. Like alcohols, amines also can react with maleated PI through a similar ring opening reaction. Triazole moieties have been incorporated into PI using this method, giving significant hydrogen bonding of

the PI chains (Figure 1.13).[175] In a slightly different reaction, maleated PI was ring opened with methanol to give an acid and an ester (Figure 1.13).[176] The acid was transformed into an acid chloride that then underwent a condensation reaction with an amine to give a functionalized PI. Though none of the aforementioned reactions with maleated PI have led to graft copolymers, such procedures could be adapted to give the functionality required for graft copolymer formation.
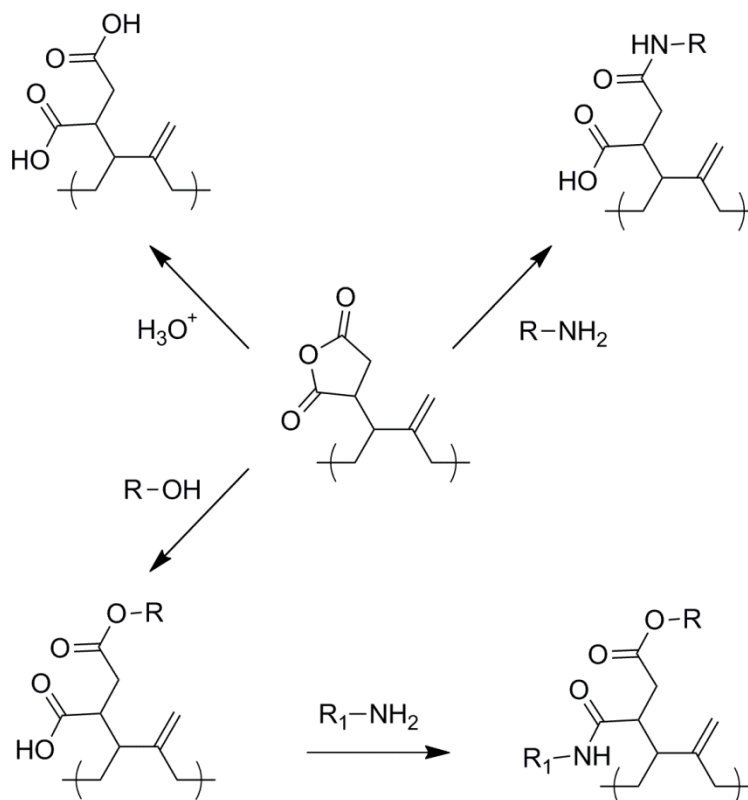
Figure 1.13. Ring opening reactions of maleated PI with aqueous acids, alcohols, and amines. The reactions yield PI with pendent acids and esters that can undergo subsequent reactions.

Reactions with epoxidized PI

PI has been epoxidized through a variety of chemical processes. With an intramolecular nucleophilic substitution reaction, HBr can be eliminated from the bromohydrin of PI to give an epoxide.[165] More commonly, PI is reacted with a peroxycarboxylic acid (e.g. meta-chloroperoxybenzoic acid) to give an epoxidized PI

(Figure 1.14).[165,177,178] In aqueous latex systems (i.e. natural rubber latex), hydrogen peroxide with formic acid can be used for the epoxidation.[178,179] The epoxide chemical handle can be used for addition reactions similar to those performed on maleated PI, but allows for more flexibility due to the number of reactions available. Carboxylic acids react with epoxidized PI through acid catalyzed ring opening addition, linking the carboxylic acid to the polymer chain by forming a ester (Figure 1.14a).[180,181,182] Likewise, amines[183] and alcohols, [184,185,186] and thiols have reacted with epoxidized PI through a nucleophilic ring opening reaction of the pendent oxiranes (Figure 1.14b-d). Phosphates will react with epoxidized PI in a facile manner to give cyclic dioxaphospholane and β-hydroxyphosphate adducts along the PI backbone (Figure 1.14e,f).[186,187,188] The phosphate adducts can bring additional functionality to PI when chemical moieties are attached to the phosphate. Moreover, the phosphates can promote chain linkages.
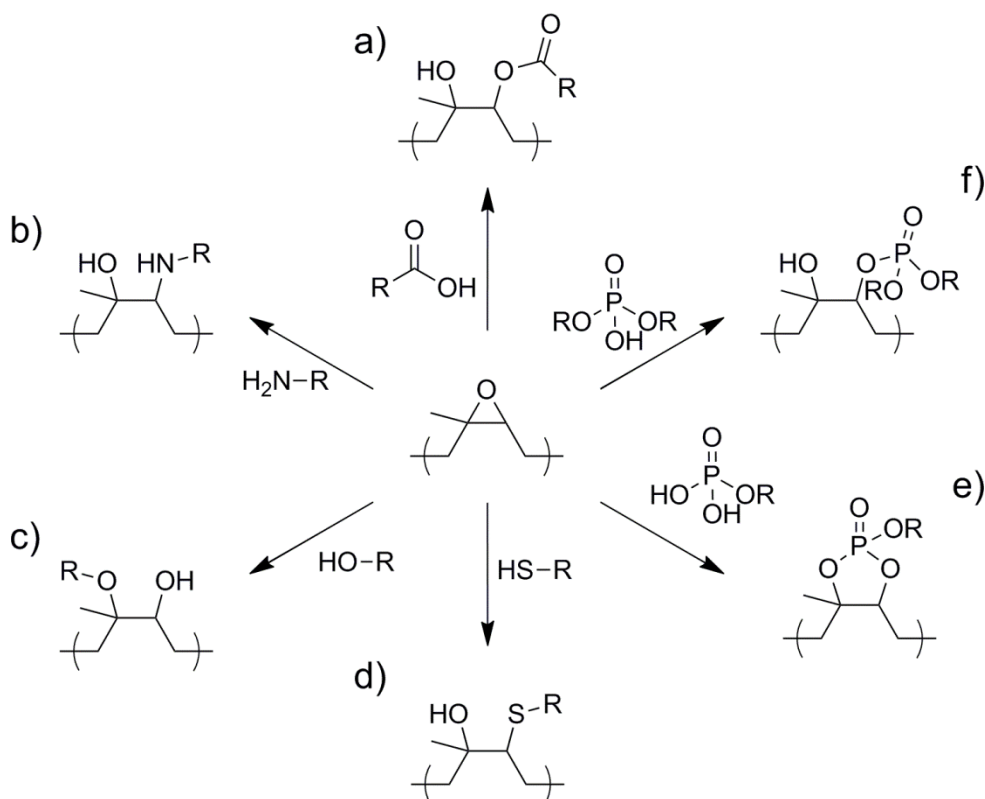
Figure 1.14. Reactions of epoxidized PI with (a) carboxylic acids, (b) amines, (c) alcohols, (d) thiols, (e,f) and phosphates.

Additionally, epoxidized PI has been used as a backbone for graft copolymer synthesis through RAFT controlled radical polymerization. Sodium *N,N*-diethyldithiocarbamate (DEDT-Na) reacted with epoxidized PI in both aqueous environments and polar solvents to give RAFT agent functionalized PI (PI-CTA) (Figure 1.15).[189] The PI-CTA macroinitiator was used for graft polymerization of methyl methacrylate (MMA), styrene, and methacrylonitrile.[190] The fastest graft polymerizations occurred in the bulk for MMA and styrene, but graft copolymerizations of these monomers could be accomplished in the latex environment. Other graft copolymers were formed off epoxidized natural rubber latex using phosphonate monomers.[191] These monomers photopolymerized to high yields in the aqueous latex to give core shell particles.
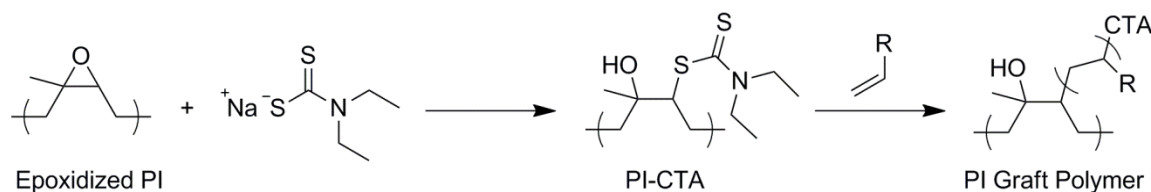
Figure 1.15. Reaction scheme to synthesize PI graft polymers from the RAFT CTA functionalized epoxidized PI.

Hydroboration-oxidation of PI

Hydroboration-oxidation of PI directly places hydroxyl groups along the PI chain. The hydroxyl functionalization is non-specific when carried out by diborane in tetrahydrofuran, giving hydroxyl groups off all the isomers present in PI.[160,192] Conversely, when 9-borabicyclo[3.3.1]nonane is used for the boration, the reaction is stereospecific towards the 3,4 and 1,2 isomers of PI.[193,194,195] Hydroboration with subsequent oxidation of the 1,2 and 3,4 isomers of PI gives the anti-Markovnikov product – a primary alcohol. Hydroxyl groups also can be placed on the PI backbone by the reaction of the double bonds with haloacetic acids followed by saponification.[196] The pendent hydroxyl groups produced by any of these processes can then be subjected to additional reactions. Hydroxyl functionalized PI has been reacted with acid chlorides[169,193,194] to impart additional functionality such as RAFT agents. Reactions of

anhydrides with hydroxylated PI have led to acetylated and acrylated products capable of additional reactions.[160,192]

As the preceding examples demonstrate, an array of post-polymerization methods exists for the functionalization of PI. These methods sometimes require several steps to reach the desired functionality, are limited in the types of functional groups available, and can be non-specific. Ideally, one highly efficient reaction could put any desired chemical moiety onto the PI backbone. The so called "click chemistry" reactions are functional group tolerant, efficient, and modular.[197,198,199,200] Intrigued by these salient features, we investigated methods to functionalize PI post-polymerization using click chemistry in Chapter 3.

1.3.3 Copolymerization of PI

Isoprene can be polymerized through many catalytic and propagation mechanisms. Industrially practiced polymerizations of isoprene are metal catalyzed (e.g. Ziegler-Natta, metallocene), cationic, and ionic systems typically targeting high *cis* or *trans*-1,4 microstructure.[201] Copolymerizations of isoprene and styrene,[202,203,204,205,206,207,208] butadiene,[209,210,211,212] isobutene,[213,214,215,216] and ethylene[217,218,219] proceed under these aforementioned mechanisms. However, as the reported comonomers suggest, these polymerization techniques are not amenable to the polar functional groups present in functional monomers.[220,221]

Fortunately, radical polymerizations are robust enough to handle a wide range of functional groups and monomer type, making them an attractive option for the copolymerization of isoprene and a hydroxyl containing monomer.[222] Furthermore, recent developments of controlled radical polymerizations allow for the targeted synthesis of isoprene homopolymers and a resurgence into the investigation of radical polymerizations of isoprene. Isoprene has be polymerized through controlled radical methods such as nitroxide mediated polymerization (NMP),[223,224,225,226,227,228,229,230] atom transfer radical polymerization (ATRP),[231] and reversible addition-fragmentation transfer (RAFT) polymerization.[232,233,234,235,236,237,238,239] These controlled radical methods allow for the synthesis of controlled molecular weights and narrow distribution polymers.

A rather limited number of radical copolymerizations of isoprene and functional monomers exist in literature, but several distinct types of monomers have been investigated (Figure 1.16). For example, the cyano-group containing 2,4-dicyano-but-1-ene (DCB), a β-disubstituted alkene, copolymerizes with isoprene in an alternating manner with one isoprene following one DCB repeat unit.[240,241] The pendent cyano-groups could be used for subsequent reactions to make more complex polymer structures. Conjugated dienes substituted at the α-position also have been copolymerized with isoprene. Ajellal et al.[242] investigated the NMP of isoprene and methyl-1,3-butadiene-1-phosphonate in an attempt to incorporate flame resistance into the polymer. The phosphonate monomer was incorporated as a minor component of a mostly isoprene backbone at nearly its feed ratio.

2,4-dicyano-but-1-ene   methyl 1,3-butadiene-1-phosphonate   para substituted styrene

maleic anhydride   maleate monoester   functionated maleimide

tert-butyl acrylate   methyl acrylate   acrylic acid

methyl methacrylate   glycidyl methacrylate   2-hydroxyethyl methacrylate
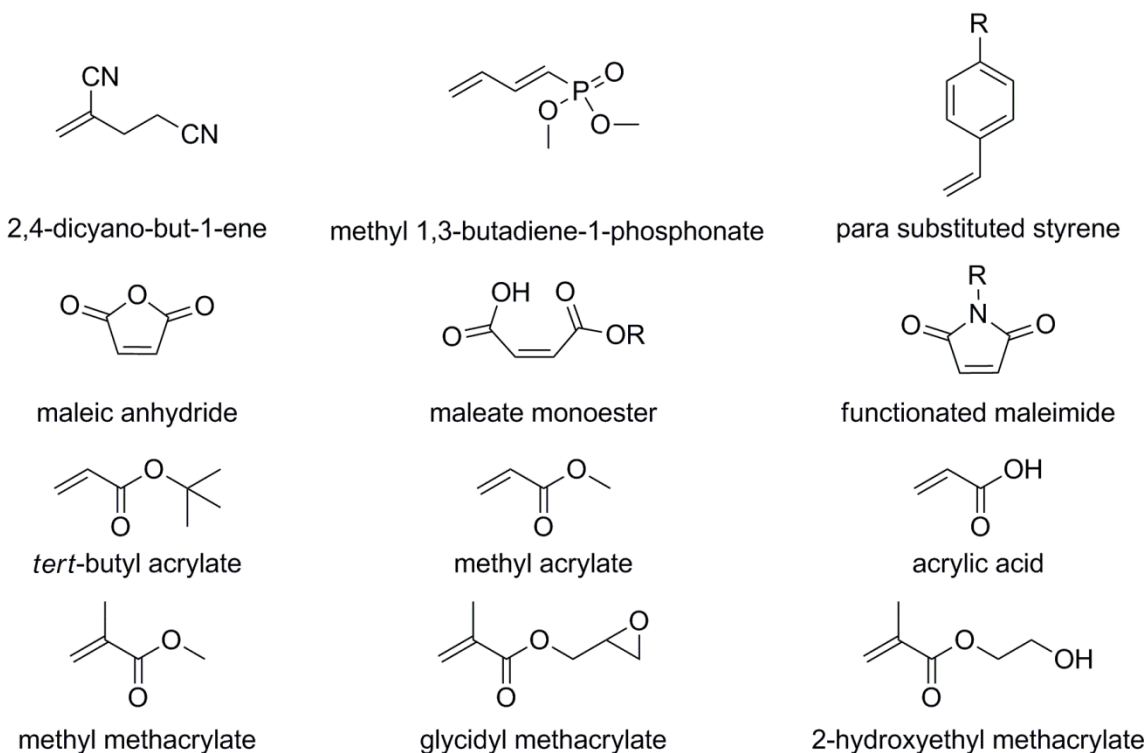
Figure 1.16. Comonomers radically copolymerized with isoprene in literature.

Maleic anhydride and its derivatives have been copolymerized with isoprene using radical mechanisms. The alternating copolymerization of isoprene and maleic

anhydride has been reported, though not in great detail.[243] In a more complete study, maleic anhydride was reacted with a series of primary alcohols to give maleate monoesters.[244] These monomers underwent an alternating copolymerization with isoprene, initiated by azobisisobutyronitrile (AIBN) at 70 °C. Similarly, functionalized maleimides underwent an alternating copolymerization with isoprene in separate studies.[245,246] Maleic anhydride and its derivatives undergo alternating copolymerizations with isoprene due to the donor-acceptor nature of the monomer system. Consequently, the reactivity ratios of each monomer go to zero, consistent with the alternating structure observed. One complication observed with the copolymerization of isoprene and maleimides was a Diels–Alder side reaction between isoprene and the maleimide, reducing the overall yield of material.[245,246] The rate of the side reaction was on the order of the copolymerization between 40 and 60 °C. Since maleic anhydride and the maleate monoesters have similar structures to the maleimides, a Diels–Alder reaction likely occurred as well.

Styrene monomers functionalized at the para-position have been copolymerized in both emulsion[247] and bulk controlled radical systems.[229] The styrene sulfonate was preferentially polymerized over the isoprene leading to compositional drift in the copolymers. The polymers initiated earlier had higher sulfonate content than those initiated later. Controlled NMP of isoprene and functionalized styrene gave materials with narrow molecular weight distributions at 120 °C.[229] In the nitroxide mediated copolymerizations, no analysis was made to determine the microstructure of the copolymers.

Another class of monomers copolymerized with isoprene is acrylates (including methacrylates). Copolymerization of methyl methacrylate at 20 °C with isoprene led to an alternating copolymer.[248] Similar copolymerizations of methyl acrylate also give alternating copolymers.[249] Both the methyl methacrylate and methyl acrylate copolymerizations compete with a Diels–Alder reaction between isoprene and each comonomer. The rate of Diels–Alder adduct formation occurs at a rate similar to polymerization. Other copolymerizations with a wide range of acrylates do not report the Diels–Alder reaction, but it likely occurs due to the high temperatures used for

polymerizations. These examples are the isoprene copolymerization with GMA at 70 °C[250] and the controlled radical copolymerizations of tert-butyl acrylate, acrylic acid, 2-hydroxyethyl methacrylate, and methyl methacrylate at 120 °C.[229] In spite of possible side reactions in these examples, the radical copolymerization of isoprene and a comonomer incorporates the comonomer's functionality into the PI chain. Though not explored in literature, these functionalized copolymers could be used as macroinitiators for complex polymer architectures. Our work in Chapter 4 explores the radical copolymerization of isoprene and a hydroxyl functionalized monomer to synthesize a PI macroinitiator.

1.4 Summary

The development of sustainable polymers will eventually lead to the replacement of the current petroleum sourced polymers. Currently, few completely renewably sourced polymers are commercially available, but their growth is continuing. Of the available or soon to be available renewably sourced polymers, PLA and PI are promising materials due their potential to be sustainable. However, PLA's acceptance as a component of many consumer goods is hampered by its brittle mechanical properties. Thus, efforts are underway to improve its mechanical properties, most notably by rubber toughening through melt blending with immiscible minor components and synthesis of polylactide graft copolymers. Most of the reported blends and graft copolymers use non-renewable materials. For this reason, we investigated fully renewable, reactive melt blends as discussed in Chapter 2. Additionally, we developed potentially sustainable PI macroinitiators through post-polymerization functionalization (Chapter 3) and copolymerization (Chapter 4).

1.5 References

[1] Xie, K.; Li, W.; Zhao, W. *Energy* **2010**, *35*, 4349–4355.

[2] Dictionary.com. http://dictionary.reference.com/browse/sustain (accessed Nov. 6, 2011).

[3] Dictionary.com. http://dictionary.reference.com/browse/sustainability (accessed Nov. 6, 2011).

[4] Anastas, P. T.; Warner, J. C. Green Chemistry: Theory and Practice, Oxford University Press: New York, 1998, p.30.

[5] Eissen, M.; Metzger, J. O.; Schmidt, E.; Schneidewind, U. *Angew. Chem. Int. Ed.* **2002**, *41*, 414–436.

[6] Böchen, S.; Lenoir, D.; Scheringer, M. *Naturwissenschaften* **2003**, *90*, 93–102.

[7] Frank, H.; Campanella, L.; Dondi, F.; Mehlich, J.; Leitner, E.; Rossi, G.; Ioset, K. N.; Bringman, G. *Angew. Che. Int. Ed.***2011**, *50*, 8482–8490.

[8] Weisz, P. B. *Phys. Today* **2004**, *57*, 47–52.

[9] Smith, P. B.; Payne, G. F. The Emergence of Renewable and Sustainable Polymers. In *Renewable and Sustainable Polymers* [Online]; Payne, G. F.; Smith, P. B. Eds.; ACS Symposium Series; American Chemical Society: Washington, D. C., 2011; pp 1–10. http://pubs.acs.org/doi/abs/10.1021/bk-2011-1063.ch001 (accessed Oct 24, 2011).

[10] Nashawi, I. S.; Malallah, A.; Al-Bisharah, M. *Energy Fuels* **2010**, *24*, 1788–1800.

[11] Okada, M. *Prog. Polym. Sci.* **2002**, *27*, 87–133.

[12] Rios, L. M.; Jones, P. R.; Moore, C.; Narayan, U. V. *J. Environ. Monitor.* **2010**, *12*, 2226–2236.

[13] Buchanan, W. http://articles.sfgate.com/2007-11-19/bay-area/17271155_1_plastic-bags-compostable-blue-recycling-bins (accessed Nov 6, 2011).

[14] Hengstler, J. G.; Foth, H.; Gebel, T.; Kramer, P.-J.; Lilienblum, W.; Schweinfurth, H.; Völkel, W.; Wollin, K.-M.; Gundert-Remy, U. *Cr. Rev. Toxicol.* **2011**, *41*, 263–291.

[15] Vilaplana, F.; Strömberg, E.; Karlsson, S. *Polym. Degrad. Stabil.* **2010**, *95*, 2147–2161.

[16] Ragauskas, A. J; Williams, C. K; Davison, B. H; Britovsek, G.; Cairney, J.; Eckert, C. A; Frederick W. J. Jr; Hallett, J. P.; Leak, D. J.; Liotta, C. L.; Mielenz, J. R.; Murphy, R.; Templer, R.; Tschaplinski, T. *Science* **2006**, *311*, 484–489.

[17] Williams, C. K.; Hillmyer, M. A. *Polym. Rev.* **2008**, 48, 1–10.

[18] van Beilen, J. B.; Poirier, Y. *Plant J.* **2008**, *54*, 684–701.

[19] Luckachan, G. E.; Pillai, C. K. S. *J. Polym. Environ.* **2011**, *19*, 637–676.

[20] Mecking, S. *Angew. Chem. Int. Ed.* **2004**, *43*, 1078–1085.

[21] Avérous, L.; Pollet, E. *MRS Bull.* **2011**, *36*, 703–710.

[22] Gandini, A. *Macromolecules* **2008**, *41*, 9491–9504.

[23] Rose, M.; Palkovits, R. *Macromol. Rapid Commun.* **2011**, *32*, 1299–1311.

[24] Vennestrøm, P. N. R.; Osmundsen, C. M.; Christensen, C. H.; Taarning, E. *Angew. Chem. Int. Ed.* [Online early access] **2011**, DOI: 10.1002/anie.201102117. Published Online: Oct 5, 2011. http://onlinelibrary.wiley.com/doi/10.1002/anie.201102117/pdf (accessed Oct 24, 2011).

[25] Zhang, L. Structure-Property Relationship of Polyurethane Flexible Foam Made from Natural Oil Polyols. Ph.D. Thesis, University of Minnesota, September 2008.

[26] Coates, G. W.; Hillmyer, M. A. *Macromolecules* **2009**, *42*, 7987–7989.

[27] de Espinosa, L. M.; Meier, M. A. R. *Eur. Polym. J.* **2011**, *47*, 837–852.

[28] Feng, X.; East, A. J.; Hammond, W. B.; Zhang, Y.; Jaffe, M. *Polym Adv. Technol.* **2011**, *22*, 139–150.

[29] Meier, M. A. R.; Metzger, J. O.; Schubert, U. S. *Chem. Soc. Rev.* **2007**, *36*, 1788–1802.

[30] Mathers, R. T. *J. Polym. Sci. Part A* [Online early access] **2011**, DOI: 10.1002/pola.24939. Published online Sep 12, 2011. http://onlinelibrary.wiley.com/doi/10.1002/pola.24939/pdf (accessed Oct 24, 2011).

[31] Gruber, P. R.; Hall, E. S.; Kolstad, J. J.; Iwen, M. L.; Benson, R. D.; Borchardt, R. L. Continuous process for the manufacture of lactide and lactide polymers. US Patent 6326458, 2001.

[32] Auras, R.; Harte, B.; Selke, S. *Macromol. Biosci.* **2004**, *4*, 835–864.

[33] Vink, E. T. H.; Davies, S.; Kolstad, J. J. *Ind. Biotechnol.* **2010**, *6*, 212–224.

[34] Anderson, K. S.; Schreck, K. M.; Hillmyer, M. A. *Polym. Rev.* **2008**, *48*, 85–108.

[35] Grijpma, D. W.; Penning, J. P.; Pennings, A. J. *Colloid Polym. Sci.* **1994**, *272*, 1068–1081.

[36] Dorgan, J. R.; Williams, J. S. *J. Rheol.* **1999**, *43*, 1141–1155.

[37] Fetters, L. J.; Lohse, D. J.; Richter, D.; Witten, T. A.; Zirkel, A. *Macromolecules* **1994**, *27*, 4639–4647.

[38] Puskas, J. E.; Gautriaud, E.; Deffieux, A.; Kennedy, J. P. *Prog. Polym. Sci.* **2006**, *31*, 533–548.

[39] Swanson, C. L.; Buchanan, R. A.; Otey, F. H. *J. Appl. Polym. Sci.* **1979**, *23*, 743–748.

[40] Whited, G. M.; Feher, F. J.; Benko, D. A.; Cervin, M. A.; Chotani, G. K.; McAuliffe, J. C.; LaDuca, R. L.; Ben-Shosha, E. A.; Sanford, K. J. *Ind. Biotechnol.* **2010**, *6*, 152–163.

[41] Castaldi, M. J.; Kwon, E.; Weiss, B.; *Environ. Eng. Sci.* **2007**, *24*, 1160–1178.

[42] Ng, S. C.; Chee, K. K. *Polymer* **1993**, *34*, 3870–3872.

[43] Hshieh, F.-Y.; Hirsh, D. B.; Beeson, H. D. *Fire Mater.* **2003**, *27*, 9–17.

[44] Schnecko, H. W. Rubber Recycling. In *Polyisoprenoids*; Koyama, T.; Steinbüchel, A.; Eds.; Biopolymers, Vol. 2; John Wiley and Sons: New York, 2001; pp 395–409.

[45] Blach, J. A.; Watson, G. S.; Busfield, W. K.; Myhra, S. *Polym. Int.* **2001**, *51*, 12–20.

[46] Bussière, P.-O.; Gardette, J.-L.; Lacoste, J.; Baba, M. *Polym. Degrad. Stabil.* **2005**, *88*, 182–188.

[47] Rose, K.; Steinbüchel, A. *Appl. Environ. Microb.* **2005**, *71*, 2803–2812.

[48] Linos, A.; Reichelt, R.; Keller, U.; Steinbüchel, A. *FEMS Microbiol. Lett.* **2000**, *185*, 155–161.

[49] Berekaa, M. M.; Linos, A.; Reichelt, R.; Keller, U.; Steinbüchel, A. *FEMS Microbiol. Lett.* **2000**, *185*, 199–206.

[50] Linos, A.; Steinbüchel, A. Biodegradation of Natural and Synthetic Rubbers. In *Polyisoprenoids*; Koyama, T.; Steinbüchel, A.; Eds.; Biopolymers, Vol. 2; John Wiley and Sons: New York, 2001; pp 321–360.

[51] Bredberg, K.; Christiansson, M.; Stenber, B.; Holst, O. Biotechnological Processes for Recycling of Rubber Products. In *Polyisoprenoids*; Koyama, T.; Steinbüchel, A.; Eds.; Biopolymers, Vol. 2; John Wiley and Sons: New York, 2001; pp 361–375.

[52] Creton, C.; Hu, G.; Deplace, F.; Morgret, L.; Shull, K. R. *Macromolecules* **2009**, *42*, 7605–7615.

[53] Pukanszky, B.; Belina, K. Tensile Properties, Creep, and Stress Relaxation. In *Polymer Characterization Techniques and Their Application to Blends*; Simor, G. P., Ed.; Oxford University Press: Oxford, 2003; pp 263–283.

[54] Bucknall, C. B. In *Polymer Blends*; Paul, D. R.; Bucknall, C. B., Eds.; John Wiley and Sons: New York, 2000; Volume 2; pp 59-82.

[55] ASTM Standard D256, *Standard Test Methods for Determining the Izod Pendulum Impact Resistance of Plastics*; ASTM Standards International, 2010.

[56] Anderson, K. S.; Schreck, K. M.; Hillmyer, M. A. *Polym. Rev.* **2008**, *48*, 85–108.

[57] Lui, H.; Zhang, J. *J. Polym. Sci. Part B* **2011**, *49*, 1051–1083.

[58] Brown, H. R. *Macromolecules* **1991**, *24*, 2752–2756.

[59] Kramer, E. J. *Adv. Polym. Sci.* **1983**, *52*, 1–56.

[60] Argon, A. S.; Cohen, R. E.; Gebizliouglu, O. S.; Schwier, C. E. *Adv. Polym. Sci.* **1983**, *52*, 275–335.

[61] Friedrich, K. *Adv. Polym. Sci.* **1983**, *52*, 225–274.

[62] Dasari, A.; Zhang, Q.-X.; Yu, Z.-Z.; Mai, Y.-M. *Macromolecules* **2010**, *43*, 5734–5739.

[63] Sauer, J. A.; Chen. C. C. *Adv. Polym. Sci.* **1983**, *52*, 169–224.

[64] Perkins, W. G. *Polym. Eng. Sci.* **1999**, *39*, 2445–2460.

[65] Bucknall, C. B.; Paul, D. R. *Polymer* **2009**, *50*, 5539–5548.

[66] Scott, C. E.; Macosko, C. W. *Polymer* **1995**, *36*, 461–470.

[67] Shih, C. K.; Tynan, D. G.; Denelsbeck, D. A. *Polym. Sci. Eng.* **1991**, *31*, 1670–1673.

[68] Sundararaj, U.; Macosko, C. W. *Macromolecules* **1995**, *28*, 2647–2657.

[69] Hudson, S. D.; Jamieson, A. M. In *Polymer Blends*; Paul, D. R.; Bucknall, C. B.,Eds.; Volume 1; Wiley: New York, 2000; pp 461-495.

[70] Favis, B. D. *J. Appl. Polym. Sci.* **1990**, *39*, 285–300.

[71] Wu, S. *Polym. Eng. Sci.* **1987**, *27*, 335–343.

[72] Wu, S. *Polymer* **1985**, *26*, 1855–1863.

[73] Wu, S. *J. Appl. Polym. Sci.* **1988**, *35*, 549–561.

[74] Jerome, R. In *Macromolecular Engineering*; Matyjaszewski, K.; Gnanou, Y.; Leibler, L., Eds.; Volume 3; Wiley-VCH: Weinheim, 2007; pp 1753–1782.

[75] Perkins, W. G. *Poly. Eng. Sci.* **1999**, *39*, 2445–2460.

[76] Shull, K. R.; Kramer, E. J. *Macromolecules* **1990**, *23*, 4769–4779.

[77] Noolandi, J.; Hong, K. M. *Macromolecules* **1982**, *15*, 482–492.

[78] Noolandi, J.; Hong, K. M. *Macromolecules* **1984**, *17*, 1531–1537.

[79] Lepers, J.; Favis, B. D. *AIChE J.* **1999**, *45*, 885–895.

[80] Dai, K. H.; Kramer, E. J.; Shull, K. R. *Macromolecules* **1992**, *25*, 220–225.

[81] Favis, B. D. *Polymer* **1994**, *35*, 1552–1555.

[82] Macosko, C. W.; Guegan, P.; Khandpur, A. K.; Nakayama, A.; Marechal, P.; Inoue,T. *Macromolecules* 1**996**, *29*, 5590–5598.

[83] Gent, A. N. *J. Mater. Sci.* **1980**, *15*, 2884–2888.

[84] Creton, C.; Kramer, E. J.; Hui, C.; Brown, H. R. *Macromolecules* **1992**, *25*, 3075–3088.

[85] Na, Y.; Yong, H.; Shuai, X.; Kikkawa, Y.; Doi, Y.; Inoue, Y. *Biomacromolecules* **2002**, *3*, 1179–1186.

[86] Wang, Y.; Hillmyer, M. A. *J. Polym. Sci. Part A* **2001**, *39*, 2755–2766.

[87] Anderson, K. S.; Lim, S. H.; Hillmyer, M. A. *J. Appl. Polym. Sci.* **2003**, *89*, 3757–3768.

[88] Anderson, K. S.; Hillmyer, M. A. *Polymer* **2004**, *45*, 8809–8823.

[89] Iannace, S.; Ambrosio, L.; Huang, S. J.; Nicolais, L. *J. Appl. Polym. Sci.* **1994**, *54*, 1525–1536.

[90] Blümm, E.; Owen, A. J. *Polymer* **1995**, *36*, 4077–4081.

[91] Zhang, L.; Xiong, C.; Deng, X. *Polymer* **1996**, *37*, 235–241.

[92] Yoon, J.-S.; Lee, W.-S.; Kim. K.-S.; Chin, I.-J.; Kim, M.-N.; Kim, C. *Eur. Polym. J.* **2000**, *36*, 435–442.

[93] Focarete, M. L.; Scandola, M.; Dobrzynski, P.; Kowalczuk, M. *Macromolecules* **2002**, *35*, 8472–8477.

[94] Takagi, U.; Yasuda, R.; Yamaoka, M.; Yamane, T. *J. Appl. Polym. Sci.* **2004**, *93*, 2363–2369.

[95] Kikkawa, Y.; Suzuki, T.; Tsuge, T.; Kanesata, M. Doi, Y.; Abe, H. *Biomacromolecules*, **2006**, *7*, 1921–1928.

[96] Noda, I.; Satkowski, M. M.; Dowrey, A. E.; Marcott, C. *Macromol. Biosci.* **2004**, *4*, 269–275.

[97] Gao, Y.; Kong, L.; Zhang, L.; Gong, Y.; Chen, G.; Zhao, N.; Zhang, X. *Eur. Polym. J.* **2006**, *42*, 764–775.

[98] Schreck, K. M.; Hillmyer, M. A. *J. Biotechnol.* **2007**, *132*, 287–295.

[99] Vilay, V.; Mariatti, M.; Ahmad, Z.; Pasomsouk, K.; Todo, M. *J. Appl. Polym. Sci.* **2009**, *114*, 1784–1792.

[100] Shibata, M.; Inoue, Y.; Miyoshi, M. *Polymer* **2006**, *47*, 3557–3564.

[101] Fan, X.; Ruan, J.; Chen, Q.; Chen, J.; Zhou, Z.; Zou, J. *J. Macromol. Sci. Part B* **2011**, *50*, 493–502.

[102] Lu, J.; Qiu, Z.; Yang, W. *Polymer* **2007**, *48*, 4196–4204.

[103] Ishida, S.; Nagasaki, R.; Chino, K.; Dong, T.; Inoue, Y. *J. Appl. Polym. Sci.* **2009**, *113*, 558–566.

[104] Jin, H.-J.; Chin, I.-J.; Kim, M.-N.; Kim, S.-H.; Yoon, J.-S. *Eur. Polym. J.* **2000**, *36*, 165–169.

[105] Bitinis, N.; Verdejo, R.; Cassagnu, P.; Lopez-Manchado, M. A. *Mater. Chem. Phys.* **2011**, *129*, 823–831.

[106] Zhang, C.; Man, C.; Pan, Y.; Wang, W.; Jiang, L.; Dan, Y. *Polym. Int.* **2011**, *60*, 1548–1555.

[107] Michinobu, T.; Bito, M.; Tanimura, M.; Katayama, Y.; Masai, E.; Nakamura, M.; Otsuka, Y.; Ohara, S.; Shigehara, K. *Polym. J.* **2009**, *41*, 843–848.

[108] Stoclet, G.; Seguela, R.; Lefebvre, J.-M. *Polymer* **2011**, *52*, 1417–1425.

[109] Zhang, J.; Jiang, L.; Zhu, L.; Jane, J.-I.; Mungura, P. *Biomacromolecules* **2006**, *7*, 1551–1561.

[110] Sarazin, P.; Li, G.; Orts, W. J.; Favis, B. D. *Polymer* **2008**, *49*, 599–609.

[111] Robertson, M. L.; Chang, K.; Gramlich, W. M.; Hillmyer, M. A. *Macromolecules* **2010**, *43*, 1807–1814.

[112] Robertson, M. L.; Paxton, J. M.; Hillmyer, M. A. *ACS Appl. Mater. Interfaces* **2011**, *3*, 3402–3410.

[113] Yeh, J.-T.; Tsou, C.-H.; Lu, W.; Li, Y.-M.; Xiao, H. W.; Huang, C.-Y.; Chen, K.-N.; Wu, C.-S.; Chai, W.-L. *J. Polym. Sci. Part B* **2010**, *48*, 913–920.

[114] Wang, L.; Ma, W.; Gross, R. A.; McCarthy, S. P. *Polym. Degrad. Stabil.* **1998**, *59*, 161–168.

[115] Braun, B.; Dorgan, J. R.; Knauss, D. M. *J. Polym. Environ.* **2006**, *14*, 49–58.

[116] Yang, Q.; Hirata, M.; Lu, D.; Nakajima, H.; Kimura, Y. *Biomacromolecules***2011**, *12*, 354–358.

[117] Semba, T.; Kitagawa, K.; Ishiaku, U. S.; Hamada, H. *J. Appl. Polym. Sci.* **2006**, *101*, 1816–1825.

[118] Semba, T.; Kitagawa, K.; Ishiaku, U. S.; Kotaki, M.; Hamada, H. *J. Appl. Polym. Sci.* **2007**, *103*, 1066–1074.

[119] Kanzawa, T.; Tokumistsu, K. *J. Appl. Polym. Sci.* **2011**, *121*, 2908–2918.

[120] Coltelli, M.-B.; Bronco, S.; Chinea, C. *Polym. Degrad. Stabil.* **2010**, *95*, 332–341.

[121] Wang, R.; Wang, S.; Zhang, Y.; Wan, C.; Ma, P. *Polym. Eng. Sci.* **2009**, *49*, 26–33.

[122] Dubois, P.; Narayan, R. *Macromol. Symp.* **2003**, *198*, 233–243.

[123] Orozco, V. H.; Brostow, W.; Chonkaew, W.; López, B. L. *Macromol. Symp.* **2009**, *277*, 69–80.

[124] Huneault, M. A.; Li, H. *Polymer* **2007**, *48*, 270–280.

[125] Leadprathom, J.; Suttiruengwong, S.; Threepopnatkul, P.; Seadan, M. *J. Met. Mater. Min.* **2010**, *20*, 87–90.

[126] Hassouna, F.; Raquez, J.-M.; Addiego, F.; Dubois, P.; Toniazzo, V.; Ruch, D. *Eur. Polym. J.* **2011**, *47*, 2134–2144.

[127] Singh, G.; Bhunia, H.; Rajor, A.; Jana, R. N.; Choudhary, V. *J. Appl. Polym. Sci.* **2010**, *118*, 496–502.

[128] Singh, G.; Bhunia, H.; Rajor, A.; Choudhary, V. *Polym. Bull.* **2011**, *66*, 939–953.

[129] Ho, C.-H.; Wang, C.-H.; Lee, Y.-D. *Polymer* **2008**, *49*, 3902–3910.

[130] Choudhary, P.; Mohanty, S.; Nayak, S. K.; Unnikrishnan, L. *J. Appl. Polym. Sci.* **2011**, *121*, 3223–3237.

[131] Takayama, T.; Todo, M. *J. Mater. Sci.* **2006**, *41*, 4989–4992.

[132] Takayama, T.; Todo, M.; Tsuji, H.; Arakawa, K. *J. Mater. Sci.* **2006**, *41*, 6501-6504.

[133] Harada, M.; Iida, K.; Okamoto, K.; Hayashi, H.; Hirano, K. *Polym. Eng. Sci.* **2008**, *48*, 1359-1368.

[134] Harada, M.; Ohya, T.; Iida, K.; Hayashi, H.; Hirano, K.; Fukuda, H. *J. Appl. Polym. Sci.* **2007**, *106*, 1813–1820.

[135] Vannaladsaysy, V.; Todo, M.; Takayama, T.; Jaafar, M.; Ahmad, Z.; Pasomsouk, K. *J. Mater. Sci.* **2009**, *44*, 3006–3009.

[136] Kim, M. W.; Hong, S. M.; Lee, D.; Park, K.; Kang, T. J.; Youn, J. R. *Adv. Compos. Mater.* **2010**, *19*, 331–348.

[137] Yu, L.; Petinakis, E.; Dean, K.; Liu, H.; Yuan, Q. *J. Appl. Polym. Sci.* **2011**, *119*, 2189–2195.

[138] Zhang, J.; Guan, L.; Su, Y.; Qi, R.; Ye, D.; Yu, J.; Huang, S. *J. Appl. Polym. Sci.* [Online early access]. DOI: 10.1002/app.34951. Published Online: Sep 1, 2011. http://onlinelibrary.wiley.com/doi/10.1002/app.34951/pdf (accessed Oct 28, 2011).

[139] Corre, Y.-M.; Duchet, J.; Reignier, J.; Maazouz, A. *Rheol. Acta.* [Online early access]. DOI: 10.1007/s00397-011-0538-1. Published online: Mar 1, 2011 http://www.springerlink. com/content/ f406672514632t0w/ fulltext.pdf (accessed July 24, 2011).

[140] Liu, H.; Chen, F.; Liu, B.; Estep, G. Zhang, J. *Macromolecules* **2010**, *43*, 6058–6066.

[141] Liu, H.; Song, W.; Chen, F.; Gou, L.; Zhang, J. *Macromolecules* **2011**, *44*, 1513–1522.

[142] Oyama, H. T. *Polymer* **2009**, *50*, 747–751.

[143] Su, Z.; Li, Q.; Liu, Y.; Hu, G.-H.; Wu, C. *Eur. Polym. J.* **2009**, *45*, 2428–2433.

[144] Sun, S.; Zhang, M.; Zhang, H.; Zhang, X. *J. Appl. Polym. Sci.* [Online early access]. DOI 10.1002/app.34111. Published Online: Jul 6, 2011. http://onlinelibrary.wiley.com /doi/10.1002/app.34111/pdf (accessed Oct 29, 2011).

[145] Zhang, N.; Wang, Q.; Ren, J.; Wang, L. *J. Mater. Sci.* **2009**, *44*, 250–256.

[146] Hashima, K.; Nishitsuji, S.; Inoue, T. *Polymer* **2010**, *51*, 3934–3939.

[147] Kim, Y. F.; Choi, C. N.; Kim, Y. D.; Lee, K. Y.; Lee, M. S. *Fiber Polym.* **2004**, *5*, 270–274.

[148] Li, Y.; Shimizu, H. *Eur. Polym. J.* **2009**, *45*, 738–746.

[149] Gramlich, W. M.; Robertson, M. L.; Hillmyer, M. A. *Macromolecules* **2010**, *43*, 2313–2321.

[150] Grijpma, D. W.; Nijenhuis, A. J.; van Wijk , P. G. T.; Pennings, A. J. *Polym. Bull.* **1992**, *29*, 571–578.

[151] Grijpma, D. W.; Van Hofslot, R. D. A.; Supèr, H.; Nijenhuis, A. J.; Pennings, A. J. *Polym. Eng. Sci.* **1994**, *34*, 1674–1684.

[152] Pitet, L. M.; Hillmyer, M. A. *Macromolecules* **2009**, *42*, 3674–3680.

[153] Haynes, D.; Naskar, A. K.; Singh, A.; Yang, C.-C.; Burg, K. J.; Drews, M.; Harrison, G.; Smith, D. W. Jr. *Macromolecules* **2007**, *40*, 9354–9360.

[154] Grijpma, D. W.; Joziasse, C. A. P.; Pennings, A. J. *Makromol. Chem. Rapid. Commun.* **1993**, *14*, 155–161.

[155] Jing, F.; Hillmyer, M. A. *J. Am. Chem. Soc.* **2008**, *130*, 13826–13827.

[156] Theryo, G.; Jing, F.; Pitet, L. M.; Hillmyer, M. A. *Macromolecules* **2010**, *43*, 7394–7397.

[157] Gauthier, M. A.; Gibson, M. I.; Klok, H.-A. *Angew. Chem. Int. Ed.* **2009**, *48*, 48–58.

[158] Feng, C.; Li, Y.; Yang, D.; Hu, J.; Zhang, X.; Huang, X. *Chem. Soc. Rev.* **2011**, *40*, 1282–1295.

[159] Schulz, D. N.; Turner, S. R.; Golub, M. A. *Rubber Chem. Technol.* **1982**, *55*, 809–859.

[160] Pinazzi, C.; Brosse, J. C.; Pleurdeau, A.; Reyx, D. *Appl. Polym. Symp.* **1975**, *26*, 73–98.

[161] McGrath, M. P.; Sall, E. D.; Tremont, S. J. *Chem. Rev.* **1995**, *95*, 381–398.

[162] Brosse, J. C.; Campistron, I.; Derouet, D.; El Hamdaoui, A.; Houdayer, S.; Reyx, D.; Ritoit-Gillier, S. *J. Appl. Polym. Sci.* **2000**, *78*, 1461–1477.

[163] Davidock, D. A.; Hillmyer, M. A.; Lodge, T. P. *Macromolecules* **2004**, *37*, 397–407.

[164] Bielinski, D. M.; Slusarski, L.; Affrossman, S.; Hartshorne, M.; Pethrich, R. A. *J. Appl. Polym. Sci.* **1995**, *56*, 853–867.

[165] Burfield, D. R.; Lim, K.-L.; Law, K.-S. *J. Appl. Polym. Sci.* **1984**, *29*, 1661–1673.

[166] Gauthier, M.; Lin, W.-Y.; Teertstra, S. J.; Tzoganakis, C. *Polymer* **2010**, *51*, 3123–3129.

[167] Derouet, D.; Tran, Q. N.; Thuc, H. H. *Eur. Polym. J.* **2007**, *43*, 1806–1824.

[168] Lishanski, I. S.; Tsitokhtsev, V. A. *J. Polym. Sci. Part C* **1968**, *22*, 277–287.

[169] Wang, G.; Fan, X.; Huang, J. *J. Polym. Sci. Part A* **2010**, *48*, 3797–3806.

[170] Saelao, J.; Phinyocheep, P. *J. Appl. Polym. Sci.* **2005**, *95*, 28–38.

[171] Derouet, D.; Phinyocheep, P.; Brosse, J. C.; Boccaccio, G. *Eur. Polym. J.* **1990**, *26*, 1301–1311.

[172] Derouet, D.; Phinyocheep, P.; Brosse, J. C.; Boccaccio, G. *Eur. Polym. J.* **1990**, *26*, 1313–1320.

[173] Derouet, D.; Phinyocheep, P.; Boccaccio, G.; Brosse, J. C. *J. Nat. Rubb. Res.* **1991**, *6*, 39–54.

[174] Visconte, L. L. Y.; Andrade, C. T.; Azuma, C. *Polym. Adv. Technol.* **1993**, *4*, 490–495.

[175] Chino, K.; Ashiura, M. *Macromolecules* **2001**, *34*, 9201–9204.

[176] Moriguchi, N.; Tsugaru, T.; Amiya, S. *J. Mol. Struct.* **2001**, *562*, 205–213.

[177] Burfield, D. R.; Lim, K.-L.; Law, K.-S.; Ng, S. *Polymer* **1984**, *25*, 995–998.

[178] Hallensleben, M. L.; Schmidt, H. R.; Schuster, R. H. *Angew. Makromol. Chem.* **1995**, *227*, 87–99.

[179] Perera, M. C. S.; Elix, J. A.; Bradbury, J. H. *J. Polym. Sci. Part A* **1988**, *26*, 637–651.

[180] Soutif, J.-C.; Brosse, J.-C. *Makromol. Chem.* **1984**, *185*, 839–846.

[181] Derouet, D.; Brosse, J. C.; Tillekeratne, L. M. K. *J. Nat. Rubb. Res.* **1990**, *5*, 296–300.

[182] Brosse, J.-C.; Klinpituksa, P.; Soutif, J.-C. *Makromol. Chem.* **1992**, *193*, 315–321.

[183] Jayawardena, S.; Reyx, D.; Durand, D.; Pinazzi, C. P. *Makromol. Chem.* **1984**, *185*, 2089–2097.

[184] Park, D.; Weinman, C. J.; Finlay, J. A.; Fletcher, B. R.; Paik, M. Y.; Sundaram, H. S.; Dimitriou, M. D.; Sohn, K. E.; Callow, M. E.; Callow, J. A.; Handlin, D. L.; Willis, C. L.; Fisher, D. A.; Kramer, E. J.; Ober, C. K. *Langmuir* **2010**, *26*, 9772–9781.

[185] Weiman, C. J.; Finaly, J. A.; Park, D.; Paik, M. Y.; Krishnan, S.; Sundaram, H. S.; Dimitriou, M.; Sohn, K. E.; Callow, M. E.; Callow, J. A.; Handlin, D. L.; Willis, C. L.; Kramer, E. J.; Ober, C. K. *Langmuir* **2009**, *25*, 12266–12274.

[186] Derouet, D.; Mulder-Houdayer, S.; Brosse, J.-C. *J. Appl. Polym. Sci.* **2005**, *95*, 39–52.

[187] Derouet, D.; Morvan, F.; Brosse, J.-C. *J. Nat. Rubb. Res.* **1996**, *11*, 9–25.

[188] Derouet, D.; Morvan, F.; Brosse, J.-C. *Eur. Polym. J.* **2001**, *37*, 1297–1313.

[189] Derouet, D.; Tran, Q. N.; Thuc, H. H. *Eur. Polym. J.* **2007**, *43*, 1806–1824.

[190] Derouet, D.; Tran, Q. N.; Thuc, H. H. *J. Appl. Polym. Sci.* **2009**, *114*, 2149–2160.

[191] Derouet, D.; Intharapat, P.; Tran, Q. N.; Gohier, F.; Nakason, C. *Eur. Polym. J.* **2009**, *45*, 820–836.

[192] Minoura, Y.; Ikeda, H. *J. Appl. Polym. Sci.* **1971**, *15*, 2219–2236.

[193] Kawahara, S.; Kakubo, T.; Sakdapipanich, J. T.; Isono, Y.; Tanaka, Y. *Polymer* **2000**, *41*, 7483–7488.

[194] Ishizu, K.; Hosokawa, T. *Polym. Int.* **2001**, *50*, 1186–1192.

[195] Lee, K. M.; Han, C. D. *Macromolecules* **2002**, *35*, 760–769.

[196] Kim, Y. H.; Pandya, A. *Macromolecules* **1991**, *24*, 6505–6511.

[197] Sumerlin, B. S.; Vogt, A. P. *Macromolecules* **2010**, *43*, 1–13.

[198] Inglis, A. J.; Barner-Kowollik, C. *Macromol. Rapid Commun.* **2010**, *31*, 1247–1266.

[199] Becer, C. R.; Hoogenboom, R.; Schubert, U. S. *Angew.Chem. Int. Ed.* **2009**, *48*, 4900–4908.

[200] Fournier, D.; Hoogenboom, R., Schubert, U. S. *Chem. Soc. Rev.* **2007**, *36*, 1369–1380.

[201] Senyek, M. Polyisoprene. *Kirk-Othmer Encyclopedia of Chemical Technology*; John Wiley & Sons Inc., 2011.

[202] Annunziata, L.; Duc, M.; Carpentier, J.-F. *Macromolecules* **2011**, *44*, 7158–7166.

[203] Valente, A.; Zinck, P.; Mortreux, A.; Visseaux, M. *J. Polym. Sci. Part A* **2011**, *49*, 1615–1620.

[204] Rabagliati, F. M.; Muñoz, L. A.; Quijada, R. *Polym. Bull.* **2011**, *67*, 1425–1434.

[205] Quinebèche, S.; Navarro, C.; Gnanou, Y.; Fontanille, M. *Polymer* **2009**, *50*, 1351–1357.

[206] Rodrigues, A.-S.; Kirillov, E.; Vuillemin, B.; Razavi, A.; Carpentier, J.-F. *Polymer* **2008**, *49*, 2039–2045.

[207] Zhang, H.; Luo, Y.; Hou, Z. *Macromolecules* **2008**, *41*, 1064–1066.

[208] Cuomo, C.; Serra, M. C.; Maupoey, M. G.; Grassi, A. *Macromolecules* **2007**, *40*, 7089–7097.

[209] Liu, D.; Cui, D. *Dalton Trans.* **2011**, *40*, 7755–7761.

[210] Ricci, G.; Zetta, L.; Alberti, E.; Motta, T.; Canetti, M.; Bertini, F. *J. Polym. Sci. Part A* **2007**, *45*, 4635–4646.

[211] Kaita, S.; Doi, Y.; Kaneko, K.; Horiuchi, A. C.; Wakatsuki, Y. *Macromolecules* **2004**, *37*, 5860–5862.

[212] Nath, D. C. D.; Shiono, T.; Ikeda, T. *J. Polym. Sci. Part A* **2002**, *40*, 3086–3092.

[213] Vierle, M.; Zhang, Y.; Santos, A. M.; Köhler, K.; Haeßner, C.; Herdtweck, E.; Bohnenpoll, M.; Nuyken, O.; Kühn, F. E. *Chem. Eur. J.* **2004**, *10*, 6323–6332.

214 Tse, C. K. W.; Penciu, A.; McInenly, P. J.; Kumar, K. R.; Drewitt, M. J.; Baird, M. C. *Eur. Polym. J.* **2004**, *40*, 2653–2657.

215 Kumar, K. R.; Penciu, A.; Drewitt, M. J.; Baird, M. C. *J. Organomet. Chem.* **2004**, *689*, 2900–2904.

216 Garratt, S.; Carr, A. G.; Langstein, G.; Bochmann, M. *Macromolecules* **2003**, *36*, 4276–4287.

217 Perrin, L.; Bonnet, F.; Chenal, T.; Visseaux, M.; Maron, L. *Chem. Eur. J.* **2010**, *16*, 11376–11385.

218 Capacchione, C.; Saviello, D.; Avagliano, A.; Proto, A. *J. Polym. Sci. Part A* **2010**, *48*, 4200–4206.

219 Li, X.; Nishiura, M.; Hu, L.; Mori, K.; Hou, Z. *J. Am. Chem. Soc.* **2009**, *131*, 13870–13882.

220 Zhang, Z.; Cui, D.; Wang, B.; Liu, B.; Yang, Y. *Struct. Bond* **2010**, *137*, 49 – 108.

221 Friebe, L.; Nuyken, O.; Obrecht, W. *Adv. Polym. Sci.* **2006**, *204*, 1 – 154.

222 Yagci, Y.; Mishra, M. K. The Fundamentals. In *Handbook of Vinyl Polymers*, 2nd ed.; Mishra, M. K.; Yagci, Y., Eds.; Taylor & Francis Group, LLC: Boca Raton, FL, 2009.

223 Banik, S. M.; Monnot, B. L.; Weber, R. L.; Mahanthapa, M. K. *Macromolecules* **2011**, *44*, 7141–7148.

224 Hong, S. C. *Elastom. Comp.* **2009**, *44*, 55–62.

225 Greene, A. C.; Grubbs, R. B. *J. Polym. Sci. Part A* **2009**, *47*, 6342–6352.

226 Iovu, M. C.; Craley, R.; Jeffries-El, M.; Krankowski, A. B.; Zhang, R.; Kowalewski, T.; McCullough, R. D. *Macromolecules* **2007**, *40*, 4733–4735.

227 Grubbs, R. B.; Wegrzyn, J. K.; Xia, Q. *Chem. Commun.* **2005**, 80–82.

228 Miura, Y.; Miyake, K. *J. Polym. Sci. Part A* **2005**, *43*, 6153–6165.

229 Benoit, D.; Harth, E.; Fox, P.; Waymouth, R. M.; Hawker, C. J. *Macromolecules* **2000**, *33*, 363–370.

230 Georges, M. K.; Hamer, G. K.; Listigovers, N. A. *Macromolecules* **1998**, *31*, 9087–9087.

[231] Asandei, A. D.; Yu, H. S. Cu-Mediated Isoprene Polymerizations Initiated from Sulfonyl Halides. *Proceedings of the 241st ACS National Meeting*, Anaheim, CA, March 27–31, 2011.

[232] Bertrand, A.; Chen, S.; Souharce, G.; Ladabière, C.; Fleury, E.; Bernard, J. *Macromolecules* **2011**, *44*, 3694–3704.

[233] Bartels, J. W.; Cauët, S. I.; Billings, P. L.; Lin, L. Y.; Zhu, J.; Fidge, C.; Pochan, D. J.; Wooley, K. L. *Macromolecules* **2010**, *43*, 7128–7138.

[234] Chen, S.; Bertrand, A.; Chang, X.; Alcouffe, P.; Ladavière, C.; Gérard, J.-F.; Lortie, F.; Bernard, J. *Macromolecules* **2010**, *43*, 5981–5988.

[235] Bar-Nes, G.; Hall, R.; Sharma, V.; Gaborieau, M.; Lucas, D.; Castignolles, P.; Gilbert, R. G. *Eur. Polym. J.* **2009**, *45*, 3149–3163.

[236] Germack, D. S.; Wooley, K. L. *Macromol. Chem. Phys.* **2007**, *208*, 2481–2491.

[237] Jitchum, V.; Perrier, S. *Macromolecules* **2007**, *40*, 1408–1412.

[238] Germack, D. S.; Wooley, K. L. *J. Polym. Sci. Part A* **2007**, *45*, 4100–4108.

[239] Germack, D. S.; Harrisson, S.; Brown, G. O.; Wooley, K. L. *J. Polym. Sci. Part A* **2006**, *44*, 5218–5228.

[240] Cowie, J. M. G.; Cree, S. H. *J. Polym. Sci. Part A* **1989**, *27*, 2907–2924.

[241] Cowie, J. M. G.; Cree, S. H.; Ferguson, R. *J. Polym. Sci. Part A* **1990**, *28*, 515–524.

[242] Ajellal, N.; Thomas, C. M.; Carpentier, J.-F. *Polymer* **2008**, *49*, 4344–4349.

[243] Gaylord, N. G.; Tomono, T.; Mandal, B. M. *J. Polym. Sci. Polym. Chem.* **1976**, *14*, 1283–1285.

[244] Nanu, I.; Andrei, C. *J. Polym. Sci. Polym. Chem.* **1974**, *12*, 231–240.

[245] Lokaj, J.; Pivcová, H.; Krabák, F. *Macromol. Mater. Eng.* **1986**, *144*, 207–218.

[246] Lokaj, J.; Bílá, J. *Acta Polym.* **1992**, *43*, 54–57.

[247] Siadat, B.; Lenz, R. W. *J. Polym. Sci.: Polym. Chem. Ed.* **1980**, *18*, 3273–3287.

[248] Ebdon, J. R.; Gabbott, N. P. *Polymer* **1983**, *24*, 565 – 572.

[249] Bamford, C. H.; Han, X.-Z. *J. Chem. Soc., Faraday Trans. 1* **1982**, *78*, 869 – 879.

[250] Safa, K. D.; Nasirtabrizi, M. H.; Tofangdarzadeh, S. *Iran. Polym. J.* **2008**, *17*, 39–47.

Chapter 2

Reactive Compatibilization of Poly(L-lactide) and Conjugated Soybean Oil[i]

In this chapter, we discuss the reactive blending of end-functionalized poly(L-lactide) (PLLA) with conjugated soybean oil (CS). The end-functionalized PLLA was synthesized through the ring opening bulk polymerization of L-lactide using *N*-2-hydroxyethylmaleimide (HEMI) as the initiator and tin(II) 2-ethylhexanoate as the catalyst, giving HEMI-PLLA. We prepared CS from soybean oil and confirmed the Diels–Alder reaction between it and HEMI-PLLA in a series of small scale blends. Larger scale melt blends of HEMI-PLLA and CS were prepared in which HEMI-PLLA reacted with CS to high conversion — coupling the two immiscible components and forming compatibilizer. Blends of HEMI-PLLA and 5 wt % CS resulted in a greater than 17 fold increase in elongation to break compared to PLLA homopolymer and more than doubled the elongation to break compared to a 5 wt % CS blend with unreactive PLLA. Analysis of the blend morphology indicated that the in situ formation of the compatibilizer decreased the CS droplet diameter compared to unreactive binary blends and that an optimum droplet diameter exists for toughening PLLA with CS.

2.1 Introduction

As discussed in Chapter 1, PLLA has been blended with many different insoluble minor phases in an effort to rubber toughen with a majority of the components being derived from non-sustainable sources (i.e. petroleum). Consequently, few examples of a fully sustainable and tough PLLA blend exist. In an effort to develop a fully sustainable, tough PLLA, we investigated soybean oil (SO) as a blend partner for PLLA.

SO and its derivatives have been investigated as blending partners for polyesters similar to polylactide and polylactide itself. Poly(3-hydroxybutyrate-*co*-3-hydroxyvalerate) (PHBV) has been blended with both SO and epoxidized soybean oil (ESO).[1] SO proved to be immiscible with PHBV, and did not improve impact resistance without the addition of a compatibilizer. ESO plasticized the PHBV and resulted in an increase in toughness with a reduction in elastic modulus. The plasticization and subsequent increase of the elongation at break of polyester resin,[2] poly(L-lactide-*co*-polycaprolactone),[3] and poly(L-lactide)(PLLA)[4] by ESO have also been reported. Due to the immiscibility of SO and PLLA, a compatibilized SO/PLLA blend could possibly toughen polylactide without plasticization. Block copolymers of polylactide and polyisoprene have been used to affect the morphology of SO/PLLA blends, indicating that compatibilization of SO and PLLA is possible using preformed block copolymers.[5] Block copolymers have also been used to compatibilize blends of polymerized SO and PLLA.[6] These previous examples suggest that blends of SO and PLLA could be compatibilized under the correct conditions.

Though preformed block copolymers have been successful in compatibilizing blends (see Chapter 1), their use can be limiting. The preformed block copolymer must diffuse to the interface of the immiscible components to compatibilize the blend, which does not happen with 100% efficiency as some block copolymer is wasted in the formation of micelles. Additionally, a preformed block copolymer that adequately compatibilizes the materials may be difficult to synthesize. To address these concerns, reactive blending schemes have been developed to produce compatibilizers in situ.[7] The compatibilizers form at the interface of the immiscible components eliminating the need for them to diffuse and simplifying their synthesis.

Reactive blending strategies have been employed for polylactide through several general methods. The majority of the reported reactive blends of polylactide use its terminal hydroxyl to undergo the desired reaction as discussed in Chapter 1. Synthesizing polylactide with other end groups (end-functionalized polylactide) for reactive blending is an uncommon practice. To our knowledge, end-functionalized polylactide has not been used in a reactive melt blending scheme to couple two immiscible components. A miscible blend of end-functionalized poly(L-lactide) (PLLA) and poly(D-lactide) (PDLA) has been reactively coupled in a melt blend to produce block copolymers, suggesting that similar reactions are feasible for immiscible components in the melt.[8] More commonly, end-functionalized polylactide has been reacted with another polymer using solution chemistry.[9,10,11,12] Use of end-functionalized polylactide allows for flexibility in the reactions and polymers used in the melt blends. Our aim is to develop reactive end-functionalized polylactide that can be used in industrially relevant compounding strategies such as melt blending.

A reactive functional group of interest is maleimide, which has proven to be reactive towards several chemical groups: nitrones,[13] thiols,[9,14] conjugated dienes,[15,16] and amines.[17] For example, *N*-2-hydroxyethylmaleimide (HEMI) has been used as a hydroxyl-containing initiator for the ring opening polymerization of lactide, producing a maleimide functionalized polylactide (HEMI-PLLA). [9,10,17] While typical SO does not contain functional groups reactive towards maleimide (see Appendices A and B for attempts at HEMI-PLLA reactions with polyisoprene and SO), conjugated dienes can be catalytically produced on the fatty acid chains to create conjugated soybean oil (CS).[18,19]

We have explored the reaction between HEMI-PLLA and CS both in solution and in the melt to produce coupled products with varying architectures. Melt blends of CS and either HEMI-PLLA or PLLA were prepared in a twin screw mixer to form blended materials with improved tensile toughness. In the HEMI-PLLA blends, in situ formation of compatibilizer during mixing decreased the CS droplet size, which resulted in a further enhancement of the tensile toughness compared to corresponding parent PLLA blends. An optimum CS particle size for toughening of PLLA was determined. Collectively,

these results demonstrate that reactive compatibilization of PLLA and CS can lead to completely sustainable blends with enhanced toughness compared to the parent PLLA.

2.2 Experimental Details

2.2.1 Materials and General Methods

All chemicals were purchased from Aldrich and used without further purification unless otherwise stated. L-lactide (Purac) was purified through recrystallization in ethyl acetate and then dried under vacuum at room temperature. Dry toluene (HPLC grade) was purified by passing it through a home built solvent purification system with activated alumina column and a supported copper catalyst. Commercial grade poly(L-lactide) homopolymer (PLLA-49) was provided by the Toyota Motor Corporation. All other polymers were synthesized using the techniques given below. An overview of all polymers used can be found in Table 2.1.

^{1}H NMR spectroscopy was performed on a Varian Inova 500 MHz spectrometer in CDCl$_3$ unless otherwise noted. Size exclusion chromatography (SEC) was performed on an Agilent 1100 high-pressure liquid chromatograph at 35 °C equipped with a PLgel (Varian) 5 μm guard column followed by three PLgel columns with varying pore sizes with HPLC grade chloroform as the mobile phase. Molecular weights and polydispersity index (PDI) were measured by a Hewlett-Packard P1047A refractometer calibrated with polystyrene standards (Polymer Laboratories). Electrospray ionization–mass spectroscopy (ESI-MS) was performed on a BioTOF II (Bruker) spectrometer with methanol as the carrier solvent.

2.2.2 Synthesis of *N*-2-hydroxyethylmaleimide (HEMI)

Synthesis of 4,10-Dioxatricyclo[5.2.1.0^{2,6}]dec-8-ene-3,5-dione (Furan-A) intermediate: Furan (92.5 g) and maleic anhydride (100 g) were added to a round bottom flask with ethyl acetate (125 mL). The reaction mixture was stirred for 24 hrs at room temperature, after which a colorless crystal was removed via suction filtration and dried under vacuum. The product (Furan-A) was used without further purification (yield 87.6%). Furan-A synthesis confirmed by ^{1}H NMR spectroscopy.[20] ^{1}H-NMR (500 MHz, DMSO-*d$_6$*) *δ*: 6.573 (s, 2H, –CHC*H*=C*H*CH–), 5.343 (s, 2H, –C*H*CH=CHC*H*–), 3.305 (s,

2H, O=CC*H*). *Synthesis of 4-(2-Hydroxy-ethyl)-10-oxa-4-aza-tricyclo[5.2.1.0^{2,6}]-dec-8-ene-3,5-dione (HEMI-A) intermediate*: Furan-A (100 g) and ethanol (150 mL) were added to a round bottom flask with a stir bar. A solution of monoethanolamine (MEA) (37.4 mL) and ethanol (30 mL) was added drop wise to the Furan-A solution at a 1.03 molar excess of MEA to Furan-A. The resulting mixture was refluxed at 85 °C for 4 hrs, during which the solution turned a deep orange. After the reaction, the solution was cooled overnight and the crystallized product was removed via suction filtration. The collected crystals were dried under vacuum at room temperature. The yellow to colorless product (HEMI-A) was used without further purification (yield 49.3%). HEMI-A synthesis confirmed by ^{1}H NMR spectroscopy.20[20] ^{1}H-NMR (500 MHz, DMSO-d_6) δ: 6.549 (s, 2H, –CHC*H*=C*H*CH–), 5.121 (s, 2H, –C*H*CH=CHC*H*–), 4.798 (br, 1H, NCH$_2$CH$_2$O*H*), 3.412 (m, 4H, NC*H$_2$*C*H$_2$*OH), 2.926 (s, 2H, O=CC*H*). *Synthesis of 1-(2-Hydroxyethyl)-1H-pyrrole-2,5-dione (HEMI) from HEMI-A*: HEMI-A (2.5 g) and toluene (50 mL) were added to a 3-neck round bottom flask with a stir bar. The reactor was continuously purged with nitrogen while the solution was refluxed at 110 °C for 5 hrs. Upon cooling at 0 °C for 2 hrs, a white solid (HEMI) was collected through suction filtration and washed with petroleum ether (yield 81.5%). The product was further purified (>99% purity) via sublimation under vacuum at 75 °C. HEMI synthesis confirmed by ^{1}H NMR spectroscopy.[20] ^{1}H NMR (500 MHz, DMSO-d_6) δ: 7.009 (s, O=CC*H*=C*H*C=O), 4.786 (s, 1H, NCH$_2$CH$_2$O*H*), 3.452 (m, 4H, NC*H$_2$*C*H$_2$*OH); (500 MHz, CDCl$_3$) δ: 6.736 (s, O=CC*H*=C*H*C=O), 3.782 (t, J = 4.9 Hz, 2H, NC*H$_2$*CH$_2$OH), 3.723 (t, J = 4.8 Hz, 2H, NCH$_2$C*H$_2$*OH), 2.090 (br, 1H, NCH$_2$CH$_2$O*H*).

2.2.3 Synthesis of HEMI-PLLA using tin(II) 2-ethylhexoate [Sn(Oct)$_2$] as the catalyst

Purified L-lactide (10 g) was added to a dry 48 mL pressure vessel along with HEMI (1.410 g) and 0.1 wt % Sn(Oct)$_2$ (10 mg) in air. After addition of a magnetic stir bar, the vessel was sealed and placed in an oil bath at 130 °C. After 2 hrs the vessel was removed and cooled in an ice bath to quench the polymerization. The resulting solid was dissolved in CH$_2$Cl$_2$ and precipitated in 10X excess hexanes. The resulting polymer

suspension was centrifuged to collect the material. Upon drying under vacuum, a 1.1 kg/mol HEMI-PLLA (HEMI-PLLA-1) was recovered (96% lactide conversion, 90% HEMI-PLLA yield). HEMI-PLLA polymers with higher molecular weights and at larger scales were precipitated in 10X excess of methanol. HEMI-PLLA at 100 g scale was removed from the reaction vessel without dissolution and pressed into pellets before melt mixing. Additional molecular weights were achieved by varying the monomer to initiator molar ratio and the L-lactide conversion. See Table 2.1 for a summary of HEMI-PLLA polymers synthesized. ^{1}H NMR spectroscopy chemical shifts of HEMI-PLLA end-group protons (500 MHz, CDCl$_3$) δ 6.720 (s, –CH=CH–), 4.344 (m, HO–CH– and N–CH$_2$–CHH–O), 4.259 (m, N–CH$_2$–CHH–O), 3.788 (m, N–CH_2–CH$_2$–O), 2.671 (br, HO–CH–); ^{1}H NMR spectroscopy chemical shifts of HEMI-PLLA repeat unit protons (500 MHz, CDCl$_3$) δ 5.157 (q, J = 6.9 Hz, O–CH–CH$_3$), 1.576 (d, J = 7.8 MHz, O–CH–CH_3).

2.2.4 Synthesis of conjugated soybean oil (CS)

Following the procedure of Larock et al.,[18] Wesson soybean oil purchased from a local grocery store (23 g) was dissolved in 75 mL of benzene with 0.5 mol % RuHCl(CO)(PPh$_3$)$_3$ (0.39 g) in an air free flask. The solution was degassed and heated at 60 °C for 48 hrs under an argon atmosphere. After cooling, the benzene was removed by evaporation and the crude product dried under vacuum at 35 °C. The crude product was then dissolved in CH$_2$Cl$_2$ (200 mL) in a nitrogen dry box and P(CH$_2$OH)$_3$ (0.5 g) was then added. The solution was stirred for 48 hrs at room temperature at which point the mixture was passed through a silica gel column with 1.5 L CH$_2$Cl$_2$ to remove the catalyst.[21] The solvent was removed by rotary evaporation and dried under vacuum to collect CS (89.7% yield). Conjugation of bis-allylic double bonds was 96%. ^{1}H NMR spectroscopy (500 MHz, CDCl$_3$) δ 6.286 (m, 0.4 H, *Z*- =CH–CH=CH–), 5.974 (m, 1.9 H, *E*- =CH–CH=CH–), 5.654 (m, 0.4 H, *Z,E*- =CH–CH=CH–), 5.552 (m, 1.6 H, *E,E*- =CH–CH=CH–), 5.376 (m, 3.6 H, *Z*- =CH–CH=CH– and =CH–), 5.261 (m, 1 H, OCH$_2$CHCH$_2$O), 4.289 (dd, J = 11.8 Hz, J = 5.0 Hz, 2 H, OCH$_a$$H_b$CHCH$_a$$H_b$O), 4.14 (dd, J = 12.7 Hz, J = 5.8 Hz, 2 H, OCH_aH$_b$CHCH_aH$_b$O), 2.305 (t, J = 7.9 Hz, 6 H,

CH_2C=O), 2.20-1.90 (m, 12H, =CHCH_2), 1.602 (s, 6.6 H, CH_2CH=O), 1.40-1.20 (br m, 52.8 H, CH$_2$), 0.877 (t, J = 6.9 Hz, 9H, CH$_2$CH_3).

2.2.5 Synthesis of 1-(2-(trimethylsilyloxy)ethyl)-1H-pyrrole-2,5-dione (TMSOEMI)

Using a modified procedure from Ahn et al.,[22] HEMI (2.00 g) was dissolved in 350 mL of THF (dried over molecular sieves) in air. Once HEMI was in solution, one molar equivalent of Et$_3$N (1.98 mL) was added to the flask and allowed to activate. After 1 hr, 1.2 molar equivalents of TMSCl (2.17 mL) were added to the vessel upon which a white precipitate formed. After 4 hrs, the reaction mixture was passed through an alumina plug. Solvent was removed by rotary evaporation and the solid was dried under vacuum. The resulting solid was purified by sublimation (vacuum, 40 °C) to produce pure TMSOEMI (57% yield). ^{1}H NMR (500 MHz, CDCl$_3$): δ: 6.701 (s, 2H), 3.708 (t, 2H, J = 6.5 Hz), 3.661 (t, 2H, J = 5.3 Hz), 0.066 (s, 9H).

2.2.6 Model blend of TMSOEMI and the methyl ester of conjugated linoleic acid (CLAME)

To a 2-neck round bottom flask, TMSOEMI (132 mg) was dissolved in toluene (1 mL) with CLAME (100 μL) to give a 2 molar excess of TMSOEMI. The contents were refluxed (110 °C) for 21 hr and product was collected by removing the solvent under vacuum. The products were purified using flash column chromatography using silica gel as the stationary phase and a 5:2 hexanes:ethyl acetate mobile phase. The TMSOEMI coupled to CLAME came off the column at an R$_f$ = 0.6. Fractions containing only the TMSOEMI and CLAME product were combined and concentrated by rotoevaporation to give the final purified product. The final product was then dried under vacuum over night. The purified reaction products were analyzed by ^{1}H NMR spectroscopy and ESI-MS.

2.2.7 Synthesis of exploratory small scale reactive blends of CS and HEMI-PLLA

CS and HEMI-PLLA were blended in both solution and the melt. As an example solution blend, HEMI-PLLA (350 mg) was dissolved in 3 mL of dry toluene in a 10 mL round bottom flask with a magnetic stir bar. CS (200 mg) was added to the solution

which was placed in an oil bath at 110 °C to reflux for 18 hrs. Melt blends were performed as follows. HEMI-PLLA and CS were added to a glass test tube in the same proportions as in the solution blend. The glass test tube was lowered into an oil bath at 190 °C and an overhead mechanical stirrer was used to mix the components for 10 min after which the test tube was removed from the oil bath. Upon cooling in ice water, the reaction mixtures (both solution and melt) were analyzed by ^{1}H NMR spectroscopy and SEC. The concentration ratios of conjugated dienes to HEMI-PLLA ([C=C-C=C]/[HEMI]) initially present in blends were calculated by using the molecular weights of CS (872 g/mol) and the HEMI-PLLA polymers, the average number of conjugated dienes per molecule of CS (1.2, as determined by ^{1}H NMR spectroscopy), and the known mass of each component. Control blends were synthesized by heating the individual components following the protocols described above. ^{1}H NMR spectra and SEC of the heated components were compared against the original material. Analysis of the ^{1}H NMR spectra for the control blends indicated that the maximum error for the measured conversions was ±8%, which was determined by comparing the original spectra of the homopolymers and CS to their spectra after heating.

2.2.8 Synthesis melt blends of HEMI-PLLA-67 and PLLA-49 with CS

All larger scale blends were made in a twin screw batch mixer (DACA Instruments) at 190 °C and 100 RPM screw speed. Prior to mixing, HEMI-PLLA and PLLA were dried overnight at 60 °C to remove moisture and CS was heated slightly above room temperature so that it would be a liquid and easier to work with. To the 190 °C mixer, the matrix polymer was added first and allowed to mix for 5 min prior to the addition of CS, allowing for complete melting of the polymer. CS was added drop wise to the mixer at the desired ratio (total blend mass of 4 g) over 1 min of mixing. After the polymer and CS were compounded for 10 minutes, the blend was collected from the mixer. The blends were cooled in liquid nitrogen upon being removed from the mixer and were stored in a negative 20 °C freezer until the samples could be further processed.

2.2.9 Characterization of melt blends of HEMI-PLLA-67 and PLLA-49 with CS

Blends were analyzed by SEC and ^{1}H NMR spectroscopy. In addition, the blends were compression molded at 190 °C for 5 min into "dog bone" tensile bars (gap dimensions, 15 mm X 3 mm X 0.4 mm) and cooled to room temperature in the press. It should be noted that though the bar dimensions do not follow any testing standard, literature values for the mechanical properties of PLLA were obtained.[23] A minimum of 3 bars were tested for each blend on a Rheometrics Instruments MINIMAT tensile tester at a cross head speed of 10 mm/min. Differential scanning calorimetry was performed on the blends after tensile testing. A sample of tensile bar (5-10 mg) was placed in a standard aluminum pan and was analyzed on a Texas Instruments TA Q1000 instrument with a scan rate of 10 °C/min from 0 °C to 220 °C. Blend T_g and crystallinity were determined from the initial heating curve. The heat of fusion used for an infinite crystal of PLLA was 94 J/g.[24]

Scanning electron microscopy images for particle analysis were taken on JEOL 6500 and 6700 microscopes. Samples were taken from the middle section of a piece of extrudate from the mixer. Prior to imaging, the surface of each sample was polished by cryo-microtomy (Reichert Ultracut S) with a glass knife at -120 °C to provide a smooth surface for image analysis. The microtomed surfaces were coated with 5-10 nm of Pt via sputtering and imaged at a 5.0 kV acceleration voltage. Microtomy of the samples resulted in the CS being pulled from the matrix, creating dark holes that were used for particle analysis. Image analysis was performed with ImageJ software to calculate the area of each CS particle. The area of the particle was used to calculate the diameter of the equivalent circle. A log-mean diameter (d_{lm}) and distribution parameter (σ_{lm}), a measure of the dispersion of the particle diameters, were calculated.[25] The matrix ligament thickness (MLT) was calculated using Equation 1:

$$MLT = d_{lm}\left[\left(\frac{\pi}{6\phi}\right)^{1/3}\exp(1.5\ln^2\sigma_{lm}) - \exp(0.5\ln^2\sigma_{lm})\right] \tag{1}$$

where ϕ is the volume fraction of CS incorporated into the blend (found by ^{1}H NMR spectroscopy).[25]

2.3 Results and Discussion

2.3.1 HEMI Synthesis

N-2-Hydroxyethylmaleimide (HEMI) was synthesized by adapting the procedure of Heath et al.[20] The synthesis consists of three reactions (Figure 2.1): Diels–Alder between furan and maleic anhydride to give Furan-A, nucleophilic ring-opening and subsequent ring closing of monoethanolamine reacting with Furan-A to give HEMI-A, and retro Diels–Alder to give HEMI. Our major contribution towards the improvement of HEMI synthesis was including a final sublimation step to give highly pure HEMI. See (Figure 2.2) for ^{1}H NMR spectra of HEMI and its intermediates.
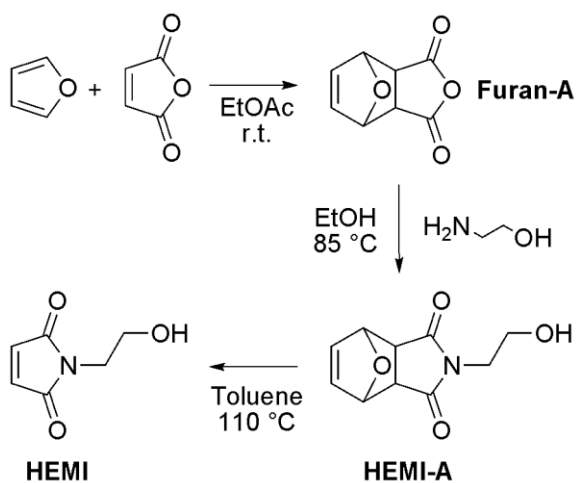
Figure 2.1. HEMI synthesis scheme starting with maleic anhydride.
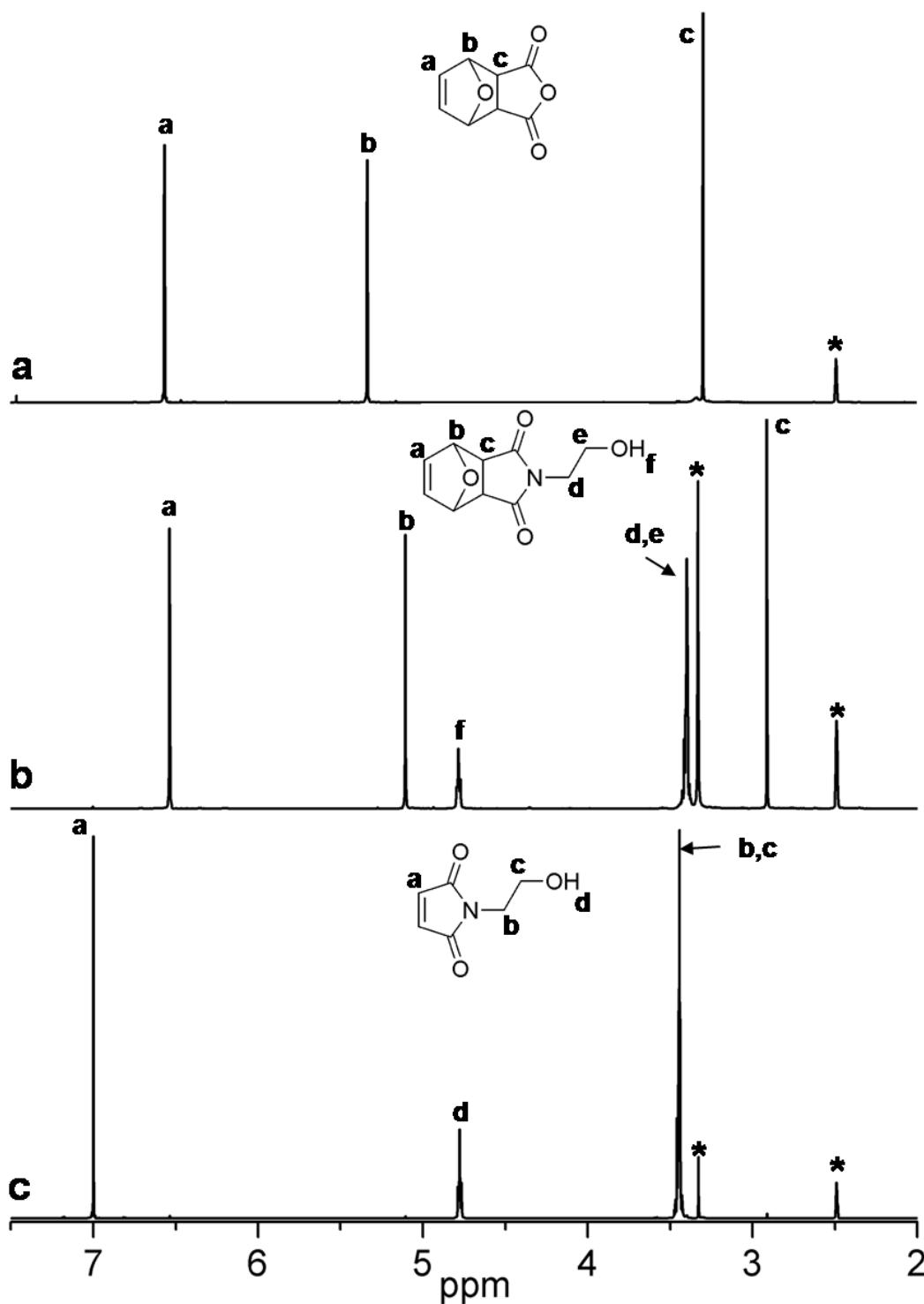
Figure 2.2. ^{1}H NMR spectra and assignments of (a) Furan-A, (b) HEMI-A, and (c) HEMI (500 MHz, DMSO-d_6). Asterisks (*) indicate chemical shifts due to solvent (DMSO-d_6) and residual water in the NMR solvent.

2.3.2 HEMI-PLLA synthesis

HEMI-PLLA was synthesized using HEMI as an initiator for the melt ring-opening polymerization of L-lactide (Figure 2.3) with tin(II) 2-ethylhexanoate ($Sn(Oct)_2$) as the catalyst. The monomer to initiator ratio as well as the polymerization times were varied to achieve a wide range of molecular weights. In Figure 2.4 the measured number average molecular weight (M_n) of HEMI-PLLA is plotted against the expected M_n as calculated from the monomer to initiator ratio and overall conversion of monomer. A linear fit of the data gives a slope close to one and an intercept of zero – indicative of a controlled polymerization. Variation of the measured M_n compared to the expected M_n at higher molecular weights may be due to increased error from end-group analysis when integrating the smaller end-group peaks in ^{1}H NMR spectra.
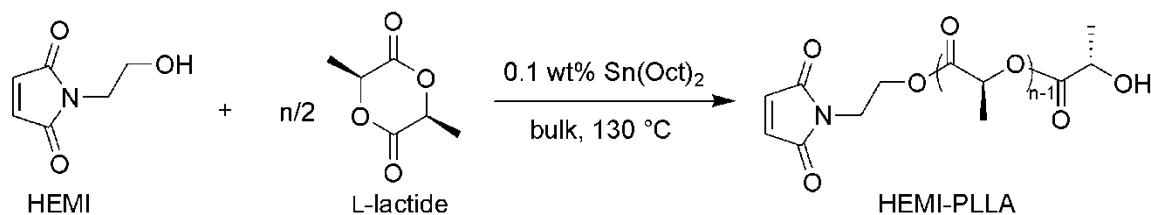
Figure 2.3. Synthesis scheme of the ring opening polymerization of L-lactide using HEMI as the hydroxyl initiator to give HEMI-PLLA. $Sn(Oct)_2$ is used as the catalyst at 0.1 wt % loading as compared to L-lactide monomer.
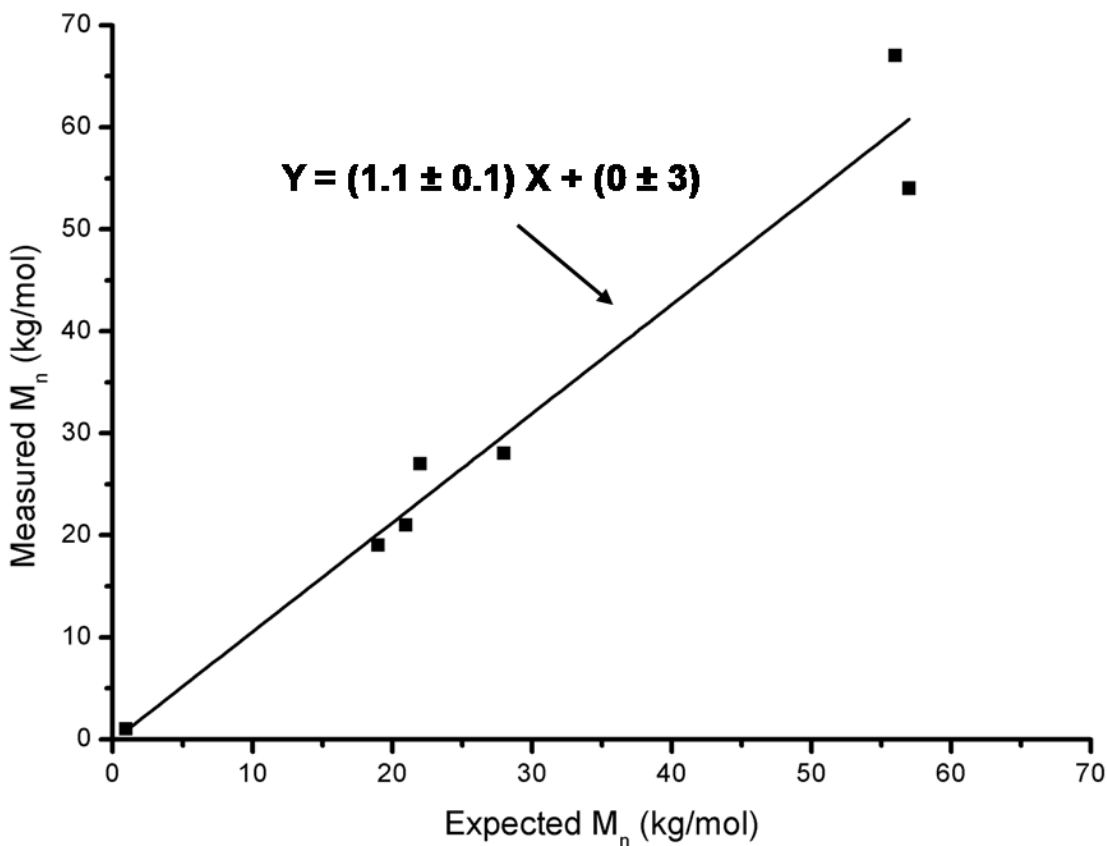
Figure 2.4. Measured M_n for HEMI-PLLA plotted against expected M_n for HEMI-PLLA. Expected M_n was calculated using the fed monomer to initiator ratio and overall conversion of L-lactide monomer. Measured M_n was calculated by ^{1}H NMR end-group analysis of the precipitated polymers. Line is linear fit using least squares method. Error of slope and intercept are the standard error of the fit.

Three samples of HEMI-PLLA were prepared for blending using different monomer to initiator ratios to control the average molar mass (Table 2.1). The polydispersity index (PDI) values of HEMI-PLLA samples were less than 1.25 at conversions greater than 90%, and lower PDI values were achieved at lower conversions (ca. 80%). Broadening of the molar mass distribution at higher monomer conversions is likely due to transesterfication reactions or depropagation – both are enhanced near the equilibrium monomer concentration.[26,27]

Table 2.1:Summary of PLLA and HEMI-PLLA homopolymers used in blends

Sample code	$M_n{}^a$ (kg/mol)	$M_w{}^b$ (kg/mol)	PDI[b]
PLLA-49[c]	49	138	1.85
HEMI-PLLA-1	1.1	2.0	1.24
HEMI-PLLA-20	20	37	1.05
HEMI-PLLA-67	67	129	1.24

[a]Determined using ^{1}H NMR spectroscopy end-group analysis. [b]Determined from SEC using polystyrene standards. [c]Obtained from Toyota Motor Corporation.

Comparison of the ^{1}H NMR spectra of HEMI (Figure 2.5a) and precipitated HEMI-PLLA-1 (Figure 2.5b) indicate high initiation efficiencies. Resonances associated with protons in HEMI attached to PLLA shifted relative to free HEMI. Furthermore, the ^{1}H NMR spectrum of HEMI-PLLA agrees with that of previous syntheses using other catalysts.[14,17] We successfully carried out the HEMI-PLLA synthesis on a 100 g scale outside of a dry box.
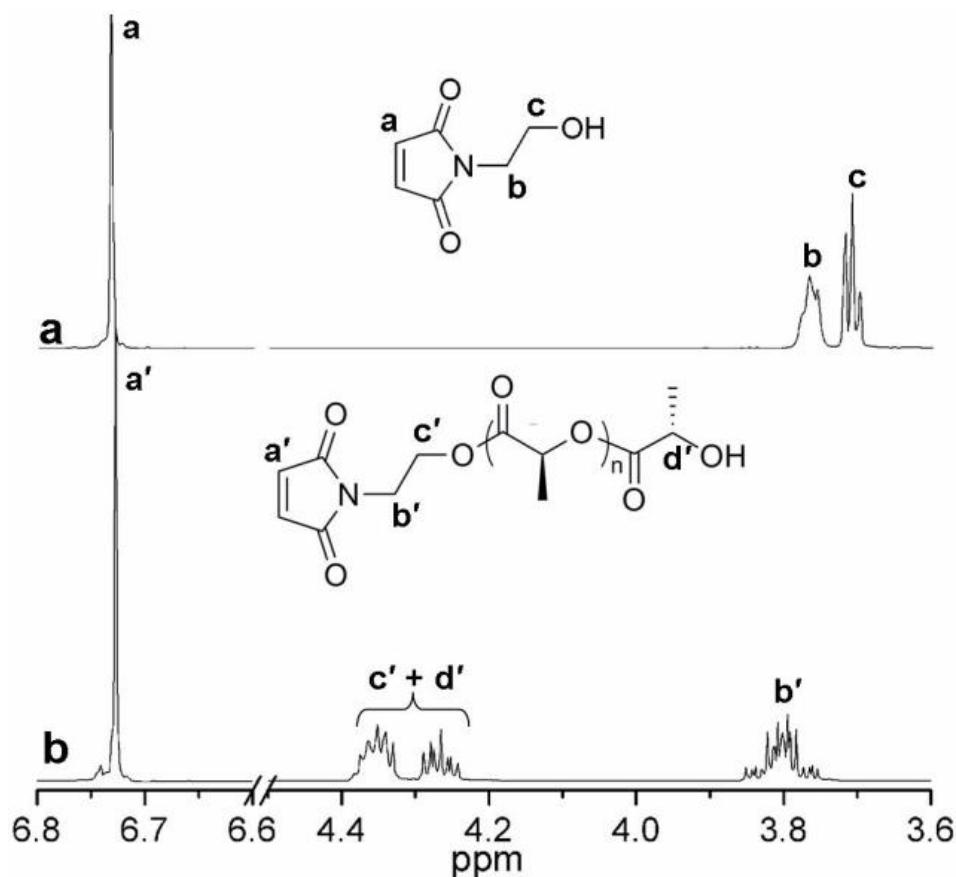
Figure 2.5. Expanded ^{1}H NMR (500 MHz, CDCl$_3$) spectra of (a) HEMI and (b) HEMI-PLLA-1. Synthesis of HEMI-PLLA shifts the peak locations of protons on the HEMI end-group.

2.3.3 Synthesis of conjugated soy (CS)

CS was prepared following the procedure of Larock et al. (Figure 2.6).[18] Both linoleic and linolenic fatty acid residues in soybean oil (SO) contain disubstituted olefins in the *Z* configuration separated by one (bis-allylic) carbon atom. Analysis of the ^{1}H NMR spectrum of SO (Figure 2.7) indicates that 4.1 carbon-carbon double bonds exist per SO molecule with 3.8 of these bonds per SO molecule separated by a bis-allylic carbon. Isomerization of these isolated olefins by RuHCl(CO)(PPh$_3$)$_3$ gives dienes amendable to the Diels–Alder coupling with the HEMI group. After reaction of SO with RuHCl(CO)(PPh$_3$)$_3$, ^{1}H NMR spectroscopic analysis of the product indicated that 96% of the bis-allylic carbons were absent, indicating effective isomerization (Figure 2.8). Due to

the isomerization mechanism, in the product diene a mixture of *E* and *Z* isomers are produced.[19] In our case, 64% of the conjugated dienes adopted the *E,E* configuration with the balance being *Z,E* and *E,Z* isomers as determined by ^{1}H NMR spectroscopy (Figure 2.8).
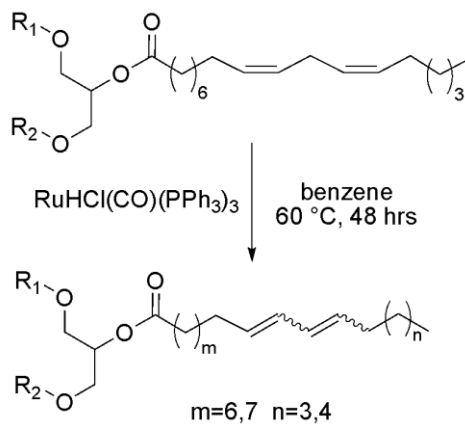
Figure 2.6. Reaction scheme for the conjugation of linoleic fatty acid residue in soybean oil. R_1 and R_2 represent the other fatty acid residues of the triglyceride, which may contain other conjugated chains in CS. Linolenic acid residues will undergo a similar conjugation.
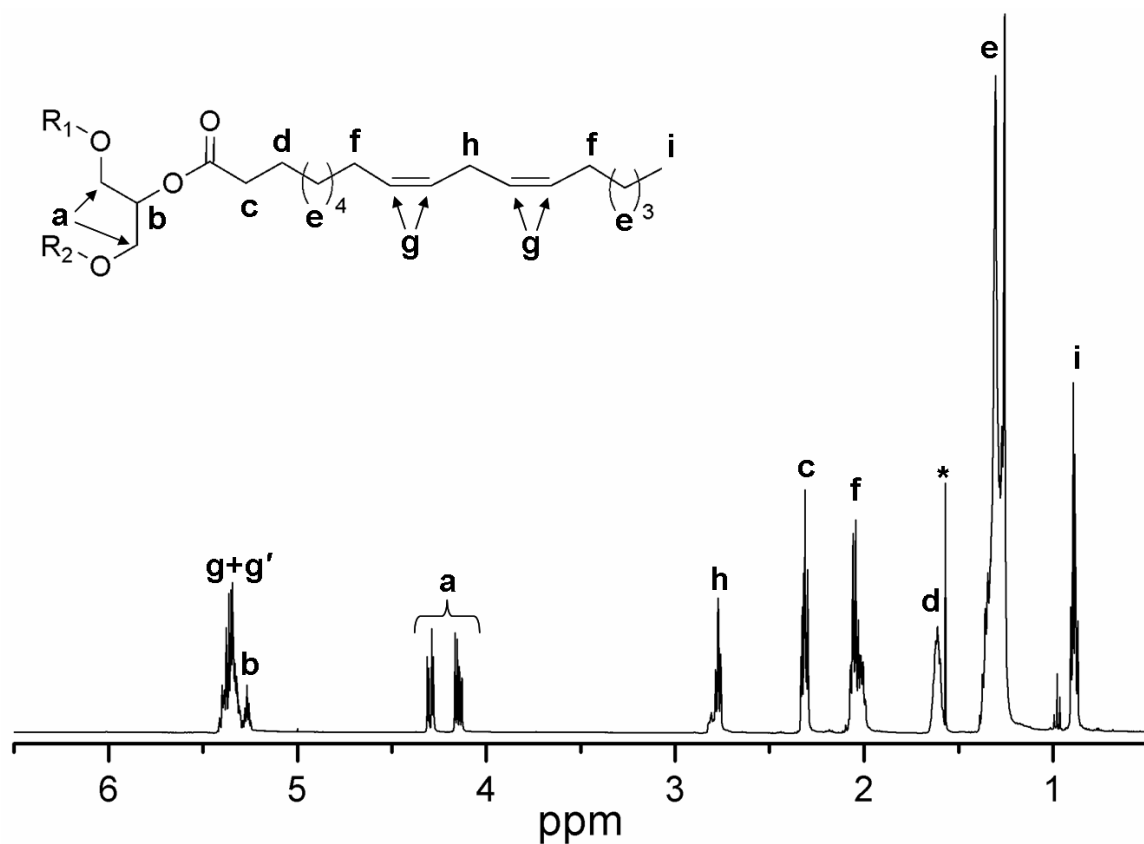
Figure 2.7. ^{1}H NMR spectrum with assignments for soybean oil (500 MHz, CDCl$_3$). Assignments are given for the linoleic acid residue in soybean oil triglyceride. R$_1$ and R$_2$ are any of the possible soybean fatty acid residues.[19] Assignment g′ designates olefinic protons of the remaining unsaturated fatty acid residues present in soybean oil. Asterisk (*) denotes H$_2$O present in solvent.
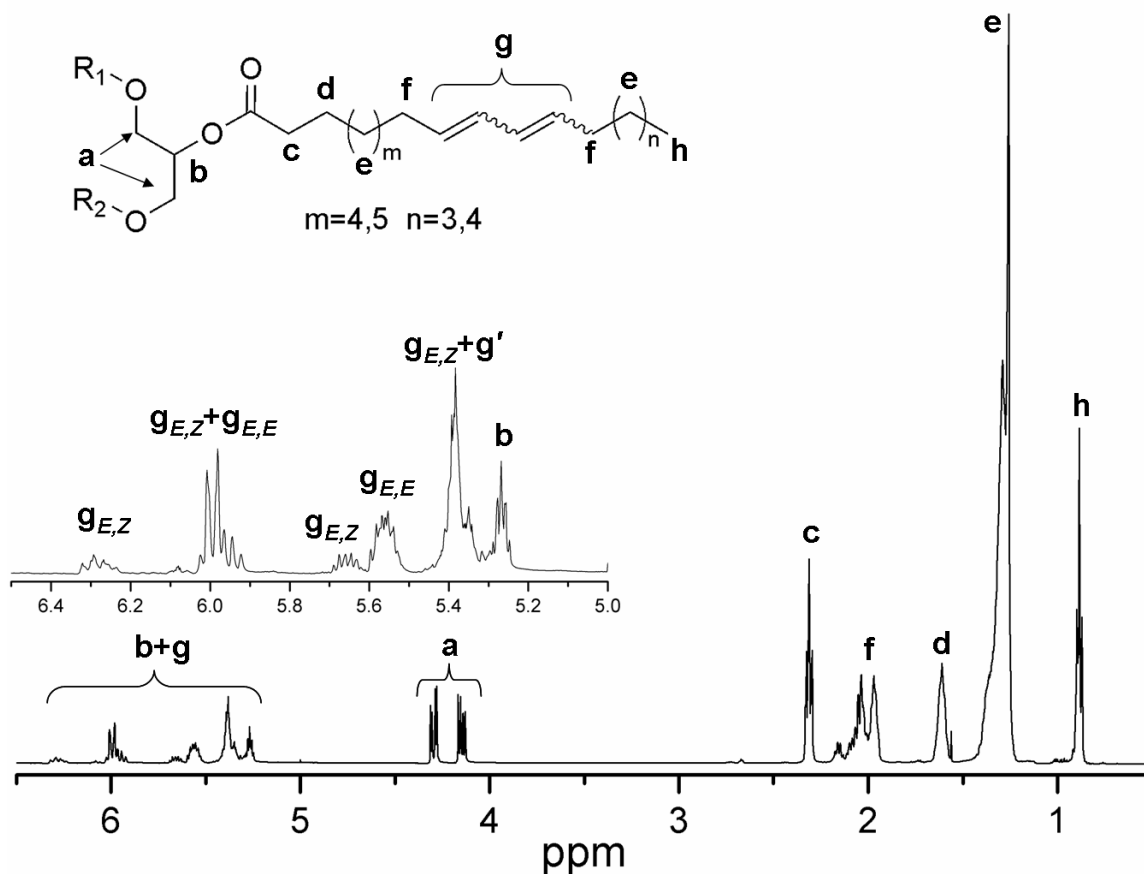
Figure 2.8. ^{1}H NMR spectrum and expanded region with assignments of conjugated soybean oil (CS) (500 MHz, CDCl$_3$). Assignments made for conjugated linoleic acid residue in CS. Conjugated stereoisomers are produced: *9Z,11E* (*10E,12Z*) and *E,E* during the conjugation of soybean oil. Peak assignments are made for the olefinic protons of each isomer.[19] Assignment g′ designates olefinic protons of the remaining unsaturated fatty acids residues in soybean oil.

2.3.4 Model reactions for structure elucidation

With both HEMI-PLLA and CS synthesized, model blends of analogous small molecules were synthesized to characterize the possible Diels–Alder reaction products. The methyl ester of conjugated linoleic acid (CLAME) was used as the CS analog (Figure 2.9). CLAME contains the three possible conjugated diene stereoisomers as evidenced by its ^{1}H NMR spectrum (Figure 2.9). The majority (83 mol %) of the conjugated dienes have the *E,Z* (or *Z,E*) configuration, while *E,E* and the *Z,Z* isomers account for 8 and 9 mol %, respectively. The stereoisomer composition of CLAME

differs significantly from that of CS, but all isomers are present, allowing for Diels–Alder reaction products between each isomer to be identified. To create a HEMI-PLLA analog, the hydroxyl group of HEMI was protected with trimethyl silane (TMSOEMI) to prevent possible alcohol-ester reactions between HEMI and CLAME when heating. We synthesized TMSOEMI following a modified procedure of Ahn *et al.*,[22] giving highly pure material as evidenced by ^{1}H NMR spectroscopy (Figure 2.10).
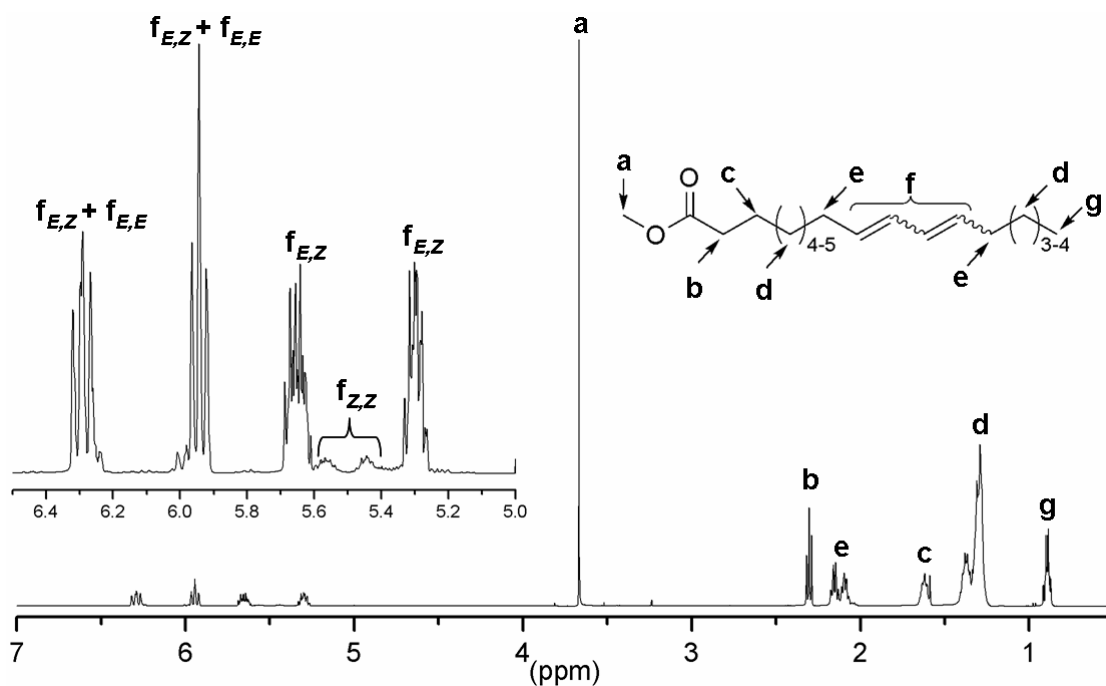
Figure 2.9. ^{1}H NMR spectrum with expanded region for CLAME, including peak assignments (500 MHz, CDCl₃). Peaks associated with the different conjugated diene stereoisomers are labeled with the corresponding subscript.
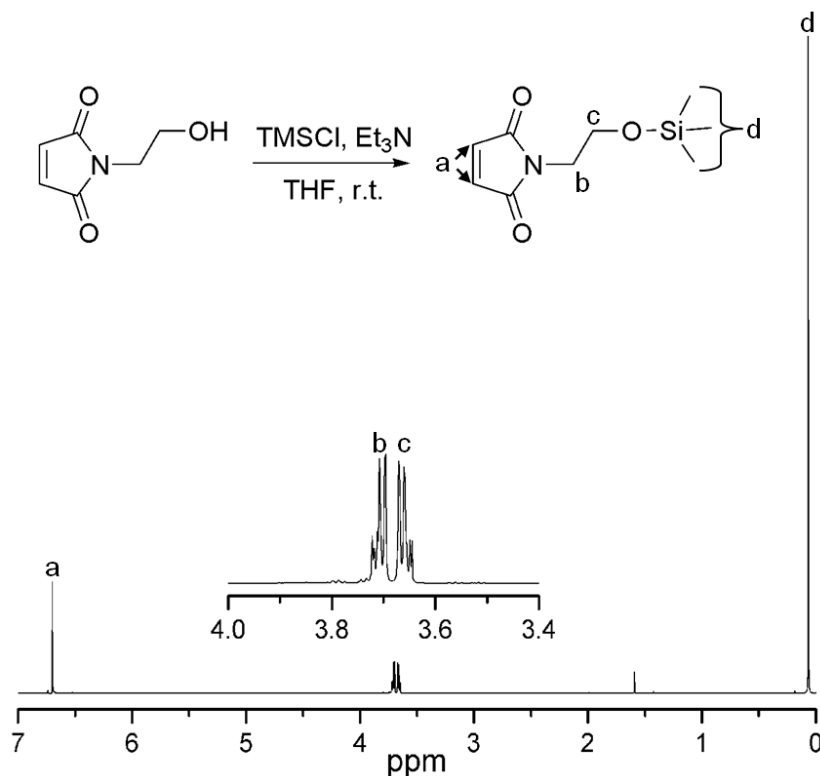
Figure 2.10. Synthesis scheme and ^{1}H NMR spectrum with expanded region for TMSOEMI (500 MHz, CDCl$_3$). Peak at 1.56 ppm belongs to water in the CDCl$_3$ NMR solvent.

As a model reaction, a blend of 2 molar excess TMSOEMI to CLAME was dissolved in toluene and refluxed overnight. Analysis of the product by electrospray ionization mass spectroscopy (ESI-MS) (Figure 2.11) indicates that the product contains material with a mass equivalent to one TMSOEMI molecule adding to one CLAME molecule (with a sodium cation), consistent with a Diels–Alder mechanism. ^{1}H NMR spectroscopic analysis of the purified reaction product (Figure 2.12) further supports the coupling of TMSOEMI and CLAME by a Diels–Alder mechanism. As a result of the TMSOEMI reacting with the different diene isomers, the reaction gives two diastereomers. When TMSOEMI reacts with the symmetric *E,E* and *Z,Z* isomers, equivalent protons occur on both sides of the ring, giving three peaks in ^{1}H NMR spectroscopy corresponding to the six protons of the ring.[28] Conversely, when TMSOEMI reacts with the *E,Z* or *Z,E* isomer of CLAME, the reaction site is asymmetric,

resulting in each proton of the six member ring being in a different electronic environment as evidenced by the six peaks for the six protons of the ring. With the above spectroscopic analysis, we can apply it to blends of HEMI-PLLA and CS to characterize the reactivity of HEMI-PLLA to the different isomers of CS.
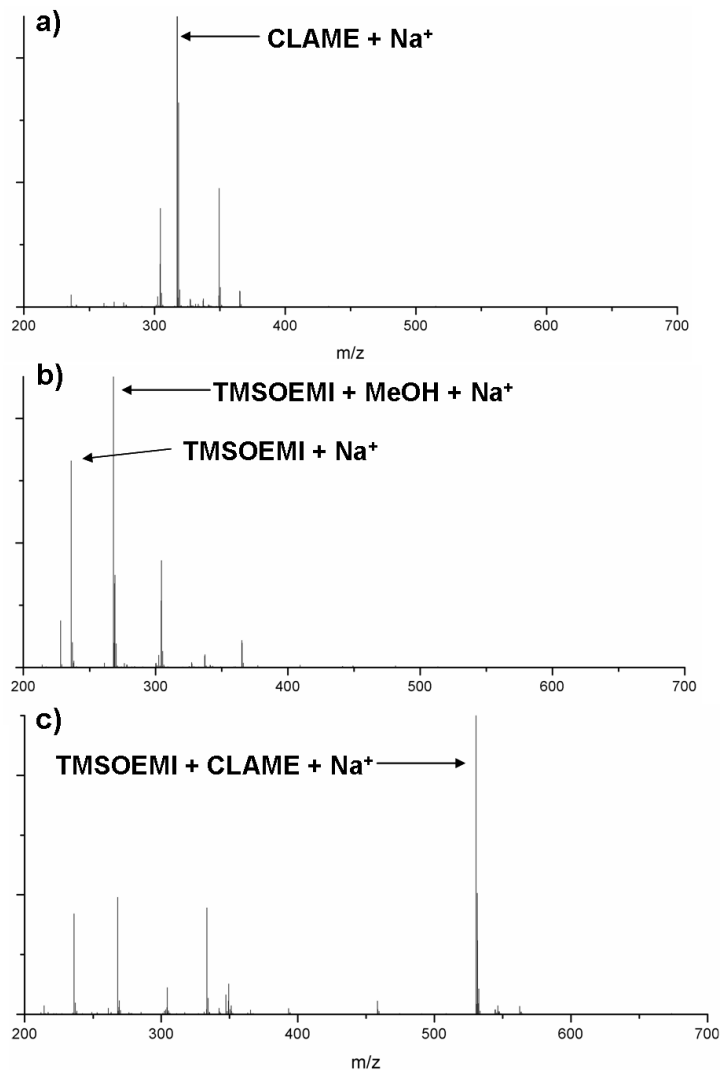
Figure 2.11. Low resolution ESI-MS spectra of (a) CLAME, (b) TMSOEMI, and (c) the reaction product of TMSOEMI and CLAME. In spectrum (a) the peak that corresponds to CLAME + Na$^+$ occurs at 317.4 m/z (317.5 calculated theoretical). In spectrum (b) two peaks are observed, the expected for TMSOEMI + Na$^+$ at 236.2 m/z (236.3 calculated theoretical) and a peak at 268.2 m/z that appears to correspond to TMSOEMI + MeOH + Na$^+$ (268.3 calculated theoretical). In spectrum (c), the starting materials are observed along with an apparent reaction product at 530.6 m/z that corresponds to TMSOEMI + CLAME + Na$^+$ (530.7 calculated).
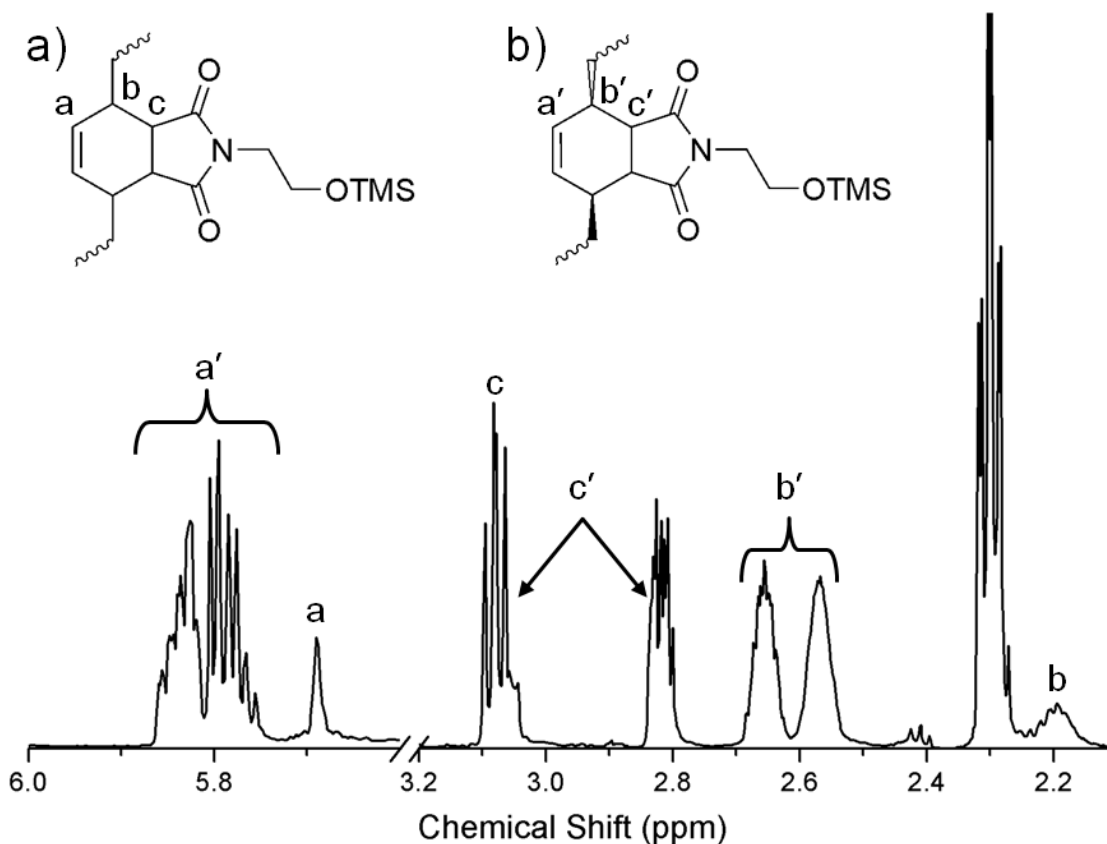
Figure 2.12. Expanded ^{1}H NMR spectrum of the purified reaction product of CLAME and TMSOEMI reaction (500 MHz, CDCl₃). Peak assignments are given for TMSOEMI reacting with the (a) *E,E* and *Z,Z* isomers and the (b) *E,Z* (or *Z,E*) isomers. Product (b) results in protons with different axial or equatorial positions leading to separate peaks for each proton in the six member ring, resulting in two peaks for each proton labeled.

2.3.5 Exploratory small scale reactive blends

Small scale blends of CS and HEMI-PLLA were prepared to explore the reactivity of HEMI-PLLA towards CS under both melt and solution (toluene) conditions. The composition and resulting conversion of the reactive species for these blends are given in Table 2.2. HEMI-PLLA-1 blends were prepared using an approximately 1:1 molar ratio of HEMI-PLLA to CS, while HEMI-PLLA-20 blends were synthesized using an excess of CS. Using ^{1}H NMR spectroscopy, conversions of the *E,E* ($X_{E,E}$) and *E,Z* (includes *Z,E*) isomers ($X_{E,Z}$) of CS were monitored along with the conversion of the HEMI end-group of HEMI-PLLA (X_{HP}). In all blends, $X_{E,E}$ of CS was greater than that of

$X_{E,Z}$ consistent with decreased steric hindrance of the *E,E* isomer reaction site as compared to the *E,Z* (and *Z,E*) isomers as is typical for Diels–Alder reactions.

Table 2.2: Composition of Small scale HEMI-PLLA and CS Blends.

HEMI-PLLA	conditions[a]	[C=C-C=C]/[HEMI][b]	$X_{E,E}$ (%)[c]	$X_{E,Z}$ (%)[d]	X_{HP} (%)[e]
HEMI-PLLA-1	toluene	0.93	100	30	70
HEMI-PLLA-1	melt	0.89	100	38	94
HEMI-PLLA-20	toluene	15	21	10	100
HEMI-PLLA-20	melt	17	22	17	82

[a]Blends in toluene were synthesized at 110 °C, melt blends were prepared at 190 °C [b]Molar ratio of conjugated double bonds to HEMI end-groups in each blend (see Experimental Details) [c]Conversion of all *E,E* isomers of CS, by ^{1}H NMR spectroscopy [d]Conversion of all *E,Z* and *Z,E* isomers of CS, by ^{1}H NMR spectroscopy [e]Conversion of HEMI end-groups of HEMI-PLLA, by ^{1}H NMR spectroscopy. All calculated conversions have an error of ± 8% (see Experimental Details).

The ^{1}H NMR spectrum of the product (Figure 2.13a) is consistent with the Diels–Alder reaction product of the *E,E* isomer of CS and HEMI-PLLA (Figure 2.14) as peaks formed and decreased in intensity as compared to the starting components (Figure 2.13b and c). The majority of HEMI-PLLA reacted with *E,E* isomer of CS and likely is due to its reaction site being less hindered than the *E,Z* isomer (Figure 2.14). Even though the *E,Z* isomers of CS are more hindered, they still react (Table 2.2), though to a lesser extent. Unfortunately, resonances associated with the Diels–Alder adduct with the *E,Z* isomer were not observed, presumably due to the smaller percentage of the *E,Z* isomers initially present and their reduced conversion.
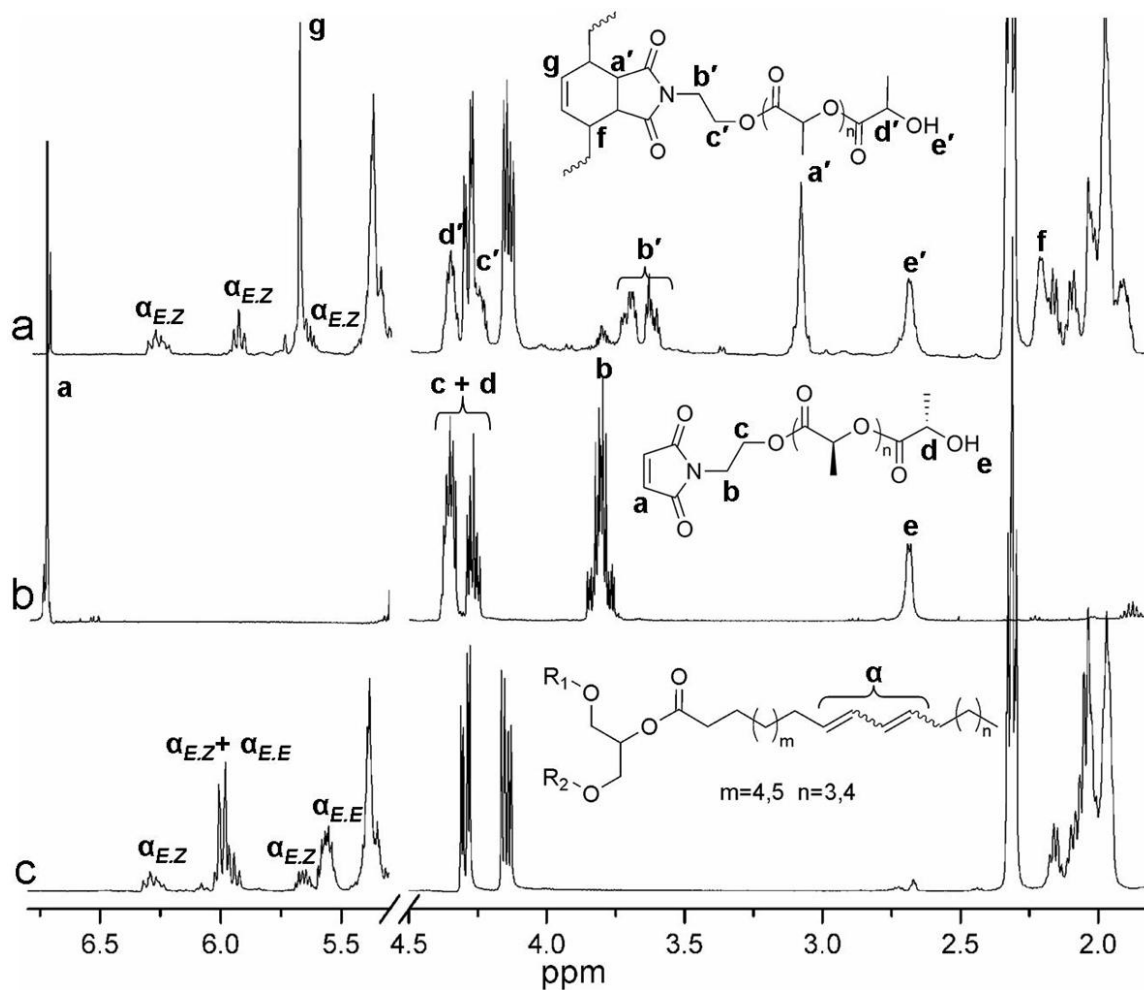
Figure 2.13. Assigned and expanded ^{1}H NMR spectra of (a) reaction product of HEMI-PLLA-1 and CS, (b) HEMI-PLLA-1, and (c) CS (500 MHz, CDCl$_3$). The formation of new peaks observed in (a) indicate that HEMI-PLLA-1 reacted with CS. Peak assignments indicate that HEMI-PLLA predominately reacts with the *E,E* isomers of CS. ^{1}H NMR spectra of other blends of HEMI-PLLA and CS show peaks at the same chemical shifts.
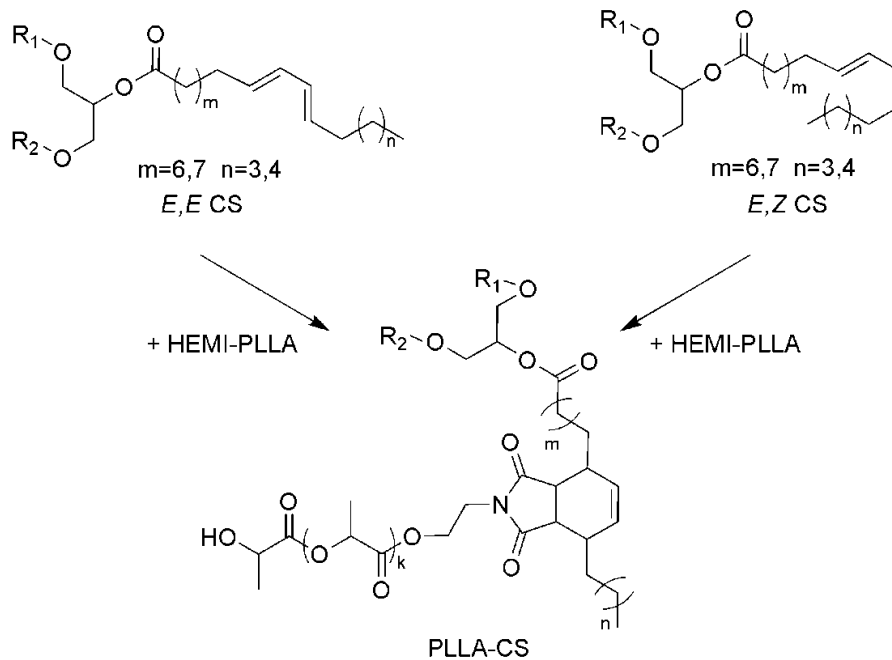
Figure 2.14. Diels–Alder reaction product of CS and HEMI-PLLA. Both isomers of CS (*E,E* and *E,Z*) are shown in the correct conformation for a Diels–Alder reaction with the *E,Z* isomer the more hindered of the two. The maleimide functionality of HEMI-PLLA reacts with the conjugated diene of CS by a Diels–Alder reaction mechanism to produce a PLLA grafted CS (PLLA-CS).

SEC data for the reactive blends with HEMI-PLLA-1 (Figure 2.15a) corroborate the reaction of HEMI-PLLA-1 with CS in both solution and the melt as evidenced by the shift of the products to lower elution volumes as compared to HEMI-PLLA-1. For the HEMI-PLLA-20 blends with CS (Figure 2.15b), the shifts in elution volume are not surprisingly less pronounced. Removal of the free CS by preparatory GPC indicates the presence of CS in the high molecular weight region of the HEMI-PLLA-20 blend, confirming the reaction between HEMI-PLLA and CS. Interestingly, the melt blend of HEMI-PLLA-20 resulted in an SEC elution curve with several distinct peaks at apparent molar masses that are two (PLLA-CS-PLLA) and three (3-arm star-PLLA) times that of the HEMI-PLLA-20. The formation of these higher molecular weight products suggests that multiple reactions of HEMI-PLLA can occur with one CS molecule. Each of the three fatty acid residues in CS can contain conjugated double bonds, and the multiple additions of HEMI-PLLA to CS are likely responsible for the additional products

observed in the SEC trace.[29] Heating either HEMI-PLLA-1 or HEMI-PLLA-20 without CS does not alter its SEC elution curve, confirming that the higher molecular weight products were not a result of HEMI-PLLA self coupling.
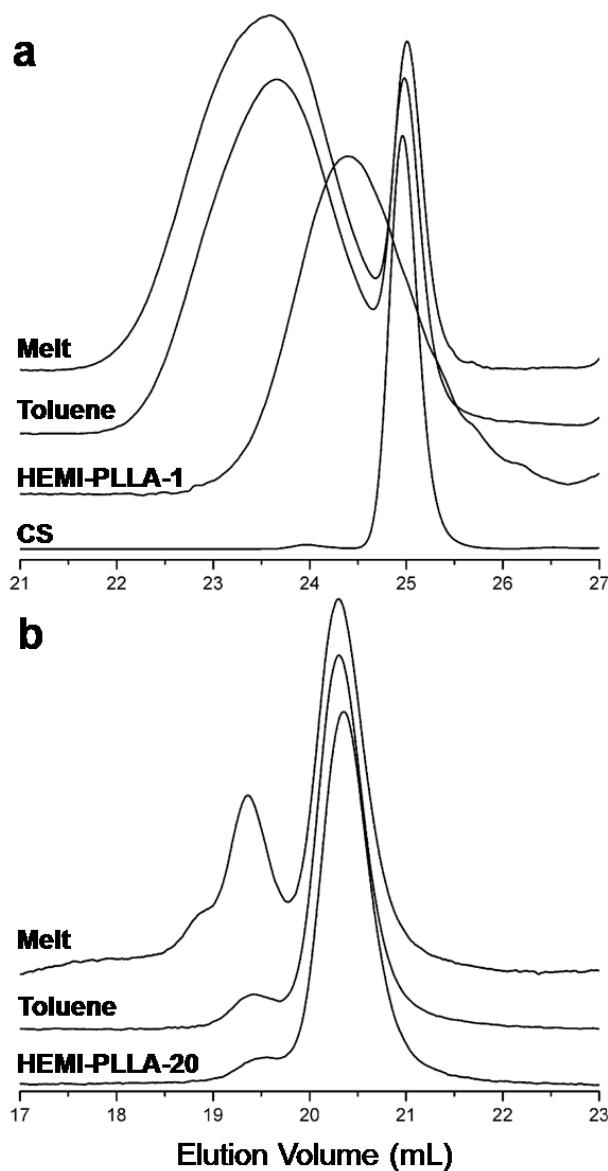
Figure 2.15. Normalized SEC elution curves for blends of HEMI-PLLA and CS. Blends of CS with (a) HEMI-PLLA-1 at a 1:1 molar ratio of HEMI-PLLA to CS and (b) HEMI-PLLA-20 at a molar excess of CS were conducted in both the melt (190 °C) and in toluene (110 °C) as indicated on the SEC chromatogram. In each chromatogram the HEMI-PLLA homopolymer elution curve is also given. The curves are offset from the baseline to improve clarity. Note the different x-axis ranges for (a) and (b) due to the different molecular weights of the products.

Multiple peaks were not observed in the SEC data for the HEMI-PLLA-1 blends as they were observed in the melt blend for HEMI-PLLA-20. Statistically, a majority of the CS molecules have more than one set of conjugated double bonds. Since most of the conjugated double bonds (greater than 75%) reacted in both HEMI-PLLA-1 blends, we expect that multiple additions of HEMI-PLLA-1 should have occurred in both blends. Separate peaks that correspond to the multiple coupling products were likely not resolved due to the small difference in molecular weights that these products would have compared to the single addition of HEMI-PLLA-1 to CS.

The SEC of the HEMI-PLLA-20 blend in the melt signifies that multiple coupling occurred between the two molecules. A high molecular weight shoulder off the HEMI-PLLA-20 peak (Figure 2.15b) was present before blending, possibly due to transesterfication or radical coupling reactions during its synthesis. The shoulder is observed in the SEC of the HEMI-PLLA-20 blend in solution at a comparable relative height to the main peak, suggesting that multiple coupling reactions did not occur in solution. Conversely, the SEC of the HEMI-PLLA-20 blend in the melt indicates multiple additions to CS, even though the two blends have similar conversions. We attribute the distinct behaviors of the two HEMI-PLLA-20 blends as observed by SEC to inherent phase separation of the HEMI-PLLA-20 and CS in the melt and not in solution. In the melt, reactions between HEMI-PLLA-20 and CS occur at the interface of the two materials, resulting in the formation of the PLLA-CS compatibilizer. The coupled CS molecule remains at the interface where it would more likely react with another HEMI-PLLA-20, giving the multiple addition products observed. In solution, no interface exists so there is actually the opposite bias. Once a CS molecule has reacted the probability for a second addition is reduced due to steric arguments. Along with the steric effects, the large molar excess of CS molecules to HEMI-PLLA-20 molecules contributes to single additions of HEMI-PLLA-20 to CS in solution.

2.3.6 Melt blends of HEMI-PLLA-67 and PLLA-49 with CS

Larger scale (4 g) melt blends of HEMI-PLLA-67 and CS were synthesized in a twin screw batch mixer. Blends of PLLA-49 and CS were also prepared as control groups for the reactive blends. CS blends with HEMI-PLLA-67 were compared to those of PLLA-49 due to their similar weight average molecular weight (Table 2.1). Components were compounded in the mixer at 190 °C for 10 min at which time blends were collected from the mixer for analysis and further processing. Both HEMI-PLLA-67 and PLLA-49 homopolymers were compounded in the mixer following the same protocol as controls. A summary of the blend analysis can be found in Table 2.3.

At high weight fractions of CS added (e.g. 15 wt %), excess CS pooled at the bottom of the mixer during compounding and was not fully incorporated. The unincorporated CS drained from the mixer when it was opened to remove the product. ^{1}H NMR spectroscopy was used to calculate the actual concentration of CS incorporated into the blends. Blends with 5 wt % or less added CS appeared to incorporate all the CS into the polylactide matrix. We determined that a maximum of 9 wt % CS could be incorporated into the blends under the conditions tested, and this required addition of 15 wt % CS to the mixer. The incomplete incorporation of the oil is due to the large difference in viscosities between the polylactide and CS[30] and has been observed in previous blends of PLLA and soybean oil.[5,6]

The formation of compatibilizers by the Diels–Alder coupling of CS and HEMI-PLLA-67 during blending was also monitored by ^{1}H NMR spectroscopy. In blends containing a molar excess of CS (15 and 5 wt % added), over 90% of the HEMI end groups were converted (Table 2.3). As the molar excess of CS to HEMI-PLLA-67 was reduced the conversion of the HEMI end-groups (X_{HP}) decreased and the conversion of the CS *E,E* isomers (X_{CS}) increased. The blend of HEMI-PLLA-67 and 2 wt % CS had a nearly one to one mole ratio of HEMI end groups to *E,E* isomers, which is reflected by the nearly equivalent X_{HP} and X_{CS} values. ^{1}H NMR spectroscopy (Figure 2.16) confirmed the formation of the Diels–Alder products between CS and HEMI-PLLA-67.

Table 2.3. Physical properties of melt blends of CS with PLLA-49 and HEMI-PLLA-67. The given errors are one standard deviation.

Matrix Polymer	W_{CS0} (%)[a]	W_{CS} (%)[b]	E (GPa)[c]	σ_b (MPa)[d]	ε_b (%)[e]	X_{HP} (%)[f]	X_{CS} (%)[g]	d_{lm} (µm)[h]	σ_{lm} (µm)[i]	MLT (µm)[j]	T_g (°C)[k]	Crystallinity (%)[l]
PLLA-49			2.4 ± 0.3	58 ± 3	5 ± 2						59	19
HEMI-PLLA-67			3.0 ± 0.2	67 ± 9	4 ± 1						57	39
PLLA-49	15	9	2.4 ± 0.3	28 ± 4	22 ± 7			1.81	1.8	3.1	59	40
HEMI-PLLA-67	15	7	2.0 ± 0.5	34 ± 2	50 ± 30	100	14	0.91	2	2.2	55	19
PLLA-49	5	4	2.1 ± 0.3	38 ± 1	30 ± 10			1.17	2	3.6	55	12
HEMI-PLLA-67	5	7	2.5 ± 0.2	37 ± 2	70 ± 30	98	44	0.7	2.1	2	54	19
PLLA-49/HEMI-PLLA-67[m]	5	6	2.3 ± 0.3	36 ± 3	20 ± 10	96	39	0.96	1.8	2.1	51	53
PLLA-49	2	2	2.6 ± 0.1	51 ± 1	5 ± 2			0.3	2	1.3	56	12
HEMI-PLLA-67	2	3	2.5 ± 0.2	54 ± 5	4 ± 2	66	70	0.35	1.3	0.5	55	18

[a]Weight fraction of CS added to melt mixer. [b]Weight fraction of CS incorporated into blends, by ^{1}H NMR spectroscopy. [c]Elastic modulus. [d]Stress at break. [e]Elongation to break. [f]Conversion of HEMI end-groups for blends with HEMI-PLLA-67. [g]Conversion of *E,E* isomers of CS added to mixer. [h]Log-mean average CS droplet diameter. [i]Log-mean CS droplet size distribution parameter. [j]Matrix ligament thickness. [k]Glass transition temperature from DSC. [l]Crystallinity of PLLA in tensile bar from DSC. [m]Matrix polymer was a 50/50 blend of PLLA-49 and HEMI-PLLA-67.
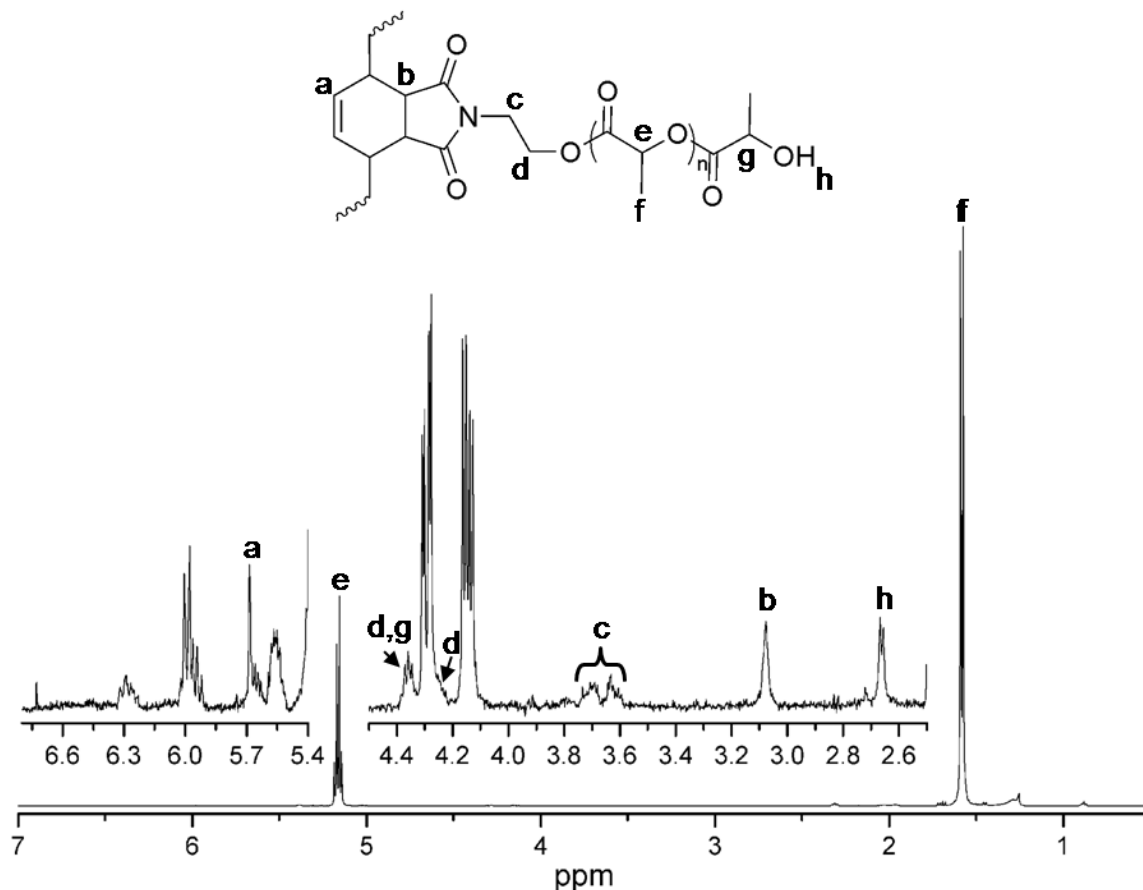
Figure 2.16. Representative ^{1}H NMR spectrum and expanded region for HEMI-PLLA-67 blend with CS with assignments (500 MHz, CDCl₃). Specifically, Figure 2.16 is the ^{1}H NMR spectrum for 5 wt % CS melt blend with HEMI-PLLA-67. The fully expanded structure demonstrates the small mole percent of CS that is present in the blend.

To probe the architecture of the products formed, the SEC chromatograms of HEMI-PLLA-67 blends with CS were compared to HEMI-PLLA-67 (Figure 2.17). The HEMI-PLLA-67 homopolymer was heated at 190 °C in the mixer, mimicking the blending protocol. The SEC of the heated homopolymer broadened and increased in elution volume slightly as compared to the pure HEMI-PLLA-67. The small change is likely due to some thermal degradation of the polymer, which has been observed for PLLA at similar temperatures.[31] While no additional peak was observed after heating HEMI-PLLA-67, a new peak is observed in the chromatogram at 18 mL for all reactive blends, which corresponds to twice the molecular weight of the original polymer. The

formation of the new peak suggests that not only PLLA-CS was synthesized but also PLLA-CS-PLLA. Whether or not 3-arm star-PLLA was formed is not clear since the predicted elution volume (17.4 mL) of such a product falls under the peak belonging to PLLA-CS-PLLA and therefore could be obscured.
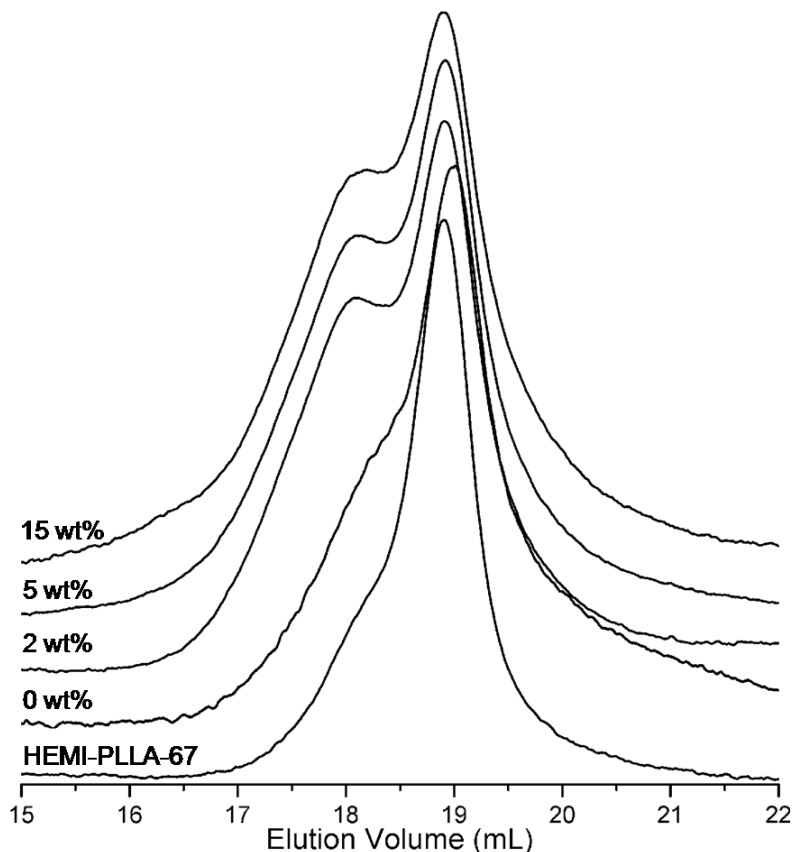
Figure 2.17. SEC elution curves of HEMI-PLLA-67 melt blends with CS. The 0 wt % curve represents HEMI-PLLA-67 compounded in the mixer under the same protocol as used for the blends. The HEMI-PLLA-67 curve corresponds to the original homopolymer.

Compression molded samples of the blends were utilized for tensile testing. Blends with more than 2 wt % CS resulted in an increase in elongation to break (ε_b) as compared to the corresponding polylactide homopolymer (Table 2.3). Blends with PLLA-49 resulted in 4–6 times the ε_b as compared to the PLLA-49 homopolymer. The ε_b values for blends with only 2 wt % percent CS were similar to that of the homopolymers, suggesting that there was a critical CS concentration for toughening. Using HEMI-PLLA-

67 as the matrix polymer increased the ε_b further, presumably due to the in situ formation of compatibilizer. Blending 5 wt % CS into HEMI-PLLA-67 increased the elongation to break by a factor of more than 17 compared to homopolymer HEMI-PLLA-67 and more than doubled the elongation to break as compared to a similar blend with PLLA-49. The stress at break (σ_b) of the blends decreased with the addition of CS. The σ_b did not significantly vary between the blends with 15 wt % and 5 wt % CS added, since all those blends had similar amounts of CS incorporated (Table 2.3). The moduli of the blends decreased slightly as compared to the parent homopolymer, which is expected with the replacement of stiff material (polylactide) with the low modulus CS, but remained above 2.0 GPa for all blends.

To determine if the mechanism of toughening the blend was due to plasticization, differential scanning calorimetry (DSC) was performed on the tested tensile bars (Figure 2.18). Four distinct thermal transitions were typically observed: glass transition (T_g), cold crystallization (T_c), melt crystallization, and melt transition (T_m). The melt crystallization exotherm directly preceding the melt endotherm is commonly observed in PLA that is pure L-lactide.[32,33] The T_g for the polylactide in the blends was not significantly different than the polylactide homopolymers. All blends and homopolymers had T_g values between 54 and 59 °C, indicating that significant plasticization did not occur. The crystallinity of the blends was calculated by subtracting the enthalpy of the two crystallization transitions from the melting transition. Generally, crystallinity of the PLLA in the blends ranged between 10 and 20 percent, similar to the homopolymers (Table 2.3). Several materials had higher degrees of crystallinity (ca. 40%) which were repeatable throughout the blend. Slower cooling rates after making the tensile bars may account for the higher crystallinity.
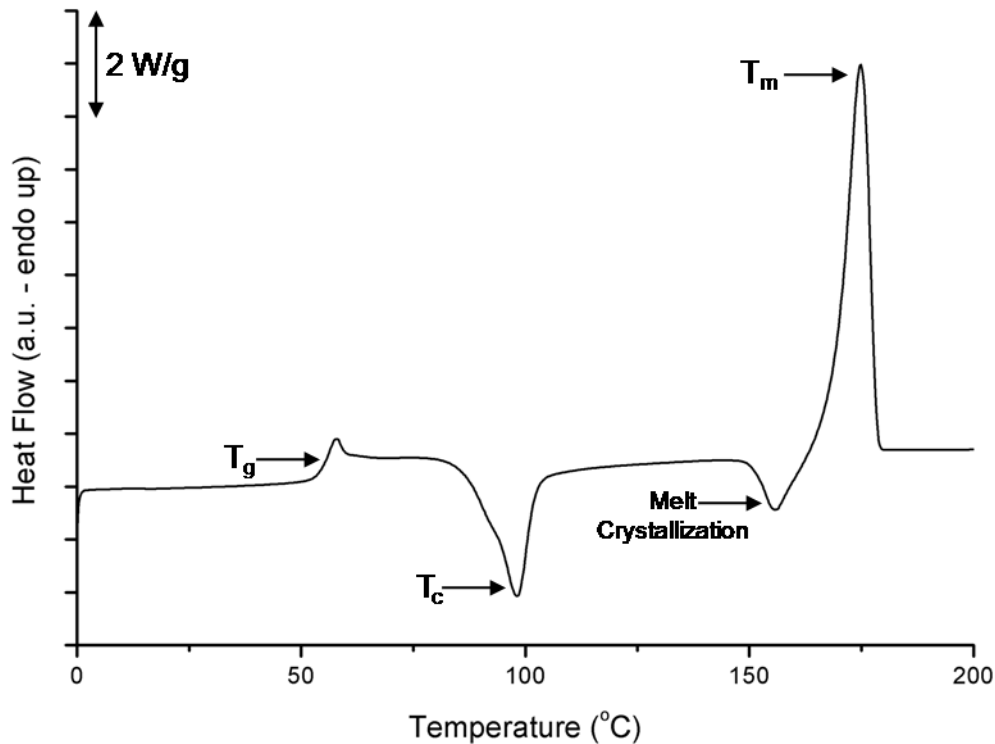
Figure 2.18. Representative differential scanning calorimetry (DSC) thermogram of HEMI-PLLA/CS blends. The thermal transitions observed are labeled as the glass transition temperature (T_g), crystallization temperature (T_c), melting temperature (T_c), and melt crystallization exotherm.

The morphology of the CS particles dispersed in the polylactide matrix was investigated with scanning electron microscopy (SEM). Samples were polished by cryo-microtomy prior to imaging to give a smooth surface suitable for image analysis. Representative SEM micrographs of PLLA-49 and HEMI-PLLA-67 blends with CS are shown in Figure 2.19. Reactive HEMI-PLLA-67 blends qualitatively appear to have smaller CS domains compared to the unreactive blends with PLLA-49. The log-mean CS particle diameter (d_{lm}) and the log-mean particle distribution parameter (σ_{lm}) were calculated from the SEM images for each blend (Table 2.3). As observed qualitatively in the SEM micrographs, analysis indicates the reactive blends with HEMI-PLLA-67 resulted in smaller d_{lm} as compared to the corresponding PLLA-49 blends, presumably due to the formation of compatibilizer at the interface. Compatibilizers in melt blends

have been known to reduce the particle size of the minor phase by decreasing the interfacial tension between the two phases and inhibiting droplet coalescence.[34,35] Since compatibilizer formed during blending, the interfacial tension between the two phases decreased, resulting in smaller droplets in the blends. The matrix ligament thickness (MLT), a measure of the interparticle distance, was also calculated for all blends (Table 2.3). The MLT was reduced for all reactive blends compared to their unreactive counterparts. Such a reduction in MLT (interparticle distance) is due to conservation of volume. The reactive and unreactive blends have the same amount (volume) of CS, but the reactive blends average diameter of the CS is less than the unreactive blend, giving more particles in the reactive blend than in the unreactive blend to conserve volume. An increase in the number of particles in a set volume of PLLA would result in the particles being closer together (smaller MLT) assuming an average distance between each particle.
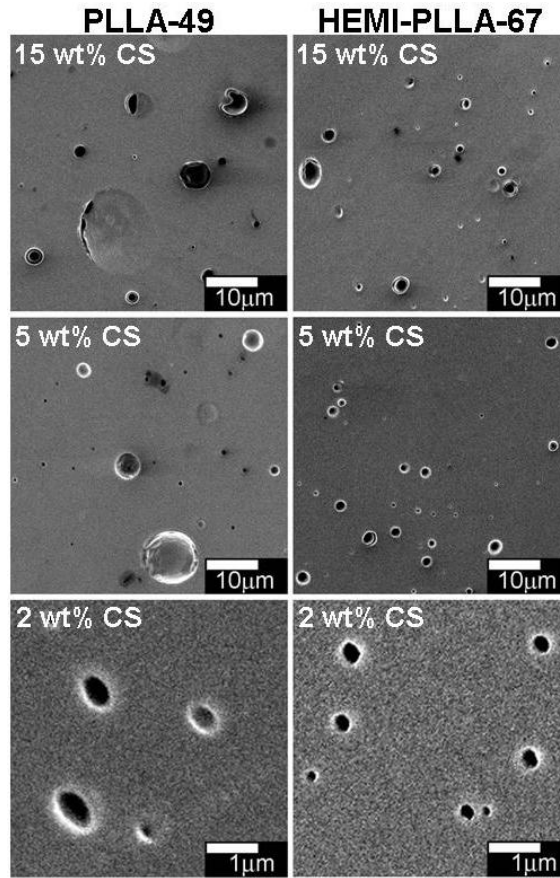
Figure 2.19. Representative SEM images of cryo-microtomed surfaces of CS binary blends with PLLA-49 (left column) and HEMI-PLLA-67 (right column). Samples are labeled by the amount of CS initially added to the mixer. See Table 2.3 for amount of CS incorporated. Cryo-microtomy of the samples removed CS at the surface creating the dark holes seen in the images.

In previous PLLA toughening schemes, a critical particle diameter and MLT for toughening were found.[36,37] For the CS blends, as the diameter of the CS domains decreases (Figure 2.20), the ε_b increases until a maximum is achieved at an optimal particle diameter. The MLT (Figure 2.20) also has a similar trend where the elongation to break sharply drops off around an MLT of 2 μm. For many brittle polymers, an optimal particle diameter is required for toughening.[38] Rubber toughening in brittle polymers relies heavily on the particles acting as craze terminators. More particles can provide sites for craze termination, but as the number of particles increase their size decreases at fixed dispersed phase content. Smaller particles are less efficient at terminating crazes, leading

to a balance between number of particles and toughening efficiency. For the polylactide and CS blends, the optimal particle diameter occurs somewhere between 0.5 and 0.9 μm.
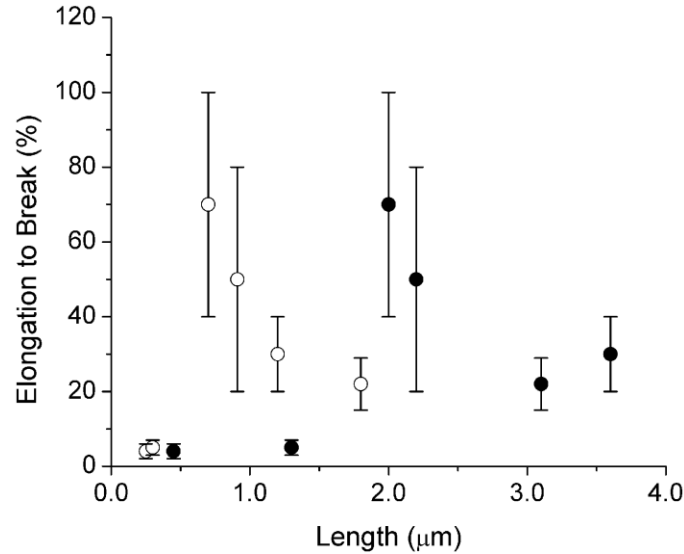
Figure 2.20: Correlation of average elongation to break with d_{lm} (open circles) and MLT (closed circles) for binary blends of CS with PLLA-49 and HEMI-PLLA-67. Error bars indicate standard deviation of elongation to break.

As discussed previously, varying amounts of CS were incorporated into the blends (Table 2.3). The amount of CS present can affect both the d_{lm} and MLT so it should be considered in the analysis. Generally, the HEMI-PLLA-67 blends with CS had similar amounts of CS incorporated as compared to the respective PLLA-49 blends. The comparable amounts of CS present suggest that a change in d_{lm} or MLT is mostly due to the reactive compatibilization that occurred and not a difference in CS content. Since the HEMI-PLLA-67 blends with 5 wt % and 15 wt % added to the mixer had the same amount of CS incorporated, their particle diameters were included in the range for the optimum particle diameter. Presumably, the two blends are nearly identical in composition, though the blend with 15 wt % CS added would initially have a greater concentration of CS with which HEMI-PLLA-67 could react and therefore may have a slightly different amount of compatibilizers present at the particle interface. Variation in the relative amount of compatibilizer affects the degree of compatibilization and subsequently the CS particle diameter. The small variation in the average ε_b values for

the HEMI-PLLA-67 blends with 5 wt % and 15 wt % CS added (both exhibiting 7 wt % incorporation) likely results from this difference in the particle diameters.

In SEM images of the tensile bar fracture surfaces (Figure 2.21), samples with improved elongation to break had deformed CS particles, indicative of matrix shear yielding. Typically, blends toughened by energy dissipation mechanisms such as shear yielding and cavitation have a critical MLT.[39,40] The MLT appears to have an optimal value around 2 μm, which contradicts previous results where a critical MLT for rubber toughening PLLA was observed.[6,36,37] Corté et al. have theorized that the critical MLT for a particular polymer matrix is a function of particle diameter in semicrystalline polymers.[40] According to their theory, the blends with smaller particles (2 wt % CS) should have a smaller critical MLT than the blends with larger CS particles (5 wt % and 15 wt % added). Perhaps, in these blends the critical MLT for the "small" particles was not reached while the critical MLT for the "large" particles was, qualitatively explaining the apparent optimum MLT value. Consequently, the data suggest that both crazing and shear yielding could be acting as energy dissipation mechanisms that give the observed improvement in elongation to break at an apparent optimal particle diameter.
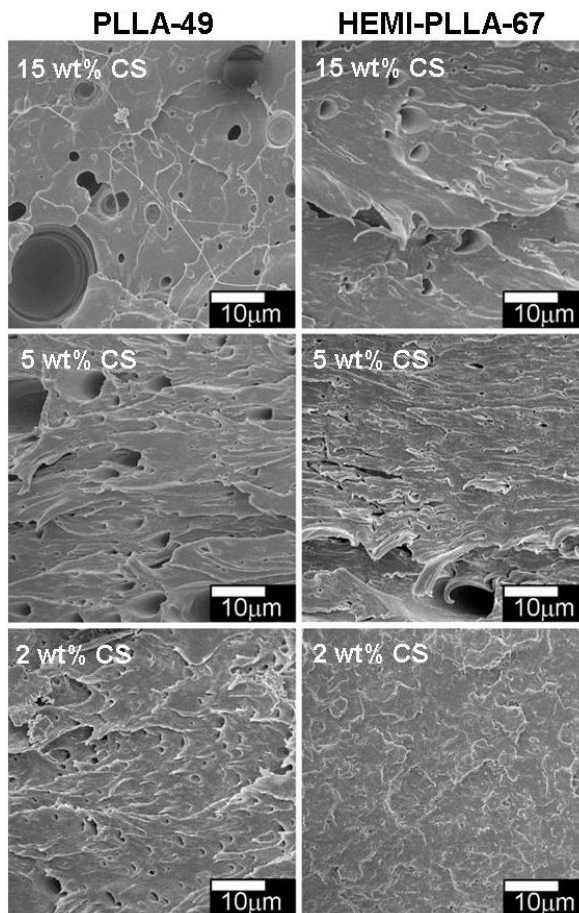
Figure 2.21. Representative SEM images of tensile bar fracture surfaces for melt blends of CS with PLLA-49 (left column) and HEMI-PLLA-67 (right column) labeled by the amount of CS added to the mixer.

To reduce the amount of reactive PLLA added, a ternary blend was synthesized in the melt mixer that contained a matrix phase composed of half HEMI-PLLA-67 and half PLLA-49 and 5 wt % CS. Interestingly, the blend had mechanical properties similar to the PLLA-49 and 5 wt % CS blend despite containing HEMI-PLLA-67 (Table 2.3). ^{1}H NMR spectroscopy confirms that the HEMI-PLLA-67 reacted to form compatibilizer and SEC (Figure 2.22) indicates that the architecture of the compatibilizer formed was similar to that of the other reactive blends. Due to the decreased loading of HEMI-PLLA-67, the number of compatibilizer molecules in the blend did decrease which could reduce the overall compatibilization of the blend. The d_{lm} of the blend (0.96 μm) was slightly less than the d_{lm} of the corresponding PLLA-49 blend (1.17 μm), indicating that the reaction

products were compatibilizing the blend. While the MLT looked close to optimal (2.1 μm), the ternary blend d_{lm} was somewhat greater than that of the apparent optimum particle diameter and consequently the ε_b of the blend did not increase beyond that of the unreactive binary blend. The ternary blend had significantly higher crystallinity than tough blends, which may account for the lower ε_b as well. The results of the ternary blend further suggest that an optimal d_{lm} exists for the blends as opposed to an optimal/critical MLT. A majority of the matrix polymer should be HEMI-PLLA to achieve the required d_{lm} and subsequent increase to the elongation to break.
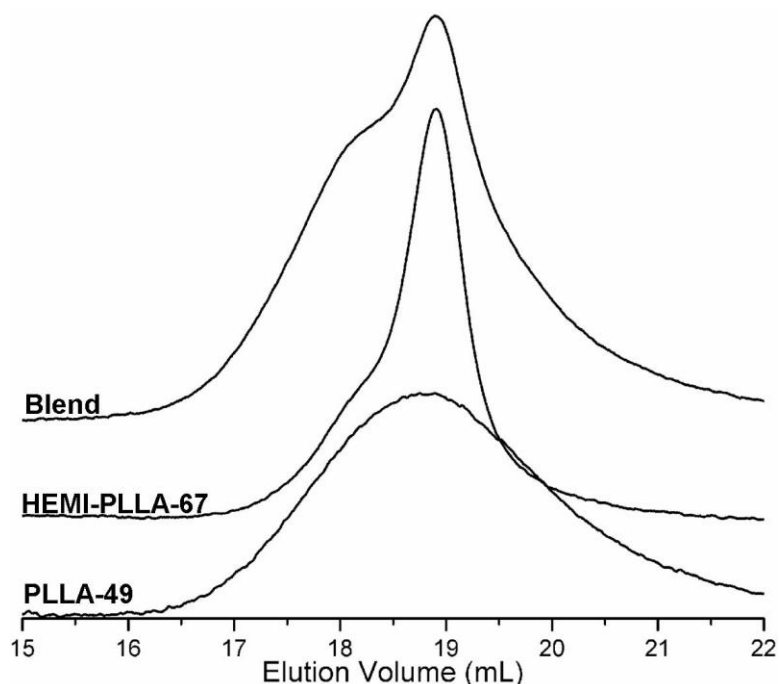
Figure 2.22. SEC of tertiary 50/50 blend of HEMI-PLLA-67 and PLLA-49 with 5 wt % CS. SEC elution curves of the HEMI-PLLA-67 and PLLA-49 are given as a comparison. Growth of a peak in the SEC of the blend at about twice the molecular weight of the HEMI-PLLA-67 peak is indicative of compatibilizer formation.

2.4 Conclusions

We investigated reactive melt blends of HEMI-PLLA and CS to synthesize tough sustainable materials. HEMI-PLLA was synthesized using $Sn(Oct)_2$ to give an end functionalized PLLA reactive towards CS through a Diels–Alder mechanism. Small scale blends of HEMI-PLLA and CS, in solution and in the bulk, demonstrated that the two

components can react to give a PLLA coupled to CS. These small scale blends demonstrated that up to three HEMI-PLLA chains can react with CS to form compatibilizers with varying architectures. Larger scale melt blends of CS with either PLLA or HEMI-PLLA resulted in toughened polylactide with the HEMI-PLLA blends showing double the elongation to break of the unreactive PLLA blends. The reactively formed compatibilizer with only 5 wt % CS resulted in a 17-fold increase in elongation to break as compared to the parent homopolymer. The increase in elongation to break was likely due to crazing as indicated by an observed optimal CS particle diameter.

2.5 References

[1] Choi, J. S.; Park, W. H. *Macromol. Symp.* **2003**, *197*, 65-76.

[2] Haq, M.; Burgueño, R.; Hohanty, A. K.; Misra, M. *Comp. Sci. Tech*. **2008**, *68*, 3344 – 3351.

[3] Brostöm, J.; Boss, A.; Chronakis, I. S. *Biomacromolecules* **2004**, *5*, 1124-1134.

[4] Ali, F.; Chang, Y.-W.; Kang, S. C.; Yoon, J. Y. *Polymer Bulletin* **2009**, *62*, 91-98.

[5] Chang, K.; Robertson, M. L.; Hillmyer, M. A. *Accepted to ACS Applied Materials and Interfaces* **2009**.

[6] Robertson, M. L.; Chang, K.; Gramlich, W. M.; Hillmyer, M. A. *Submitted* **2009**.

[7] Jerome, R. In *Macromolecular Engineering*; Matyjaszewski, K.; Gnanou, Y.; Leibler, L.; Eds.; 3; Wiley-VHC: Weinheim; p 1753-1782.

[8] Masutani, K.; Kawabata, S.; Aoki, T.; Kimura, Y. *Polym. Int*. **2010**, *59*, 1526-1530.

[9] Stanford, M. J.; Dove, A. P. *Macromolecules* **2009**, *42*, 141-147.

[10] Stanford, M. J.; Pflughaupt, R. L.; Dove, A. P. *Macromolecules* **2010**, *43*, 6538-6541.

[11] Gao, H.; Wang, Y. N.; Fan, Y.G.; Ma, J. B. *J. Control Release* **2005**, *107*, 158-173.

[12] Liu, X.; Li, K.; Feng, X.; Cao, Y. *J. Macromol. Sci. A* **2009**, *46*, 937-942.

[13] Zhu, J.; Lines, B. M.; Ganton, M. D.; Kerr, M. A.; Workentin, M. S. *J. Org. Chem.* **2008**, *73*, 1099-1105.

[14] Pounder, R. J.; Standford, M. J.; Brooks, P.; Richards, S. P.; Dove, A. P. *Chem. Commun*. **2008**, 5158-5160.

[15] Aydan, D.; Durmaz, H.; Tunca, U.; Hizal, G. *J. Poly. Sci. Part A: Polym. Chem.* **2009**, *47*, 178-187.

[16] Zhu, J.; Ganton, M. D.; Kerr, M. A.; Workentin, M. S. *J. Am. Chem. Soc.* **2007**, *129*, 4904-4905.

[17] Xu, N.; Du, F.-S.; Li, Z.-C. *J. Polym. Sci Part A: Polym. Chem.* **2007**, *45*, 1889-1898.

[18] Larock, R. C.; Dong, X.; Chung, S.; Reddy, C. K.; Ehlers, L. E. *J. Am. Oil Chem. Soc.* **2001**, *78*, 447-453.

[19] Andjelkovic, D. D.; Min, B.; Ahn, D.; Larock, R. C. *J. Agric. Food Chem.* **2006**, *54*, 9535-9643.

[20] Heath, W. H.; Palmieri, F.; Adams, J. R.; Long, B. K.; Chute, J.; Holcombe, T. W.; Zieren, S.; Truitt, M. J.; White, J. L.; Willson, C. G. *Macromolecules* **2008**, *41*, 719-726.

[21] Davidock, D. A. Novel Fluorinated Block Copolymers by Selective Chemical Modification: Chemistry and Thermodynamics. Ph.D. Thesis, University of Minnesota, Minneapolis, MN, 2004.

[22] Ahn, K.-D.; Kang, J.-H.; Yoo, K.-W.; Choo, D.-J. *Macromol. Symp.* **2007**, *254*, 46-53.

[23] Auras, R.; Harte, B.; Selke, S. *Macromol. Biosci.* **2004**, *4*, 835-864.

[24] Anderson, K. S. High Impact Polylactide Composites. Ph.D. Thesis, University of Minnesota, Minneapolis, MN, 2004.

[25] Liu, Z. H.; Zhang, X. D.; Zhu, X. G.; Li, R. K. Y.; Qi, Z. N.; Wang, F. S.; Choy, C. L. *Polymer* **1998**, *39*, 5019-5025.

[26] Witzke, D.R.; Narayan, R.; Kolstad, J. J. *Macromolecules* **1997**, *30*, 7075-7085.

[27] Nijenhuis, A. J.; Grijpma, D. W.; Pennings, A. J. *Macromolecules* **1992**, *25*, 6419-6424.

[28] Zhu, J.; Ganton, M. D.; Kerr, M. A.; Workentin, M. S. *J. Am. Chem. Soc.* **2007**, *129*, 4904-4905.

[29] Switek, K. A.; Bates, F. S.; Hillmyer, M. A. *Macromolecules* **2004**, *37*, 6355-6361.

[30] Scott, C. E.; Joung, S. K. *Polym. Eng. Sci.* **1996,** *36*,1666-1674.

[31] Sodergard, A.; Nasman, H. *Polym. Degrad. Stab.* **1994**, *46*, 25-30.

[32] Ke, T.; Sun, X. *J. Appl. Polym. Sci.* **2003**, *89*, 1203 - 1210.

[33] Liu, Y.; Wang, L.; He, Y.; Fan, Z.; Li, S. *Polym. Int.* **2010**,*59*, 1616 - 1621.

[34] Macosko, C. W.; Guegan, P.; Khandpur, A. K.; Nakayama, A.; Marechal, P.; Inoue, T. *Macromolecules* **1996**, *29*, 5590-5598.

[35] Lepers, J.; Favis, B. D. *AICHE J.* **1999**, *45*, 885-895.

[36] Anderson, K. S.; Lim, S. H.; Hillmyer, M. A. *J. Appl .Polym. Sci.* **2003**, *89*, 3757-3768.

[37] Anderson, K. S.; Hillmyer, M. A. *Polymer* **2004**, *45*, 8809-8823.

[38] Perkins, W. G. *Poly. Eng. Sci.* **1999**, *39*, 2445

[39] Wu, S. *Polymer* **1985**, *26*, 1855-1863.

[40] Corte, L.; Leibler, L. *Macromolecules* **2007**, *40*, 5606-5611.

Chapter 3

Conjugated Polydienes for Post-polymerization Functionalization[i]

In this chapter we discuss the catalytic isomerization of the isolated double bonds on polydienes to give a synthetic handle for Diels–Alder click chemistry. Both polyisoprene (PI) and polycyclooctadiene (PCOD) were catalytically isomerized with $RuHCl(CO)(PPh_3)_3$ to conjugated PI (CPI) and PCOD (CPCOD). The reaction time and temperature were varied to control the number of conjugated dienes generated along the polydiene backbones. To demonstrate conjugated polydiene utility, small molecules were coupled to them through the Diels–Alder click reaction to produce an array of post polymerization functionalized polymers. Such chemistry allows for one parent conjugated polymer to be functionalized with an array of chemical moieties. In one example, *N*-2-hydroxyethylmaleimide (HEMI) was coupled to CPI to produce a hydroxylated material. L-lactide was then polymerized from this macroinitiator with both tin(II) octoate $(Sn(Oct)_2)$ and 1,5,7-triazabicyclo[4.4.0]dec-5-ene (TBD) to produce poly(L-lactide) (PLLA) grafted from PI (PI-*g*-PLLA) with a monomodal SEC distribution at 95 wt % PLLA content.

3.1 Introduction

As discussed in Chapter 1, synthetic polyisoprene (PI) can be produced from renewable materials and has a low glass transition temperature (T_g) – properties that make it an interesting material for renewable adhesives and toughening agents. The isolated carbon-carbon double bonds along the PI chain allow for a number of post-polymerization chemical modifications to give complex architectures for a wide range of applications.

One emerging method to facilitate the post polymerization functionalization of polymers is "click" chemistry because these click reactions are high yield, modular, and yield no side products.[1,2,3,4] For these reasons, click reactions provide a versatile and efficient method to functionalize polymers post polymerization. Common functionalizations include thiol-ene,[5] azide-alkyne,[4] and Diels–Alder reactions.[6] Among these reactions, typically, only the Diels–Alder reaction does not require a catalyst or initiator.[1] Diels–Alder reactions have been used to produce star polymers,[7,8] block polymers,[9] graft copolymers,[6] reversibly crosslinked polymers,[10] and small molecule functionalized polymers.[11,12,13] For PI to undergo similar Diels–Alder reactions, it must contain conjugated dienes or a reactive dienophile.

Conjugation of the double bonds on PI has been accomplished using several methods with the final goal often being conducting polymers. Perhaps the most discussed method to conjugate PI is doping the polymer with molecular iodine (I_2).[14] However, the I_2 doped polymers do not only contain conjugated dienes and polyene segments, they also have multiple intermediates from the conjugation process such as charge complexes, cation-radical intermediates, and iodated double bonds.[15,16,17,18] Other oxidants such as $SbCl_5$ and $TiCl_4$ have also been used to conjugate polydienes with similar results and intermediates.[19,20] Although the aforementioned techniques effectively produce conducting polymers, they do not necessarily provide the functionality and stability required for the desired Diels–Alder reactions due to the high concentration of undesirable side products (see Appendix C). Elimination of brominated poly(isobutylene-*co*-isoprene) has produced conjugated dienes available for Diels–Alder reactions, but at low concentrations (0.1 mmol/g polymer).[21,22] The limitations of previous approaches to

PI conjugation for post-polymerization modifications motivate the development of new conjugation methods.

Transition metal catalysts are widely used to isomerize and migrate carbon-carbon double bonds in small molecules.[23,24,25,26,27] Typically, these reactions conserve the original number of carbon-carbon double bonds, only moving double bonds along the carbon chain. Under appropriate conditions, the double bonds will migrate over several carbon atoms to reach the most energetically favorable position, for example adjacent to another π-orbital containing functional group.[28,29] If additional carbon-carbon double bonds are present in the molecule, systems of conjugated dienes can be formed as has been demonstrated with linoleic acids and esters.[30,31,32] Much like fatty acids, PI contains isolated double bonds along its chain, suggesting that PI can be conjugated with similar transition metal catalysts.

In analogy to the conjugation of vegetable oils and related fatty acids, we investigated the ability of the $RuHCl(CO)(PPh_3)_3$ catalyst as a model system to conjugate olefins along the PI backbone. We successfully synthesized conjugated PI with varying degrees of conjugation. To demonstrate the range of syntheses possible the small molecule squalene and polycyclooctadiene were also conjugated. The conjugated dienes along CPI and conjugated PCOD (CPCOD) reacted with small molecules through the Diels–Alder click reaction to produce tailored functionality along the polymer backbones. As an example of the utility of this approach, we functionalized a sample of CPI with primary hydroxyl groups. The hydroxyl functionalized CPI was used as macroinitiator for the ring opening polymerization of L-lactide, creating poly(L-lactide) (PLLA) graft CPI copolymers (PI-*g*-PLLA). Previous work in our group has shown that similar graft copolymers of PLA with an incompatible, low glass transition temperature polymer backbone result in materials with high toughness.[33] In Appendix E, we synthesized a variety of PI-*g*-PLA materials and investigated their physical and morphological properties.

3.2 Experimental Details

3.2.1 Materials and general methods

All chemicals were purchased from Aldrich and used without further purification unless otherwise noted. *N*-2-hydroxyethylmaleimide was synthesized by a previously published procedure.[11] L-lactide and D,L-lactide (Purac) were purified by recrystallization in ethyl acetate and then dried under vacuum at room temperature. The RuHCl(CO)(PPh$_3$)$_3$ catalyst and P(CH$_2$OH)$_3$ ligand were purchased from Strem Chemicals and used without further purification. HPLC grade toluene and cyclohexanes were dried on a home built solvent column by passing them over an activated alumina column and a supported copper catalyst. HPLC grade CH$_2$Cl$_2$ was dried on an MBraun solvent purification system. PCOD was synthesized following a previously reported procedure.[34] All other materials were synthesized as described below.

^{1}H NMR spectroscopy was performed on a Varian Inova 500 MHz spectrometer in CDCl$_3$ (Cambridge) using the residual CHCl$_3$ peak as reference. Size exclusion chromatography was performed on an Agilent 1100 high-pressure liquid chromatograph at 35 °C equipped with a PLgel (Varian) 5 μm guard column followed by three PLgel columns with varying pore sizes with HPLC grade chloroform as the mobile phase. Molecular weights and polydispersity index (PDI) were measured by a Hewlett-Packard P1047A refractometer calibrated with polystyrene standards (Polymer Laboratories). DSC analysis was performed on a Texas Instruments TA Q1000 calorimeter at a 10 °C/min temperature ramp rate. PI/CPI samples were cycled between -90 and 30 °C with two heating and one cooling cycle. PCOD/CPCOD samples were cycled between -120 and 100 °C with two heating and cooling cycles. The DSC traces given for all samples are from the second heating ramp.

3.2.2 Anionic polymerization of isoprene

Isoprene was polymerized anionically following a previously published procedure and apparatus setup.[35,36,37] Briefly, isoprene was degassed by three freeze-pump-thaw cycles, dried over n-BuLi twice, and then vacuum distilled to a tared burette. To a flame dried reactor under 5 psig argon atmosphere, the purified isoprene monomer (50 g), dry

cyclohexane (800 mL), and sec-BuLi (1.4 M solution in hexanes, 1.28 mL) were added. The reactor was heated at 40 °C in a water bath for 4 h at which time the reaction was quenched with a degassed 50/50 methanol/isopropanol solution. The reaction solution was precipitated in 3 volume excess 50/50 methanol/isopropanol solution and subsequently dried under vacuum at 45 °C to yield PI (M_n= 25 kg/mol, 94% yield). ^{1}H NMR spectroscopy (500 MHz, CDCl$_3$) **δ** 5.124 (s, C=C*H* *trans* and *cis*-1,4 PI), 4.8-4.6 (m, C=C*H$_2$* 3,4 PI), 2.042 (s, C=CH-C*H$_2$trans* and *cis*-1,4 PI), 1.678 (s, -C*H$_3$cis*-1,4 PI), 1.599 (s, -C*H$_3$trans*-1,4 PI).

3.2.3 Conjugation of polydienes and squalene

As an example, PI (800 mg) was dissolved in benzene (4.5 mL) in a 20 mL scintillation vial. RuHCl(CO)(PPh$_3$)$_3$ (18 mg) was added to the polymer solution and stirred to create a slurry. The slurry was transferred to a 10 mL side arm pressure vessel. The solution was degassed by three freeze-pump-thaw cycles and backfilled with 3 psig argon. The vessel was then transferred to a 60 °C oil bath to heat for 160 h. Reaction temperatures and times were varied as well as solvents. Toluene and xylenes were substituted for benzene at reaction temperatures higher than 90 °C. At 60 °C under the same reaction conditions, conjugation of PI in either toluene or benzene resulted in similar degrees of conjugation. After the desired reaction time, solvent was removed by vacuum at ambient temperature over several days. To remove the catalyst, the sealed flask was brought into a N$_2$ atmosphere dry box where dry CH$_2$Cl$_2$ (6.75 mL) and P(CH$_2$OH)$_3$ (23 mg) were added to the flask. The vessel was sealed in the dry box and removed to stir for several days – until the solution had become cloudy white. The cloudy solution was passed through a silica gel column with 150 mL of CH$_2$Cl$_2$. The solution was concentrated by rotary evaporation followed by the addition of BHT (8 mg). The remaining solvent was removed under vacuum at room temperature over several days to give CPI (69.9 % yield). *^{1}H NMR spectroscopic assignments for conjugated squalene CSQ* (500 MHz, CDCl$_3$) **δ** 6.40 (d, *J* = 16.8 Hz, *Z2* –CH=C-C*H*=CH-), 6.22 (dd, *J* = 14.0 Hz, *J* = 11.9 Hz, *E1* –C=CH-C*H*=CH-), 6.04 (m, *E2* –CH=C-C*H*=CH-), 5.81 (d, *J* = 10.8 Hz, *E1* –C=C*H*-CH=CH-), 5.65 (br, *Z2* –CH=C-CH=C*H*-), 5.53 (br m, *E2* –CH=C-

CH=C*H*- and *E1* –C=CH-CH=C*H*-), 5.36 (br m, *E2* –C*H*=C-CH=CH-), 5.30 (m, =C*H*-CH$_2$-C*H*=), 5.25 (br, *Z2* –C*H*=C-CH=CH-), 5.20-5.06 (br, vinyl =C*H*-), 2.80-2.60 (=CH-C*H*$_2$-CH=), 2.20-1.90 (=CH-C*H*$_2$-), 1.79 (m, *Z2* -C*H*$_3$), 1.74 (s, *E1* -C*H*$_3$), 1.73 (s, *E2* -C*H*$_3$), 1.68 (s, isolated -CH=C-C*H*$_3$), 1.60 (s, isolated -CH=C-C*H*$_3$), 0.99-0.94 (m, -C*H*$_2$-), and 0.90-0.85 (m, -C*H*$_3$).^{1}*H NMR spectroscopic assignments for CPI* (500 MHz, CDCl$_3$) **δ** 6.41 (d, *J* = 14.8 Hz, *Z2* -CH=C-C*H*=CH-), 6.24-6.09 (br s, *E1* -C=CH-C*H*=CH-), 6.05 (d, *J* = 12.9 Hz, *E2* =C-CH$_2$-CH=C-C*H*=), 6.02 (d, *J* = 14.7, *E2* –CH=C-C*H*=CH-), 5.96-5.72 (br m, *E1* -C=C*H*-CH=CH-), 5.63 (br m,*Z2* -CH=C-C*H*=CH-), 5.51 (m, *E1* -C=CH-CH=C*H*- and *E2* –CH=C-CH=C*H*-), 5.45 (m, *E2* =C-CH$_2$-C*H*=C-CH=), 5.35 (d, *J* = 7.2 *E2* –C*H*=C-CH=CH-), 5.30 (m, =C*H*-CH$_2$-C*H*=), 5.23 (s, *Z2* -C*H*=C-CH=CH-), 5.20-5.00 (m, isolated =C*H*-), 4.8-4.6 (m, *H*$_2$C=C-), 2.9-2.5 (m, =CH-C*H*$_2$-CH=), 2.30-1.85 (br, =CH-C*H*$_2$-), 1.79 (s, *Z2*, -C*H*$_3$), 1.72 (s, *E2*, -C*H*$_3$), 1.68 (s, *cis*-1,4, -C*H*$_3$), 1.60 (s, *trans*-1,4, -C*H*$_3$), 0.96 (br m, -C*H*$_2$-), and 0.87 (br m, -C*H*$_3$).^{1}*H NMR spectroscopic assignments for CPCOD* (500 MHz, CDCl$_3$) **δ** 6.60-6.35 (br m, *Z-E-Z* order of isomers =CH-C*H*=C*H*-CH=), 6.29 (m, *E-Z* -CH=CH-C*H*=CH-), 6.20-6.05 (br m, *E-E-E* =CH-C*H*=C*H*-CH=), 6.00 (d, *J* = 12.7 Hz, *E-E* =CH-C*H*=CH-), 5.98 (m, *E-Z* –CH=C*H*-CH=), 5.67 (m, *E-E-E* =CH-CH=CH-C*H*=), 5.65 (m, *E-Z* –C*H*=CH-CH=), 5.56 (m, *E-E* =CH-CH=C*H*-), 5.40 (br m, *E-Z* –CH=CH-C*H*= and isolated vinyl protons), 2.90-2.60 (br m,=CH–C*H*$_2$-CH=), 2.20-1.90 (br m, all =CH-C*H*$_2$-), and 1.50-1.25 (br m, -C*H*$_2$-).

3.2.4 Small molecule and CPI or CPCOD coupling reactions

As a general example, CPI was dissolved in toluene at 3.3% (w/v) concentration. Subsequently, liquid small molecules were added to the solution by syringe at the desired volume to give the targeted ratio of small molecule to reactive conjugated dienes. For solid small molecules (HEMI and MA), the desired mass was dissolved in minimal CH$_2$Cl$_2$ and then the resulting solution was added to the CPI solution. For reactions to be performed at 160 °C, 5 wt % (relative to CPI) BHT was added to the solution. Once all the components solubilized, the solutions were transferred to side arm pressure vessels where they were degassed by three freeze-pump-thaw cycles and backfilled with 3 psig

argon. The sealed reactors were placed in an oil bath at the desired temperature (110 °C or 160 °C) to react for varying times. Upon completion, the flasks were removed from the oil bath to cool to ambient temperature. The resulting solutions were precipitated three times from CH_2Cl_2 into 10X excess methanol. The product was dissolved in CH_2Cl_2 and 1 wt % BHT was added to the solution. The solution was concentrated with blowing N_2 and dried under vacuum at room temperature for several days. Control blends of PI and the small molecules were synthesized as discussed above by substituting PI for CPI. Products were analyzed with ^{1}H NMR spectroscopy and SEC. The following gives the new peaks observed in the coupled products' ^{1}H NMR spectra.*^{1}H NMR spectroscopic analysis of CPI-g-HEMI*(500 MHz, CDCl$_3$) **δ** 5.54 (s, ring -C*H*=C-), 3.64 (s, N-C*H$_2$*-CH$_2$-O), 3.62 (s, N-CH$_2$-C*H$_2$*-O), 3.25-2.89 (m, ring O=C-C*H*-C*H*-C=O), and 1.75 (s, ring –C*H$_3$*). *^{1}H NMR spectroscopic analysis of CPI-g-MA* (500 MHz, CDCl$_3$) **δ** 5.48 (s, ring -C*H*=C-), 3.50-3.10 (m, ring O=C-C*H*-C*H*-C=O), and 1.76 (s, ring –C*H$_3$*). *^{1}H NMR spectroscopic analysis of CPI-g-HEA* (500 MHz, CDCl$_3$) **δ** 5.54 (m, ring -C*H*=C-), 4.22 (s, O-C*H$_2$*-CH$_2$-OH), 3.82 (s, O-CH$_2$-C*H$_2$*-OH), and 2.69 (s, ring –C*H*-C=O). *^{1}H NMR spectroscopic analysis of CPI-g-HEMA* (500 MHz, CDCl$_3$) **δ** 5.45 (m, ring -C*H*=C-), 4.30-4.05 (m, O-C*H$_2$*-CH$_2$-OH), and 3.86-3.68 (m, O-CH$_2$-C*H$_2$*-OH). *^{1}H NMR spectroscopic analysis of CPCOD-g-HEMI* (500 MHz, CDCl$_3$) **δ** 5.71 (s, ring -C*H*=C*H*-), 3.66 (s, N-C*H$_2$*-CH$_2$-O), 3.61 (s, N-CH$_2$-C*H$_2$*-O), 3.11 (s, ring O=C-C*H*-C*H*-C=O), 2.22 & 2.15 (s, ring =CH-C*H*-), and 1.92 & 1.78 (br, =CH-C*H$_2$*-CH-CH=). *^{1}H NMR spectroscopic analysis of CPCOD-g-MA* (500 MHz, CDCl$_3$) **δ** 5.81 (s, ring -C*H*=C*H*-), 3.35 (s, ring O=C-C*H*-C*H*-C=O), 2.22 & 2.16 (s, ring =CH-C*H*-), and 1.86 & 1.78 (br, =CH-C*H$_2$*-CH-CH=).

3.2.5 CPI-*g*-PLLA synthesis

CPI-*g*-HEMI with 19 hydroxyl groups per molecule was synthesized using the above method for Diels–Alder reactions with CPI and subsequently used as the macroinitiator for CPI-*g*-PLLA synthesis. All reactions targeted 95 wt % L-lactide monomer (0.475 g) and 5 wt % macroinitiator (25 mg), were setup in a N_2 dry box, and were performed in 48 mL pressure vessels. After the polymerization reaction, solutions

were diluted in CH_2Cl_2 and precipitated in 10X excess methanol. The precipitated polymers were collected by suction filtration and dried under vacuum at room temperature. The specific synthetic details for each catalyst used follow. *Sn(Oct)$_2$ catalyzed reaction*. The macroinitiator and monomer were dissolved in dry toluene (3.5 mL). Sn(Oct)$_2$ was added at a monomer to catalyst ratio of 5000:1 as a stock solution of Sn(Oct)$_2$ in toluene. The reaction vessel was heated at 100 °C for 21 h in an oil bath, after which the vessel was removed from heat and allowed to cool to ambient temperature to quench the reaction. *AlEt$_3$ catalyzed reaction*. The macroinitiator was dissolved in dry toluene (4.1 mL). AlEt$_3$ solution (1M in hexanes) was added at a 2:1 hydroxyl group to catalyst ratio (7.8 μL) and the resulting solution was left to stir 16 h in the dry box. Subsequently, the monomer was added to the solution and the vessel was placed in a 90 °C oil bath for 5 h. One drop of acid water (4:1 DI water to concentrated HCl) was added to quench the reaction. *TBD catalyzed reaction*. The macroinitiator and monomer were dissolved in dry CH_2Cl_2. TBD (0.5 mg) was added as a stock solution in dry CH_2Cl_2. The solution was allowed to react for 4 h at room temperature and then quenched with benzoic acid (4.3 mg) solution in CH_2Cl_2. PLLA repeat unit ^{1}H NMR spectroscopy assignments (500 MHz, CDCl$_3$) **δ** 5.158 (q, *J* = 7.2 Hz, O-C*H*-CH$_3$), 1.576 (d, *J* = 8.1 Hz, O-CH-C*H$_3$*). End-group ^{1}H NMR spectroscopic assignments (500 MHz, CDCl$_3$) **δ** 4.35 (m, PLLA methine -C*H*-OH), 4.26 & 4.09 (s, N-CH$_2$-C*H$_2$*-O), and 3.64 (br, N-C*H$_2$*-CH$_2$-O).

3.3 Results and Discussion

3.3.1 Conjugation of squalene

The feasibility of PI conjugation with RuHCl(CO)(PPh$_3$)$_3$ was investigated first with the small molecule analog squalene, allowing for easier handling and analysis. A variety of reaction conditions (Table 3.1) were investigated to produce conjugated squalene (CSQ) at a catalyst loading ([Ru]/[C=C]) of 1.6×10^{-3}. Reactions in solution at 60 and 90 °C for 44 h isomerized a significant fraction of the isolated olefins to conjugated dienes. Not surprisingly, the increase in reaction temperature led to a greater conversion of isolated olefins to conjugated dienes over the same reaction time – consistent with an increase in

reaction rate. In an effort to remove solvent from the system, we performed a bulk isomerization reaction (CSQ-0.23) at 90 °C. The conversion of the isolated olefins in the bulk system is significantly less than that in the similar solution reaction (CSQ-0.95) (Table 3.1). The low conversion is attributed to poor catalyst solubility in the melt system as the system was cloudy. Since the catalyst was not in solution, it was not available to undergo reactions. At the temperatures investigated a homogeneous system gives the highest conversions.

Table 3.1. CSQs synthesized at $[Ru]/[C=C] = 1.6 \times 10^{-3}$ catalyst loading under various conditions for 44 h.

Sample Designation[a]	Solvent	Reaction Temperature (°C)	% C=C Conjugated[b] (%)
CSQ-0.29	Benzene	60	10
CSQ-0.23	None	90	8
CSQ-0.95	Toluene	90	39

[a]CSQ = conjugated squalene and the number following is the average number of *E,E* conjugated dienes per squalene molecule. [b]Percentage of all the olefins in squalene that are now in conjugated systems.

The proposed conjugated diene synthesis mechanism for CSQ and CPI (Figure 3.1) follows those for the isomerization of small molecules.[24] The reaction passes through series of intermediates where the ruthenium-hydride catalyst adds across a double bond and then undergoes reductive elimination. The addition and subsequent elimination can isomerize the isolated carbon-carbon double bond (*e.g. E* to *Z* conformation) or lead to migration of the bond along the polymer/squalene chain. One such migration event in squalene and PI brings carbon-carbon double bonds closer together in a bis-allylic configuration. Subsequent isomerizations/migrations to the bis-allylic intermediate result in conjugated dienes with varying stereochemistry (Figure 3.1).
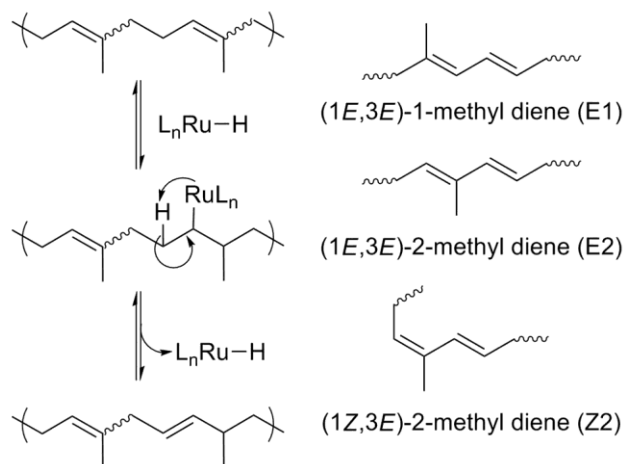
Figure 3.1. Proposed isomerization mechanism of polyisoprene and squalene by ruthenium hydride catalyst and the structures of the major conjugated diene isomers present in CPI and CSQ. At least two isomerization events are required to produce conjugated dienes along the polymer chain. Conjugated diene isomers are named according to the conformation of the more substituted double bond and placement of methyl group (E1, E2, and Z2).

A representative ^{1}H NMR spectrum of the CSQs (Figure 3.2) supports the proposed CSQ synthesis scheme (Figure 3.1). Comparison of the CSQ spectrum to the squalene spectrum in the 5.25–6.50 and 2.5–3.0 ppm regions, shows that peaks not present in the spectrum of squalene are now present in CSQ. The peaks in the 3.0–2.5 ppm region are consistent with bis-allylic protons, while the peaks in the 6.50–5.25 ppm region belong to conjugated diene protons. The formation of bis-allylic protons as well as conjugated diene protons in CSQ validates the proposed isomerization mechanism (Figure 3.1). From the ^{1}H NMR spectrum of the CSQ, the two major conjugated diene isomers are identified as E2 and E1. The *E,E* isomer formation in CSQ is favored for two reasons: (1) the original isolated olefins in squalene all have the *E* configuration and (2) the RuHCl(CO)(PPh$_3$)$_3$ catalyst under the reaction conditions investigated, preferentially isomerizes double bonds to the *E* configuration.[11] With no olefins in the *Z* configuration initially and the catalyst preferring to produce *E* isomers, few Z2 isomers are seen in the CSQ product.
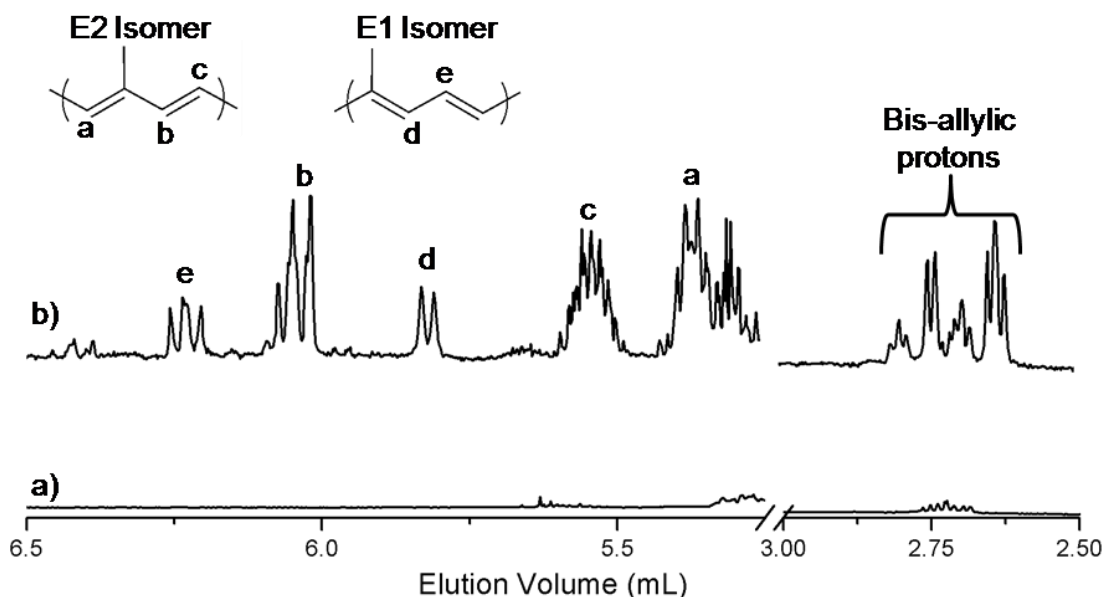
Figure 3.2. Expanded ^{1}H NMR spectra of (a) squalene and (b) isomerized squalene CSQ-0.29 with peak assignments (500 MHz, CDCl$_3$). The spectra have been expanded to show regions where new peaks form in the CSQ-0.29 spectrum.

3.3.2 Conjugation of polyisoprene

With the proof of concept demonstrated by the production of CSQ, conjugated PI (CPI) was synthesized from anionically polymerized PI (see Experimental Details) using RuHCl(CO)(PPh$_3$)$_3$ at [Ru]/[C=C] = 1.6×10^{-3} in benzene (Table 3.2). Generally, the CPIs have similar number average molecular weights (M$_n$) and only slightly larger polydispersity index (PDI) values as compared to the original PI when measured by size exclusion chromatography (SEC) using polystyrene standards. The SEC traces (Figure 3.3) of the CPIs have a higher molecular weight shoulder that is consistent with a small amount of coupling and a tail consistent with some limited degradation likely due to the increased reactivity of the conjugated products. Addition of the antioxidant butylated hydroxytoluene (BHT) to the product prevented coupling and degradation as shown in Figure 3.3b compared to the original PI trace (Figure 3.3a).

Table 3.2. Selected CPIs conjugated at 60 °C and $[Ru]/[C=C] = 1.6 \times 10^{-3a}$

Sample Designation[b]	Reaction Time (h)	Percent Conjugated[c] (%)	C=C $M_n{}^d$ (kg/mol)	PDI[d]
PI			50	1.05
CPI-4.4	44	6	42	1.20
CPI-17	160	20	48	1.08
CPI-30	400	31	44	1.11

[a]Concentration of polymer in benzene was 20% w/v, BHT was added to samples after conjugation to prevent coupling and degradation. [b]CPI = conjugated polyisoprene, the number following is the average number of E2 dienes per CPI molecule, calculated by ^{1}H NMR spectroscopy; M_n of PI = 25 kg/mol. [c]Of all the olefins along the polymer backbone, this is the percentage that are in conjugation as calculated by ^{1}H NMR spectroscopy. [d]Measured using SEC calibrated with polystyrene standards.
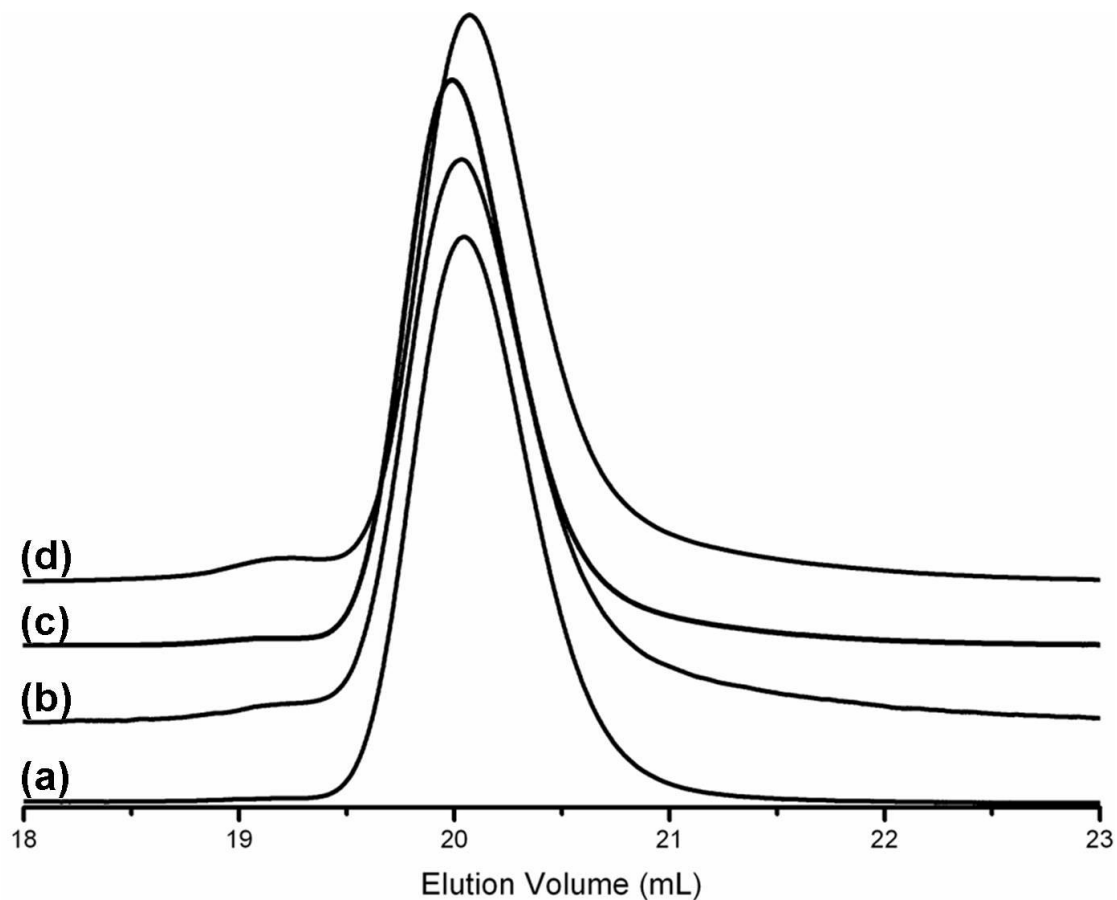
Figure 3.3. SEC elution curves of (a) PI, (b) CPI-4.4, (c) CPI-17, and (d) CPI-30. The SEC traces of the CPIs show little evidence of degradation or coupling (i.e. tailing and shoulders).

Analysis of the conjugation reaction products by proton ^{1}H NMR spectroscopy (Figure 3.4 and Figure 3.5) confirms the formation of both the intermediate bis-allylic protons (2.5–3.0 ppm) and the formation of the conjugated dienes (5.4–6.5 ppm). Other resonances at chemical shifts consistent with conjugated diene formation are also present as well as peaks corresponding to the original PI. Three major conjugated diene stereoisomers were identified (Figure 3.1): E1, E2, and Z2. The E2 and Z2 isomers make up the bulk of the conjugated dienes in nearly equal proportion, while the E1 isomer comprises the remaining 5–10% of the conjugated dienes. The distribution of conjugated diene isomers in CPI is different from that of CSQ due to differences in the content of the starting isomers of the isolated olefins present in each molecule. While the olefins of

squalene are all the *E* isomer (or *trans*) initially, the olefins of PI are a mixture of *E* and *Z* isomers (*trans* and *cis*) with approximately 40% of the initial olefins being the *E* isomer. During the conjugation reaction, the *Z* isomers isomerize to *E* isomers prior to conjugation, increasing the total number of *E* isomers in CPI as compared to the original PI.
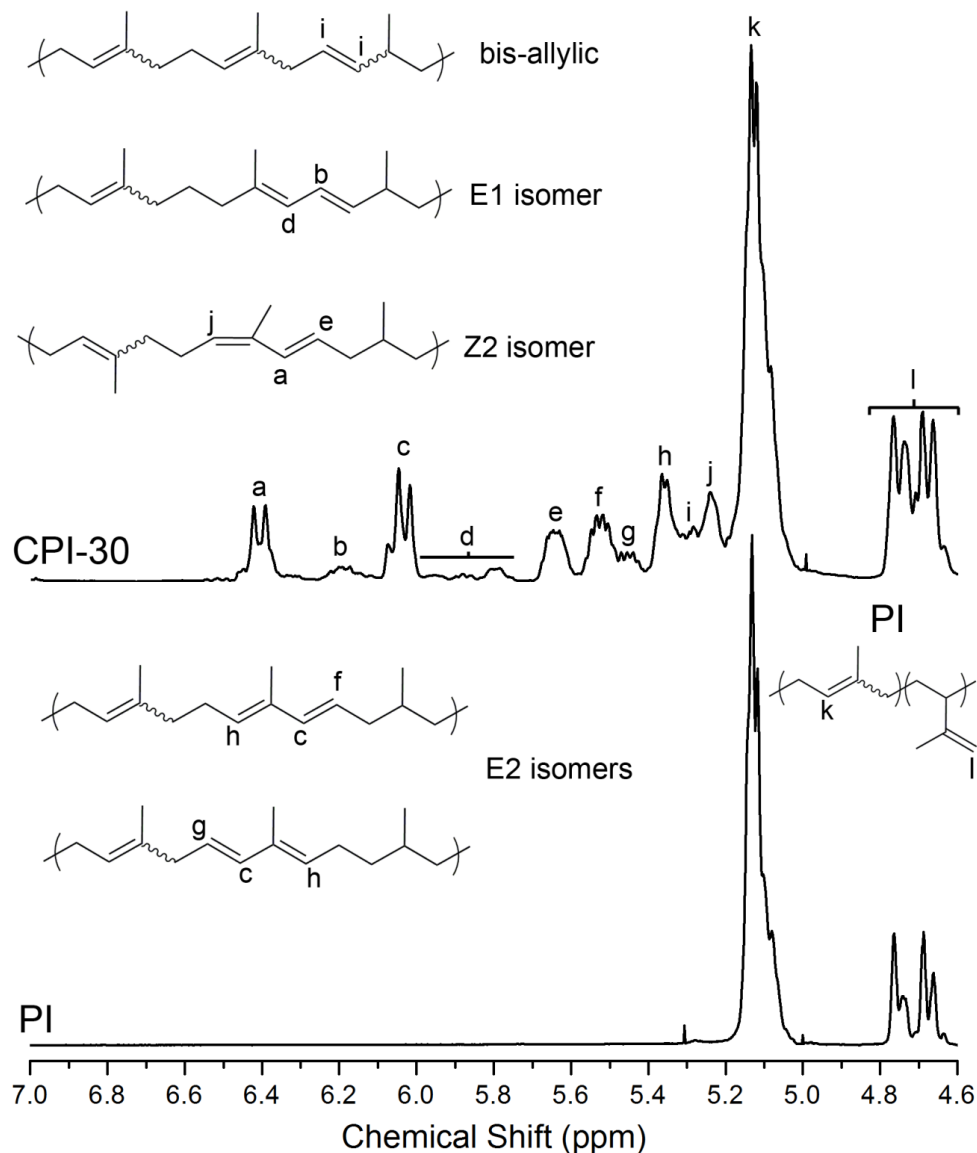
Figure 3.4. Detailed ¹HNMR spectra and peak assignments for CPI-30 and PI in the 7.0–4.6 ppm range (500 MHz, CDCl₃). Structures are given for the E1, E2, Z2, and bis-allylic structures. Peaks belonging to both the original PI polymer and CPI are present.
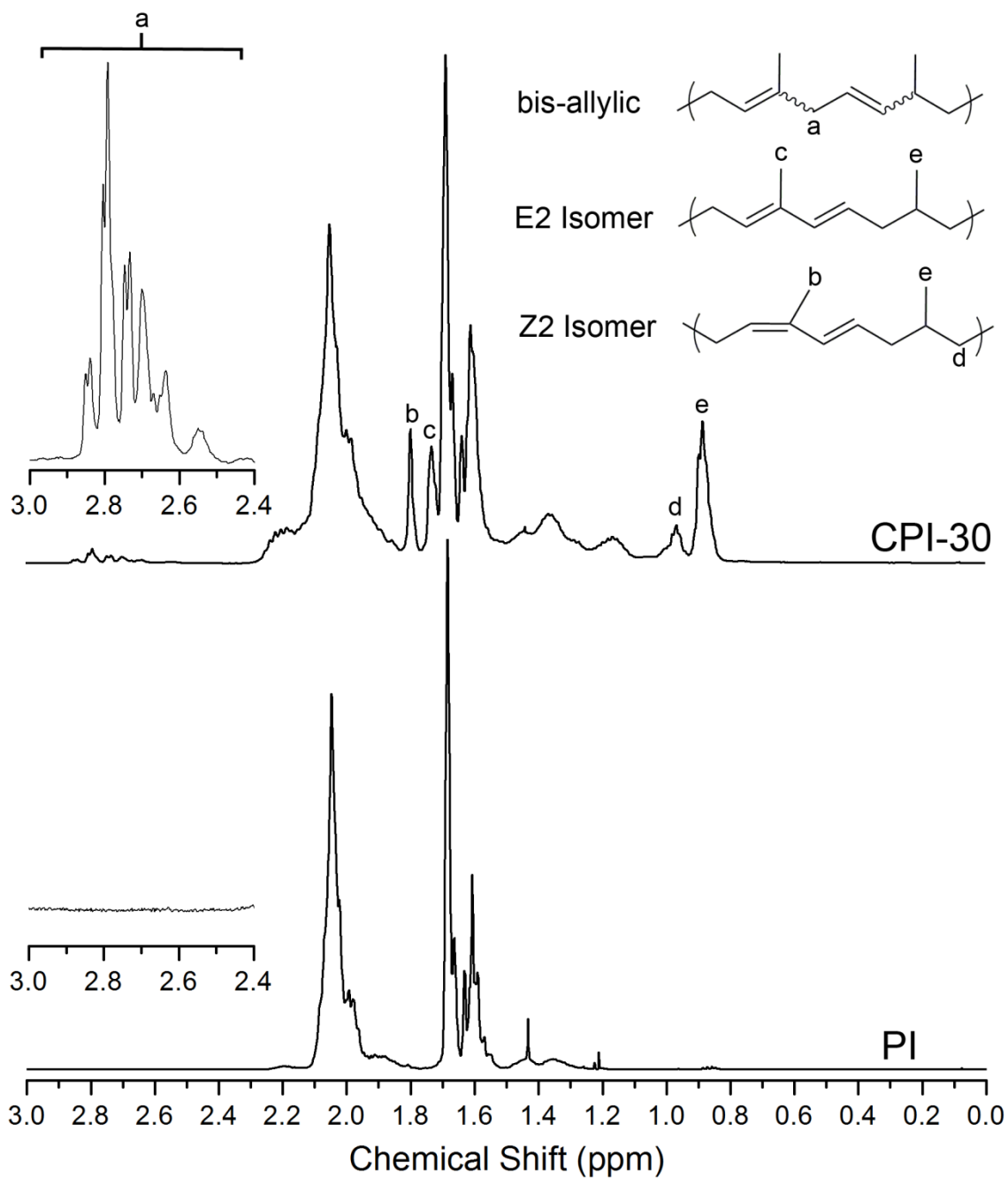
Figure 3.5. Detailed ^{1}HNMR spectrum and peak assignments for CPI-30 in the 3.0–0.0 ppm range (500 MHz, CDCl$_3$). The ^{1}H NMR spectrum of PI is included as a comparison.

Reaction time, temperature, and catalyst loading were varied to investigate the degree of conjugation attainable. The percent of carbon-carbon double bonds conjugated increased from 6 to 31% with the reaction time climbing from 44 to 400 h at 60 °C

(Table 3.2). The long times required for higher degrees of conjugation at 60 °C are likely due to the low catalyst loading (1.6×10^{-3} [Ru]/[C=C]). Typically, isomerization reactions on small molecules with $RuHCl(CO)(PPh_3)_3$ at similar temperatures and in solvent are performed at catalyst loadings ten times greater than used to conjugate PI and reach completion in a matter of hours.[28,38,39] In an effort to increase the reaction rate, catalyst loading was increased from 1.6×10^{-3} [Ru]/[C=C] to 4.9×10^{-3} [Ru]/[C=C] while keeping all other reaction conditions the same (benzene, 60 °C, 44 h). Once heated to 60 °C, the additional catalyst did not dissolve as evidenced by the solution being cloudy and brown. At the lower catalyst loadings, the fully soluble catalyst in solution at 60 °C is yellow. Analysis of the higher catalyst loading product indicates that the conversion of isolated olefins to conjugated dienes is 4%. The product synthesized at lower catalyst loading has 6% conversion of the isolated olefins into conjugated dienes. Presumably, the limited solubility of the catalyst in benzene leads to the similar conversions in both systems. The result also suggests that the benzene solution at 60 °C is saturated in catalyst around 1.6×10^{-3} [Ru]/[C=C] (4.0 mg catalyst/mL benzene) as an increase in conjugated dienes is expected (at 44 h) if more catalyst goes into solution.

Increasing reaction temperature (75–120 °C) in an effort to increase reaction rate gave mixed results. Generally, at each temperature investigated, as reaction time increases the percent of olefins that are conjugated dienes goes up (Figure 3.6a), but some variations exist for this trend. After 44 h of reaction, temperatures greater than 60 °C gave higher degrees of conjugation as compared to those values obtained at 60 °C. However, when the higher temperature reactions were run longer, the attainable degrees of conjugation remained similar to the values obtained at the shorter reaction times. Examples of this effect can be seen at 90 °C, where increasing the reaction time from 44 h to 160 h results in a slight increase in the percent conjugation (notably the level of conjugation is less than that at 160 h for the 60 °C sample). Similar effects are seen at 75 °C where increasing the reaction time from 160 h to 400 h results in a decrease in percent conjugation, less than that of 400 h reaction at 60 °C. Such data suggest that the catalyst deactivates over the course of the reaction.
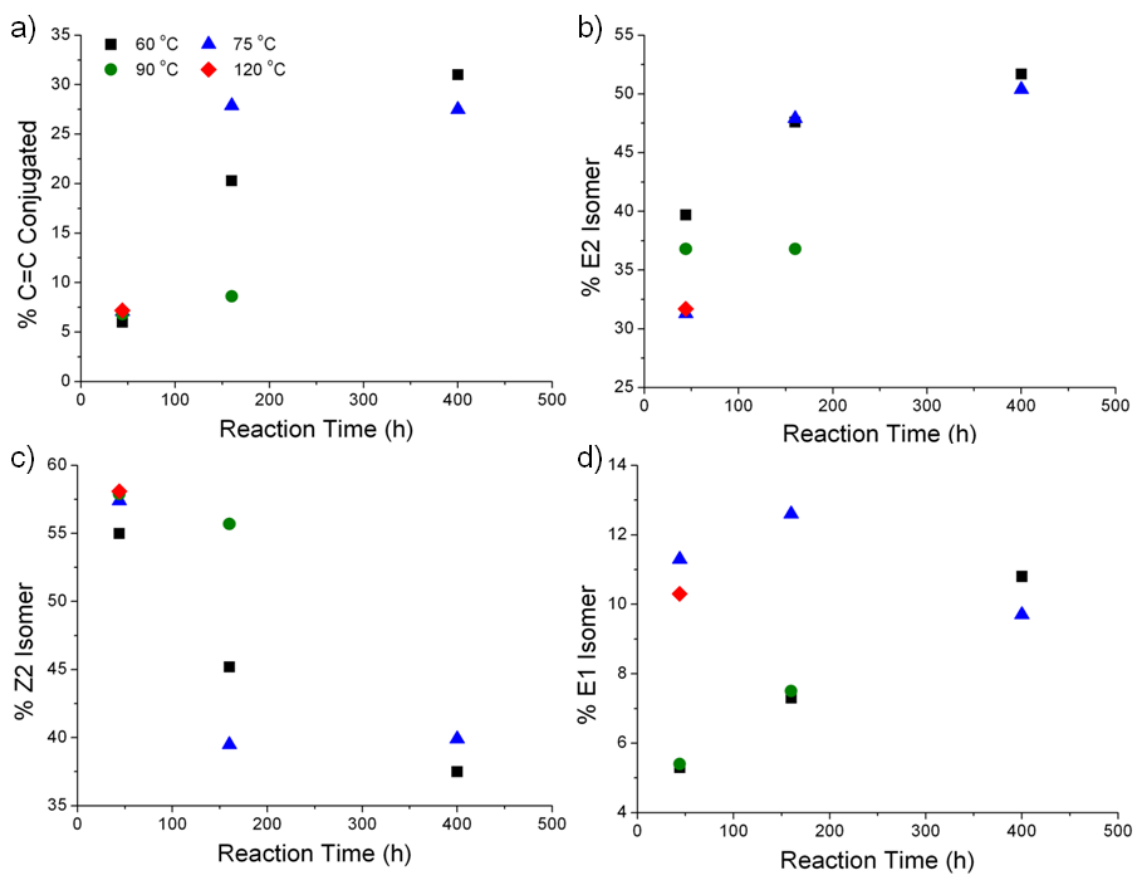
Figure 3.6. Plots of (a) % C=C conjugated and % of conjugated dienes as (b) E2 isomers, (c) Z2 isomers, and (d) E1 isomers as functions of time and temperature for PI reacting with $[Ru]/[C=C] = 1.6 \times 10^{-3}$. Values were calculated by ^{1}H NMR spectroscopy.

The exact cause for deactivation of the catalyst is unclear. Thermal degradation is unlikely as the RuHCl(CO)(PPh$_3$)$_3$ catalyst effectively conjugates vegetable oils at temperatures up to 210 °C in an inert atmosphere.[30,40] For the reactions performed at 90 and 120 °C, the color of the reaction mixture changed from yellow/orange to green over the course of the reaction. Also, small dark insoluble particles were observed in these solutions. The change in color and formation of solid precipitate corresponded with the decreased activity of the catalyst (i.e. lower conversion to conjugated double bonds). Such a color change is consistent with oxidized catalyst.[41,42] Although the reaction mixture was degassed, the degassing procedure may not have removed all the oxygen from the system. Another possible cause of the observed color change is that the Ru-H

species could have been converted to ruthenium alkyl, alkyl-alkene, or allylic complexes that may be insoluble in the solvent, supported by the observation of insoluble particles.[28,39] Such ruthenium species could be inactive at the temperatures investigated.[28,42] Thus, both explanations of the color change would be consistent with the deactivated catalyst behavior that was observed. Possibly increasing the reaction temperature further may result in the dormant ruthenium complexes activating once again, yielding faster rates of conjugation.

The isomer composition of the conjugated dienes changed with both reaction time and temperature. CPIs synthesized at reaction temperatures above 75 °C have a higher fraction of E1 isomers compared to those synthesized at 60 °C (Figure 3.6d), presumably due to the increased available energy to conjugate across the pendent methyl group along the backbone (Figure 3.1). As the reaction time is increased, the fraction of E2 isomers (Figure 3.6b) goes up while the fraction of the Z2 isomer decreases (Figure 3.6c), suggesting that *Z* isomers are being isomerized to *E* isomers. Such results are consistent with the major isomer observed at short reaction times being Z2 while at longer times it is E2. As previously stated, the $RuHCl(CO)(PPh_3)_3$ catalyst prefers to isomerize double bonds to the *E* configuration. Initially, the majority of carbon-carbon double bonds in PI are the *Z* isomer, allowing for the initial conjugated dienes to be the Z2 isomer with just one double bond migrating. Over time, the carbon-carbon double bonds will be isomerized to the *E* configuration prior conjugation, resulting in a higher concentration of E2 isomer in the final product at longer reaction times.

3.3.3 Conjugation of polycyclooctadiene

PCOD was conjugated following the procedure used for both squalene and PI to investigate the utility of the chemistry. Two conjugated PCOD (CPCOD) samples were synthesized as comparisons to the CPI samples. The most notable result is, with all aspects of the reaction being equal, the conversion of isolated olefins to conjugated dienes is greater when the parent polymer is PCOD as compared to PI (Table 3.3). Under the reaction conditions 60 °C and 44 h reaction time, CPI-4.4 has 6% of its olefins as conjugated dienes while CPCOD-12 has 32%. The apparent increase in catalyst reactivity

toward PCOD compared to PI is likely due to the different chemical structures of the two polymers. The pendant methyl group along the backbone of PI imparts steric hindrance to the coordination of the Ru catalyst, generating a thermodynamic barrier to the catalyst's activation.[43] PCOD does not have such a barrier as it has no pendant groups; consequently, it is more reactive than PI.

Table 3.3. PCOD conjugated at $[Ru]/[C=C] = 1.6 \times 10^{-3}$ catalyst loading.[a]

Sample Designation[b]	Reaction Temperature (°C)	Reaction Time (h)	Percent C=C Conjugated (%)[c]	M_n (kg/mol)[d]	PDI[d]
PCOD				10	1.79
CPCOD-12	60	44	32	14	1.79
CPCOD-23	75	160	61	15	2.19

[a]Concentration of polymer in benzene was 20% w/v, BHT was added to samples after conjugation to prevent coupling and degradation. [b]Sample designation CPCOD-### where ### indicates the number of *E,E* conjugated dienes per polymer chain. [c]Calculated from ^{1}H NMR spectroscopy. [d]Calculated from SEC calibrated with polystyrene standards.

Analysis of the ^{1}H NMR spectrum of CPCOD (Figure 3.7b) indicates the presence of two major conjugated diene isomers − *E,Z* and *E,E*. As a consequence of the original PCOD primarily containing *E* olefins and the catalyst preferring to isomerize to the *E* olefin, a majority of the conjugated dienes of CPCOD are the *E,E* isomer. Peaks in the CPCOD ^{1}H NMR spectrum at 6.05–6.20 and 6.30–6.60 ppm ranges are consistent with protons existing in conjugated systems of more than two carbon-carbon double bonds.[44,45,46,47] Such multiple conjugated double bond systems are short enough so that the CPCOD products remained colorless. The ability of CPCOD to form larger conjugated systems as compared to the isolated dienes of CPI likely is due to the increased reactivity of PCOD and lack of pendant methyl groups that act as a barrier for double bond migration in PI.
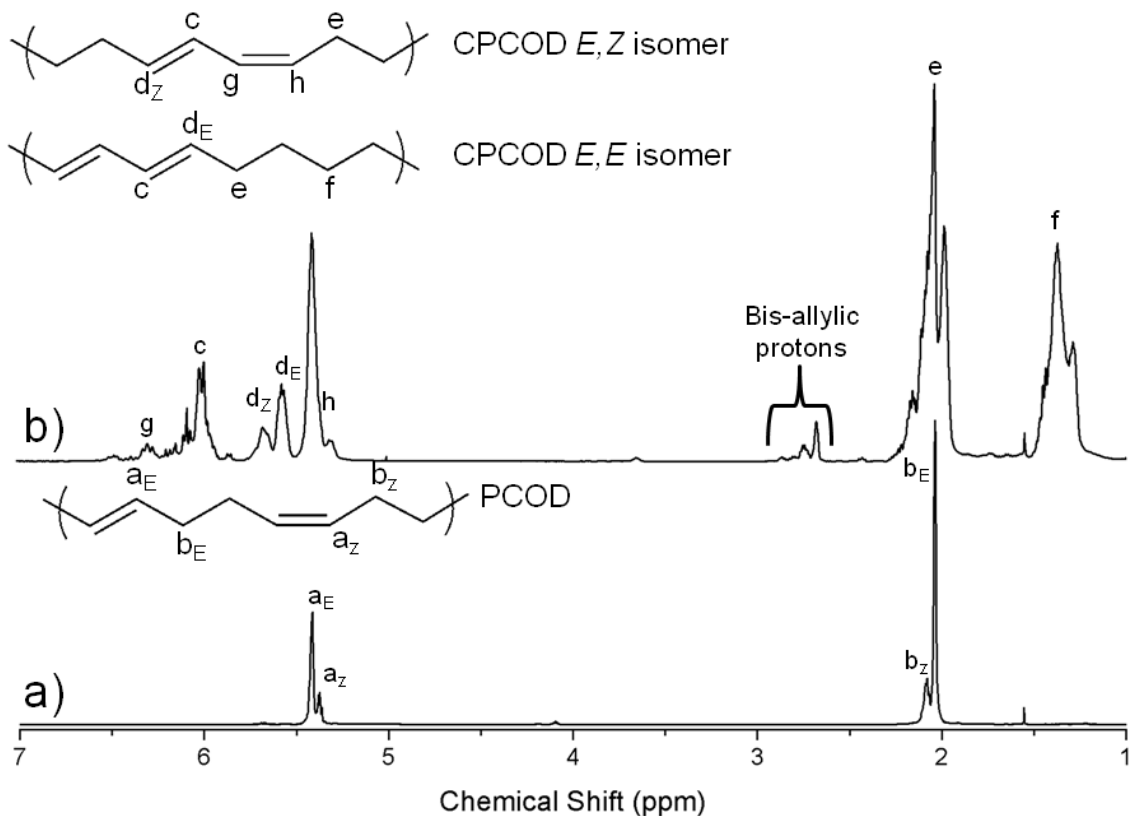
Figure 3.7. ^{1}H NMR spectra with peak assignments for (a) PCOD and (b) CPCOD-23 (500 MHz, CDCl$_3$). The chemical structures for the two most common conjugated diene isomers present in CPCOD are given. The appearance of new peaks in the CPCOD indicates the formation of conjugated dienes.

SEC elution curves of the CPCOD (Figure 3.8) differ somewhat from the original PCOD chromatogram as the CPCOD curves are shifted to lower elution volume (higher molecular weight). The larger measured molecular weight may be due to CPCOD radical chain coupling during the conjugation reaction or change in the hydrodynamic radius due to the conjugation. Both CPCOD-12 and CPCOD-23 have a similar increase in molecular weight (Table 3.3), suggesting that the increase is inherit to the conjugation process and independent of conjugation time and temperature.
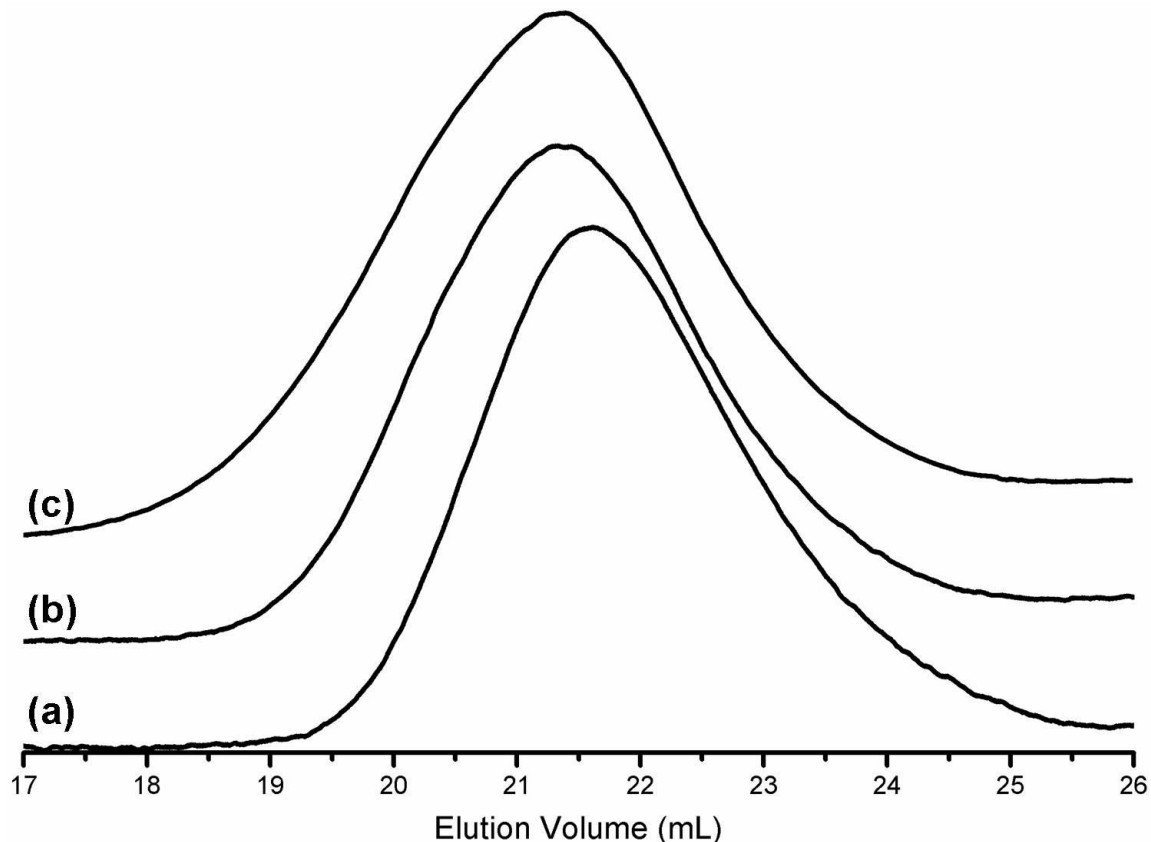
Figure 3.8. SEC elution curves of (a) PCOD, (b) CPCOD-12, and (c) CPCOD-23. The CPCOD samples shift slightly to lower elution volume, indicating an increase in the calculated molecular weight calibrated with polystyrene standards.

3.3.4 Thermal behavior of conjugated polydienes

The glass transition temperature (T_g) of the CPIs increases with higher degrees of conjugation (Figure 3.9). The higher T_g values are an indication of stiffening of the polymer chain due to the introduction of the more rigid conjugated diene systems and saturated portions (polyethylene-*alt*-polypropylene) with T_g values similar to PI.[48,49,50] Similarly, the T_g of CPCOD was higher than that of the original PCOD (Figure 3.10). The PCOD is semicrystalline as indicated by the multiple melting transition temperatures (T_m) in the thermogram. In the CPCOD, the relative intensity of the melting transition decreased as well as the T_m. The decrease in relative intensity of the melting endotherm suggests that the conjugated dienes impede the ability of CPCOD chains to crystallize

and shorten the segments of the polymer chain that are able to crystallize, reducing the T_m. The decreased crystallinity of the CPCOD was further evidenced by the observed properties of the polymer. The original PCOD was a waxy solid at room temperature while the CPCOD was a viscous liquid.
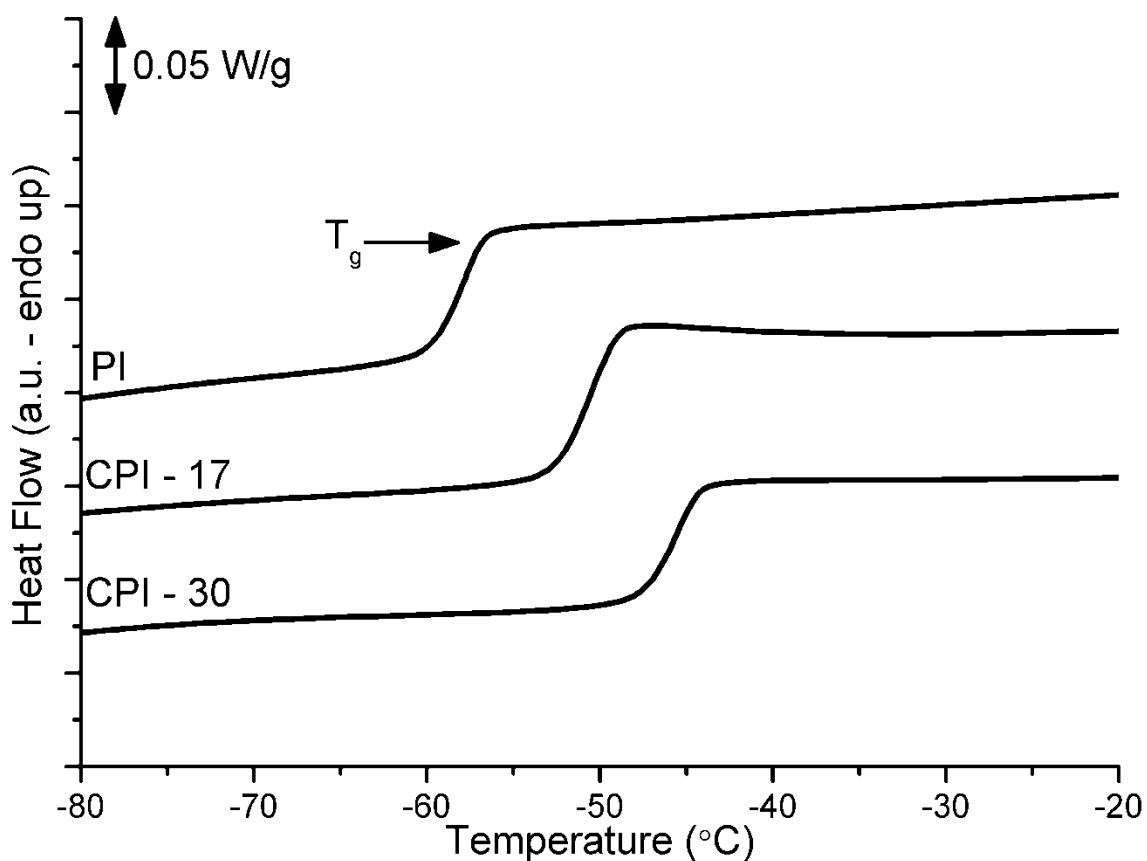
Figure 3.9. Normalized DSC thermograms of original PI and select CPIs. The thermal transitions are labeled. The T_g increases with the degree of conjugation.
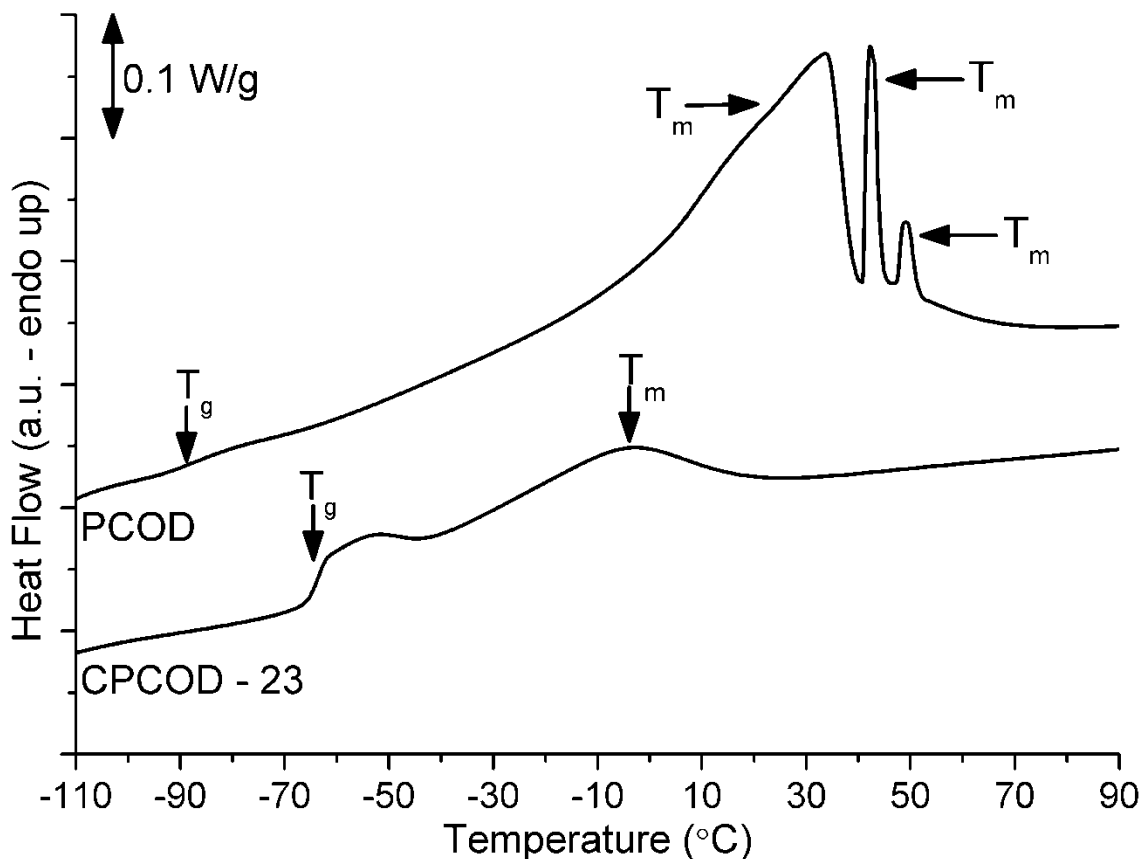
Figure 3.10. Normalized DSC thermograms of PCOD and CPCOD-23. The thermal transitions are labeled. The DSC curve of PCOD has a slight glass transition and strong melting endotherms. The CPCOD-23 curve has a higher T_g and a lower T_m.

3.3.5 Diels–Alder Reactions with CPI

To functionalize PI post conjugation, we investigated the reactions of small molecule dienophiles (R) and macromolecular end-functionalized PLLA with select CPIs. To probe the susceptibility of the CPI to a Diels–Alder reaction, the small molecules we studied varied in "dienophilicity" (Table 3.4). Analysis of the reaction products by ^{1}H NMR spectroscopy suggests that the E2 isomer is the preferred conjugated diene to undergo a Diels–Alder reaction with dienophile as its conversion (X_{E2}) is significantly greater than that of the other diene isomers for the blends investigated (Table 3.4). Dienophiles prefer to react with the E2 isomer of CPI over the other major isomers due steric hindrance in the reaction site when the conjugated diene

adopts the correct s-*cis* conformation for the Diels–Alder addition (Figure 3.11).[51] When the Z2 isomer adopts the correct conformation, the polymer chain protrudes into the reaction site, providing a steric barrier to reaction. Likewise, the E1 isomer in the correct conformation has a steric penalty to reaction due to the methyl group present in the reaction site. Since the methyl group of the E1 isomer is less steric hindering than the polymer chain of the Z2 isomer, less hindrance to reaction is present. Consequently, the conversion of the E1 isomer (X_{E1}) is typically greater than that of the Z2 isomer (X_{Z2}), reflecting the difference in steric hindrance (Table 3.4).

Table 3.4. Reaction conditions and results of small molecule reactions with CPI-30.

R^a	$[R]/[E2]^b$	T_r^c (°C)	t_r^d (h)	X_{E2}^e (%)	X_{Z2}^f (%)	X_{E1}^g (%)	Grafts per Polymer[h]	M_n^i (kg/mol)	PDI^i
HEMI	1.0	110	20	95	0^h	22	30	49	1.23
MA	1.1	110	20	100	6	34	33	44	1.16
HEA	1.0	160	111	83	7	19	26	40	1.24
HEMA	1.0	160	111	52	12	0	8	29	1.38

[a]Small molecule to be grafted to polymer; HEMI = N-2-hydroxyethyl maleimide, MA = maleic anhydride, HEA = 2-hydroxyethyl acrylate, HEMA = 2-hydroxyethyl methacrylate. [b]Ratio of moles of small molecule (R) to moles of E2 CPI isomer. [c]Couplingreaction temperature. [d]Coupling reaction time. [e]Conversion of E2 isomer in CPI, found from ^{1}H NMR spectroscopy. [f]Conversion of Z2 isomer in CPI, found from ^{1}H NMR spectroscopy. Note: negative value gives an estimate in the error associated with the calculation as the conversion should not be a negative number. [g]Conversion of E1 isomer in CPI, found from ^{1}H NMR spectroscopy. [h]Number of small molecule grafts to polymer, found from ^{1}H NMR spectroscopy. [i]Calculated from SEC calibrated by polystyrene standards. [h]The calculated value of X_{Z2} for the HEMI reaction was less than zero (-4%) which is not physically possible. Likely, the X_{Z2} is close to zero and the less than zero value is indicative of the error present when calculating the conversions using ^{1}H NMR spectroscopy.
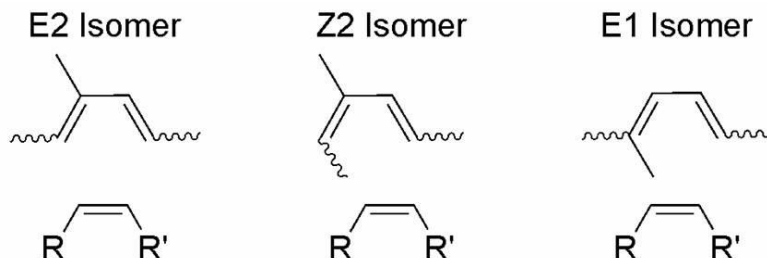
Figure 3.11. Conformations of CPI isomers required for Diels–Alder cycloaddition of small molecules. Dienophile is represented by olefin with generic R and R′ groups.

Both *N*-2-hydroxyethylmaleimide (HEMI) and maleic anhydride (MA) coupled with CPI-30 to near completion in 20 h (110 °C) when loaded at a [HEMI or MA]/[E2] = 1. The formation of new peaks in the[1]H NMR spectra of the HEMI (Figure 3.12) and MA (Figure 3.13) reaction products with CPI-30 is consistent with HEMI and MA grafting to CPI-30 to give CPI-*g*-HEMI and CPI-*g*-MA respectively. SEC analysis of the grafted products (Figure 3.14b and c) indicates that grafting at 110 °C does not significantly change the molecular weight distribution of the product compared to the original CPI. The broadening of the product curves as compared to the original CPI-30 trace is likely a result of some polymer degradation and coupling, likely through a radical mechanism.
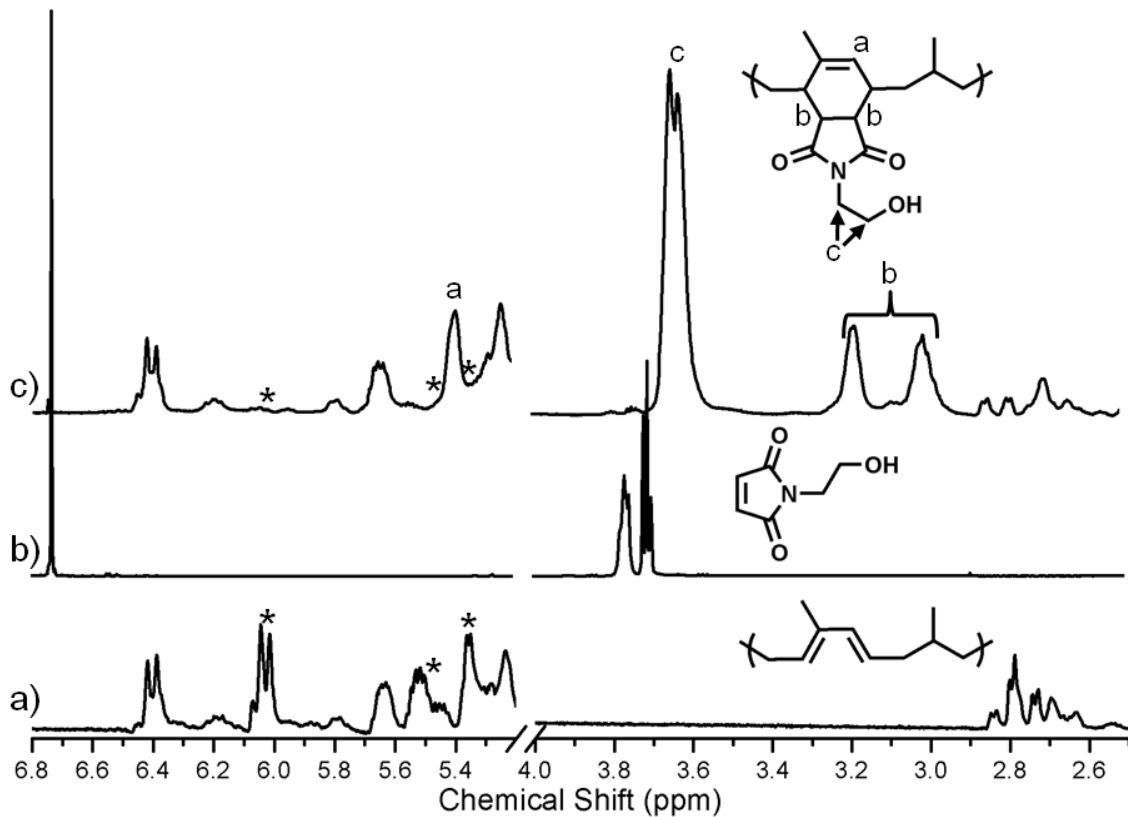
Figure 3.12. Expanded ^{1}H NMR spectra of (a) CPI-30, (b) HEMI, and (c) CPI-*g*-HEMI (500 MHz, CDCl$_3$). Asterisks indicate peaks associated with the E2 isomer of CPI in the starting material and final product. The generation of new peaks in the CPI-*g*-HEMI spectrum as compared to the spectra of the reactants is consistent with the coupling of HEMI and CPI-30.
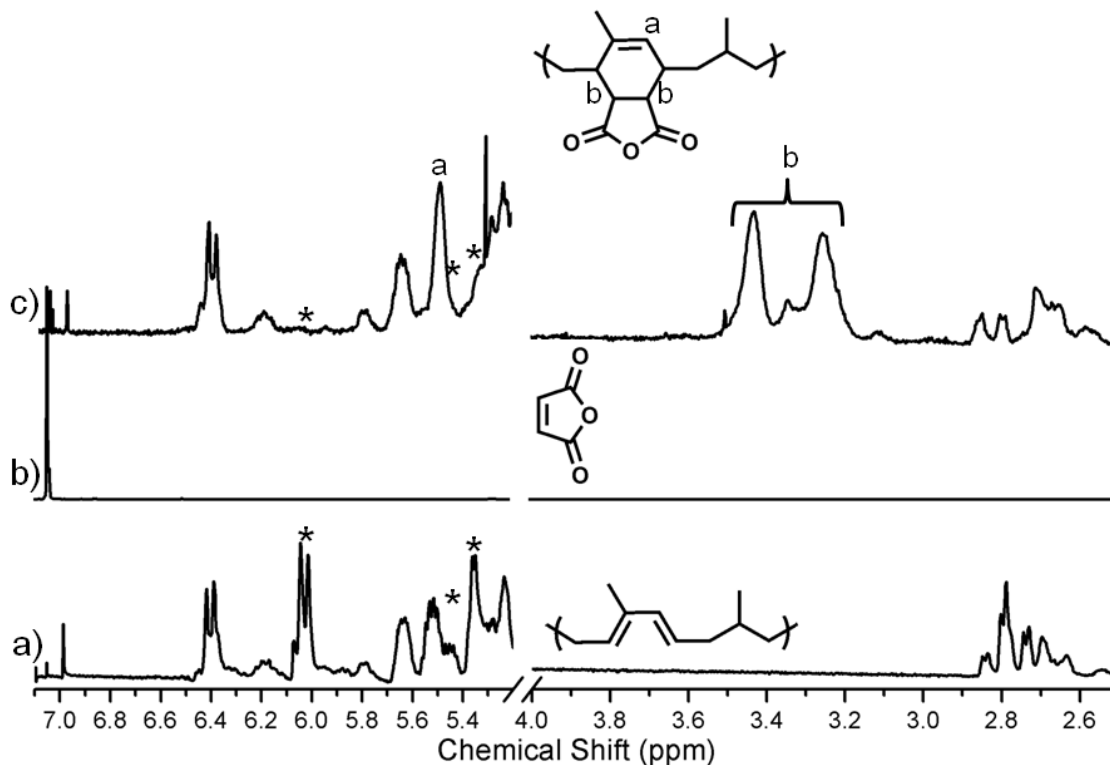
Figure 3.13. Expanded ¹H NMR spectra of (a) CPI-30, (b) MA, and (c) CPI-*g*-MA (500 MHz, CDCl₃). Asterisks indicate peaks associated with the E2 isomer of CPI in the starting material and final product. The generation of new peaks in the CPI-*g*-MA spectrum as compared to the spectra of the reactants is consistent with the coupling of MA and CPI-30.
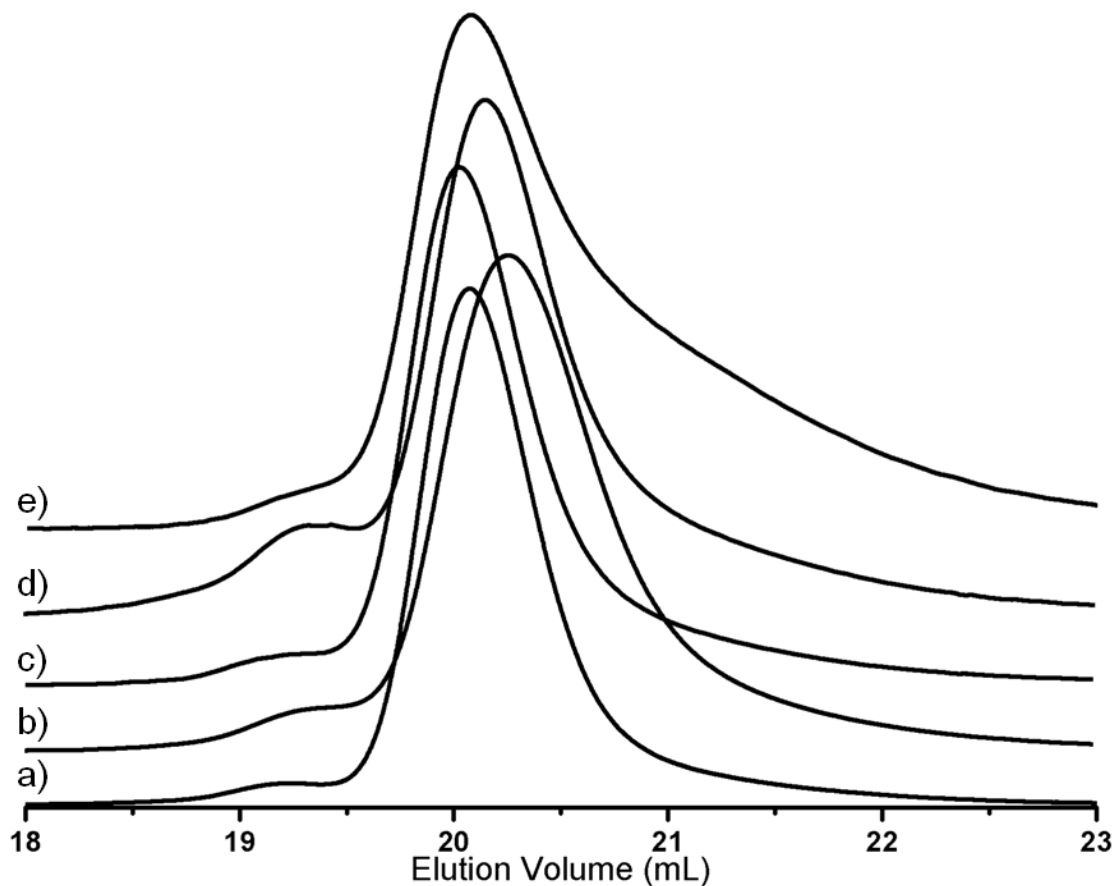
Figure 3.14. SEC elution curves of (a) CPI-30, (b) CPI-*g*-HEMI, (c) CPI-*g*-MA, (d) CPI-*g*-HEA, and (e) CPI-*g*-HEMA. Shoulders and tailing off the main peaks of CPI-*g*-HEA and CPI-*g*-HEMA indicate coupling and degradation respectively.

Under similar reaction conditions to the HEMI and MA blends, the poorer dienophiles vinyl acetate (VA), 2-hydroxyethyl acrylate (HEA), 2-hydroxyethyl methacrylate (HEMA), and 1-vinyl-2-pyrrolidone (V2P) did not graft onto the CPI backbone. By increasing the reaction temperature to 160 °C and time to 111 h, HEA and HEMA reacted with the E2 isomer to form CPI-*g*-HEA (Figure 3.15) and CPI-*g*-HEMA (Figure 3.16), respectively. The apparent decrease in reactivity of HEMA compared to HEA as evidenced by the degree that each coupled to CPI-30 is likely due to the extra methyl group of HEMA increasing the bulkiness of the molecule. VA and V2P still did not react with CPI at 160 °C for 115 h, presumably due to the electron donating groups present in each molecule.[51] Increasing the reaction time and temperature allowed for

HEMA and HEA to graft, but consequently the PDI of the CPI broadened and the M_n decreased significantly. SEC traces of the products (Figure 3.14d and e) have features that are both consistent with CPI degradation and coupling caused by thermally induced free radical reactions.
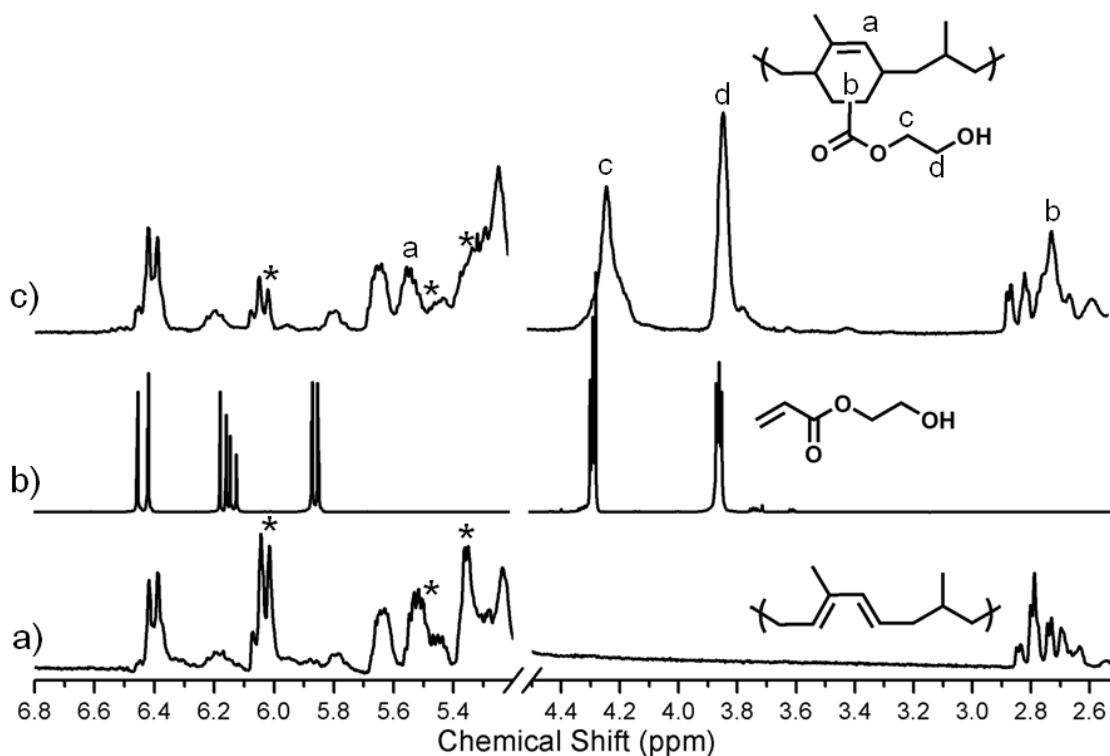
Figure 3.15. Expanded ^{1}H NMR spectra of (a) CPI-30, (b) HEA, and (c) CPI-*g*-HEA (500 MHz, CDCl$_3$). Asterisks indicate peaks associated with the E2 isomer of CPI in the starting material and final product. The generation of new peaks in the CPI-*g*-HEA spectrum as compared to the spectra of the reactants is consistent with the coupling of HEA and CPI-30.
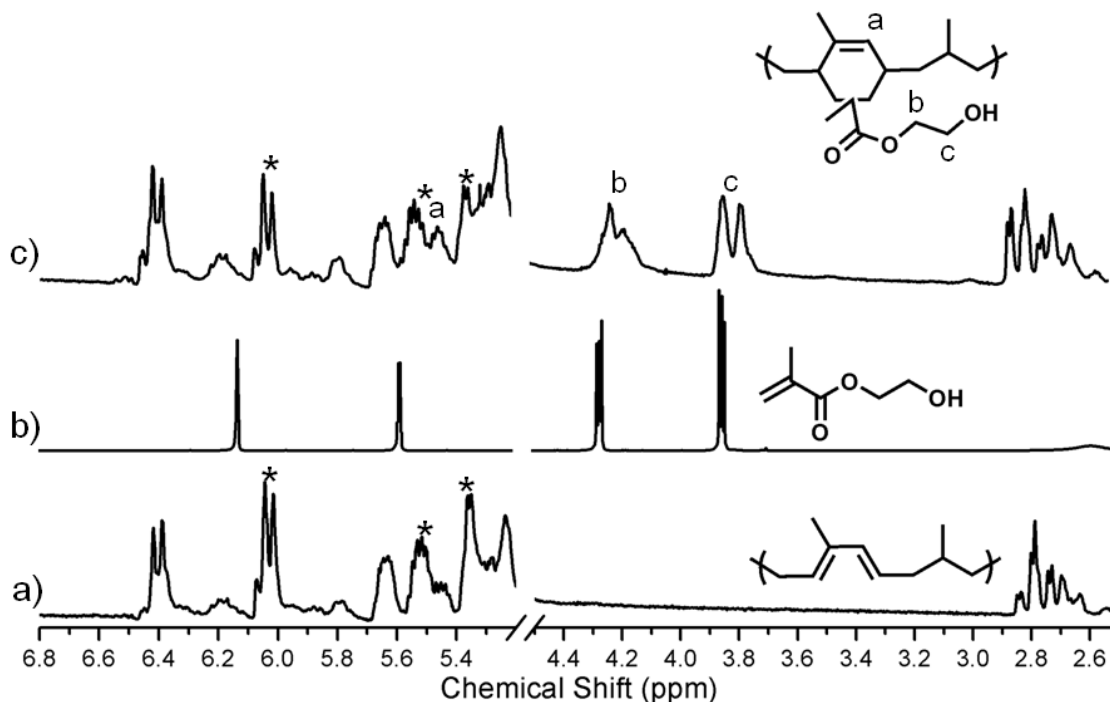
Figure 3.16. Expanded ^{1}H NMR spectra of (a) CPI-30, (b) HEMA, and (c) CPI-*g*-HEMA (500 MHz, CDCl$_3$). Asterisks indicate peaks associated with the E2 isomer of CPI in the starting material and final product. The generation of new peaks in the CPI-*g*-HEMA spectrum as compared to the spectra of the reactants is consistent with the coupling of HEMA and CPI-30.

Control blends of the small molecules in Table 3.4 with PI were synthesized under the same reaction conditions discussed above for blends with CPI. Both HEMI and MA blends with PI at 110 °C for 20 h show no signs of reaction with PI, confirming that coupling of HEMI and MA to CPI proceeds through the Diels–Alder reaction mechanism only under the conditions tested. Blends of HEA and HEMA with PI at 160 °C resulted in the apparent grafting of HEA and HEMA to PI. Peaks in the PI/HEA and PI/HEMA ^{1}H NMR spectra correspond to HEA and HEMA coupled to PI (see 4.4–3.8 ppm region in Figure 3.15 and Figure 3.16). Since no conjugated dienes exist in PI, the small molecules presumably couple through a free radical mechanism. For the HEA/PI reaction 5 HEA grafts per chain are present as compared to 26 grafts per chain for the HEA/CPI reaction. The HEMA/PI product has one graft per chain while the HEMA/CPI product has 8 grafts per chain. The reduced number of grafts for the PI reactions as compared to the CPI

reactions suggests that primarily HEA and HEMA react with CPI through a Diels–Alder mechanism as well as possible coupling reactions occurring through a free radical mechanism.

3.3.6 Diels–Alder Reactions with CPCOD

Given the successful grafting to CPI, HEMI and MA were reacted with CPCOD-23 in a manner similar to reactions with CPI-30 (Table 3.5). The CPCOD reacts with both HEMI and MA by a Diels–Alder mechanism as indicated by the generation of new peaks in their respective ^{1}H NMR spectra (Figure 3.17) consistent with the formation of Diels–Alder products. Like the E2 isomer of CPI, the *E,E* isomer of CPCOD is more reactive as compared to the *E,Z* isomer of CPCOD as demonstrated by the conversion of the *E,E* isomer (X_E) being significantly greater than that of the *E,Z* isomer (X_Z) for both HEMI and MA. Similar to the isomer preference in CPI, the higher reactivity of the *E,E* isomer in CPCOD towards dienophiles is due to the steric hindrance present in the *E,Z* isomer when adopting the correct conformation for reaction. Much like the CPI coupling reactions, the SEC elution curves of the CPCOD-*g*-HEMI and CPCOD-*g*-MA products (Figure 3.18) do not differ greatly from that of the starting material. The similar behaviors of CPCOD and CPI towards Diels–Alder reactions with dienophiles suggest that such behavior would occur with other likewise conjugated polymers and good dienophiles.

Table 3.5. Small molecule reactions with CPCOD-23 at 110 °C.

R^a	$[R]/[E]^b$	$X_E{}^c$ (%)	$X_Z{}^d$ (%)	Grafts per Polymer[e]	$M_n{}^f$ (kg/mol)	PDI[f]
HEMI	0.8	75	5	16	19	2.23
MA	0.7	71	6	12	17	2.28

[a]Small molecule coupled to CPCOD. [b]Ratio of moles of small molecule (R) per moles of *E,E* isomer in CPCOD. [c]Conversion of *E,E* isomer in CPCOD, found by ^{1}H NMR spectroscopy. [d]Conversion of *E,Z* isomer in CPCOD, found by ^{1}H NMR spectroscopy. [e]Number of grafts of small molecule per polymer chain, found by ^{1}HNMR spectroscopy. [f]Found from SEC elution curves calibrated with polystyrene standards. Original CPCOD-23 had $M_n = 15$ kg/mol and PDI = 2.19.
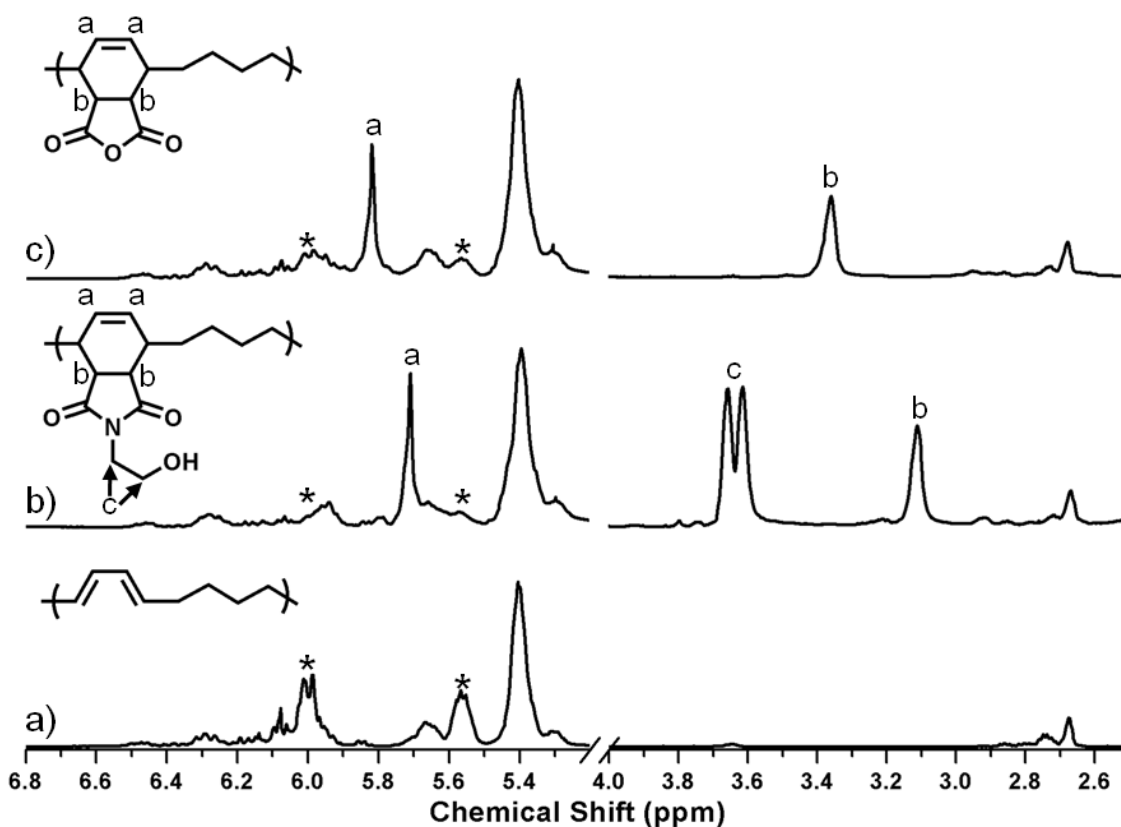
Figure 3.17. Expanded ^{1}H NMR spectra of (a) CPCOD-23, (b) CPCOD-*g*-HEMI, and (c) CPCOD-*g*-MA (500 MHz, CDCl₃). Peaks associated with the *E,E* isomer of CPCOD-23 are marked with asterisks and decrease in relative intensity when reacted with dienophiles. Structures are given for the *E,E* isomer reaction product with MA and HEMI with the new peaks present in the product ^{1}H NMR spectrum appropriately labeled.
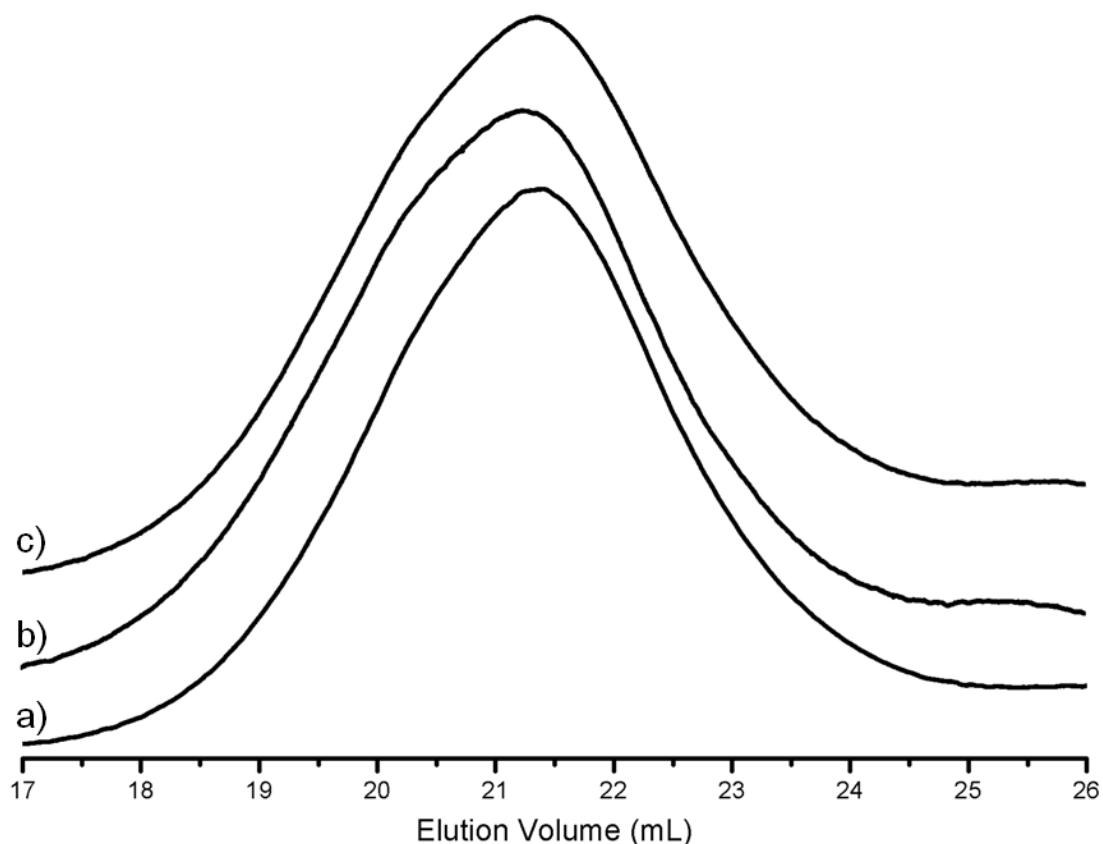
Figure 3.18. SEC elution curves of (a) CPCOD-23, (b) CPCOD-*g*-HEMI, and (c) CPCOD-*g*-MA. The SEC elution curves of the coupled products do not differ greatly from the initial CPCOD.

3.3.7 CPI coupling with end-functionalized polylactide

The reactivity of CPI was explored further by coupling it with HEMI end-functionalized poly(L-lactide) (HEMI-PLLA) in solution. CPI-17 and HEMI-PLLA (67 kg/mol) were coupled following the same reaction conditions (110 °C, toluene) as used for the HEMI/CPI blends. The composition of the reaction mixture allowed for a 2.4 molar excess of E2 dienes compared to HEMI end-groups. ^{1}H NMR spectroscopic analysis, as with the small molecule reactions, confirmed that HEMI-PLLA reacts primarily with the E2 isomer of CPI. The reaction rate, under the conditions investigated, is significantly slower for the HEMI-PLLA reaction than for the HEMI reaction. After 136 h of heating, 92% of the HEMI end-groups reacted (43% conversion of the E2

isomers) as opposed to the complete conversion of HEMI in 20 h. The difference in apparent rates of reaction is that the HEMI-PLLA coupling reaction had a reactive group concentration 40 times less than the HEMI reaction. The solubility in toluene and molecular weight of HEMI-PLLA limits the maximum concentration of reactive end groups attainable, hence the lower concentration. The steric hindrance caused by having a bulky PLA chain may have attributed to the slower reaction rate as well.

Even though the reaction was slow and did not reach completion, graft copolymer (CPI-*g*-PLLA) was formed as evidenced by a shift to lower elution volume in the SEC elution curve of the product compared to the starting materials. A control reaction of PI and HEMI-PLLA under the same conditions does not couple, confirming that the Diels–Alder reaction between HEMI-PLLA and CPI is responsible for the graft copolymer formation. Compared to the starting materials, the molecular weight (from SEC) of the graft copolymer increased to 250 kg/mol and the distribution broadened to give a PDI of 1.51. A small lower molecular weight peak at 19 min in the CPI-*g*-PLLA trace corresponds to unreacted HEMI-PLLA. The remaining HEMI-PLLA underscores the difficulties that arise from synthesizing graft copolymers using a "grafting to" approach where unreacted homopolymers can linger that will affect the purity of the final product. The reaction between HEMI-PLLA and CPI demonstrates the reactivity of CPI towards end-functionalized polymers, but to synthesize pure polylactide graft copolymer, a "grafting from" approach is ideal.
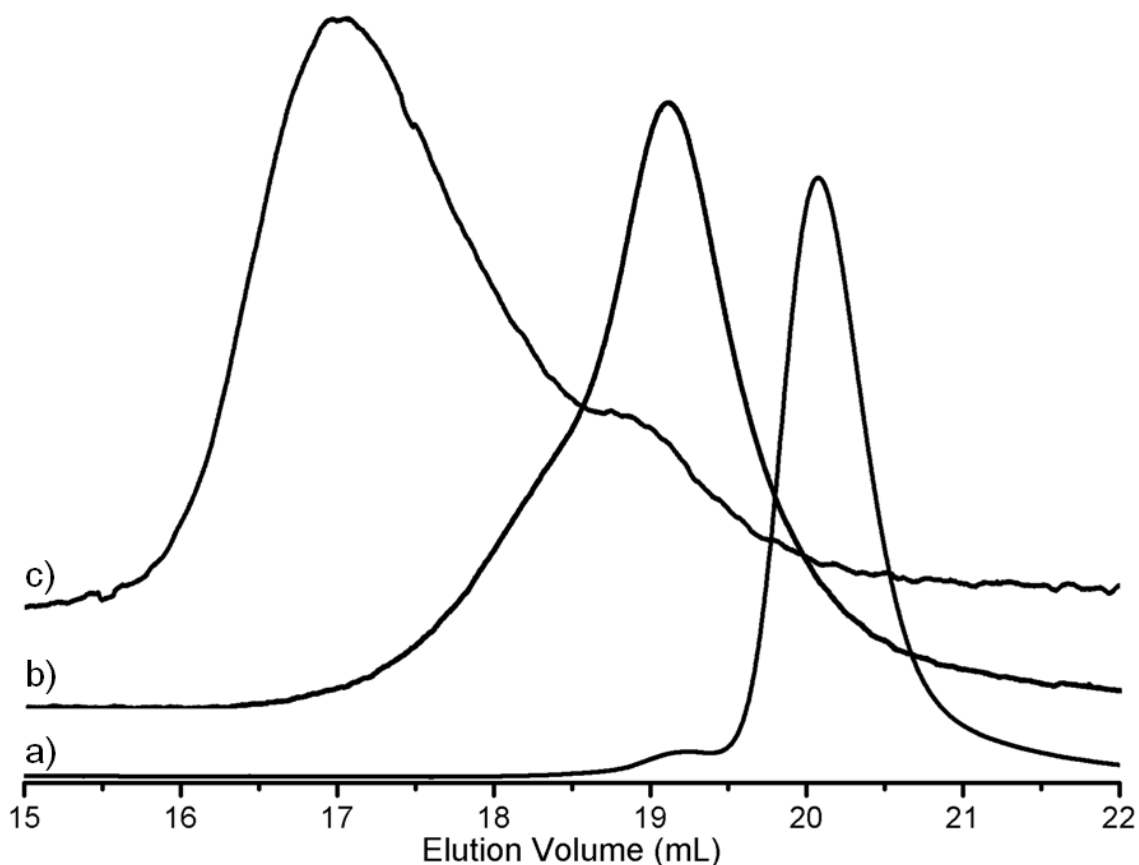
Figure 3.19. SEC elution curves of (a) CPI-30, (b) HEMI-PLLA, and (c) CPI-*g*-PLLA. The HEMI-PLLA used had a M_n equal to 67 kg/mol (^{1}H NMR spectroscopy) and a PDI of 1.24 (SEC). The CPI-*g*-PLLA shifts to lower elution volume consistent with graft copolymer formation.

3.3.8 Synthesis of CPI-*g*-PLLA

CPI-17 functionalized with 19 HEMI molecules was used as the macroinitiator for CPI-*g*-PLLA synthesis with a target of 95 wt % PLLA. Three widely used lactide polymerization catalysts were investigated: tin(II) octoate (Sn(Oct)$_2$), 1,5,7-triazabicyclo[4.4.0]dec-5-ene (TBD), and AlEt$_3$. The AlEt$_3$ polymerization led to a product with a multimodal SEC distribution (Figure 3.20b) and low conversion. Conversely, the Sn(Oct)$_2$ and TBD catalyzed reactions produced graft copolymers with monomodal distributions (Figure 3.20c and d) and PDI values of 1.08 and 1.11, respectively. The shift to lower elution volume in the SEC traces is consistent with graft

copolymer formation. A small broad peak exists in the SEC trace of the $Sn(Oct)_2$ synthesized CPI-*g*-PLLA which may correspond to a low level of PLLA homopolymer. In both the SEC traces for the $Sn(Oct)_2$ and TBD catalyzed polymerizations, the peak associated with the macroinitiator is absent, suggesting that all or nearly all of the macroinitiator reacted.
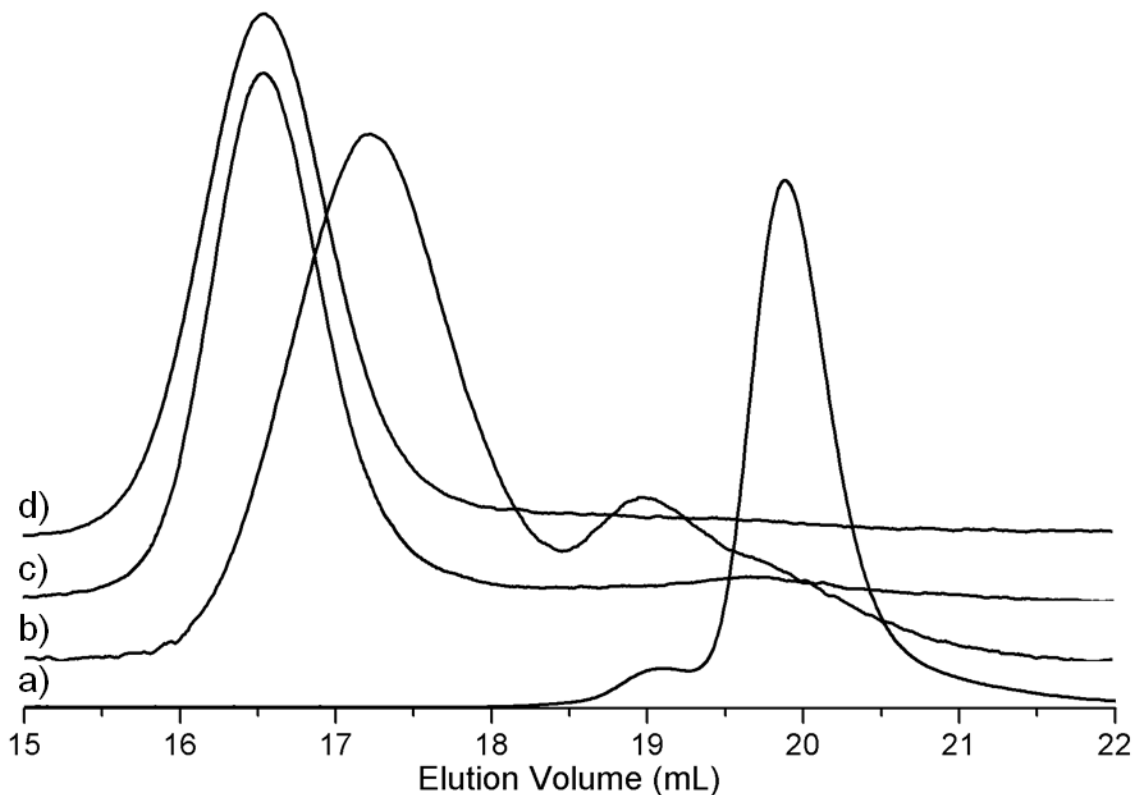
Figure 3.20. SEC elution curves of (a) CPI-*g*-HEMI macroinitiator and CPI-*g*-PLLA synthesized using (b) $AlEt_3$, (c) $Sn(Oct)_2$, and (d) TBD catalysts respectively. All CPI-*g*-PLLA products shifted to lower elution volume, consistent with the formation of graft copolymers.

^{1}H NMR spectroscopy confirms the synthesis of CPI-*g*-PLLA (Figure 3.21) from CPI-*g*-HEMI. Peaks associated with the methylene protons of HEMI grafted from CPI (Figure 3.21a) shift downfield with the formation of PLLA. Peaks consistent with the PLLA end groups (4.4 ppm and 2.6 ppm) as well as the PLLA repeat units appeared, verifying the formation of PLLA. The integration ratios of the HEMI and PLLA end groups agree with expectations for graft copolymer formation and complete initiation.

The M_n of the individual PLLA grafts were calculated by end group analysis from the ^{1}H NMR spectrum to be 22 kg/mol and 26 kg/mol for the $Sn(Oct)_2$ and TBD catalyzed polymerizations respectively. Considering the conversion of L-lactide (98%), the theoretical PLLA arm M_n of the TBD catalyzed polymerization (26 kg/mol) matches the experimental value, confirming that all PLLA initiated off the macroinitiator. The experimental PLLA arm M_n for the $Sn(Oct)_2$ catalyzed polymerization (91% conversion) is slightly less than the theoretical value (25 kg/mol). The apparent discrepancy between theory and experiment may be explained by the formation of PLLA homopolymer as evidenced by the low molecular weight peak in the SEC trace (Figure 3.20c).
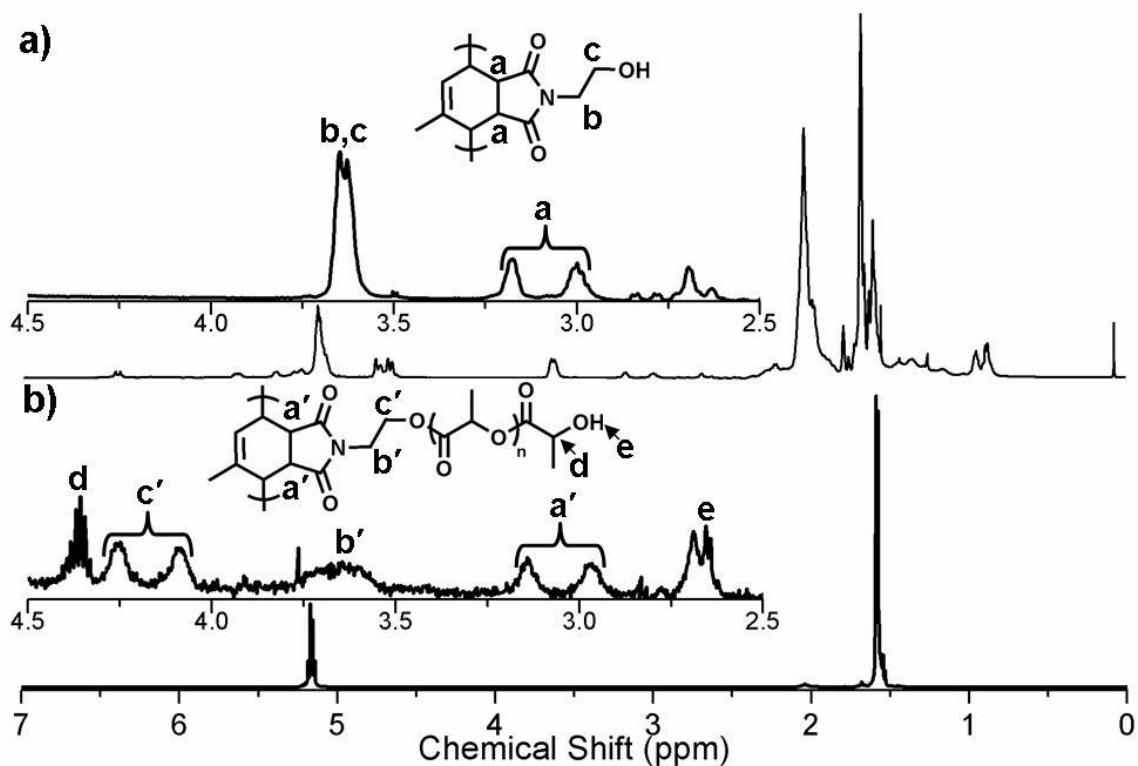
Figure 3.21. Representative ^{1}H NMR spectra and expanded regions of (a) CPI-*g*-HEMI and (b) CPI-*g*-PLLA (500 MHz, CDCl3). The CPI-*g*-PLLA contains 95 wt % PLLA grafts off the CPI polymer chain.

3.4 Conclusions

The catalytically isomerized isolated olefins produced conjugated diene synthetic handles along the backbone of polydienes. RuHCl(CO)(PPh$_3$)$_3$ proved an effective isomerization catalyst, though, solubility and temperature concerns limit the rate of isomerization. Nevertheless, both PI and PCOD were conjugated to levels acceptable to post-polymerization functionalization. Through the Diels–Alder mechanism, small molecules were grafted off the conjugated polydiene backbones to give various functionalities. As long as the small molecules were good dienophiles, grafting occurred overnight under mild conditions, retaining the molecular weight distributions initially present in the parent material. Synthesis of PLLA graft copolymers through a "grafting to" approach further demonstrated the reactivity of these conjugated polydienes. Using a HEMI functionalized CPI, PLLA graft copolymers were generated through a "grafting from" approach by polymerizing L-lactide off CPI-*g*-HEMI using a variety of ring opening catalysts. The versatility shown in the above examples indicates that conjugated diene could be a useful tool for generating functionalized materials.

3.5 References

[1]Sumerlin, B. S.; Vogt, A. P. *Macromolecules* **2010**, *43*, 1–13.

[2]Inglis, A. J.; Barner-Kowollik, C. *Macromol. Rapid Commun.* **2010**, *31*, 1247–1266.

[3] Becer, C. R.; Hoogenboom, R.; Schubert, U. S. *Angew.Chem. Int. Ed.* **2009**, *48*, 4900–4908.

[4]Fournier, D.; Hoogenboom, R., Schubert, U. S. *Chem. Soc. Rev.* **2007**, *36*, 1369–1380.

[5]Lowe, A. B. *Polym. Chem.* **2010**, *1***,** 17–36.

[6]Gacal, B.; Durmaz, H.; Tasdelen, M. A.; Hizal, G.; Tunca, U.; Yagci, Y.; Demiral, A. L. *Macromolecules* **2006**, *39*, 5330–5336.

[7]Altintas, O.; Hizal, G.; Tunca, U. *Des. Monomers Polym.* **2009**, *12*, 83–98.

[8]Sinnwell, S.; Inglis, A. J.; Stenzel, M. H.; Barner-Kowollik, C. Block, Stars, and Combs: Complex Macromolecular Architecture Polymers via Click Chemistry. In *Click*

Chemistry for Biotechnology and Materials Science; ed. J. Lahann, John Wiley and Sons, Ltd, United Kingdom, 2009, pp. 89–117.

[9]Durmaz, H.; Dag, A.; Altintas, O.; Erdogan, T.; Hizal, G.; Tunca, U. *Macromolecules* **2007**, *40*, 191–198.

[10] Inglis, A. J.; Nebhani, L.; Altintas, O.; Schmidt, F. G.; Barner-Kowollik, C. *Macromolecules* **2010**, *43*, 5515–5520.

[11] Gramlich, W. M.; Robertson, M. L.; Hillmyer, M. A. *Macromolecules* **2010**, *43*, 2313–2321.

[12] Dag, A.; Durmaz, H.; Hizal, G.; Tunca, U. *J. Polym. Sci., Part A: Polym. Chem.* **2007**, *46*, 302–313.

[13] Durmaz, H.; Karatas, F.; Tunca, U.; G. Hizal, G. *J. Polym. Sci., Part A: Polym. Chem.* **2006**, *44*, 499–506.

[14] Dai, L.; White, J. W. *Polymer* **1991**, *32*, 2120–2127.

[15] Thakur, M. *Macromolecules* **1988**, *21***,** 661–664.

[16]Owen, E. D.; Al-Moh'd, H. S. M. *Polymer* **1997**, *38*, 3533–3538.

[17] Dai, L.; Mau, A. W. H.; Griesser, H. J.; Winkler, D. A. *Macromolecules* **1994**, *27*, 6728–6735.

[18] Thakur, M.; Swamy, R.; Titus, J. *Macromolecules* **2004**, *37*, 2677–2678.

[19] Dai, L.; Mau, A. W. H. *Synthetic Metals* **1997**, *86*, 1893–1894.

[20] Yu, G.-Q.; Thakur, M. *J. Polym. Sci., Part B: Polym. Phys.* **1994**, *32*, 2099–2104.

[21] McLean, J. K.; Guillen-Castellanos, S. A.; Parent, J. S.; Whitney, R. A.; Resendes, R. *Eur. Polym. J.* **2007**, *43*, 4619–4627.

[22] Malmberg, S. M.; Parent, J. S.; Pratt., D. A.; Whitney, R. A. *Macromolecules* **2010**, *43*, 8456–8461.

[23] Kuźnik, N.; Krompiec, S. *Coord. Chem. Rev.* **2007**, *251*, 222–233.

[24] Schmidt, B. *Eur. J. Org. Chem.* **2004**, *2004*,1865–1880.

[25] Kuźnik, N.; Krompiec, S.; Bieg, T.; Baj, S.; Skutil, K.; Chrobok, A. *J. Organomet. Chem.* **2003**, *665*, 167–175.

[26] Krompiec, S.; Krompiec, M.; R. Penczek, R.; Ignasiak, H. *Coord. Chem. Rev.* **2008**, *252*, 1819–1841.

[27] Alcaide, B.; Almendros, P.; Luna, A. *Chem. Rev.* **2009**, *109*, 3817–3858.

[28] Krompiec, S.; Kuźnik, N.; Krompiec, M.; Penczek, R.; Mrzigod, J.; Tórz, A. *J. Mol. Catal. A-Chem.* **2006**, *253*, 132–146.

[29] Gauthier, D.; Lindhardt, A. T.; Olsen, E. P. K.; Overgaard, J.; Skrydstrup, T. *J. Am. Chem. Soc.* **2010**, *132*, 7998–8009.

[30] Krompiec, S.; Penczek, R.; Krompiec, M.; Pluta, T.; Ignasiak, H.; Kita, A.; Michalik, S.; Matlengiewicz, M.; Filapek, M. *Curr. Org. Chem.* **2009**, *13*, 896–913.

[31] Larock, R. C.; Dong, X.; Chung, S.; Reddy, C. K.; Ehlers, L. E. *J. Amer Oil Chem. Soc.* **2001**, *78***,** 447–453.

[32] Andjelkovic, D. D.; Min, B.; Ahn, D.; Larock, R. C. *J. Agric. Food Chem.* **2006**, *54*, 9535–9543.

[33] Theryo, G.; Jing, F.; Pitet, L. M.; Hillmyer, M. A. *Macromolecules* **2010**, *43*, 7394–7397.

[34] Pitet, L. M.; Hillmyer, M. A. *Macromolecules* **2009**, *42*, 3674–3680.

[35] Ndoni, S.; Papadakis, C. M.; Bates, F. S.; Almdal, K. *Rev. Sci. Instrum.* **1995**, *66*, 1090–1095.

[36] Hillmyer, M. A.; Bates, F. S. *Macromolecules* **1996**, *29*, 6994–7002.

[37] Schmidt, S. C.; Hillmyer, M. A. *Macromolecules* **1999**, *32*, 4794–4801.

[38] Wakamatsu, H.; Nishida, M.; Adachi, N.; Mori, M. *J. Org. Chem.* **2000**, *65*, 3966–3970.

[39] Yue, C. J.; Liu, Y.; He, R. *J. Mol. Catal. A: Chem.* **2006**, *259*, 17–23.

[40] Krompiec, J.; Sunwiński, J.; Majewski, J.; Grobelny, J. *Polish J. Appl. Chem.* **1998**, *42*, 43–48.

[41] Davidock, D. A. Novel Fluorinated Block Copolymers by Selective Chemical Modification: Chemistry and Thermodynamics. Ph.D. Thesis, University of Minnesota, Minneapolis, MN, 2004.

[42]Hallman, P. S.; McGarvey, B. R.; Wilkinson, G. *J. Chem. Soc. A.* **1968**, 3143–3150.

[43]Salvini, A.; Piacenti, F.; Frediani, P.; Devescovi, A.; Caporali, M. *J. Organomet.Chem.* **2001**, *625*, 255–267.

[44]Ma, J.; Cheon, H.-S.; Kishi, Y. *Org. Lett.* **2007**, *9*, 319–322.

[45]Colobert, F.; Kreuzer, T.; Cossy, J.; Reymond, S.; Tsuchiya, T.; Ferrié, L.; Marko, I. E.; Jourdain, P. *Synlett* **2007**, *15*, 2351–2354.

[46] Horii, N.; Arato, S.; Narayan, B.; Hosokawa, M.; Sashima, T.; Miyashita, K. *J. Amer. Oil Chem. Soc.* **2007**, *84*, 749–754.

[47]Cao, Y.; Gao, H.-L.; Chen, J.-N.; Chen, Z.-Y.; Yang, L. *J. Agric. Food Chem.* **2006**, *54*, 9004–9009.

[48]Masuda, T.; Tang, B.-Z.; Tanaka, A.; Higashimura, T. *Macromolecules* **1986**, *19*, 1459–1464.

[49]Hiemenz, P. C.; Lodge, T. P. Chapter 12: Glass Transition. *Polymer Chemistry*, Second Edition; Taylor & Francis Group: Boca Raton, 2007; pp 491–492.

[50] Luettmer-Strathmann, J. *J. Chem. Phys.* **2005**, *123*, 014910.

[51]M. B. Smith, and J. March, *March's Advanced Organic Chemistry*, 5th Ed., John Wiley and Sons, New York, 2001, pp. 1062–1075.

Chapter 4

Copolymerization of Isoprene and Hydroxyl Containing Monomers

In this chapter, the copolymerization of isoprene and hydroxyl containing monomers is discussed. Polyisoprene (PI) with pendent hydroxyl groups was synthesized by the radical copolymerization of isoprene and the hydroxyl containing comonomers 2-hydroxyethyl acrylate (HEA), 2-hydroxyethyl methacrylate (HEMA), and methylenebut-3-en-1-ol (IOH). The reversible addition-fragmentation transfer (RAFT) controlled radical and emulsion copolymerizations of isoprene with these comonomers was attempted. In the RAFT controlled radical copolymerizations, Diels–Alder reactions between the hydroxyl monomers and isoprene as well as the Diels–Alder homodimerization of isoprene occurred. Significantly more IOH comonomer was incorporated into the copolymer (39 mol %) than both HEMA (23 mol %) and HEA (3 mol %). See Appendix D for additional isoprene and HEMA RAFT controlled radical copolymerizations. Only IOH copolymerized with isoprene under emulsion conditions. The utility of the hydroxyl functionalized PI was demonstrated by using it as a macroinitiator for the ring opening polymerization of D,L-lactide, yielding microphase separated polylactide graft polymers.

4.1 Introduction

As discussed in Chapter 1, Polyisoprene (PI) is an interesting backbone material for graft copolymer synthesis. Graft polymers with a PI backbone and glassy side chains can lead to tough and thermoplastic elastomeric materials.[1,2,3] Various PI graft copolymers have been synthesized by grafting from approaches such as metallation,[4] radical polymerization,[5,6] and post-polymerization functionalization.[7,8,9] However, these methods are limited by the monomers that can polymerize and the extra steps needed to yield a macroinitiator. Hydroxyl functionalized PI is interesting as it allows for the synthesis of polylactide graft copolymers with a rubbery backbone, which can be quite tough materials.[10]

Of the polymerization schemes available, only a radical propagation mechanism is sufficiently functional group tolerant to allow for the copolymerization of isoprene and a hydroxyl containing comonomer. Furthermore, with the advent of controlled radical polymerizations of isoprene, PI macroinitiators with targeted molecular weights and narrow molecular weight distributions can be synthesized (see Chapter 1). Radical copolymerizations of isoprene and functional monomers have been performed to give functionalized polyisoprene (see Chapter 1).[11,12,13,14,15,16,17,18,19,20,21,22] However, isoprene is known to dimerize by a Diels–Alder mechanism.[23] When the polymerization temperature is sufficiently high, the dimer formation can compete with polymerization, reducing the achievable yields.[24] Additionally, comonomers can act as dienophiles. These competing reactions have been observed in isoprene copolymerizations with maleimides,[17,20] methacrylates,[16] and acrylates.[15] Consumption of the monomers by side reactions affects the copolymerization kinetics, distribution of functional groups along the polymer chain, and ultimate comonomer content. Ideally, the comonomer would copolymerize randomly to give a homogenous distribution of hydroxyl groups along the polymer chain at the feed concentration.

In an effort to develop a hydroxyl functionalized PI macroinitiator, we investigated copolymerizations of isoprene with the commercially available, hydroxyl containing monomers 2-hydroxyethyl acrylate (HEA) and 2-hydroxyethyl methacrylate

(HEMA). NMP copolymerizations of HEMA and other acrylates with isoprene have been reported by Benoit et al.,[11] but the products were not investigated as macroinitiators. To combat the anticipated Diels–Alder side reaction between the hydroxyl monomer and isoprene, we also investigated 2-methylenebut-3-en-1-ol (IOH) as a comonomer. IOH has been used for organic syntheses[25,26,27,28,29] and copolymerized in patent literature,[30,31,32,33] but to our knowledge it has not been copolymerized with isoprene. The structure similarities of IOH and isoprene may allow for IOH to have isoprene comparable reaction kinetics towards Diels–Alder and polymerization reactions.

To this end, HEA, HEMA, and IOH were copolymerized with isoprene using a RAFT controlled radical process. Monomer conversions to polymer and Diels–Alder side products were monitored to compare the behavior of the different comonomers. In an effort to eliminate the Diels–Alder side reaction during polymerization, HEA, HEMA, and IOH copolymerizations with isoprene were also attempted in an emulsion setting at room temperature. The resulting pendent hydroxyl containing copolymers from both the RAFT controlled radical and emulsion polymerizations subsequently were used as macroinitiators for polylactide graft copolymer synthesis.

4.2 Experimental Details

4.2.1 General methods and materials

All chemicals were purchased from Sigma-Aldrich and used without further purification unless otherwise noted. HPLC grade CH_2Cl_2 was dried on an MBraun solvent purification system. Isoprene was purified by passing it through neutral alumina prior to use unless otherwise noted. D,L-lactide (Purac) was recrystallized from ethyl acetate and stored under nitrogen prior to use. HEA and HEMA were passed through basic alumina prior to use. The RAFT CTA (2-((((dodecylthio)carbonothioyl)thio)-2-methylpropanoic acid) was synthesized following a previously reported procedure.[34]

^{1}H NMR spectroscopy was performed on a Varian Inova 500 MHz spectrometer in $CDCl_3$ (Cambridge) using the residual $CHCl_3$ peak as reference. Size exclusion chromatography was performed on an Agilent 1100 high-pressure liquid chromatograph

at 35 °C equipped with a PLgel (Varian) 5 μm guard column followed by three PLgel columns with varying pore sizes with HPLC grade chloroform as the mobile phase. Molecular weights and polydispersity index (PDI) were measured by a Hewlett-Packard P1047A refractometer calibrated with either polystyrene (Polymer Laboratories) or polyisoprene (Scientific Polymer Products Inc.) standards. Differential scanning calorimetry (DSC) was performed on a TA Instruments Discovery Series instrument with the P(I-co-IOH) samples cycled between -85 and 200 °C with two heating and one cooling cycle. Glass transition temperatures were measured from the second heating ramp. Infrared spectroscopy was performed on a Nicolet Magna-IR 550 (Thermo Scientific) on NaCl plates at ambient temperature.

4.2.2 Synthesis of 1-bromo-2-methylbut-3-en-2-ol (IBrOH)

De-ionized water (2 L) was cooled to less than 5 °C in a round-bottom-flask followed by isoprene (192 mL) and stirred to create a suspension. *N*-bromosuccinimide (310.6 g) was added portion wise such that the reactor temperature remained below 5 °C. The solution was stirred at 5 °C for 3 h and sat overnight at room temperature. The aqueous phase was extracted twice with diethyl ether and the organic fractions were combined, washed with brine, dried with $MgSO_4$, and concentrated with rotary evaporation. Concentrated product was purified by reduced pressure distillation (38 – 42 °C, 5 torr) to give a clear product, 47% yield. ^{1}H NMR spectroscopy (300 MHz, $CDCl_3$) **δ** 5.90 (dd, *J* = 17.6 Hz *J* = 10.9 Hz, -C*H*=CH$_a$H$_b$), 5.37 (d, *J* = 18.3 Hz, -CH=C*H$_a$*H$_b$), 5.19 (d, *J* = 9.5 Hz, -CH=CH$_a$*H$_b$*), 3.48 (s, -C*H$_2$*-Br), 2.19 (s, -O*H*), and 1.43 (s, -C*H$_3$*).

4.2.3 Synthesis of 2-methyl-2-vinyloxirane (MVO)

IBrOH (100 mL) was cooled to 0 °C in a round-bottom-flask and a 30% aqueous NaOH solution (120 mL) was added drop wise over 1 h, keeping the reactor temperature below 5 °C. Upon complete addition of NaOH solution, two phase mixture was stirred for 1.5 h at 0 °C. The organic fraction was separated from the aqueous fraction and used without further purification (97% pure, 98% yield). ^{1}H NMR spectroscopy (300 MHz, $CDCl_3$) **δ** 5.63 (dd, *J* = 17.1 Hz *J* = 10.8 Hz, -C*H*=CH$_a$H$_b$), 5.35 (d, *J* = 17.6 Hz, -

CH=CH_aH$_b$), 5.23 (d, J = 11.7 Hz, -CH=CH$_a$H$_b$), 2.82 (d, J = 5.2 Hz, OCH_aH$_b$), 2.73 (d, J = 5.1 Hz, OCH$_a$H$_b$), and 1.45 (s, -CH_3).

4.2.4 Synthesis of IOH using lithium diisopropyl amine (LDA)

Using either MVO synthesized in house or MVO purchased from Alfa-Aesar, the MVO was degassed by three freeze-pump-thaw cycles prior to synthesizing IOH. Building on a reported literature procedure,[28] to a degassed 3-neck flask, nBuLi (2.5 M, 62 mL) in hexanes was cannula transferred and the hexanes were removed by evacuating the system. The nBuLi was cooled in ice and anhydrous Et$_2$O (240 mL) was cannula transferred to the flask. The nBuLi/Et$_2$O solution was cooled in dry ice/acetone and degassed diisopropylamine/Et$_2$O (20.2 mL/40 mL) was cannula transferred to the 3-neck reactor. The solution was stirred for 30 min prior to addition of MVO (10 g) by syringe to the cold mixture. The dry ice/acetone bath was removed system warmed up slowly to room temperature. Once the solution had become orange (20 min), it was poured into ice cold 2 M HCl (250 mL per 10 g MVO) to quench the reaction. The organic fraction was separated from the aqueous and the aqueous fraction was washed 3 times with Et$_2$O. The organic fractions were combined and washed with sodium bicarbonate solution, brine, and dried over MgSO$_4$. The dry fractions were dried by rotary evaporation at room temperature and 250 torr. The solvents were distilled off at atmospheric pressure. IOH was distilled from the remaining product (45 °C, 14 torr) to give 98% pure IOH (18.4% overall yield, 54% purification yield). By massing a known volume of the purified IOH, the density of IOH was estimated to be 0.9 g/mL at 25 °C. Solubility of IOH was estimated by ^{1}H NMR spectroscopy by adding IOH to D$_2$O (99.9 % purity) until two phases were realized. The D$_2$O phase was collected, analyzed by ^{1}H NMR spectroscopy, and the integrations of representative IOH resonances were compared to the integration of the residual solvent H$_2$O peak to give an approximate solubility (8 g/L). ^{1}H NMR spectroscopy (500 MHz, CDCl$_3$) δ 6.39 (dd, J = 18.0 Hz J = 11.4 Hz, -CH=CH$_a$H$_b$), 5.29 (s, -C=CH_aH$_b$), 5.27 (d, J = 18.3 Hz, -CH=CH_aH$_b$), 5.15 (s, -C=CH$_a$H$_b$), 5.12 (d, J = 11.4 Hz, -CH=CH$_a$H$_b$), 4.35 (s, -CH_3), and 1.58 (br s, -OH). ^{13}C NMR (125 MHz, CDCl$_3$) δ 145.2, 136.3, 115.7, 114.1, and 62.6. FT-IR (cm^{-1}) 3337 (-OH stretch), 3090, 3008 (H-C=

stretch), 2981, 2927, 2871 (-CH- stretch), 1597 (-C=C- stretch), 1083 (C-O stretch), 1023, and 903 (C=C-H, vibrations).

4.2.5 Alternative Synthesis of IOH with bis(trimethylsilyl)amide (LiHMDS)

Following a modified literature procedure[27] and using either MVO synthesized by the above procedure or MVO purchased from Alfa-Aesar, the MVO was degassed by three freeze-pump-thaw cycles. In a N_2 dry box, LiHMDS (37 g) was added to a 500 mL side arm round-bottom-flask sealed with a septum. The flask was removed from the glove box, dry THF (150 mL) was cannula transferred to LiHMDS. Anhydrous Et_2O (150 mL) was cannula transferred to a degassed 3-neck flask fitted with a condenser and septum. The THF/LiHMDS solution was subsequently cannula transferred to the 3-neck flask. Flask was backfilled with 3 psig argon, MVO (14.3 g) was added drop wise by syringe, and the mixture was heated to 60 °C for 20 h. Reaction was quenched by pouring the solution into ice cold 2 M HCl (250 mL per 10 g MVO). The organic fraction was separated from the aqueous fraction, which was washed 3 times with anhydrous Et_2O. The combined organic fractions were washed with sodium bicarbonate solution, brine, and dried over $MgSO_4$. The organic fractions were concentrated by rotary evaporation at room temperature and 250 torr. IOH was purified by column chromatography. The sample was loaded onto silica gel column with pentanes as the mobile phase. The column was washed with pentanes. The solvent was switched to a 5:1 pentanes:Et_2O mobile phase and fractions were collected. IOH had a R_f = 0.27 in 5:1 pentanes:Et_2O. The pentanes and Et_2O were distilled off at 45 °C and atmospheric pressure. To collect IOH, the solution was vacuum distilled (800 mtorr, 33 °C), giving IOH product with 89% purity and 30% yield on purification. See Section 4.2.4 for spectroscopic analysis.

4.2.6 Controlled radical RAFT copolymer synthesis

Comonomer, TBP, and RAFT CTA were dissolved in isoprene at the desired ratios (0.06 mol of total monomer). The solution was transferred to a 10 mL side arm pressure vessel, degassed by 3 freeze-pump-thaw cycles, and backfilled with 3 psig argon. The vessel was then placed in a 125 °C oil bath to heat. To take aliquots for the kinetics study, the procedure from Germack and Wooley was followed.[35] The flask was

removed from the oil bath and placed in liquid nitrogen to freeze the reaction mixture. The mixture was thawed in an ice bath and an aliquot (ca. 500 µL) was taken under flowing argon. The flask was resealed, evacuated by 3 freeze-pump-thaw cycles, backfilled with argon, and placed by in the oil bath to continue reacting. A portion of the aliquot was placed directly into CDCl$_3$ and analyzed by ^{1}H NMR spectroscopy to give a crude solution spectrum which was used to calculate isoprene conversion to limonene and total conversion of hydroxyl comonomers. The remainder of the aliquot was diluted with tetrahydrofuran (THF) inhibited with BHT and dried under reduced pressure at 50 °C to remove all the volatile monomers and byproducts. The dried aliquots were analyzed by SEC and ^{1}H NMR spectroscopy to determine the conversion of monomers to polymer. After 24 h of total heating time and the final aliquot was taken, the remaining viscous yellow liquid was diluted in THF and precipitated in 10 volume excess methanol, twice. The product was dissolved in THF, concentrated by N$_2$, and dried under reduced pressure at 50 °C for 48 h. The product was characterized by ^{1}H NMR spectroscopy and SEC. ^{1}H NMR spectroscopy for polymer repeat units (500 MHz, CDCl$_3$) **δ** for PI isomers 5.76 (m, 1,2 isomer -C*H*=CH$_2$), 5.13 (br, *cis* and *trans* 1,4 –C*H*=C-), 5.0-4.8 (m, 1,2 isomer -CH=C*H$_2$*), 4.75-4.60 (m, 3,4 isomer -C=C*H$_2$*), 2.2-1.9 (br m, allylic), 1.68 (s, *cis* –C*H$_3$*), 1.60 (s, *trans* –C*H$_3$*), and 0.94 (s, 1,2 -C*H$_3$*); for IOH repeat units 5.41 (br, *cis* 1,4 -C*H*=C-), 5.31 (br, *trans* 1,4 -C*H*=C-), 4.11 (s, *trans* 1,4 =C-C*H$_2$*-OH), and 4.02 (s, *cis* 1,4 =C-C*H$_2$*-OH); for HEA repeat units 4.20 (br, OC-C*H$_2$*-CH$_2$-OH) and 3.81 (br, OC-CH$_2$-C*H$_2$*-OH); and for HEMA repeat units 4.20 (br, OC-C*H$_2$*-CH$_2$-OH) and 3.83 (br, OC-CH$_2$-C*H$_2$*-OH).

4.2.7 Calculation of monomer conversions for RAFT controlled radical polymerizations

Using the ^{1}H NMR spectrum of the aliquot from the crude reaction solution, the conversion of isoprene to limonene ($x_{I \to L}$) and overall conversion of the hydroxyl monomer (x_{OH}) were calculated with the following procedures. Sample calculations are given for the HEMA/isoprene copolymerization at 12 h unless otherwise noted. For $x_{I \to L}$, the integration of the limonene peak at 4.72 ppm (878.7) was subtracted by the

integration of the isoprene 3,4-addition produce peak at 4.65 ppm (99.5) to correct for the concurrent peaks at 4.72 ppm. This value was divided by the integration of the RAFT CTA peak at 3.36 ppm, corrected to give a molar equivalent (50.4/2). The value was then divided by the know ratio of isoprene to RAFT CTA added to the reactor (184.3). Sample calculation for $x_{I \to L}$ is below.

$$x_{I \to L} = \frac{\frac{(878.7 - 99.5)}{(50.4/2)}}{184.3} = 0.17$$

To x_{OH} of hydroxyl monomer (HEMA), the integration value of the peak at 4.2 ppm (282.0), corresponding to reacted monomer, was divided by the sum of the integration values of the 4.2 ppm peak and the unreacted monomer peak at 4.31 ppm (10.0). For HEA, the monomer and reacted monomer peaks were 4.32 and 4.24 ppm, respectively. Sample calculation for hydroxyl monomer conversion is below.

$$x_{OH} = \frac{282.0}{282.0 + 10.0} = 0.96$$

For the x_{OH} of IOH (12 h), the procedure above had to be modified to correct for protons with concurrent resonances. The integration of the reacted monomer region at 4.20–3.96 ppm (47.5) had the integration of the RAFT CTA peak at 3.36 ppm (10.0) subtracted from it to account for the peak overlap from protons of the terminal end of the polymer chain. The integration of the unreacted monomer peak at 4.36 ppm (8.3) was summed with the corrected value and divided the corrected value. See below for sample calculation.

$$IOH \; x_{OH} = \frac{47.5 - 10}{47.5 - 10 + 8.3} = 0.79$$

All conversions to polymer were calculated from the dried crude aliquots. Conversion of isoprene to polymer ($x_{I \to P}$) was calculated by summing the normalized integrations of the various isomers: 1,2-addition (5.76 ppm, 13.6); 3,4-addition (4.8–4.6 ppm, 36.6/2); and 1,4-addition (5.13, 472.7) products; dividing by the normalized integration of the RAFT

CTA end group (3.34 ppm, 10.7); and dividing that value by the ratio of isoprene to RAFT CTA fed to the reactor (184.3). Sample calculation is below.

$$x_{I \to P} = \frac{\dfrac{13.6 + 36.6/2 + 474.7}{10.7/2}}{184.3} = 0.31$$

Conversion of hydroxyl monomer to polymer ($x_{OH \to P}$) was calculated by dividing the normalized integration of the polymer peak (4.2 ppm, 12.6/2) by the normalized integration of the RAFT CTA peak (3.34 ppm, 10.7/2) and dividing that value by the known ratio of hydroxyl monomer to RAFT CTA fed to the reactor (5.7). Sample calculation is below.

$$x_{OH \to P} = \frac{\dfrac{12.6/2}{10.7/2}}{5.7} = 0.21$$

To calculate the x_{OHP} of IOH (12 h), the integration of the polymerized IOH peak (26.8) was corrected by subtracting the integration of the RAFT CTA resonance (10.0), divided by the integration of the RAFT CTA resonance, and then divided by the know ratio of IOH to RAFT CTA fed to the reactor (5.7). Sample calculation is below.

$$IOH\ x_{OH \to P} = \frac{\dfrac{26.8 - 10.0}{10.0}}{5.7} = 0.30$$

The validity of calculating the $x_{I \to P}$ using the CTA as an internal standard was confirmed gravimetrically. For the isoprene homopolymerization and HEMA copolymerization, aliquots of the final crude solutions (24 h) were taken and quickly massed. The aliquots were dried under reduced pressure at 50 °C to remove all volatiles and the samples were massed again, calculating the $x_{I \to P}$ by dividing the initial sample mass by the dry sample mass. The gravimetrically determined $x_{I \to P}$ of the isoprene homopolymerization and HEMA/isoprene copolymerization were 47% and 50%, respectively. These conversions compare favorably with those calculated by ^{1}H NMR spectroscopic end group analysis of the isoprene and HEMA polymerizations, which

were 46% and 50%, respectively. The close agreement of the gravimetric and spectroscopic methods to calculate monomer conversion to polymer confirms the validity of the spectroscopic method.

4.2.8 Emulsion copolymer synthesis

Following a modified literature procedure for isoprene homopolymerization,[36] sodium dodecyl sulfate (SDS) was massed into a 10 mL side arm vessel sealed with a PTFE stopcock and degassed with three evacuate/backfilled with 3 psig argon cycles. Under flowing argon, degassed deionized (DI) water was added to the flask to dissolve the SDS (69.4 mM solution). Comonomer and isoprene were mixed before adding to the reactor under flowing argon to give a 1.47 mM monomer in water emulsion. The mixture was allowed to stir for 1 h. The tBHP and TDM were added under flowing argon at the desired ratio and allowed to stir for 30 min. Under flowing argon, a 1.5 M solution of tetraethylenepentamine (TEPA) in DI water was added to start the reaction. TEPA and tBHP were always added at 1:1 ratio as the two chemicals made up the redox pair. TEPA, tBHP, and TDM were added at a 1:1:0.5 ratio, respectively. The reaction vessel was then placed in a 25 °C oil bath to keep a constant reaction temperature. After the desired polymerization time, the reaction was quenched by adding a 200 ppm hydroquinone solution in methanol at a 0.2:1 ratio to the reaction emulsion. To determine conversion by mass, a known volume of the emulsion was taken, concentrated under blowing N_2, and dried under reduced pressure over night. The bulk of the emulsion was coagulated by pouring it into excess acetone. The coagulated material was then dissolved in THF and precipitated in 10 volume excess methanol. The sample was collected by dissolving in THF, concentrating with nitrogen, and drying under reduced pressure. Polymers were a yellow to orange color due to the oxidized TEPA. The materials were characterized by ^{1}H NMR spectroscopy and SEC. ^{1}H NMR spectroscopy for the isoprene/IOH copolymer repeat units (500 MHz, CDCl$_3$) **δ** 5.76 (m, -CH=CH$_2$), 5.41 (br, IOH *cis* -CH=C-), 5.31 (br, IOH *trans* -CH=C-), 5.13 (br, isoprene *cis* and *tran* –CH=C-), 5.0-4.8 (m, -CH=CH_2), 4.75-4.60 (m, -C=CH_2), 4.11 (s, *trans* =C-CH_2-OH), 4.02 (s, *cis* =C-CH_2-OH), 2.2-1.9 (br m, allylic), 1.68 (s, *cis* –CH_3), 1.60 (s, *trans* –CH_3), and 0.94 (s, 1,2 -CH_3).

4.2.9 Homopolymerization of IOH

IOH was homopolymerized following both the RAFT controlled radical and the emulsion procedures given above for copolymerizations. Under the RAFT conditions, IOH was homopolymerized at a [M]:[CTA] = 190 for 24 h at 125 °C in the bulk. The crude product was sampled for ^{1}H NMR spectroscopy, dissolved in CH_2Cl_2, and precipitated in 10 times volume excess methanol. The product was collected and dried under reduced pressure overnight at 50 °C, yielding a brown rubbery material. Under the emulsion conditions, IOH was homopolymerized at [M]:[I] = 50 for 17 h at 25 °C. The reaction was quenched by adding a 200 ppm hydroquinone/methanol solution to the emulsion and the water was evaporated off. The product was dissolved in methanol and precipitated in 10 times volume excess hexanes. The product was collected and dried under reduced pressure overnight at 50 °C, yielding a yellow rubbery material. The materials were analyzed by ^{1}H NMR spectroscopy and FT-IR spectroscopy. ^{1}H NMR spectroscopy of RAFT synthesized PIOH (500 MHz, $CDCl_3$) **δ** 9.45 (s, O=C*H*), 5.98–5.76 (br, 1,2-addition isomer, -C*H*=CH₂), 5.65 (br, 1,4-addition isomer, -C*H*=C-), 5.40–5.20 (br, 1,2-addition isomer, -CH=C*H*₂), 5.07 and 4.92 (br, 3,4-addition isomer, -C=C*H*₂), 4.20–3.96 (br, 1,4-addition isomer, -C*H*₂OH), 4.04–3.68 (br, 3,4-addition isomer, -C*H*₂OH), 3.65 (br, 1,2-addition isomer, , -C*H*₂OH), 2.4–1.9 (br, -C*H*₂-C=), 1.9–1.2 (br, -C*H*₂-), and 1.0–0.7 (br, -C*H*₃). ^{1}H NMR spectroscopy of emulsion synthesized PIOH (500 MHz, $CDCl_3$) **δ** 5.77 (br, 1,2-addition isomer, -C*H*=CH₂), 5.45 (br, *cis*-1,4-addition isomer, -C*H*=C-), 5.34 (br, *trans*-1,4-addition isomer, -C*H*=C-), 4.11 (br, *trans*-1,4-addition isomer, -C*H*₂OH), 3.98 (br, *cis*-1,4-addition isomer, -C*H*₂OH), 3.49 (br, 1,2-addition isomer, , -C*H*₂OH), and 2.2 (br, -C*H*₂-C=). FT-IR of crude RAFT controlled radical polymerization solution, NaCl plate (cm⁻¹): 3434.3, 3080.1, 2924.1, 2871.5, 2703.6, 1724.7, 1684.8, 1644.9, 1081.2, 903.4, and 803.7. FT-IR of purified RAFT controlled radical PIOH, NaCl plate (cm⁻¹): 3448, 2924, 2955, 2871, 1727, 1647, 1457, 1083, 904, 807, and 733. FT-IR of emulsion synthesized PIOH, NaCl plate (cm⁻¹): 3306, 2919, 2853, 1665, 1577, 1541, 1454, 1233, 1005, 909, and 860.

4.2.10 PLA graft copolymer synthesis procedure at 50 wt % lactide

In a N_2 atmosphere glove box, the following components were combined in 20 mL scintillation vials. Hydroxyl copolymer macroinitiator (250 mg) and D,L-lactide (250 mg) were dissolved in dried CH_2Cl_2 (4.2 mL). To the solution, TBD (32.2 mg) was added as a stock solution in minimal CH_2Cl_2 to start the polymerization. After 5 min, a solution of benzoic acid (283 mg) in minimal CH_2Cl_2 was added to quench the polymerization. The quenched reaction solutions were removed from the glove box and precipitated twice into 10 volume excess methanol from CH_2Cl_2. The collected products were dried under reduced pressure at 50 °C for two days. The products were analyzed by SEC and ^{1}H NMR spectroscopy. ^{1}H NMR spectroscopy (500 MHz, CDCl$_3$) **δ** PLA repeat units 5.17 (m, -C*H*-) and 1.58 (m, -C*H$_3$*); PLA end-group protons 4.36 (m, -C*H*-); P(I-co-IOH) end-group protons 4.56 (br, =C-C*H$_2$*-O-CO) and 4.50 (br, =C-C*H$_2$*-O-CO); and P(I-co-HEMA) end-group protons 4.42-4.18 (br, O-C*H$_2$*-C*H$_2$*-O).

4.2.11 P(I-co-IOH)-g-PLA synthesis at 95 wt % lactide

In a N_2 dry box P(I-co-IOH) (0.5 g) was massed into a 150 mL pressure vessel and dissolved in dry CH_2Cl_2 (88 mL). D,L-lactide (9.5 g) was dissolved in solution and followed by 920 μL of a 1,5,7-triazabicyclo[4.4.0]dec-5-ene (TBD) stock solution in dry CH_2Cl_2 (20 mg/2 mL) to start the polymerization. The flask was sealed, removed from the dry box, and allowed to stir for 35 min at room temperature (ca. 22 °C). A solution of benzoic acid (81 mg) in minimal CH_2Cl_2 was added to the viscous solution to quench the polymerization. The solution was diluted with CH_2Cl_2 and precipitated in 10 volume excess methanol. The product was collected, dissolved in CH_2Cl_2, and precipitated in 10 volume excess hexanes. The collected white polymer was set to dry under reduced pressure overnight. From an aliquot of the crude solution D,L-lactide conversion was calculated to be 98% (85% yield). Product was characterized by ^{1}H NMR spectroscopy and SEC. ^{1}H NMR spectroscopy (500 MHz, CDCl$_3$) **δ** PLA repeat units 5.17 (m, -C*H*-) and 1.58 (m, -C*H$_3$*); end-group protons 4.56 (br, =C-C*H$_2$*-O-CO), 4.50 (br, =C-C*H$_2$*-O-CO), and 4.36 (m, -C*H*- and =C-C*H$_2$*-O-CO).

4.2.12 SAXS and TEM analysis of P(I-co-IOH)-g-PLA

Transmission electron microscopy (TEM) was performed on a FEI Tecnai Spirit BioTWIN at an operating voltage of 80 keV. Samples for TEM were microtomed at 25 °C on a Leica EM UC6 Ultramicrotome to a thickness of approximately 70 nm and stained with OsO_4 vapor (4 wt % aqueous solution) for 20-30 minutes prior to imaging. Room temperature synchrotron small-angle X-ray scattering (SAXS) was carried out at the Advanced Photon Source (APS) at Argonne National Laboratories at the Sector 5-ID-D beamline maintained by the Dow-Northwestern-Dupont Collaborative Access Team (DND-CAT) with a source that produces x-rays with a wavelength of 0.84 Å. Scattering intensity was monitored by a Mar 165 mm diameter CCD detector with a resolution of 2048×2048. The two-dimensional scattering patterns were integrated azimuthally, giving one-dimensional scattering profiles. In each scattering profile, the lowest spatial frequency (q) peak was designated as q* – the principle scattering peak. From the q* value, the domain spacing (d) of each sample was calculated using $d = 2\pi/q^*$.

4.2.13 Acetylation of emulsion synthesized P(I-co-IOH)

P(I-co-IOH) (50 mg) was dissolved in 3 mL of THF to which acetic anhydride (0.5 mL) and pyridine (0.5 mL) were added. The solution was allowed to stir for 20 h at which time the volatiles were blown off with N_2 and the resulting polymer was set to dry under reduced pressure. Complete acetylation of the hydroxyl groups was realized as the peaks associated with the pendent hydroxyl groups are no longer present. ^{1}H NMR spectroscopy of new peaks (500 MHz, CDCl$_3$) **δ** 4.59, 4.50, and 4.48 (s, =C-C*H$_2$*-O-CO).

4.3 Results and Discussion

4.3.1 IOH Synthesis

Of the schemes available to synthesize IOH, the general reaction pathway in Figure 4.1 is the most frequently used in literature,[27,28,] utilizing the fewest steps and common reagents. Using either the in house synthesized or purchased MVO, the oxirane isomerization was performed to give IOH. The isomerization of MVO to IOH is accomplished by the addition of a strong, non-nucleophilic base that eliminates the β-hydrogen to the oxirane, allowing for the subsequent ring opening.[37] The resulting

alkoxide is then quenched by transferring the basic solution to an aqueous acid (HCl) with the desired IOH as the product. Two bases from literature were investigated: lithium bis(trimethylsilyl)amide (LiHMDS)[27] and lithium diisopropylamide (LDA).[28] In both systems MVO was completely converted, but the LiHMDS base system had higher conversion to IOH (~100%) than the LDA system (65%). Purification of the IOH from the crude reaction solutions proved difficult when either base was used. The crude solution of the LiHMDS promoted reaction has significant hexamethyldisilazane (HMDS) byproduct present. HMDS has a similar boiling point (126 °C)[38] to IOH (126 °C),[39] resulting in HMDS coming over with the IOH during distillation. Furthermore, IOH and HMDS appear to react during the distillation as evidenced by an observed shift of resonances in the ^{1}H NMR spectrum. A majority of the HMDS can be separated by column chromatography, but a significant amount of HMDS still remains in the IOH (Figure 4.2d). Pure IOH can be obtained from the distillation of IOH from the LDA promoted reaction solution as the diisopropylamine byproduct has a significantly different boiling point (84 °C)[38] from the IOH product (Figure 4.2e). The yield in the distillation process is low (ca. 20%) as the IOH reacts while heated to form side products such as oligomers and Diels–Alder dimers.
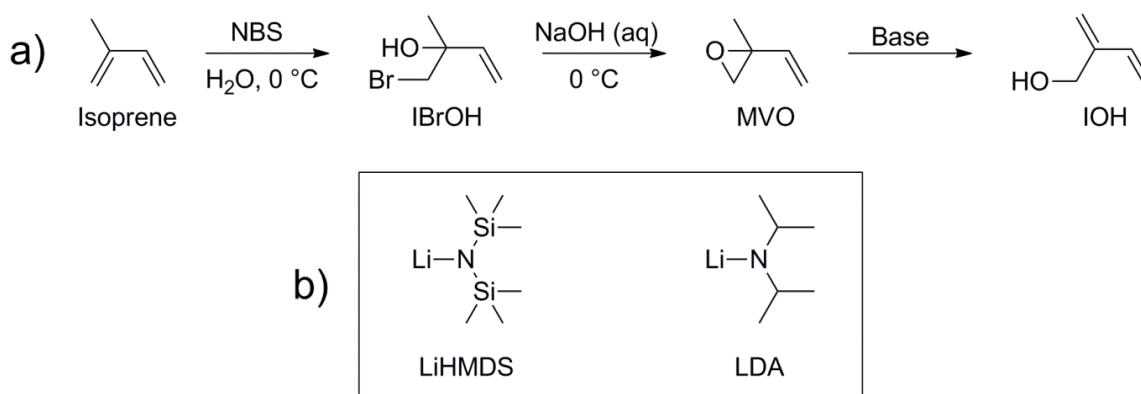
Figure 4.1. Synthesis of IOH (a) from isoprene and (b) the non-nucleophilic bases used to isomerize 2-methyl-2-vinyloxirane (MVO) to IOH. Two intermediate molecules are synthesized to give IOH. First a bromohydrin is formed to give 1-bromo-2-methylbut-3-en-2-ol (IBrOH) and second the intramolecular base catalyzed ring closure of IBrOH to give MVO.
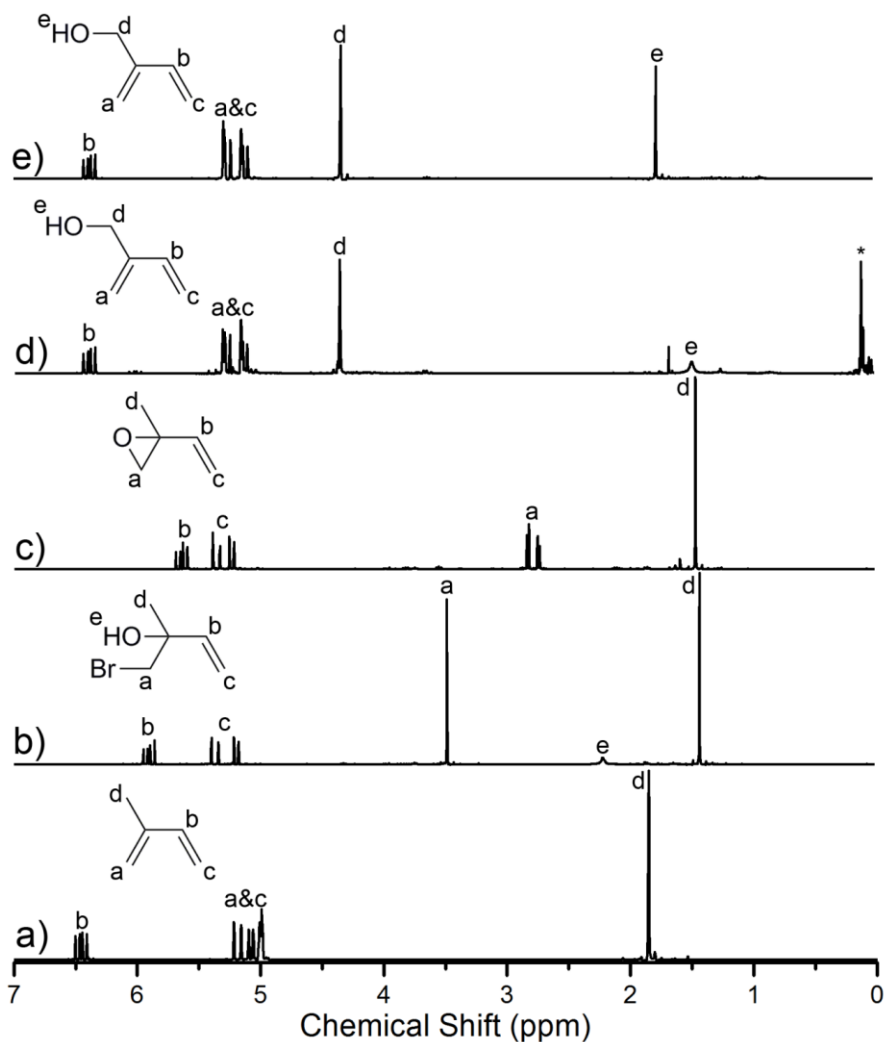
Figure 4.2. ^{1}H NMR spectra (CDCl$_3$) and peak assignments of (a) isoprene, (b) IBrOH, (c) MVO, (d) IOH synthesized using LiHMDS (asterisk marks residual HMDS), and (e) IOH synthesized using LDA. Synthesis of IOH from MVO using LDA with subsequent distillation leads to a product with minimal impurities.

4.3.2 RAFT controlled radical copolymerizations

HEA, HEMA, and IOH were copolymerized with isoprene at a feed (f$_{OH}$) of 3 mol %, following the isoprene RAFT homopolymerization procedure of Germack and Wooley (see Appendix D for additional HEMA/isoprene RAFT controlled radical copolymerizations).[35] Additionally, isoprene was homopolymerized as a control. Polymerizations were performed at 125 °C in the bulk using the trithiocarbonate, 2-

((((dodecylthio)carbonothioyl)thio)-2-methylpropanoic acid (CTA) as the RAFT chain transfer agent and *tert*-butyl peroxide (TBP) as the radical initiator. The ratio of monomer to CTA ([M]:[CTA]) was held at 190:1 with a 5 to 1 ratio of CTA to TBP. Proton nuclear magnetic resonance (^{1}H NMR) spectra of crude reaction solution aliquots were used to calculate the conversion of isoprene to limonene ($x_{I \to L}$) and the overall disappearance (i.e., conversion) of the hydroxyl monomers throughout the reaction (x_{OH}). Subsequently, the aliquots were dried under reduced pressure to remove all volatiles (i.e., residual monomers and all Diels–Alder products) and analyzed by ^{1}H NMR spectroscopy to calculate the conversion of isoprene to polymer ($x_{I \to P}$) and hydroxyl monomer to polymer ($x_{OH \to P}$). The conversion of hydroxyl monomer to Diels–Alder adducts (x_{DA}) was inferred to be the difference between the total hydroxyl monomer conversion and $x_{OH \to P}$. For both the crude and dried aliquots, the CTA was used as an internal reference to calculate $x_{I \to L}$, $x_{OH \to P}$, and $x_{I \to P}$ (see Supporting Information). In addition to the aliquots, after 24 h the polymerizations were quenched by freezing in liquid nitrogen and the polymer was collected to give hydroxyl macroinitiators for subsequent reactions (Figure 4.3a).
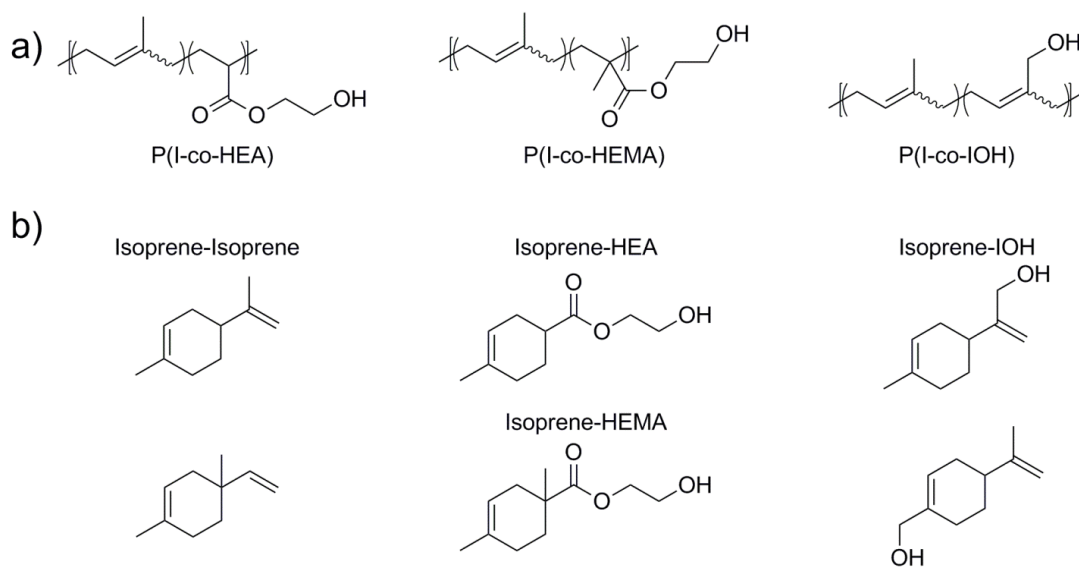
Figure 4.3. Chemical structures of (a) isoprene-hydroxyl monomer copolymers and (b) Diels–Alder side products observed during copolymerization. Shown are the isoprene dimers, HEA and HEMA adducts where isoprene is the diene, and IOH adducts where IOH acts as the diene and dienophile. Additional Diels–Alder adduct isomers are possible, but not shown for brevity.

Using the procedure described above, the $x_{I \rightarrow P}$ and $x_{OH \rightarrow P}$ were calculated and plotted as functions of polymerization time (Figure 4.4 and Figure 4.5, respectively). After 24 h the $x_{I \rightarrow P}$ for the isoprene homopolymerization and the copolymerizations have similar values (Table 4.1), suggesting that at the comonomer loading investigated, the comonomer does not significantly affect the rate of isoprene polymerization. Additionally, the $x_{I \rightarrow P}$ does not vary greatly between the homopolymerization and copolymerizations at the sampled time points (Figure 4.4). However, the $x_{OH \rightarrow P}$ values vary significantly over the polymerization depending on the monomer used (Figure 4.5). At all time points investigated, the $x_{OH \rightarrow P}$ for HEA is approximately constant (2–3 mol %), while the $x_{OH \rightarrow P}$ values for IOH and HEMA increase over time and plateau out towards polymerization termination (24 h). The observed plateaus suggest that each comonomer nears complete conversion at 24 h, but as the $x_{OH \rightarrow P}$ values at 24 h indicate (Table 4.1), not all monomer is converted to polymer.

Figure 4.4. Conversion of isoprene to polymer ($x_{I \to P}$) as a function of polymerization time for homopolymerizations and hydroxyl monomer copolymerizations. Conditions were [M]:[CTA] = 190, 125 °C reaction temperature, and initial hydroxyl monomer concentration (if used) (f_{OH}) of 3 mol %. The conversion of isoprene to polymer behaves similarly for both homopolymerizations and copolymerizations. Values were calculated by ^{1}H NMR spectroscopic end group analysis on dried aliquots from the polymerizing reaction mixture. Two separate runs of isoprene homopolymerization gave similar conversions over time, indicating that the polymerizations are repeatable.
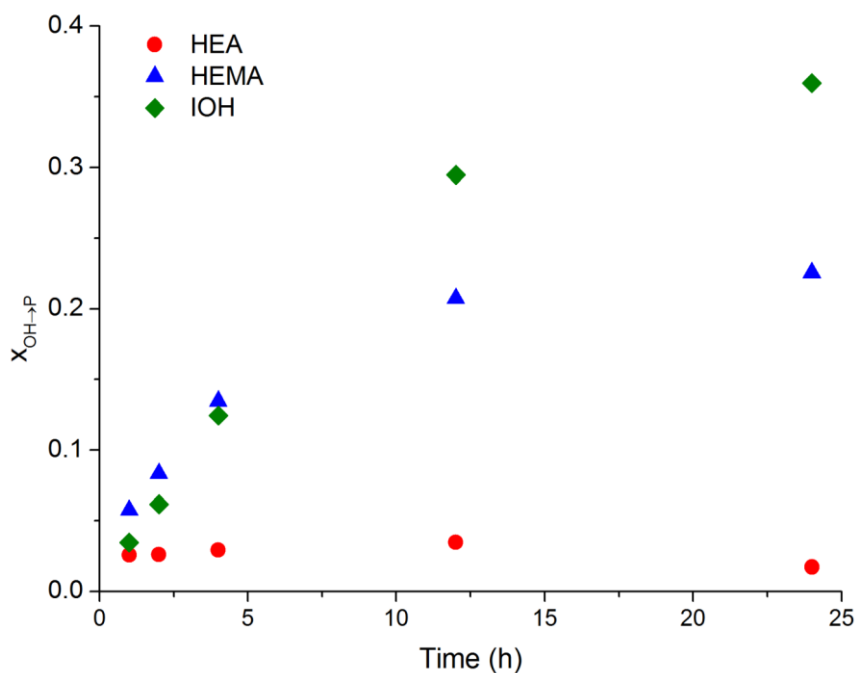
Figure 4.5. Hydroxyl monomer conversion to polymer ($x_{OH \to P}$) as a function of polymerization time for RAFT controlled radical copolymerizations. The $x_{OH \to P}$ values were calculated following the procedure described in the Experimental Details. Conditions were [M]:[CTA] = 190, 125 °C reaction temperature, and f_{OH} of 3 mol %. Of the hydroxyl comonomers, more IOH is converted into polymer.

Table 4.1. Monomer conversions to the various products and the properties of collected polymers for the RAFT controlled radical copolymerization of isoprene and hydroxyl containing monomers in the bulk at 125 °C for 24 h, [M]:[CTA] = 190, and f_{OH} = 3 mol %.

Comonomer	$x_{I \to P}$[b] (%)	$x_{OH \to P}$[c] (%)	$x_{I \to L}$[d] (%)	x_{DA}[e] (%)	F_{OH}[f] (%)	M_n[g] (kg/mol)	PDI[h]
None[a]	46		25			6.4	1.33
HEA	45	2	22	98	0.2	6.2	1.33
HEMA	50	23	23	77	1.3	6.6	1.31
IOH	45	36	24	57	2.2	6.1	1.38

[a]Isoprene homopolymerization. [b]Conversion of isoprene to polymer, calculated from ^{1}H NMR spectroscopy of dried aliquot at 24 h. [c]Conversion of hydroxyl comonomer to polymer, calculated from ^{1}H NMR spectroscopy of dried aliquot at 24 h. Error is estimated to be ± 2%, calculated as the range of $x_{I \to P}$ values for two separate homopolymerizations. [d]Conversion of isoprene to its dimer limonene, calculated from ^{1}H NMR spectroscopy of crude aliquot at 24 h. Error is estimated to be ± 3%, calculated as the range of $x_{I \to L}$ values for two separate homopolymerizations. [e]Conversion of hydroxyl monomer to Diels−Alder adduct, calculated from ^{1}H NMR spectroscopy of crude aliquot at 24 h. [f]Mole % of hydroxyl monomer in copolymer, calculated from ^{1}H NMR spectroscopy of precipitated polymer at 24 h. [g]Number average weight, calculated from ^{1}H NMR spectroscopic end-group analysis of precipitated polymer at 24 h. [h]Found by SEC calibrated with polyisoprene standards.

At 24 h, both HEA and HEMA had completely reacted while 93% of IOH reacted. The discrepancy between the $x_{OH \to P}$ and x_{OH} (Figure 4.6) for each monomer is due to the Diels−Alder side reaction. Resonances associated with the Diels−Alder adducts of each monomer (Figure 4.3b) with isoprene and isoprene dimerization are observed in the crude solution ^{1}H NMR spectra (Figure 4.7−Figure 4.10). A majority of the hydroxyl monomers converted to Diels−Alder products over the course of heating (column x_{DA} in Table 4.1). The $x_{I \to L}$ in all polymerizations at 24 h is around 25% as the isoprene dimerization is slower than the hydroxyl monomer Diels−Alder adduct formation (Figure 4.11). HEA is the most reactive comonomer towards a Diels−Alder reaction with isoprene, with the complete consumption of HEA in 4 h and 97% of HEA being converted to Diels−Alder adduct. HEMA is less reactive than HEA with an x_{DA} of 77%. As predicted, IOH is less reactive towards Diels−Alder adduct formation than HEA and HEMA, with 57% conversion to Diels−Alder products after 24 h.
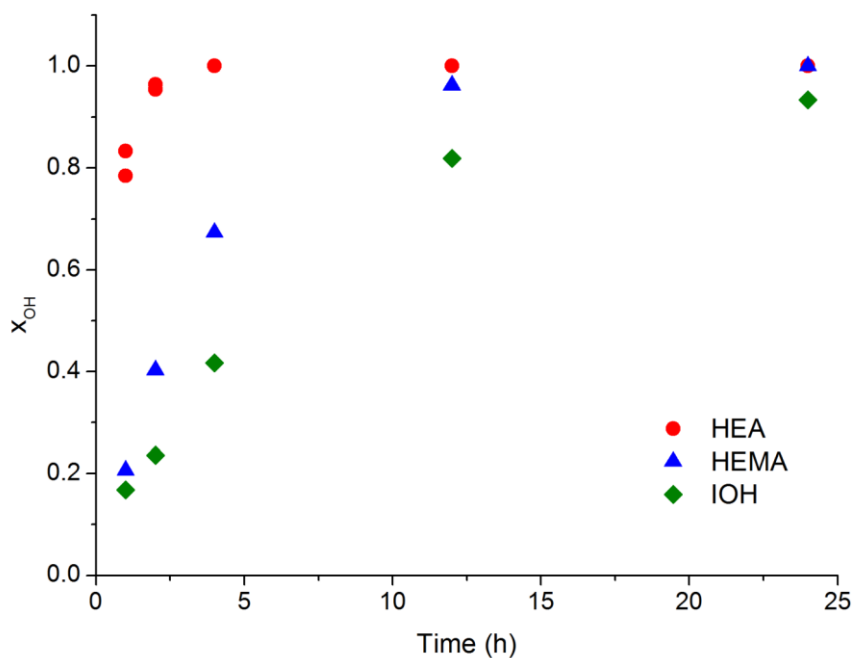
Figure 4.6. Total conversion of hydroxyl monomer (x_{OH}) as a function of reaction time for RAFT controlled radical isoprene copolymerizations at 125 °C. The total conversion for the hydroxyl comonomers was calculated from the ^{1}H NMR spectra of the crude aliquots (before drying) as discussed in the Experimental Details. HEA is completely consumed by 4 h and HEMA is completely consumed by 24 h.
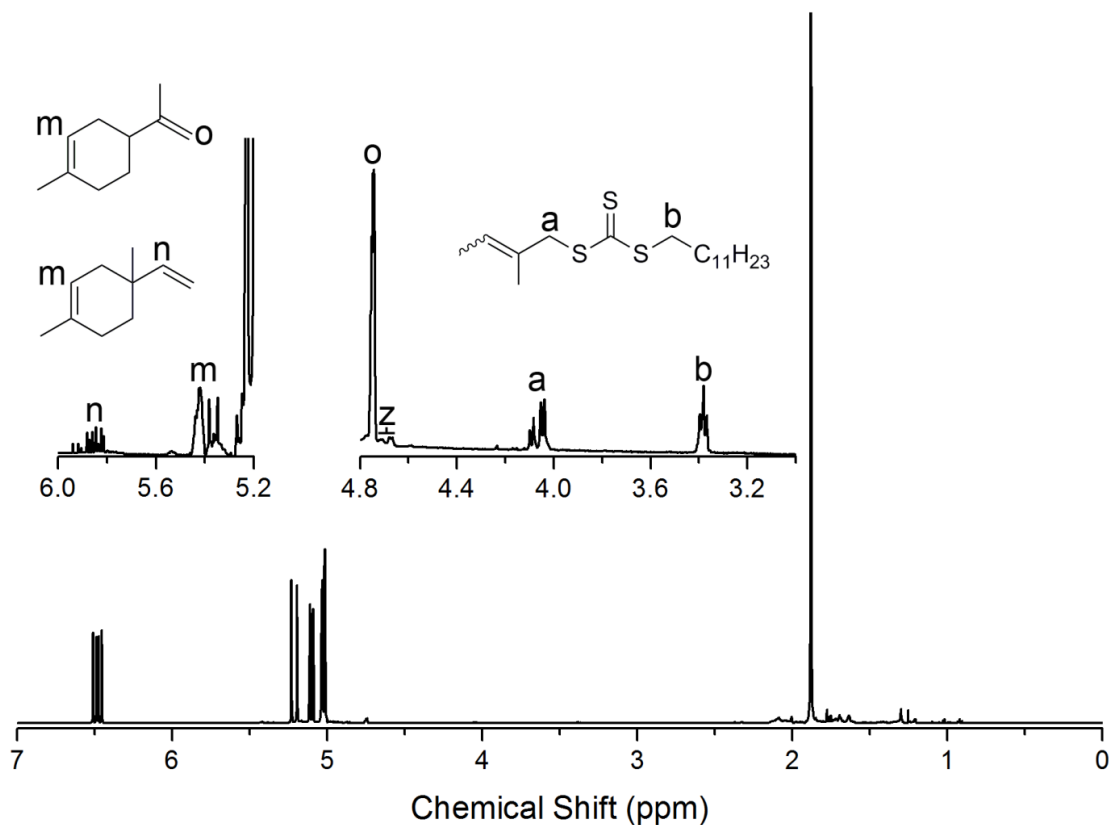
Figure 4.7. Representative ^{1}H NMR spectrum of the crude solution for the RAFT controlled radical homopolymerization of isoprene after 2 h at 125 °C. In the full axis spectrum, the prominent peaks belong to isoprene monomer. In the expanded regions, peaks that correspond to RAFT CTA end group region are labeled. The peak labeled "b" was used as an internal standard for all conversion calculations for all polymerizations. The peak labeled "o" corresponds with the isoprene homo-Diels–Alder adduct limonene. It overlaps with a set of peaks that correspond to half of the vinyl protons of the 3,4-addition product (other half is labeled "z"). See Experimental Details for sample calculations for conversion of isoprene to limonene ($x_{I \to L}$). Limonene is not the only isoprene Diels–Alder dimer formed. Additionally, the dimer 1,4-dimethyl-4-vinylcyclohex-1-ene (DMVCH) is produced as a minor product. The representative peaks corresponding to the protons of DMVCH overlap with polymer proton peaks so the conversion of isoprene to DMVCH could not be calculated directly from the crude aliquot ^{1}H NMR spectra. Heating isoprene at 125 °C for 24 h without polymerization favored the formation of limonene 4 to 1 over DMVCH. Likely, a similar ratio exists in the system when polymerization occurs.
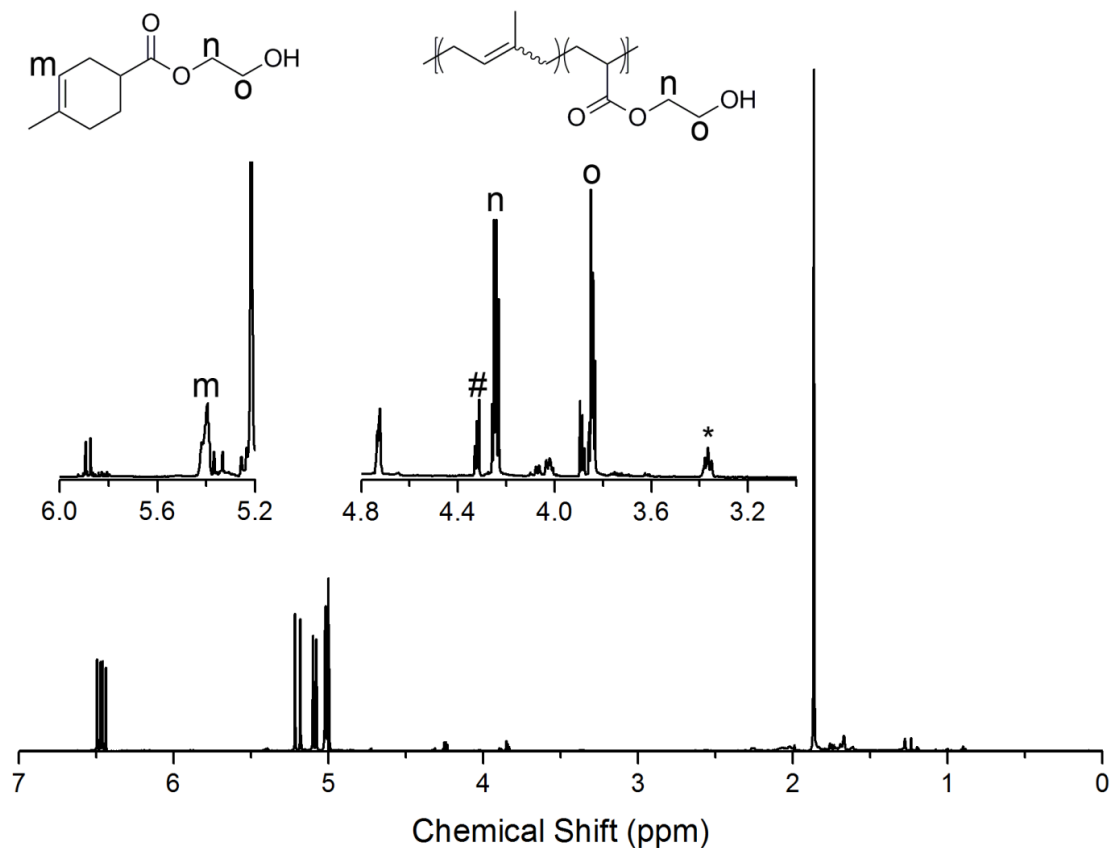
Figure 4.8. Representative ^{1}H NMR spectrum of the crude solution for the RAFT controlled radical copolymerization of isoprene and HEA after 1 h at 125 °C. The structure of HEA-isoprene Diels–Alder adduct is given with peak assignments. Protons associated with protons for both the Diels–Alder adduct and isoprene-HEA copolymer overlap as labeled on the expanded spectrum. The peak associated with residual monomer is labeled with a pound sign (#) and the peak corresponding to the RAFT CTA end-group is labeled by an asterisk (*). Total HEA monomer conversion was calculated as described in the Experimental Details.
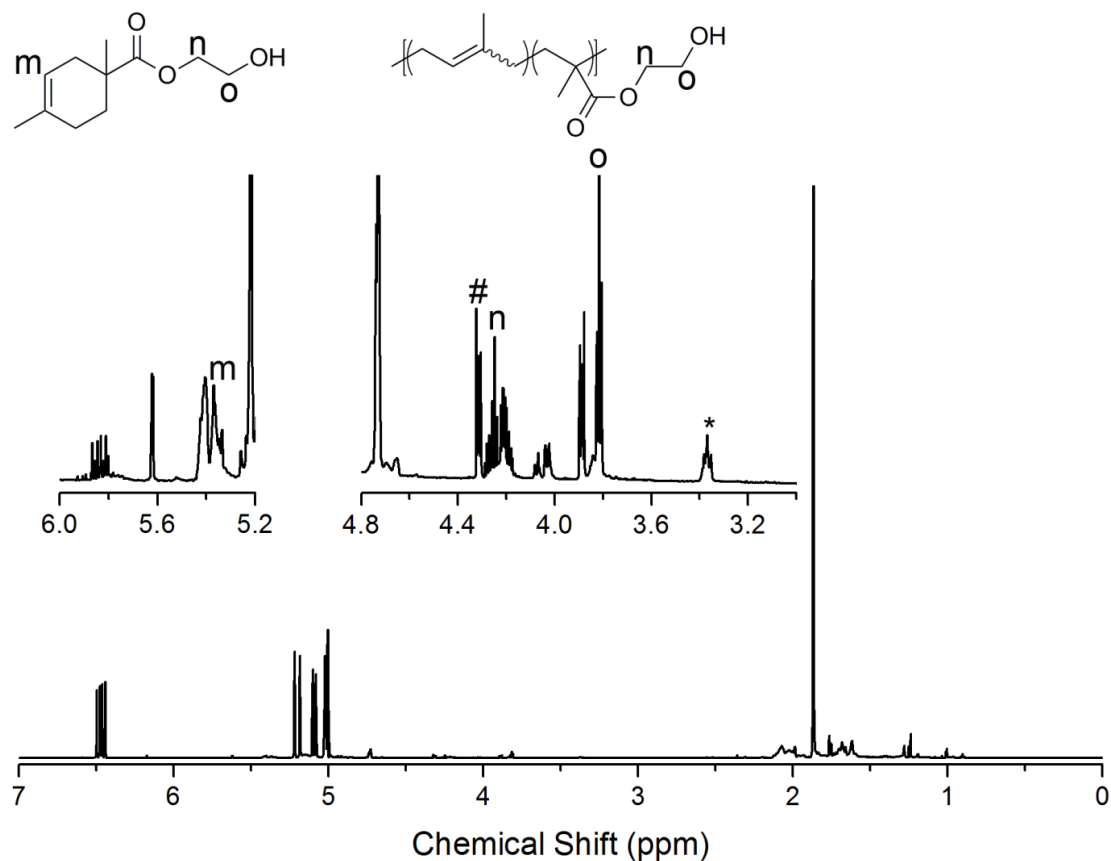
Figure 4.9. Representative ^{1}H NMR spectrum of the crude solution for the RAFT controlled radical copolymerization of isoprene and HEMA after 4 h at 125 °C. The structure of HEMA-isoprene Diels–Alder adduct is given with peak assignments. Protons associated with protons for both the Diels–Alder adduct and isoprene-HEMA copolymer overlap as labeled on the expanded spectrum. The peak associated with residual monomer is labeled with a pound sign (#) and the peak corresponding to the RAFT CTA end-group is labeled by an asterisk (*). Total HEMA monomer conversion was calculated as described in the Experimental Details.
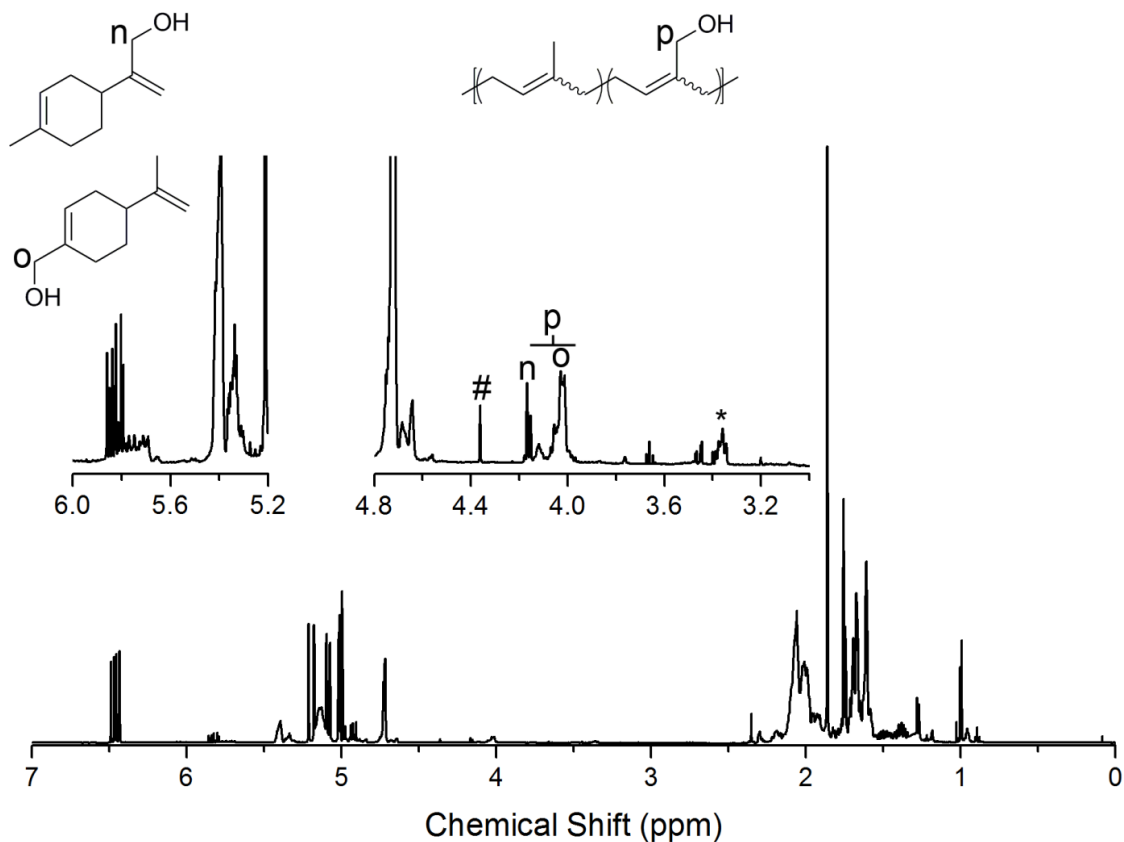
Figure 4.10. Representative ^{1}H NMR spectrum of the crude solution for the RAFT controlled radical copolymerization of isoprene and IOH after 24 h at 125 °C. Peaks are assigned for the Diels–Alder adducts of isoprene and IOH. The peak labeled "n" corresponds with the Diels–Alder adduct where IOH is the dienophile. The peak labeled "o" not only corresponds to protons on the Diels–Alder adduct where IOH is the diene, but it also corresponds to protons present on the IOH repeat units in the polymer and those that belong to the polymer end group (see Figure 4.7). The peak associated with residual monomer is labeled with a pound sign (#) and the peak corresponding to the RAFT CTA end-group is labeled by an asterisk. Total HEMA monomer conversion was calculated as described in the Experimental Details.
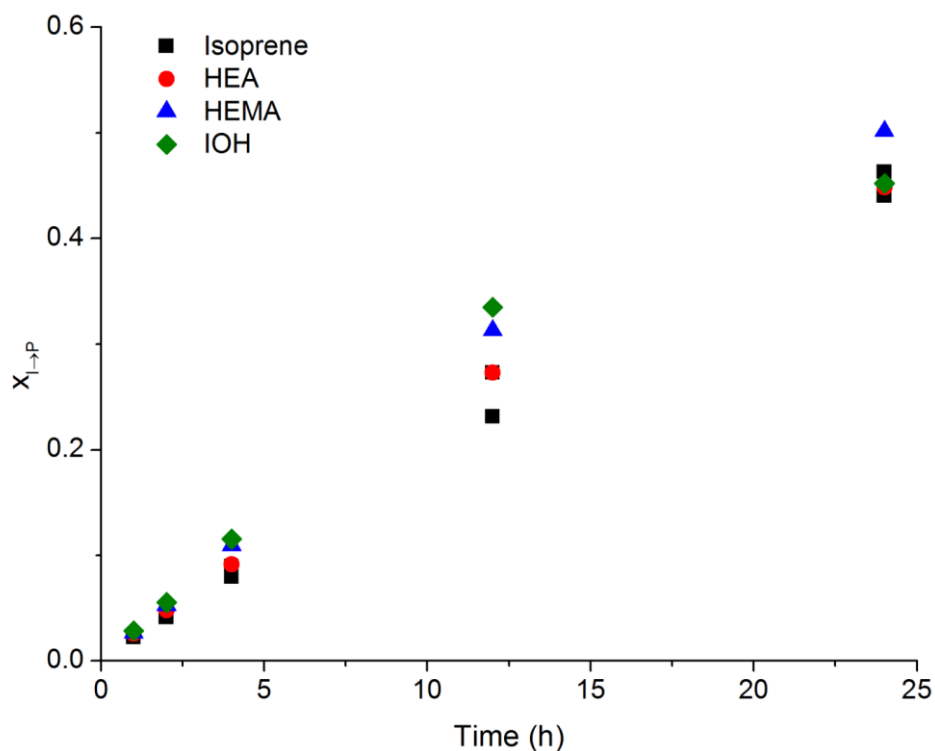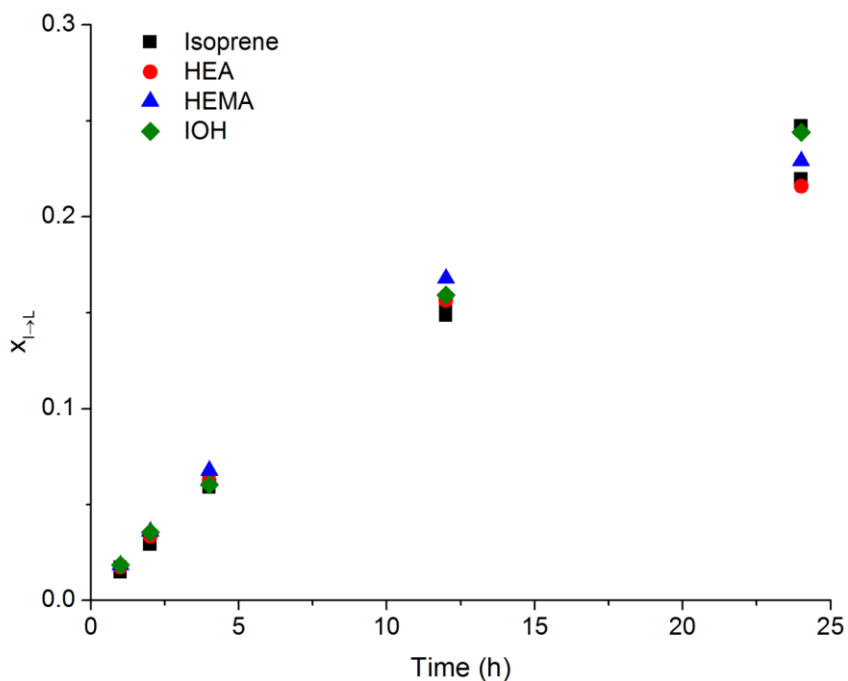
Figure 4.11. Conversion of isoprene to limonene ($x_{I \to L}$) as function of the polymerization time for isoprene homopolymerizations and hydroxyl monomer copolymerizations. Both homopolymerizations and copolymerizations exhibit similar trends in limonene production. Values are determined from ^{1}H NMR spectroscopic analysis of crude reaction solution aliquots taken during polymerization following the procedure discussed in Experimental Details.

HEA is the strongest dienophile with its pendent electron-withdrawing carbonyl group and as a result, it reacts quickly with isoprene. HEMA, though similar in structure to HEA, is significantly less reactive towards forming the Diels–Alder adduct as the methyl group provides steric hindrance and electron donation by induction. HEMA, *t*-butyl acrylate, and methyl methacrylate have been copolymerized with isoprene through a NMP process at high temperatures (ca. 120 °C), but without any mention of a Diels–Alder side reaction.[11] Since the NMP and RAFT controlled radical polymerizations occur at a similar reaction temperatures and have similar polymerization rates, the NMP copolymerizations likely also suffered from Diels–Alder side reactions. Compared to HEA and HEMA comonomers, IOH is the weakest dienophile and a lower x_{DA} results. However, unlike HEA and HEMA, IOH can be both a diene and dienophile in the Diels–Alder reaction, similar to isoprene. From analysis of the crude ^{1}H NMR spectrum (Figure 4.12), IOH undergoes the Diels–Alder reaction as the diene preferentially (2.2 to 1).
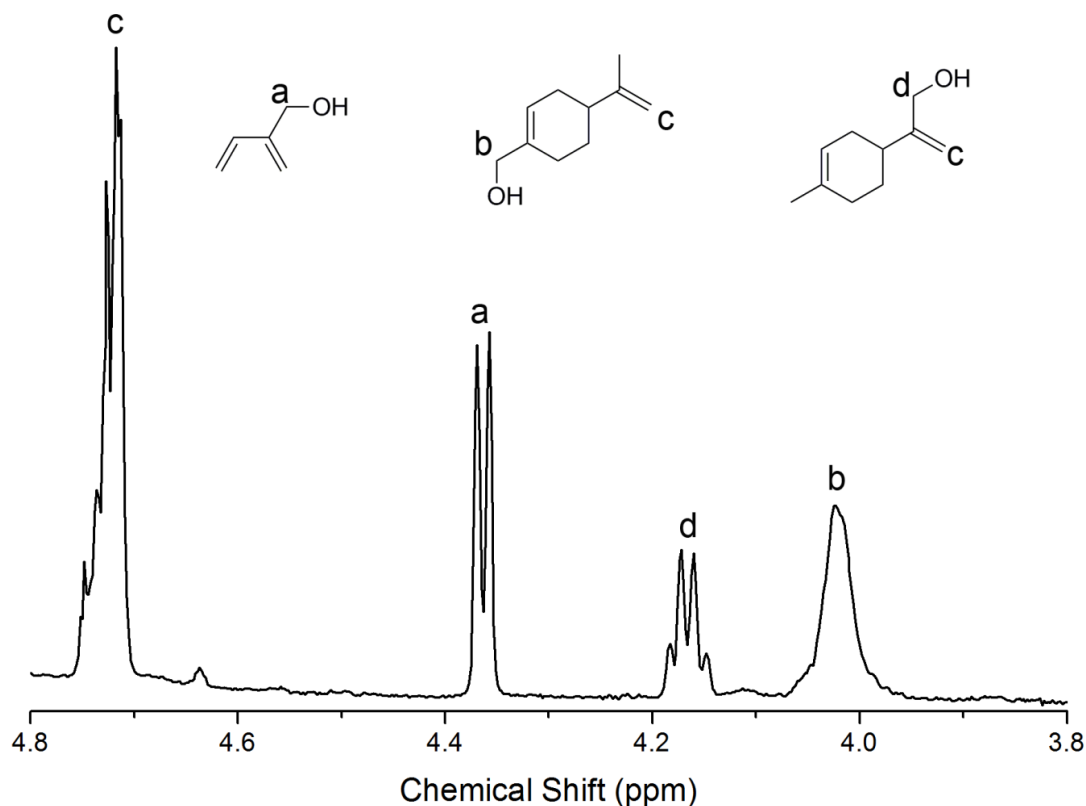
Figure 4.12. Expanded ^{1}H NMR spectrum of crude reaction solution of isoprene and IOH (3 mol % IOH) heated for 24 h at 125 °C. Peak assignments are given for the Diels–Alder adducts of isoprene and IOH where IOH is either the diene or dienophile. Other regioisomers are possible, but their structures are not shown. The peak corresponding to the remaining IOH monomer is labeled "a" and is split into a doublet by the alcohol proton. The peak labeled "c" corresponds to not only the Diels–Alder adduct of IOH and isoprene, but also the isoprene-isoprene Diels–Alder adduct. Total IOH conversion was 68% after 24 h. IOH is preferentially reacts as the diene 2.2 to 1 compared to reacting as the dienophile.

The mole fraction of hydroxyl monomer incorporated into the polymer chain (F_{OH}) was measured from the dried aliquot at each time point (Figure 4.13). The data indicate that the copolymerizations were not random as F_{OH} does not equal f_{OH} at every time point. Initially (1–4 h), the F_{OH} values for HEMA and IOH are greater than the f_{OH}, indicating that both HEMA and IOH preferentially polymerize over isoprene. Between 4 and 24 h, the F_{OH} values of all copolymerizations decrease below f_{OH}, indicating gradient copolymer formation. However, the IOH copolymer is significantly less gradient-like than the HEMA and HEA copolymers. During the copolymerization, the F_{OH} for IOH is always within 20% of f_{OH}, while the F_{OH} values of HEMA range from 210 to 46% of the f_{OH} value and little HEA is incorporated into the polymer. The gradient nature of the copolymer is a function of both the propensity of the hydroxyl monomer to copolymerize and undergo Diels–Alder reactions. The Diels–Alder reaction consumes HEA so quickly (x_{DA} at 4 h equals 97%) the monomer cannot participate in the copolymerization. HEMA polymerizes preferentially over isoprene and undergoes the Diels–Alder reaction faster than IOH so its copolymer (P(I-co-HEMA)) is more gradient-like than the IOH copolymer. IOH has polymerization and Diels–Alder kinetics similar to isoprene, giving a copolymer (P(I-co-IOH)) with comonomer contents that do not vary greatly along the polymer chain.
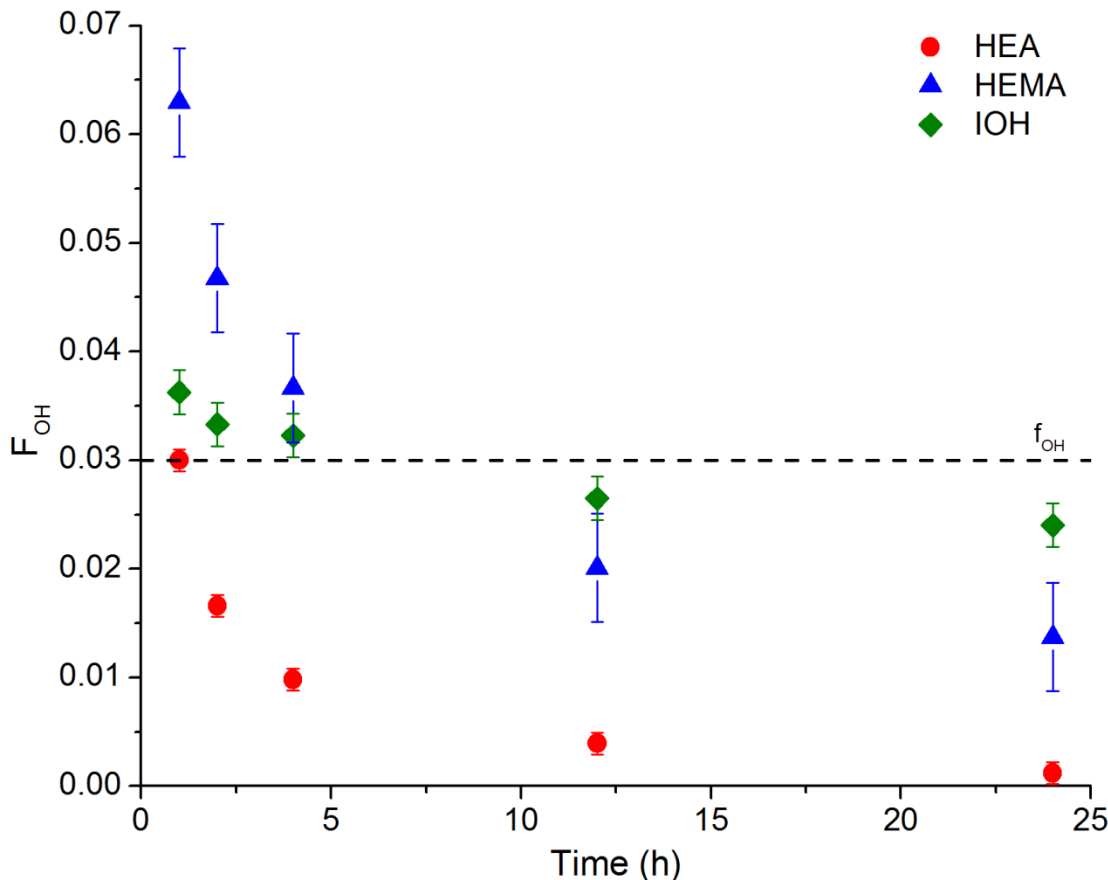
Figure 4.13. Mole fraction of hydroxyl comonomer in polymer (F_{OH}) as a function of polymerization time. Dashed line indicates hydroxyl comonomer feed mole fraction (f_{OH}) of 0.03. Polymerizations were performed at 125 °C in the bulk at a [M]:[CTA] = 190 with tert-butyl peroxide as the radical generator. Mole fractions we determined by ^{1}H NMR spectroscopy on dried aliquots at each time point. Error bars were estimated as the difference between the F_{OH} calculated from the aliquots (24 h) and the F_{OH} calculated from the precipitated polymer (24 h). For all comonomers, F_{OH} decreases as the polymerization proceeds as a result of the competing Diels–Alder reaction consuming hydroxyl comonomer.

Analysis of hydroxyl monomer content in the precipitated polymers confirms that more IOH was incorporated into the final polymer than HEA and HEMA (Table 4.1). The PI homopolymer and the copolymers have similar number average molecular weights (M_n) and polydispersity indexes (PDI = 1.3–1.4).[35,40] M_n (NMR) values were calculated assuming one CTA per polymer chain and using ^{1}H NMR spectroscopic end group analysis (Figure 4.14–Figure 4.17). This assumption was tested by comparing the

M_n measured by ^{1}H NMR spectroscopy with that measured by SEC calibrated with PI standards (Figure 4.18). The molecular weights of isoprene homopolymer closely match, while the SEC M_n is lower for HEMA and IOH copolymers. Perhaps, the deviation is due to the incorporation of hydroxyl groups changing the solvent quality and giving polymers with a different hydrodynamic radius in the SEC mobile phase.
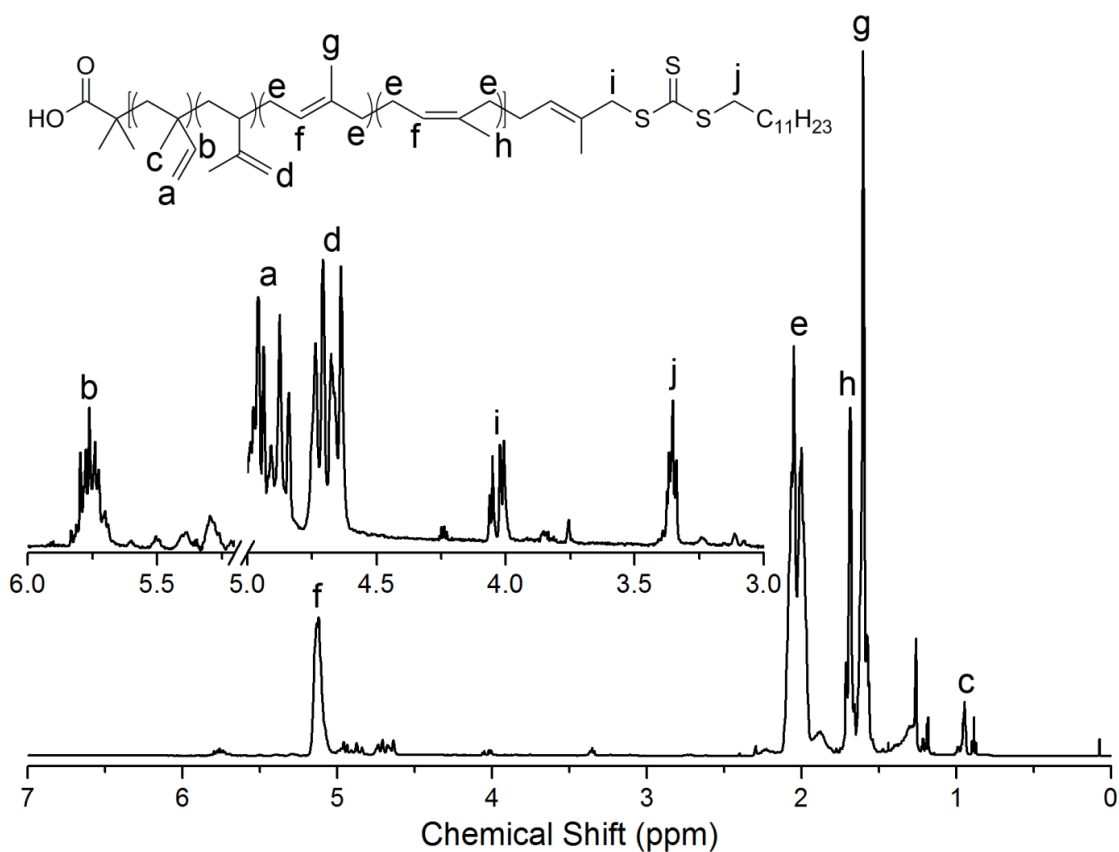
Figure 4.14. ^{1}H NMR spectrum with expanded region and peak assignments for RAFT controlled radical synthesized PI at [M]:[CTA] = 190 and 125 °C. The four possible isoprene repeat unit isomers are present in the polymer. Of the repeat units, 4.4 mol % are the 1,2-addition product; 6.0 mol % are the 3,4-addition product, and 89.6 mol % are the 1,4-addition product. Of the 1,4-addition product repeat units, 66% are of the *trans* configuration with the balance being the *cis* configuration. The isomeric composition of the PI is similar for all hydroxyl copolymers and the peaks assignments given are valid for the subsequent spectra of the hydroxyl copolymers.
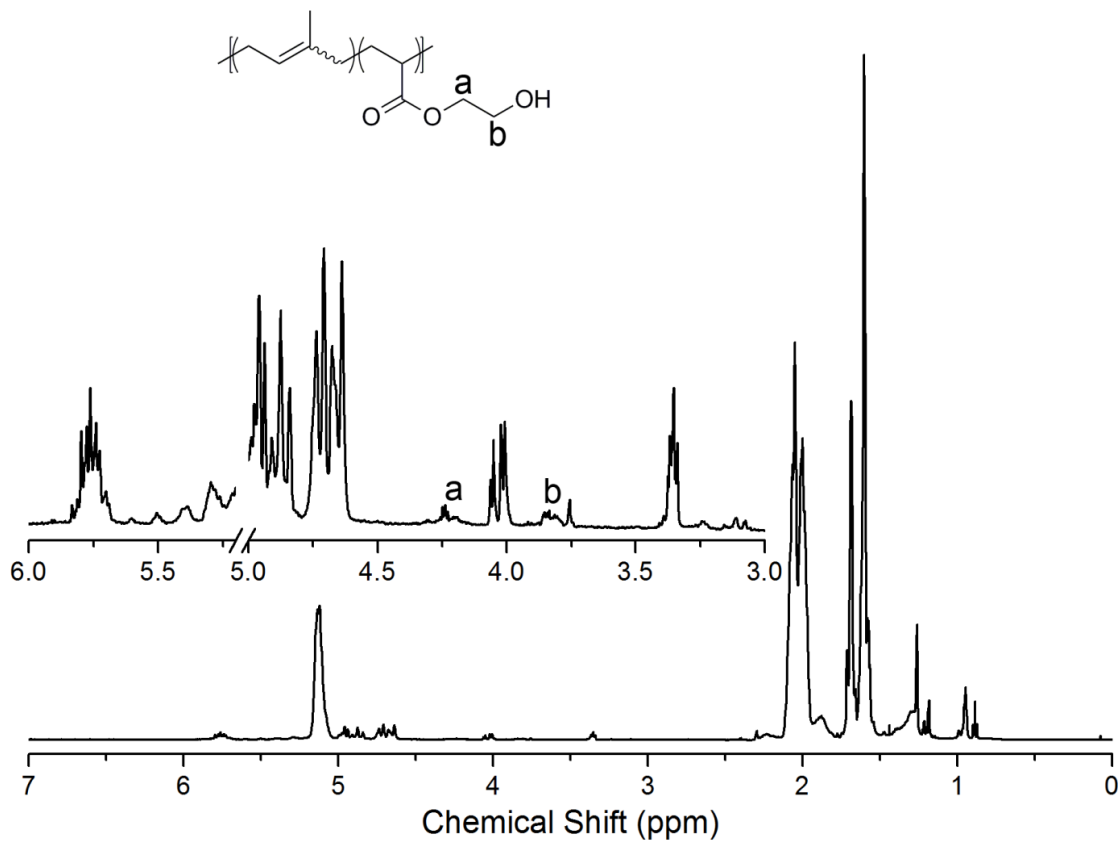
Figure 4.15. ^{1}H NMR spectrum with expanded region and peak assignments for RAFT controlled radical synthesized P(I-co-HEA) at [M]:[CTA] = 190, f_{OH} = 3 mol %, and 125 °C. PI peak assignments are given in Figure 4.14. The small labeled peaks are consistent with a limited amount of HEA copolymerized with isoprene.
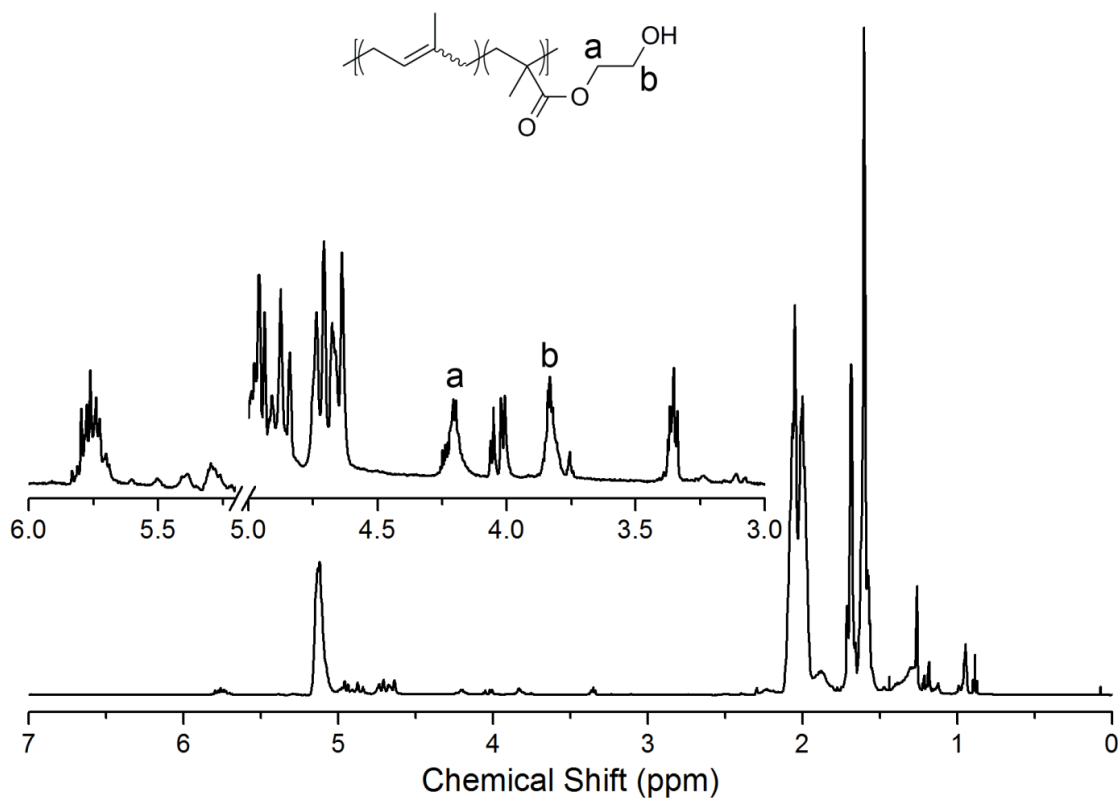
Figure 4.16. ^{1}H NMR spectrum with expanded region and peak assignments for RAFT controlled radical synthesized P(I-co-HEMA) at [M]:[CTA] = 190, f_{OH} = 3 mol %, and 125 °C. PI peak assignments are given in Figure 4.14. The small labeled peaks are consistent with the copolymerization of HEMA with isoprene.
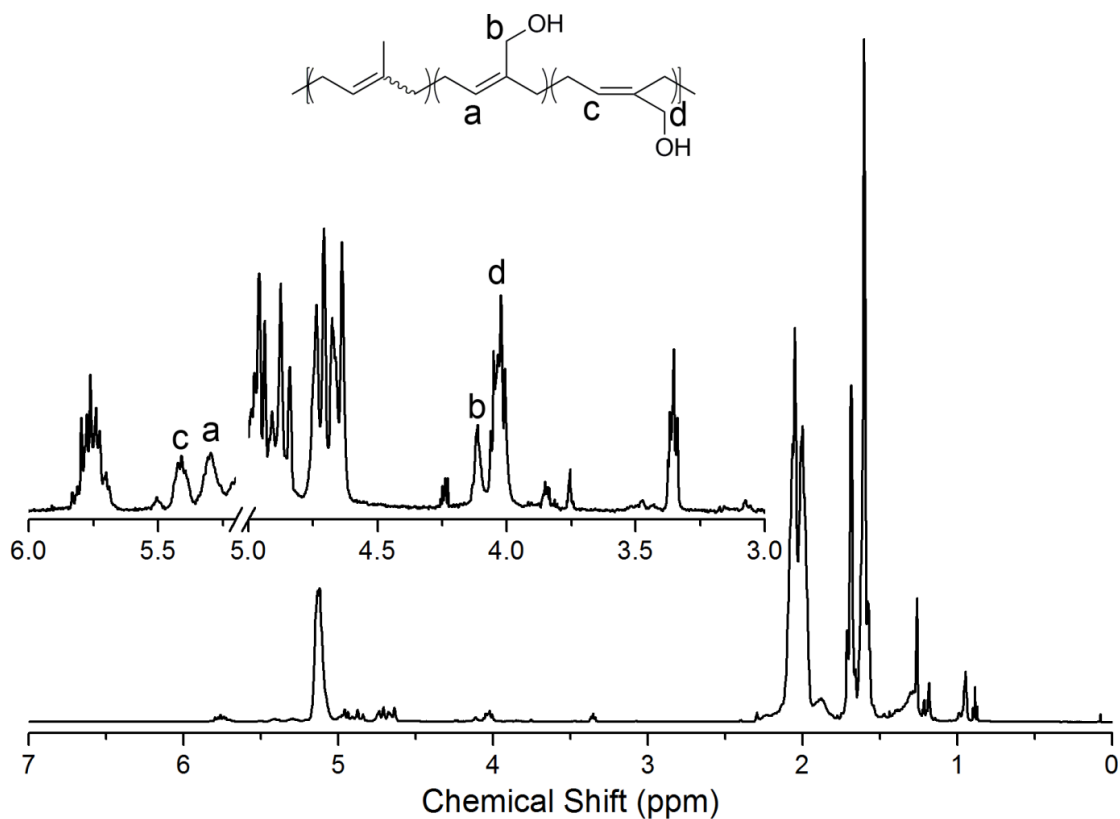
Figure 4.17. ^{1}H NMR spectrum with expanded region and peak assignments for RAFT controlled radical synthesized P(I-co-IOH) at [M]:[CTA] = 190, f_{OH} = 3 mol %, and 125 °C. PI peak assignments are given in Figure 4.14. Two of the possible isomers for the IOH repeat units are observed: *trans*-1,4-addition and *cis*-1,4-addition product. The production of the *cis* repeat units is preferred, accounting for 67% of the 1,4 isomers, with the *trans* isomers making up the balance. Significant production of the other two possible isomers of the IOH repeat unit (1,2 and 3,4) was not found. One of the peaks associated with the polymer end-group overlaps with the peak labeled "d," accounting for the multiplet observed.
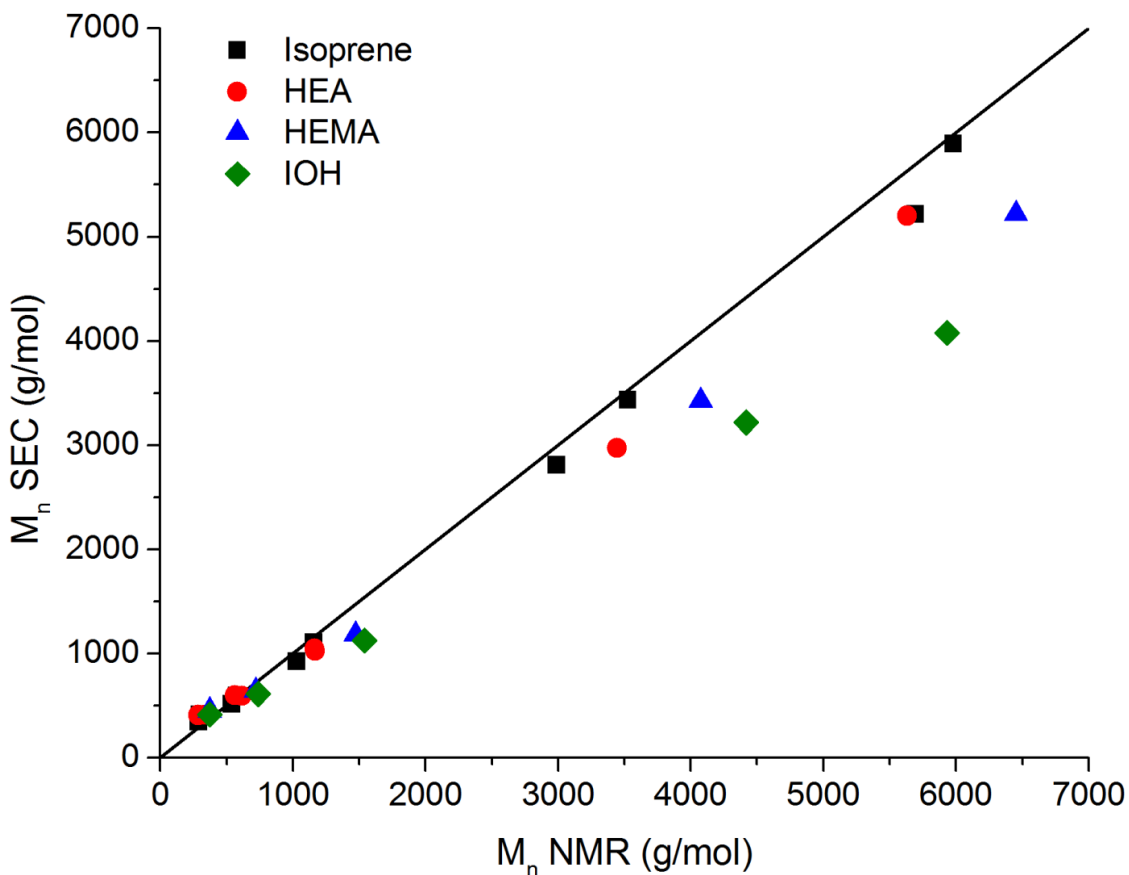
Figure 4.18. Comparison of M_n determined by SEC (M_n SEC) and ^{1}H NMR spectroscopy (M_n NMR) for isoprene homopolymerizations and hydroxyl monomer copolymerizations in the bulk at 125 °C. The solid line indicates where M_n SEC and M_n NMR are equal. Samples were taken as aliquots from the polymerizing reaction mixture. M_n NMR values were calculated by end group analysis and M_n SEC values were calculated by SEC calibrated with polyisoprene standards.

4.3.3 Emulsion copolymerization

Emulsion copolymerizations between isoprene and hydroxyl monomers were also investigated. Emulsion polymerizations generally have faster rates of polymerization than bulk radical polymerizations due to the segregation of free radicals to monomer swollen micelles.[41] The segregation limits bimolecular termination events and in the absence of significant chain transfer can lead to polymers with higher molecular weights.[41] The greater rate of polymerization allows for emulsion polymerizations to achieve high conversions at lower temperatures than corresponding bulk radical polymerizations. Emulsion polymerizations of isoprene have been performed at 25 °C and reach complete conversion in 48 h.[42] At this lower temperature the Diels–Alder reactions are expected to be significantly slower and perhaps would not negatively impact the copolymerization.

Emulsion copolymerizations of isoprene and HEA, HEMA, and IOH were investigated at a f_{OH} of 3 mol %. Sodium dodecylsulfate (SDS) was used as the surfactant for the copolymerizations at 25 °C. The initiator system was of the redox-couple type with *tert*-butylhydroperoxide (tBHP) and tetraethylenepentamine (TEPA) as a 1:1 redox pair ([I]). The CTA *tert*-dodecylmercaptan (TDM) was added at a 0.5:1 ratio to the redox initiator pair to reduce the molecular weights of the polymers formed. At a [M]:[I] equal to 50, hydroxyl monomers (HEA, HEMA, and IOH) and isoprene were copolymerized at 25 °C for 48 h. When the polymerizations were terminated, only the IOH copolymerization had significantly incorporated IOH into the final copolymer, giving a material with a F_{OH} value of 0.025. Little HEMA ($F_{OH} = 0.003$) and no HEA were incorporated into the polymer. The difference in F_{OH} values between the monomers is likely due to the different solubilities of the monomers and their oligomers. HEA and HEMA are very soluble in water, while IOH has limited (8 g/mL, see Experimental Details) solubility in water like other pentanols.[43,44,45] Patent reports of emulsion copolymerizations of IOH with monomers other than isoprene confirm the limited water solubility of IOH.[31,32] We expect that IOH will be mostly present in the isoprene droplets and HEMA and HEA will largely partition to the aqueous phase.

Different polymer molecular weights were targeted by changing the [M]:[I] (Table 4.2). By altering the [M]:[I], the average number of radicals per micelle (*n*) changes, giving different polymerization rates. Higher [M]:[I] values give lower *n*, which decreases the polymerization rate. The slower polymerization rate translates into lower total monomer conversion (x_M) (found gravimetrically) values at 48 h (Table 4.2). The M_n values (calculated from SEC, see Figure 4.19 for SEC elution curves) increase for copolymers with higher [M]:[I] as the [M]:[CTA] ratio increases and *n* decreases (Table 4.2). With less CTA and lower *n* the polymer chains are able to propagate longer before a termination event occurs, giving higher M_n. Furthermore, the probability of chain coupling and branching events increases as the conversion nears completion which leads to higher PDI values (Figure 4.20).

Table 4.2. Properties of isoprene/IOH emulsion copolymers at 25 °C for 24 h, [I]:[CTA] = 0.5 where the CTA is tert-dodecylmercaptan, and f_{IOH} = 0.03.

[M]:[I][a]	x_M[b] (%)	F_{IOH}[c]	M_n[d] (kg/mol)	PDI[d]
50	96	0.023	6	4.75
150	74	0.025	12	2.77
430	56	0.021	24	2.99

[a]Monomer to initiator ratio, where the initiator is the redox pair tetraethylenepentamine and tert-butyl hydroperoxide. [b]Total monomer conversion calculated by gravimetric analysis of the polymerization products. [c]Mole fraction of IOH incorporated in polymer. [d]Determined by SEC using polyisoprene standards.
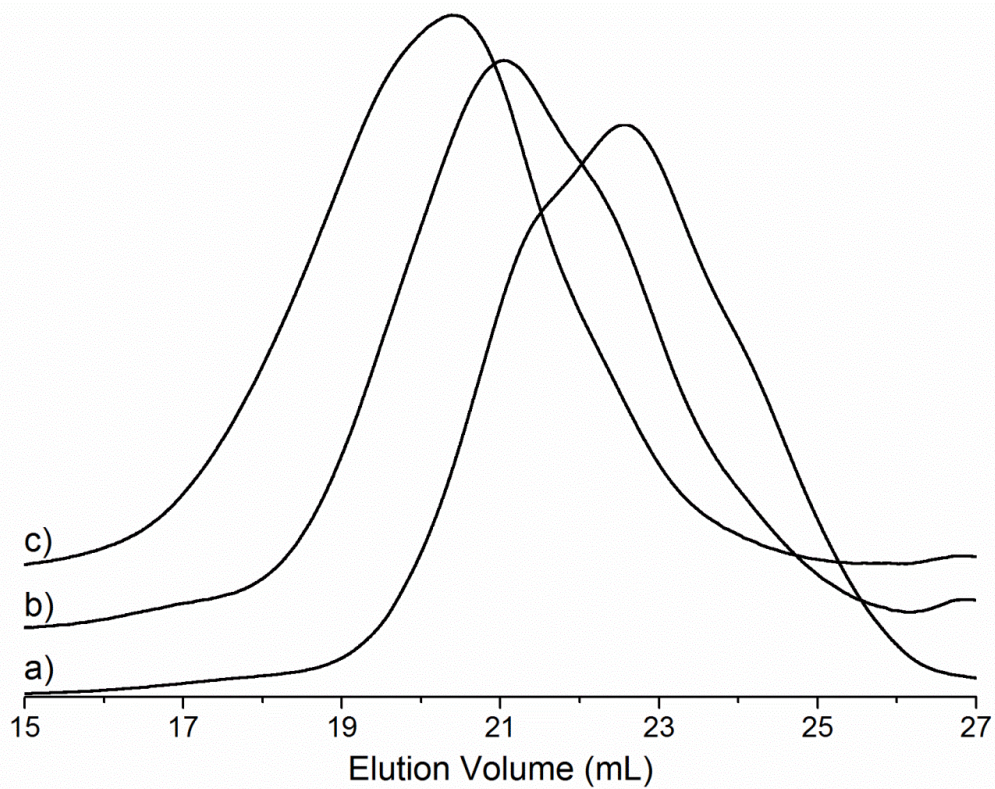
Figure 4.19. Representative SEC elution curves for emulsion copolymerizations of isoprene and IOH at [M]:[I] values of (a) 50, (b) 150, and (c) 430. As [M]:[I] increases the peak of each elution curve shifts to lower elution volume, indicative of a higher M_n. Distributions are broad (PDI > 2) and typically have a shoulder off the main peak.
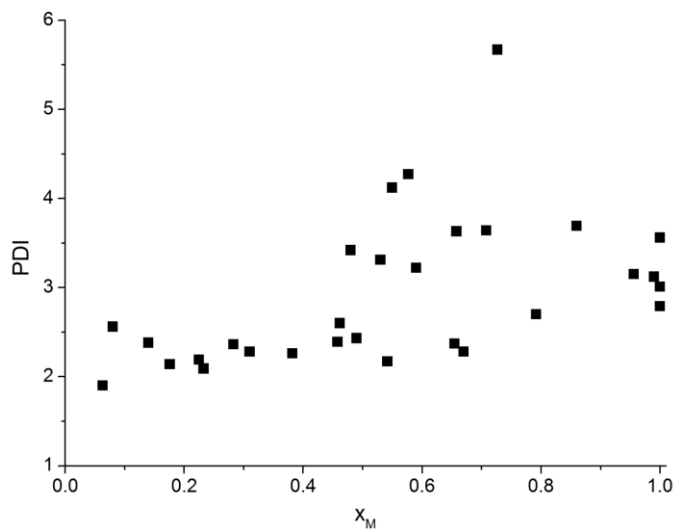
Figure 4.20. The PDI of emulsion isoprene/IOH (f_{IOH} range of 3 to 5 mol %) copolymers as a function of total monomer conversion calculated gravimetrically (x_M).

All the polymers in Table 4.2 had F_{IOH} values between 0.021 and 0.025, but it is unclear how the IOH monomer is distributed among the polymer chains. No Diels–Alder reaction was observed between IOH and isoprene under the reaction conditions investigated, so the incorporation of the IOH monomer into the copolymer is simply a function of the copolymerization kinetics. A series of polymerizations with f_{IOH} values ranging from 3 to 5 mol % were stopped at varying times to give materials with different overall monomer conversion (x_M) values (Figure 4.21). The ratio of the F_{OH} for IOH (F_{IOH}) to the f_{OH} for IOH (f_{IOH}) (F_{IOH}/f_{IOH}) increases as monomer is consumed. The copolymerization undergoes compositional drift with a value of F_{IOH}/f_{IOH} approximately equal to 0.4 initially in the polymerization and reaching 0.8–0.9 at high x_M (0.8–1). The fact that F_{IOH}/f_{IOH} is less than one at low conversion signifies that isoprene is preferentially added early in the polymerization and is the faster polymerizing monomer. The initial deviation (x_M ca. 10%) of F_{IOH}/f_{IOH} from one observed in the polymerizations at f_{IOH} circa 3 mol % also occurs for f_{IOH} values up to 30 mol % (Figure 4.22). Eventually all of the IOH should be incorporated into polymer at the end of the polymerization (x_M = 1) and F_{IOH}/f_{IOH} should equal one, but this is not observed as F_{IOH}/f_{IOH} ranges from 0.8 to 0.95 at x_M = 1. The origin of this deviation from the expected value of F_{IOH}/f_{IOH} may be

due to the uncertainty of calculating x_M or loss of high IOH content polymers during precipitation. Loss of the high IOH content polymers would result in a F_{IOH}/f_{IOH} value less than the actual value of the polymerizing emulsion.
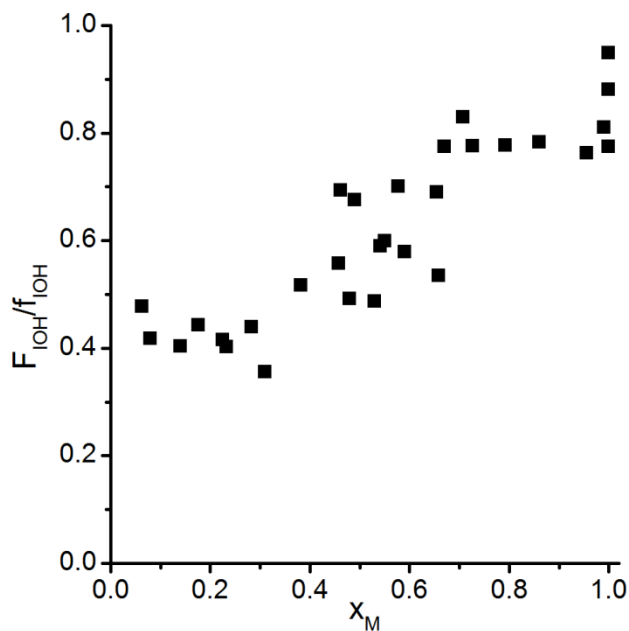
Figure 4.21. F_{IOH}/f_{IOH} as a function of the overall monomer conversion (x_M) in emulsion copolymerizations of IOH and isoprene. Each point is a separate polymerization with f_{IOH} equal to 3–5 mol %. The x_M values were calculated by massing a dried aliquot of the emulsion. As x_M increases the F_{IOH}/f_{IOH} increases.
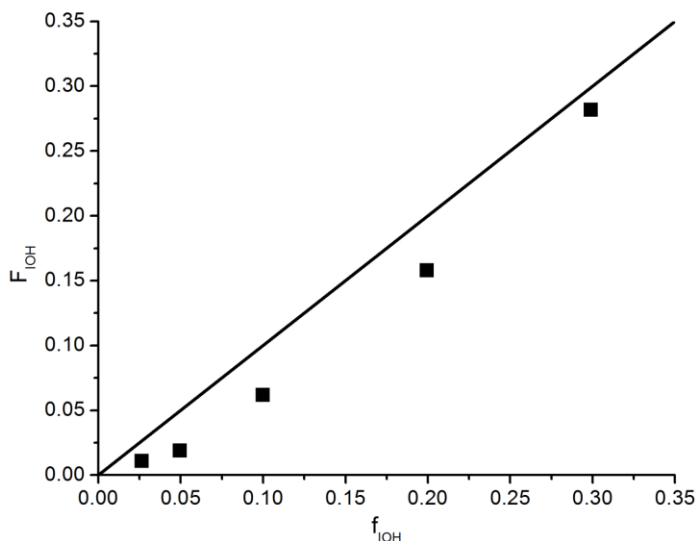
Figure 4.22. Copolymer IOH mole fraction (F_{IOH}) as a function of IOH mole fraction fed (f_{IOH}) at low x_M values (5–14%). Solid line represents where F_{IOH} equals f_{IOH}. F_{IOH} is less than f_{IOH} over the range of values investigated. Interestingly, as the f_{IOH} increases (ca. 30 mol %) the F_{IOH} and f_{IOH} values become more similar, suggesting that the composition curve may cross the $F_{IOH} = f_{IOH}$ line at higher f_{IOH}.

Differential scanning calorimetry (DSC) was performed on the copolymers with various values of F_{IOH} (Figure 4.23). With increased F_{IOH}, the glass transition temperature (T_g) of the copolymers increased. At the higher F_{IOH} values (0.158 and 0.282), the breadth of glass transition widens along with the T_g increase. The broad glass transitions observed likely are due to the compositional drift of the copolymerization creating copolymers early in the polymerization with F_{IOH} lower than the average measured and copolymers late in the polymerization with F_{IOH} higher than the average measured.
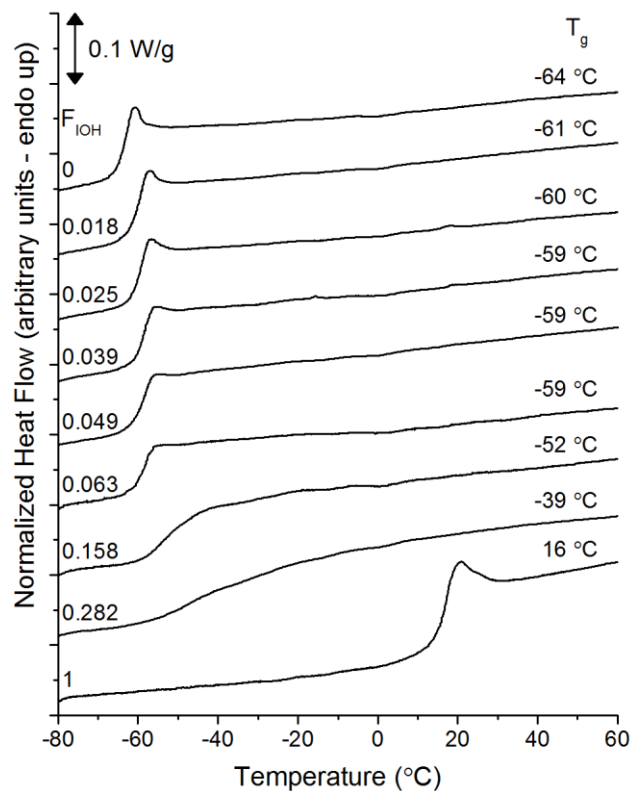
Figure 4.23. Representative DSC thermograms for emulsion polymerized P(I-co-IOH) copolymers and PIOH homopolymer. The mol % of IOH in the copolymer (F_{IOH}) and glass transition temperature (T_g) are given for their respective thermogram. Thermograms are normalized and shifted vertically to improve clarity. For all thermograms, a single glass transition temperature is observed.

4.3.4 Homopolymerization of IOH

IOH was homopolymerized in both a bulk controlled radical RAFT polymerization and emulsion polymerization. The RAFT controlled radical homopolymerization of IOH was performed following the copolymerization procedure at 125 °C for 24 h and a [M]:[CTA] equal to 190. ^{1}H NMR spectra of the crude reaction solution indicate that significant polymerization occurred as well as monomer isomerization to small molecules that contain aldehyde functionality (Figure 4.24). The collected polymer was soluble in chloroform and was analyzed by SEC and ^{1}H NMR spectroscopy (Figure 4.25 and Figure 4.26). The RAFT synthesized PIOH had a M_n (SEC calibrated with polystyrene standards) of 16 kg/mol and PDI equal to 2.75 (Figure 4.26). The broad distribution suggests the polymerization was not well controlled. The emulsion polymerization of IOH followed the procedure used for the copolymer synthesis with a [M]:[I] of 50 and a 17 h polymerization at 25 °C (43% conversion). The repeat units of the emulsion synthesized PIOH were primarily the result of 1,4-addition while the RAFT controlled radical polymerized PIOH had a nearly equimolar mixture of the 3,4 and 1,4-additions indicated by their respective ^{1}H NMR spectra (Figure 4.25). Consequently, the emulsion synthesized PIOH was insoluble in chloroform, but soluble in methanol, likely due to its differing structure. The T_g values of the emulsion polymerized PIOH and RAFT controlled radical polymerized PIOH were 16 and 13 °C, respectively. Though the different polymerization methods gave PIOH with different chemical structures, the polymerization examples demonstrate that IOH can be homopolymerized to give a polymer with pendent hydroxyl groups.
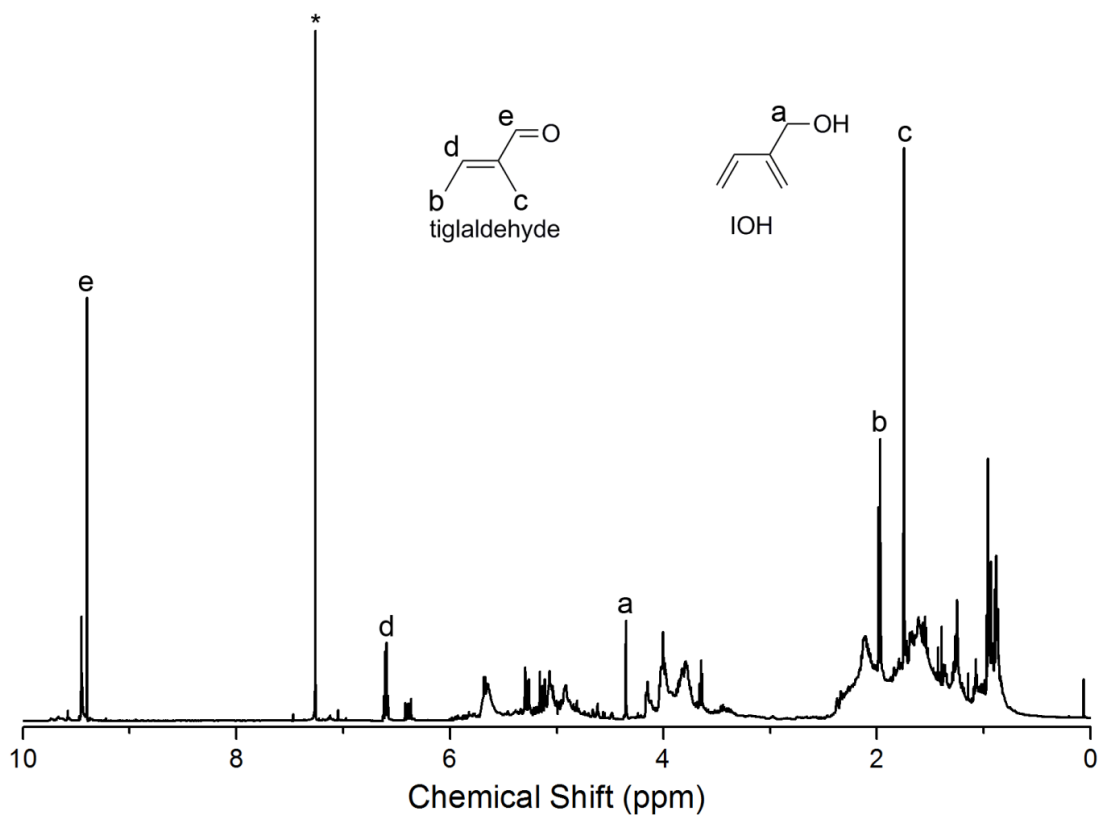
Figure 4.24. ^{1}H NMR spectrum of crude reaction solution of bulk RAFT controlled radical polymerization of IOH at 125 °C for 24 h. Original monomer remains as indicated by the peak labeled "a," but is a minor component of the mixture. Broad peaks at 6–3 ppm and 2.5–0.7 ppm resonances are indicative of polymer formation. New peaks that correspond to IOH isomerized to tiglaldehyde are now present in the mixture after heating (see labeled peaks on spectrum).[46] The exact mechanism for the isomerization of IOH to tiglaldehyde is unclear. Fourier transform-infrared (FT-IR) spectroscopy confirmed the presence of aldehydes as there was an absorption at 1725 cm^{-1}.
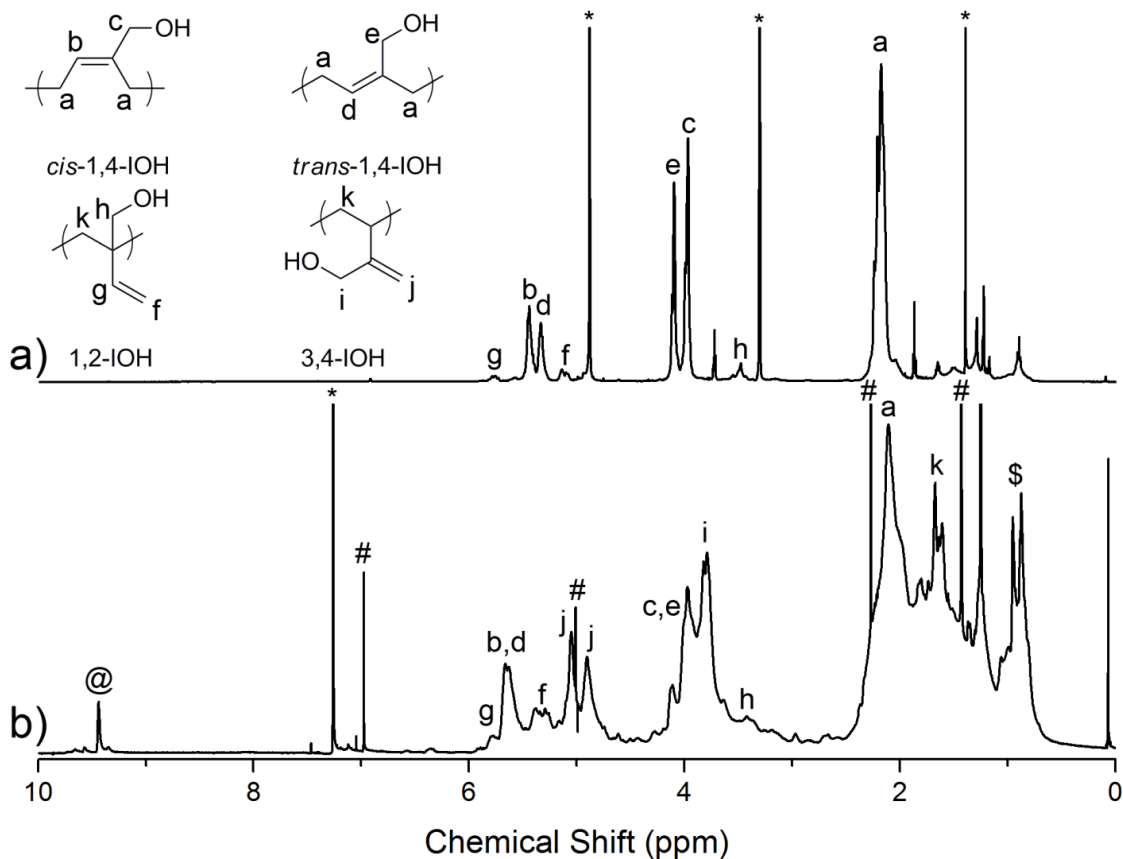
Figure 4.25. ^{1}H NMR spectra of (a) emulsion synthesized PIOH (500 MHz, CD$_3$OD) and (b) bulk RAFT control radical polymerized PIOH (500 MHz, CDCl$_3$) with tentative peak assignments. Asterisks (*) mark peaks of residual NMR solvent. The pound sign (#) denotes peaks belonging to butylated hydroxytoluene (BHT). The isomer composition of the emulsion synthesized PIOH is 5.3% 1,2-IOH, 41.8% *trans*-1,4-IOH, and 52.9% *cis*-1,4-IOH. No 3,4-addition products were observed in the emulsion polymerized PIOH. The RAFT polymerized PIOH has a significantly different molecular architecture than the emulsion PIOH with 45% 3,4-IOH, 48% 1,4-IOH, and 7% 1,2-IOH. Additionally, peaks associated with saturated methyl groups ($) and aldehydes (@) are present in the ^{1}H NMR spectrum of the RAFT synthesized PIOH, which do not correspond to any of the expected IOH repeat unit isomers. The protons that correspond to the $ and @ labeled peaks may be a result of the aldehyde side product, discussed in Figure 4.24, reacting with the growing polymer chain. FT-IR of the RAFT polymerized PIOH is consistent with the presence of aldehydes in the polymer sample (1727 cm^{-1}). The FT-IR of the emulsion polymerized PIOH is devoid of such absorptions. The different isomeric composition of the IOH homopolymers results in different solubilities. The RAFT polymerized PIOH is insoluble in hexanes and methanol while soluble in tetrahydrofuran, chloroform, and methylene chloride. The emulsion polymerized PIOH is insoluble in hexanes and chloroform, slightly soluble in tetrahydrofuran, and soluble in methanol and ethanol.
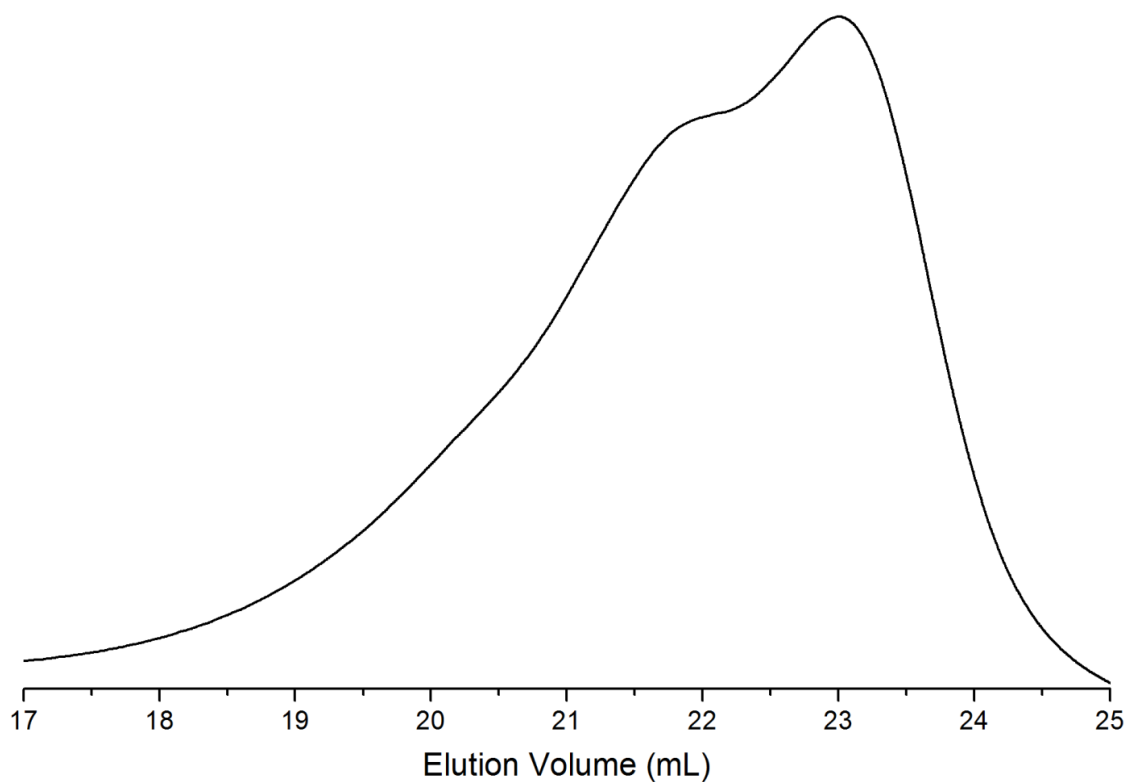
Figure 4.26. SEC elution curve of RAFT controlled radical polymerized PIOH. Using polystyrene standards, the M_n is 16 kg/mol and the PDI is 2.75. The bimodal nature of the peak and broad PDI indicate that the polymerization was not controlled. The high molecular weight tail suggests that the PIOH interacts with the column.

4.3.5 Graft copolymer synthesis

To demonstrate the availability of pendent hydroxyl group for subsequent reactions, the P(I-co-HEMA) and P(I-co-IOH) copolymers in Table 4.2 were used as macroinitiators for polylactide (PLA) synthesis. A 50/50 weight ratio of D,L-lactide and macroinitiator were targeted for each system. The polymerizations were catalyzed with 1,5,7-triazabicyclo[4.4.0]dec-5-ene (TBD) at a [M]:[TBD] of 7.5. TBD loading was higher than typical lactide homopolymerizations to counteract any potential acid-base interactions between the TBD and the carboxylic acid end groups on the RAFT macroinitiators.[47,48] SEC elution curves of the collected products shift to lower elution volumes as compared to the macroinitiators, consistent with the formation of the graft polymers P(I-co-HEMA)-g-PLA and P(I-co-IOH)-g-PLA (Figure 4.27).
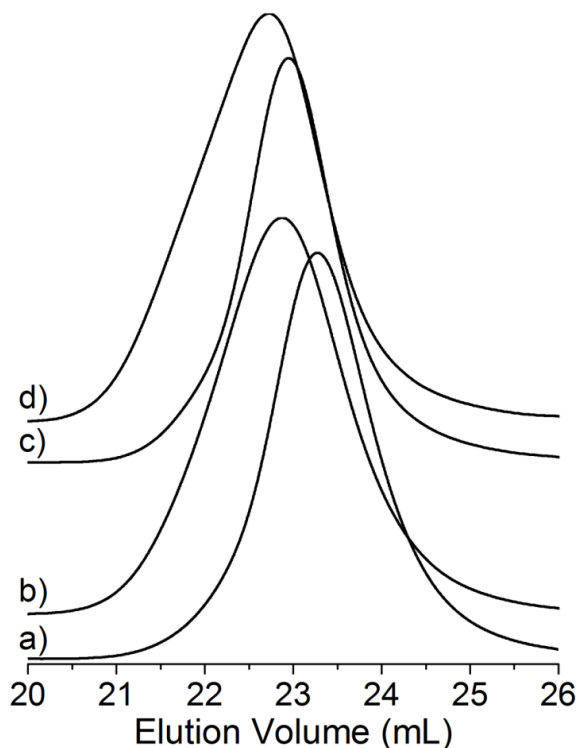
Figure 4.27. SEC of elution curves of (a) P(I-co-IOH), (b) P(I-co-IOH)-g-PLA, (c) P(I-co-HEMA), and (d) P(I-co-HEMA)-g-PLA. P(I-co-IOH) and P(I-co-HEMA) were synthesized by RAFT controlled radical copolymerization (Table 4.1). M_n (SEC, PS standards) values are 10 and 12 kg/mol, and PDI values are 1.47 and 1.44 for P(I-co-IOH)-g-PLA and P(I-co-HEMA)-g-PLA, respectively.

Analysis of the ^{1}H NMR spectra for the collected materials confirms the formation of graft copolymers (Figure 4.28 and Figure 4.29) as resonances associated with the methylene protons adjacent to the hydroxyl groups of each macroinitiator are no longer present. New peaks form in the spectra at chemical shifts that are consistent with lactide polymerization from the macroinitiator. From the ^{1}H NMR spectra, the PLA content in each graft copolymer was calculated to be 29 and 33 wt % (57 and 65% lactide conversions) for P(I-co-HEMA)-g-PLA and P(I-co-IOH)-g-PLA, respectively. The average molecular weight of the PLA arms for P(I-co-HEMA)-g-PLA was calculated to be 2.1 kg/mol as compared to the theoretical value (based off monomer conversion and number of hydroxyl groups per macroinitiator chain) of 2.0 kg/mol. Similarly close to the theoretical molecular weight, is the average PLA arm molecular weight of P(I-co-IOH)-g-PLA − 1.7 kg/mol measured versus 1.6 kg/mol theoretical. This accuracy is consistent pure graft polymers being formed without significant PLA homopolymer contamination.
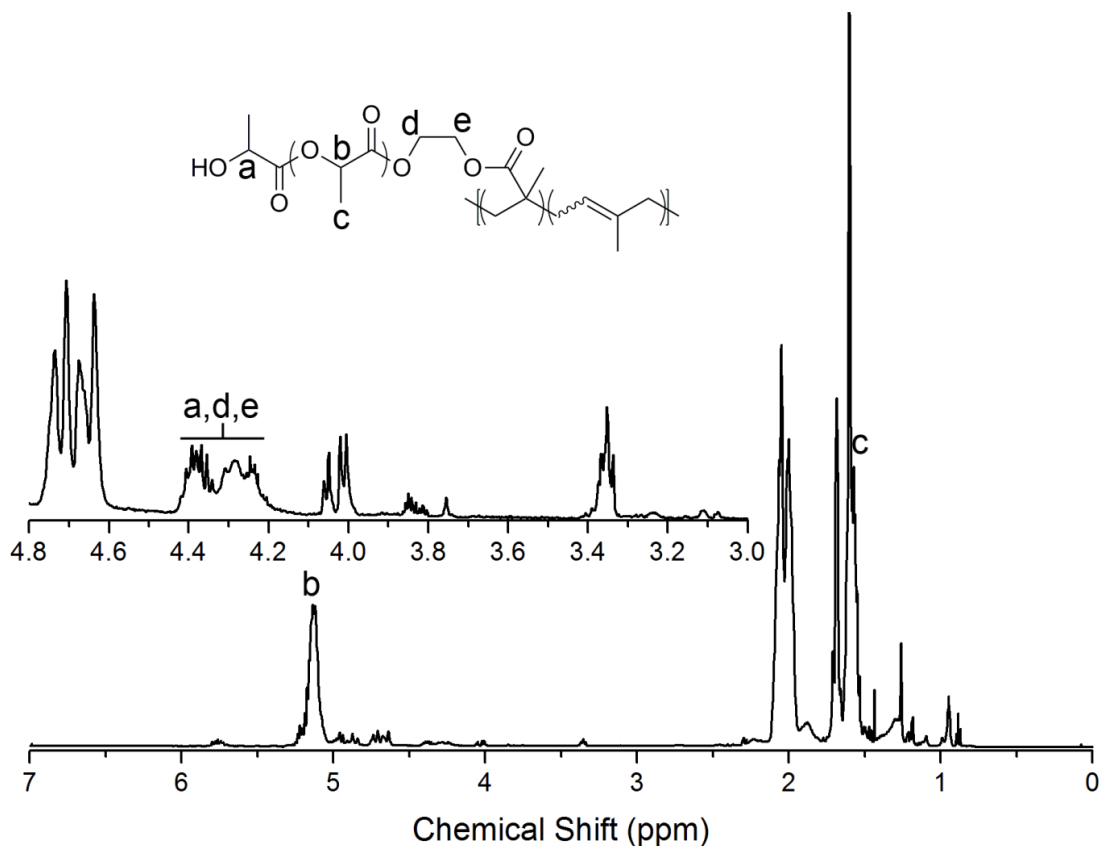
Figure 4.28. ^{1}H NMR spectra and expanded spectrum region of P(I-co-HEMA)-g-PLA. P(I-co-HEMA) macroinitiator peaks assignments are given in Figure 4.16. Peaks that correspond to PLA repeat unit protons overlap with those corresponding to the macroinitiator. The peak associated with the PLA end-group proton overlaps with the peaks belonging to the initiating HEMA group. Consequently, the region indicated by "a,d,e" on the spectrum represents five protons per PLA arm.
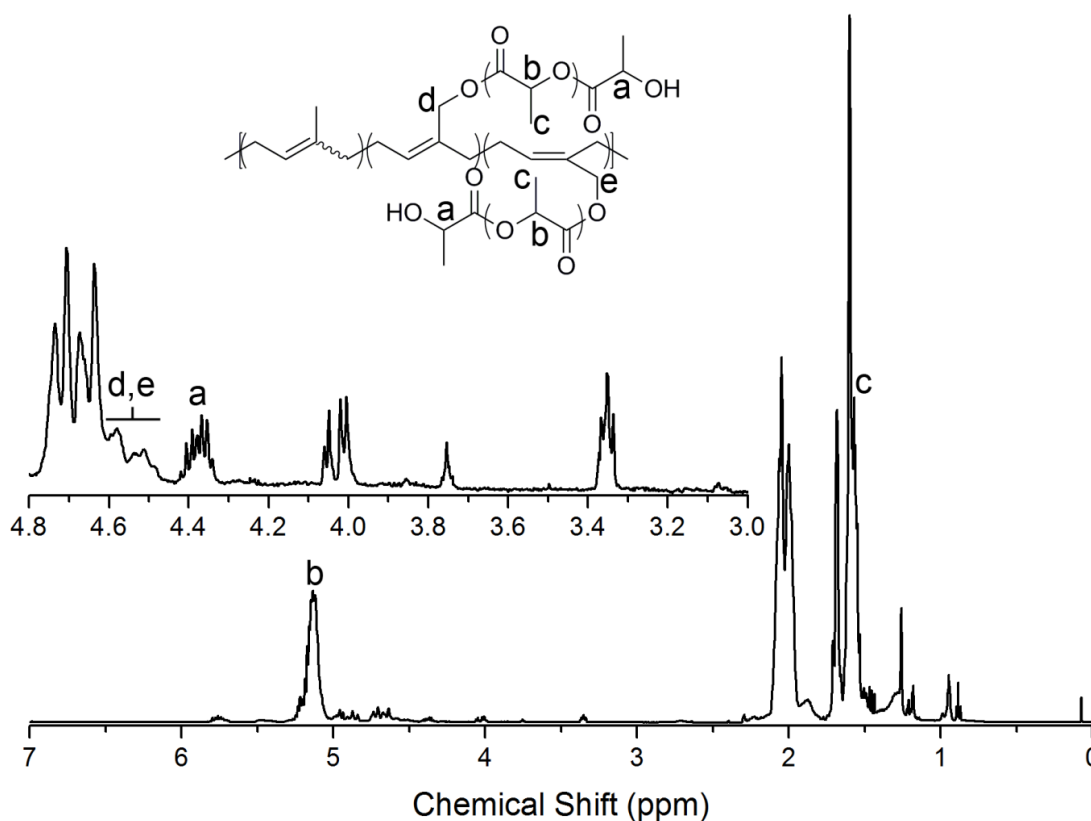
Figure 4.29. ^{1}H NMR spectra and expanded spectrum region of P(I-co-IOH)-g-PLA. P(I-co-IOH) macroinitiator peaks assignments are given in Figure 4.17. Upon initiation of the PLA polymerization, peaks associated with the methylene protons of IOH repeat unit shift downfield and are labeled "d,e".

Similarly, emulsion polymerized P(I-co-IOH) was used as a macroinitiator for PLA graft polymer synthesis to give a material containing 95 wt % PLA (Figure 4.30 and Figure 4.31). Room temperature small angle x-ray scattering (SAXS) of the 95 wt % P(I-co-IOH)-g-PLA gave an one-dimensional scattering profile with a primary reflection, corresponding to a domain spacing of 33 nm (Figure 4.32 inset). The presence of only a primary scattering peak in SAXS indicates that P(I-co-IOH)-g-PLA is microphase separated with no long range order. Transmission electron microscopy (TEM) confirms the phase separation of P(I-co-IOH) and PLA as dark domains of the macroinitiator (stained with OsO$_4$) are dispersed in a matrix of PLA (Figure 4.32). The existence of

phase separated rubbery domains is a prerequisite for tough PLA graft polymers, suggesting that tough materials could be made from P(I-co-IOH) macroinitiators (see Appendix E).[10]
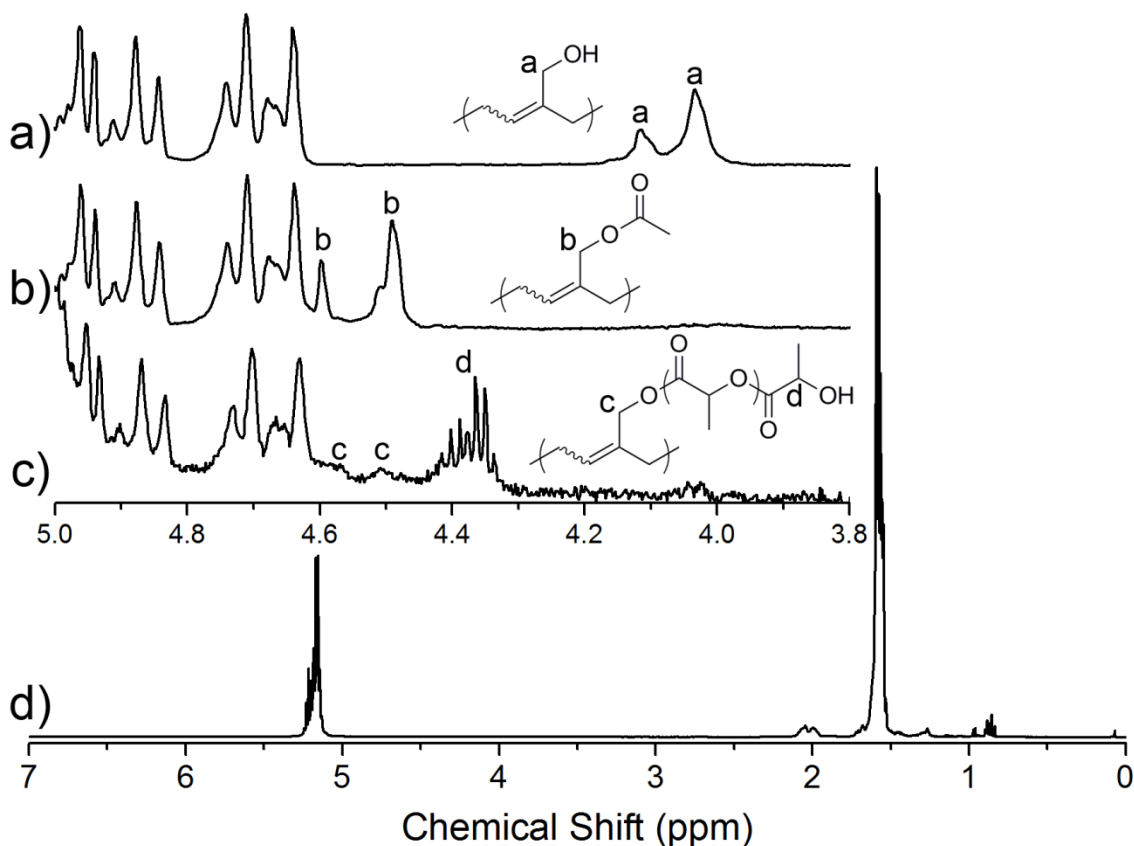
Figure 4.30. Expanded ^{1}H NMR spectra and chemical structure peak assignments for (a) emulsion synthesized P(I-co-IOH), (b) acetylated P(I-co-IOH), and (c) P(I-co-IOH)-g-PLA using the emulsion P(I-co-IOH) as a macroinitiator. The (d) full ^{1}H NMR spectrum for P(I-co-IOH)-g-PLA is also given. The peaks at 5.17 and 1.58 ppm belong to the PLA repeat units. The P(I-co-IOH) used as the macroinitiator had F_{IOH} = 0.025, a M_n (SEC with polystyrene standards) of 74 kg/mol, and a PDI of 6.35. After 35 min at room temperature, the polymerization had reached 98% conversion of D,L-lactide, giving a P(I-co-IOH)-g-PLA polymer with theoretical PLA arms with a M_n of 55 g/mol and a total theoretical M_n of 1600 kg/mol. Acetylation of the same polymer demonstrates that other types of reactions can occur with the pendent hydroxyl groups of P(I-co-IOH) and identifies the resonances for the initiating end of the PLA arms.
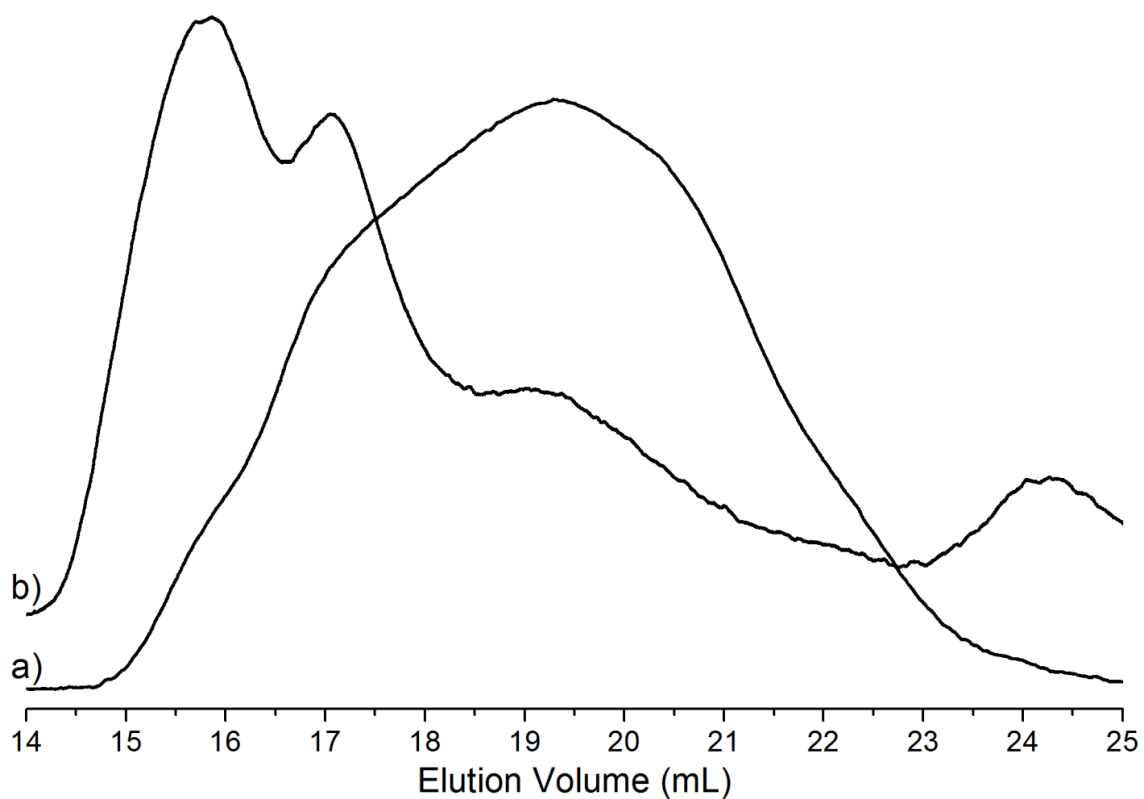
Figure 4.31. SEC elution curves for (a) P(I-co-IOH) macroinitiator (M_n = 77 kg/mol, PDI = 6.35, F_{IOH} = 2.5%) and (b) 95 wt % PLA P(I-co-IOH)-g-PLA graft copolymer (M_n = 330 kg/mol, PDI = 5.93) polymerized off the P(I-co-IOH).
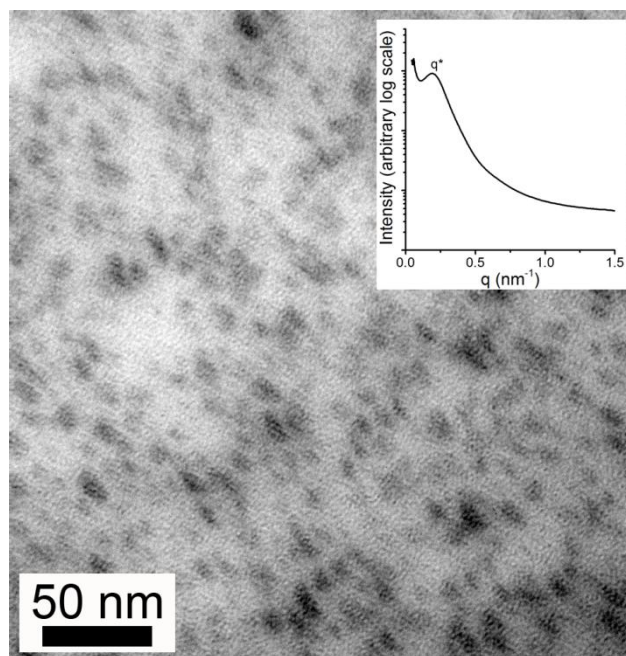
Figure 4.32. Representative TEM micrograph and (inset) room temperature one-dimensional SAXS profile plotted against spatial frequency (q) of P(I-co-IOH)-g-PLA containing 95 wt % PLA. The P(I-co-IOH) macroinitiator was synthesized by emulsion copolymerization. The SAXS profile has one principle scattering peak (q*), corresponding to a domain spacing of 33 nm. The dark regions of the TEM are P(I-co-IOH) domains stained with OsO_4.

4.4 Conclusions

Controlled radical RAFT copolymerization of isoprene and olefinic monomers containing hydroxyl functionality competes with Diels–Alder side reactions. Under the conditions investigated, the Diels–Alder reactions consume the hydroxyl monomers quicker than they are polymerized. Consequently, the resulting isoprene copolymers are gradient-like with high hydroxyl concentration initially that tapers off as the comonomer is consumed. The monomer IOH, structurally similar to isoprene, has favorable kinetics towards copolymerization. IOH copolymerizes with isoprene in a more random manner, producing P(I-co-IOH) macroinitiators with hydroxyl content close to that fed. Additionally, IOH can be copolymerized with isoprene in an emulsion setting, while HEA and HEMA cannot. The isoprene emulsion copolymers had an IOH content close to the feed composition at high monomer conversions. The hydroxyl containing isoprene

copolymers are able to undergo subsequent reactions efficiently to produce PLA graft copolymers. P(I-co-IOH) can be used as a macroinitiator to produce P(I-co-IOH)-g-PLA with 95 wt % PLA that phase separates in the bulk, allowing for the synthesis of potentially sustainable, tough materials.

4.5 References

[1] Neoh, S. B.; Hashim, A. S. *J. Appl. Polym. Sci.* **2004**, *93*, 1660–1665.

[2] Zhu, Y.; Burgaz, E.; Gido, S. P.; Staudinger, U.; Weidisch, R.; Uhrig, D.; Mays, J. W. *Macromolecules* **2006**, *39*, 4428–4436.

[3] Duan, Y.; Thunga, M.; Schlegel, R.; Schneider, K.; Rettler, E.; Weidisch, R.; Siesler, H. W.; Stamm, M.; Mays, J. W.; Hadjischristidis, N. *Macromolecules* **2009**, *42*, 415–4164.

[4] Hadjichristidis, N.; Roovers, J. *J. Polym. Sci. Polym Phys. Ed.* **1978**, *16*, 851–858.

[5] Lehrle, R. S.; Willis, S. L. *Polymer* **1997**, *38*, 5937–5946.

[6] Subramaniam, N.; Monteiro, M. J.; Taylor, J. R.; Simpson-Gomes, A.; Gilbert, R. G. *Macromol. Symp.* **2000**, *152*, 43–53.

[7] Derouet, D.; Tran, Q. N.; Thuc, H. H. *J. Appl. Polym. Sci.* **2009**, *114*, 2149–2160.

[8] Gramlich, W. M.; Hillmyer, M. A. *Polym. Chem.* **2011**, *2*, 2062–2067.

[9] Wang, G.; Fan, X.; Huang, J. *J. Polym. Sci. Part A* **2010**, *48*, 3797–3806.

[10] Theryo, G.; Jing, F.; Pitet, L. M.; Hillmyer, M. A. *Macromolecules* **2010**, *43*, 7394–7397.

[11] Benoit, D.; Harth, E.; Fox, P.; Waymouth, R. M.; Hawker, C. J. *Macromolecules* **2000**, *33*, 363–370.

[12] Nanu, I.; Andrei, C. *J. Polym. Sci. Polym. Chem.* **1974**, *12*, 231–240.

[13] Gaylord, N. G.; Tomono, T.; Mandal, B. M. *J. Polym. Sci. Polym. Chem.* **1976**, *14*, 1283–1285.

[14] Siadat, B.; Lenz, R. W. *J. Polym. Sci.: Polym. Chem. Ed.* **1980**, *18*, 3273–3287.

[15] Bamford, C. H.; Han, X.-Z. *J. Chem. Soc., Faraday Trans. 1* **1982**, *78*, 869 – 879.

[16] Ebdon, J. R.; Gabbott, N. P. *Polymer* **1983**, *24*, 565 – 572.

[17] Lokaj, J.; Pivcová, H.; Krabák, F. *Macromol. Mater. Eng.* **1986**, *144*, 207–218.

[18] Cowie, J. M. G.; Cree, S. H. *J. Polym. Sci. Part A* **1989**, *27*, 2907–2924.

[19] Cowie, J. M. G.; Cree, S. H.; Ferguson, R. *J. Polym. Sci. Part A* **1990**, *28*, 515–524.

[20] Lokaj, J.; Bílá, J. *Acta Polym.* **1992**, *43*, 54–57.

[21] Ajellal, N.; Thomas, C. M.; Carpentier, J.-F. *Polymer* **2008**, *49*, 4344–4349.

[22] Safa, K. D.; Nasirtabrizi, M. H.; Tofangdarzadeh, S. *Iran. Polym. J.* **2008**, *17*, 39–47.

[23] Lybarger, H. M. Isoprene. *Kirk-Othmer Encyclopedia of Chemical Technology*; John Wiley & Sons Inc., 2011.

[24] Hong, S. C. *Elastom. Comp.* **2009**, *44*, 55–62.

[25] Alcaraz, L.; Harnett, J. J.; Mioskowski, C.; Martel, J. P.; Le Gall, T.; Shin, D.-S.; Falck, J. R. *Tetrahedron Lett.* **1994**, *35*, 5449–5452.

[26] Bailey, W. J.; Carpenter, W. G.; Hermes, M. E. *J. Org. Chem.* **1962**, *27*, 1975–1978.

[27] Satake, Y.; Nishikawa, T.; Hiramatsu, T.; Araki, H.; Isobe, M. *Synthesis* **2010**, *12*, 1992–1998.

[28] Riley, R. G.; Silverstein, R. M.; Katzenellenbogen, J. A.; Lenox, R. S. *J. Org. Chem.* **1974**, *39*, 1957–1958.

[29] Thomas, A. F. *J. Am. Chem. Soc.* **1969**, *91*, 3281–3289.

[30] Kopecek, J.; Ulbrich, K.; Vacik, J. Method for producing new biologically tolerated polymers. Canadian Patent 1045296. December 26, 1978.

[31] Atlantic Richfield, Co. Hydroxy butadienes. GB Patent 1198582. July 15, 1970.

[32] Trementozzi, Q. A.; Gebura, S. E.; Locke, F. J. Blends of styrene-acrylonitrile resins with graft copolymers of diene rubber substrate and hydroxylic polymer superstrate. U.S. Patent 3488405. January 6, 1970.

[33] Selman, C. M.; Uraneck, C. A. Preparation of functional polymers. U.S. Patent 3993853. November 23, 1976.

[34] Lai, J. T.; Filla, D.; Shea, R. *Macromolecules* **2002**, *35*, 6754–6756.

[35] Germack, D. S.; Wooley, K. L. *J. Polym. Sci. Part A* **2007**, *45*, 4100–4108.

[36] Cheong, I. W.; Fellows, C. M.; Gilbert, R. G. *Polymer* **2004**, *45*, 769–781.

[37] Crandall, J. K.; Apparu, M. Base-Promoted Isomerizations of Epoxides. In *Organic Reactions*, Vol 29; Dauben, W. G., Ed.; John Wiley & Sons Inc., 1983; pp 345–443.

[38] *CRC Handbook of Chemistry and Physics* [Online]; http://www.hbcpnetbase.com/ (accessed October 21, 2011).

[39] Estimated using *ChemBioDraw Ultra*, Version 12.0.2.1076, CambridgeSoft, 2010.

[40] Jitchum, V.; Perrier, S. *Macromolecules* **2007**, *40*, 1408–1412.

[41] Chern, C.-S. *Principles and Applications if Emulsion Polymerization* [Online]; John Wiley and Sons: New York, 2008; pp 1–22. http://onlinelibrary.wiley.com/doi/10.1002 /9780470377949.ch1/pdf (accessed Oct. 22, 2011).

[42] Cheong, I. W.; Fellows, C. M.; Gilbert, R. G. *Polymer* **2004**, *45*, 769–781.

[43] Mun, G. A.; Nurkeeva, Z. S.; Dergunov, S. A.; Nam, I. K.; Maimakov, T. P.; Shaikhutdinov, E. M.; Lee, S. C.; Park, K. *React. Funct. Polym.* **2008**, *68*, 389–395.

[44] Chu, H.-H.; Ou, E.-D. *Polym. Bull.* **2000**, *44*, 337–344.

[45] Palit, S. R. *J. Phys. Chem.* **1947**, *51*, 837–857.

[46] Fotiadou, A. D.; Zografos, A. L. *Org. Lett.* **2011**, *13*, 4592–4595.

[47] Kiesewetter, M. K.; Shin, E. J.; Hedrick, J. L.; Waymouth, R. M. *Macromolecules* **2010**, *43*, 2093–2107.

[48] Lohmeijer, B. G. G.; Pratt. R. C.; Leibfarth, F.; Logan, J. W.; Long, D. A.; Dove, A. P.; Nederberg, F.; Choi, J.; Wade, C.; Waymouth, R. M.; Hedrick, J. L. *Macromolecules* **2006**, *39*, 8574–8583.

Bibliography

Adams, H. E.; Powers, P. O. *J. Appl. Phys.* **1946**, *17*, 325-337.

Ahn, K.-D.; Kang, J.-H.; Yoo, K.-W.; Choo, D.-J. *Macromol. Symp.* **2007**, *254*, 46-53.

Ajellal, N.; Thomas, C. M.; Carpentier, J.-F. *Polymer* **2008**, *49*, 4344–4349.

Alcaide, B.; Almendros, P.; Luna, A. *Chem. Rev.* **2009**, *109*, 3817–3858.

Alcaraz, L.; Harnett, J. J.; Mioskowski, C.; Martel, J. P.; Le Gall, T.; Shin, D.-S.; Falck, J. R. *Tetrahedron Lett.* **1994**, *35*, 5449–5452.

Ali, F.; Chang, Y.-W.; Kang, S. C.; Yoon, J. Y. *Polymer Bulletin* **2009**, *62*, 91-98.

Al-Issa, M. A.; Davis, T. P.; Huglin, M. B.; Yip, D. C. F. *Polymer* **1985**, *26*, 1869–1874.

Altintas, O.; Hizal, G.; Tunca, U. *Des. Monomers Polym.* **2009**, *12*, 83–98.

Anastas, P. T.; Warner, J. C. Green Chemistry: Theory and Practice, Oxford University Press: New York, 1998, p.30.

Anderson, K. S. High Impact Polylactide Composites. Ph.D. Thesis, University of Minnesota, Minneapolis, MN, 2004.

Anderson, K. S.; Hillmyer, M. A. *Polymer* **2004**, *45*, 8809-8823.

Anderson, K. S.; Lim, S. H.; Hillmyer, M. A. *J. Appl .Polym. Sci.* **2003**, *89*, 3757-3768.

Anderson, K. S.; Schreck, K. M.; Hillmyer, M. A. *Polym. Rev.* **2008**, *48*, 85−108.

Andjelkovic, D. D.; Min, B.; Ahn, D.; Larock, R. C. *J. Agric. Food Chem.* **2006**, *54*, 9535-9643.

Annunziata, L.; Duc, M.; Carpentier, J.-F. *Macromolecules* **2011**, *44*, 7158–7166.

Argon, A. S.; Cohen, R. E.; Gebizliouglu, O. S.; Schwier, C. E. *Adv. Polym. Sci.* **1983**, *52*, 275–335.

Asadauskas, S.; Erhan, S. Z. *J. Am. Oil Chem. Soc.* **2001**, *78*, 1029-1035.

Asandei, A. D.; Yu, H. S. Cu-Mediated Isoprene Polymerizations Initiated from Sulfonyl Halides. *Proceedings of the 241ˢᵗ ACS National Meeting*, Anaheim, CA, March 27–31, 2011.

ASTM Standard D256, *Standard Test Methods for Determining the Izod Pendulum Impact Resistance of Plastics*; ASTM Standards International, 2010.

Atlantic Richfield, Co. Hydroxy butadienes. GB Patent 1198582. July 15, 1970.

Auras, R.; Harte, B.; Seke, S. *Macromol. Biosci.* **2004**, *4*, 835-864.

Avérous, L.; Pollet, E. *MRS Bull.* **2011**, *36*, 703–710.

Aydan, D.; Durmaz, H.; Tunca, U.; Hizal, G. *J. Poly. Sci. Part A: Polym. Chem.* **2009**, *47*, 178-187.

Ayres, R. L.; Michejda, C. J.; Rack, E. P. *J. Am. Chem. Soc.* **1971**, *93*, 1389–1394.

Bailey, W. J.; Carpenter, W. G.; Hermes, M. E. *J. Org. Chem.* **1962**, *27*, 1975–1978.

Bamford, C. H.; Han, X.-Z. *J. Chem. Soc., Faraday Trans. 1* **1982**, *78*, 869 – 879.

Banik, S. M.; Monnot, B. L.; Weber, R. L.; Mahanthapa, M. K. *Macromolecules* **2011**, *44*, 7141–7148.

Bar-Nes, G.; Hall, R.; Sharma, V.; Gaborieau, M.; Lucas, D.; Castignolles, P.; Gilbert, R. G. *Eur. Polym. J.* **2009**, *45*, 3149–3163.

Bartels, J. W.; Cauët, S. I.; Billings, P. L.; Lin, L. Y.; Zhu, J.; Fidge, C.; Pochan, D. J.; Wooley, K. L. *Macromolecules* **2010**, *43*, 7128–7138.

Becer, C. R.; Hoogenboom, R.; Schubert, U. S. *Angew.Chem. Int. Ed.* **2009**, *48*, 4900–4908.

Beginn, U. *Colloid Polym. Sci.* **2008**, *286*, 1465–1474.

Benoit, D.; Harth, E.; Fox, P.; Waymouth, R. M.; Hawker, C. J. *Macromolecules* **2000**, *33*, 363–370.

Berekaa, M. M.; Linos, A.; Reichelt, R.; Keller, U.; Steinbüchel, A. *FEMS Microbiol. Lett.* **2000**, *185*, 199–206.

Bertrand, A.; Chen, S.; Souharce, G.; Ladabière, C.; Fleury, E.; Bernard, J. *Macromolecules* **2011**, *44*, 3694–3704.

Bielinski, D. M.; Slusarski, L.; Affrossman, S.; Hartshorne, M.; Pethrich, R. A. *J. Appl. Polym. Sci.* **1995**, *56*, 853–867.

Binger, P.; Freund, A.; Wdemann, P. *Tetrahedron* **1989**, *45*, 2887–2894.

Bitinis, N.; Verdejo, R.; Cassagnu, P.; Lopez-Manchado, M. A. *Mater. Chem. Phys.* **2011**, *129*, 823–831.

Blach, J. A.; Watson, G. S.; Busfield, W. K.; Myhra, S. *Polym. Int.* **2001**, *51*, 12–20.

Blümm, E.; Owen, A. J. *Polymer* **1995**, *36*, 4077–4081.

Böchen, S.; Lenoir, D.; Scheringer, M. *Naturwissenschaften* **2003**, *90*, 93–102.

Braun, B.; Dorgan, J. R.; Knauss, D. M. *J. Polym. Environ.* **2006**, *14*, 49–58.

Bredberg, K.; Christiansson, M.; Stenber, B.; Holst, O. Biotechnological Processes for Recycling of Rubber Products. In *Polyisoprenoids*; Koyama, T.; Steinbüchel, A.; Eds.; Biopolymers, Vol. 2; John Wiley and Sons: New York, 2001; pp 361–375.

Brosse, J.-C.; Campistron, I.; Derouet, D.; El Hamdaoui, A.; Houdayer, S.; Reyx, D.; Ritoit-Gillier, S. *J. Appl. Polym. Sci.* **2000**, *78*, 1461–1477.

Brosse, J.-C.; Klinpituksa, P.; Soutif, J.-C. *Makromol. Chem.* **1992**, *193*, 315–321.

Brostöm, J.; Boss, A.; Chronakis, I. S. *Biomacromolecules* **2004**, *5*, 1124-1134.

Brown, H. R. *Macromolecules* **1991**, *24*, 2752–2756.

Buchanan, W. http://articles.sfgate.com/2007-11-19/bay-area/17271155_1_plastic-bags-compostable-blue-recycling-bins (accessed Nov 6, 2011).

Bucknall, C. B. In *Polymer Blends*; Paul, D. R.; Bucknall, C. B., Eds.; John Wiley and Sons: New York, 2000; Volume 2; pp 59-82.

Bucknall, C. B.; Paul, D. R. *Polymer* **2009**, *50*, 5539–5548.

Burfield, D. R.; Lim, K.-L.; Law, K.-S. *J. Appl. Polym. Sci.* **1984**, *29*, 1661–1673.

Burfield, D. R.; Lim, K.-L.; Law, K.-S.; Ng, S. *Polymer* **1984**, *25*, 995–998.

Burlett, D. J.; Lindt, J. T. *Rubber Chem. Technol.* **1993**, *66*, 411–434.

Bussière, P.-O.; Gardette, J.-L.; Lacoste, J.; Baba, M. *Polym. Degrad. Stabil.* **2005**, *88*, 182–188.

Buzdugan, E.; Ghioca, P.; Badea, E. G.; Serban, S. *Eur. Polym. J.* **1997**, *33*, 1713–1716.

Cao, Y.; Gao, H.-L.; Chen, J.-N.; Chen, Z.-Y.; Yang, L. *J. Agric. Food Chem.* **2006**, *54*, 9004–9009.

Capacchione, C.; Saviello, D.; Avagliano, A.; Proto, A. *J. Polym. Sci. Part A* **2010**, *48*, 4200–4206.

Carlson, D.; Nie, L.; Narayan, R.; Dubois, P. *J. Appl. Polym. Sci.* **1999**, *72*, 477–485.

Carone, E. Jr; Kopcak, U.; Goncalves, M. C.; Nunes, S. P. *Polymer* **2000**, *41*, 5929–5935.

Castaldi, M. J.; Kwon, E.; Weiss, B.; *Environ. Eng. Sci.* **2007**, *24*, 1160–1178.

Chang, K.; Robertson, M. L.; Hillmyer, M. A. *Accepted to ACS Applied Materials and Interfaces* **2009**.

Chen, S.; Bertrand, A.; Chang, X.; Alcouffe, P.; Ladavière, C.; Gérard, J.-F.; Lortie, F.; Bernard, J. *Macromolecules* **2010**, *43*, 5981–5988.

Cheong, I. W.; Fellows, C. M.; Gilbert, R. G. *Polymer* **2004**, *45*, 769–781.

Chern, C.-S. *Principles and Applications if Emulsion Polymerization* [Online]; John Wiley and Sons: New York, 2008; pp 1–22. http://onlinelibrary.wiley.com/doi/10.1002

Chino, K.; Ashura, M. *Macromolecules* **2001**, *34*, 9201–9204.

Choi, J. S.; Park, W. H. *Macromol. Symp.* **2003**, *197*, 65-76.

Choi, S.-H.; Bates, F. S.; Lodge, T. P. *J. Phys. Chem. B* **2009**, *113*, 13840-13848.

Choudhary, P.; Mohanty, S.; Nayak, S. K.; Unnikrishnan, L. *J. Appl. Polym. Sci.* **2011**, *121*, 3223–3237.

Chu, H.-H.; Ou, E.-D. *Polym. Bull.* **2000**, *44*, 337–344.

Coates, G. W.; Hillmyer, M. A. *Macromolecules* **2009**, *42*, 7987–7989.

Colobert, F.; Kreuzer, T.; Cossy, J.; Reymond, S.; Tsuchiya, T.; Ferrié, L.; Marko, I. E.; Jourdain, P. *Synlett* **2007**, *15*, 2351–2354.

Coltelli, M.-B.; Bronco, S.; Chinea, C. *Polym. Degrad. Stabil.* **2010**, *95*, 332–341.

Continuous process for the manufacture of lactide and lactide polymers. US Patent 6326458, 2001.

Corre, Y.-M.; Duchet, J.; Reignier, J.; Maazouz, A. *Rheol. Acta.* [Online early access]. DOI: 10.1007/s00397-011-0538-1. Published online: Mar 1, 2011 http://www. springerlink. com/content/ f406672514632t0w/ fulltext.pdf (accessed July 24, 2011).

Corte, L.; Leibler, L. *Macromolecules* **2007**, *40*, 5606-5611.

Cowie, J. M. G.; Cree, S. H. *J. Polym. Sci. Part A* **1989**, *27*, 2907–2924.

Cowie, J. M. G.; Cree, S. H.; Ferguson, R. *J. Polym. Sci. Part A* **1990**, *28*, 515–524.

Crandall, J. K.; Apparu, M. Base-Promoted Isomerizations of Epoxides. In *Organic Reactions*, Vol 29; Dauben, W. G., Ed.; John Wiley & Sons Inc., 1983; pp 345–443.

CRC Handbook of Chemistry and Physics [Online]; http://www.hbcpnetbase.com/ (accessed October 21, 2011).

Creton, C.; Hu, G.; Deplace, F.; Morgret, L.; Shull, K. R. *Macromolecules* **2009**, *42*, 7605–7615.

Creton, C.; Kramer, E. J.; Hui, C.; Brown, H. R. *Macromolecules* **1992**, *25*, 3075–3088.

Crosslinking Peroxides and Polymer Additives; BTB Communication 2154 [Online]; Akzo Nobel Polymer Chemicals: Chicago, IL, June, 2006

Cuomo, C.; Serra, M. C.; Maupoey, M. G.; Grassi, A. *Macromolecules* **2007**, *40*, 7089–7097.

Dag, A.; Durmaz, H.; Hizal, G.; Tunca, U. *J. Polym. Sci., Part A: Polym. Chem.* **2007**, *46*, 302–313.

Dai, K. H.; Kramer, E. J.; Shull, K. R. *Macromolecules* **1992**, *25*, 220–225.

Dai, L.; Mau, A. W. H. *Synthetic Metals* **1997**, *86*, 1893–1894.

Dai, L.; Mau, A. W. H.; Griesser, H. J.; Winkler, D. A. *Macromolecules* **1994**, *27*, 6728–6735.

Dai, L.; White, J. W. *Polymer* **1991**, *32*, 2120–2127.

Dasari, A.; Zhang, Q.-X.; Yu, Z.-Z.; Mai, Y.-M. *Macromolecules* **2010**, *43*, 5734–5739.

Davidock, D. A. Novel Fluorinated Block Copolymers by Selective Chemical Modification: Chemistry and Thermodynamics. Ph.D. Thesis, University of Minnesota, Minneapolis, MN, 2004.

Davidock, D. A.; Hillmyer, M. A.; Lodge, T. P. *Macromolecules* **2004**, *37*, 397–407.

de Espinosa, L. M.; Meier, M. A. R. *Eur. Polym. J.* **2011**, *47*, 837–852.

Derouet, D.; Brosse, J. C.; Tillekeratne, L. M. K. *J. Nat. Rubb. Res.* **1990**, *5*, 296–300.

Derouet, D.; Intharapat, P.; Tran, Q. N.; Gohier, F.; Nakason, C. *Eur. Polym. J.* **2009**, *45*, 820–836.

Derouet, D.; Morvan, F.; Brosse, J.-C. *Eur. Polym. J.* **2001**, *37*, 1297–1313.

Derouet, D.; Morvan, F.; Brosse, J.-C. *J. Nat. Rubb. Res.* **1996**, *11*, 9–25.

Derouet, D.; Mulder-Houdayer, S.; Brosse, J.-C. *J. Appl. Polym. Sci.* **2005**, *95*, 39–52.

Derouet, D.; Phinyocheep, P.; Boccaccio, G.; Brosse, J. C. *J. Nat. Rubb. Res.* **1991**, *6*, 39–54.

Derouet, D.; Phinyocheep, P.; Brosse, J. C.; Boccaccio, G. *Eur. Polym. J.* **1990**, *26*, 1313–1320.

Derouet, D.; Tran, Q. N.; Thuc, H. H. *Eur. Polym. J.* **2007**, *43*, 1806–1824.

Derouet, D.; Tran, Q. N.; Thuc, H. H. *J. Appl. Polym. Sci.* **2009**, *114*, 2149–2160.

Dictionary.com. http://dictionary.reference.com/browse/sustain (accessed Nov. 6, 2011).

Dictionary.com. http://dictionary.reference.com/browse/sustainability (accessed Nov. 6, 2011).

Dorgan, J. R.; Williams, J. S. *J. Rheol.* **1999**, *43*, 1141–1155.

Duan, Y.; Thunga, M.; Schlegel, R.; Schneider, K.; Rettler, E.; Weidisch, R.; Siesler, H. W.; Stamm, M.; Mays, J. W.; Hadjischristidis, N. *Macromolecules* **2009**, *42*, 415–4164.

Dubois, P.; Narayan, R. *Macromol. Symp.* **2003**, *198*, 233–243.

Durmaz, H.; Dag, A.; Altintas, O.; Erdogan, T.; Hizal, G.; Tunca, U. *Macromolecules* **2007**, *40*, 191–198.

Durmaz, H.; Karatas, F.; Tunca, U.; G. Hizal, G. *J. Polym. Sci., Part A: Polym. Chem.* **2006**, *44*, 499–506.

Ebdon, J. R.; Gabbott, N. P. *Polymer* **1983**, *24*, 565 – 572.

Eissen, M.; Metzger, J. O.; Schmidt, E.; Schneidewind, U. *Angew. Chem. Int. Ed.* **2002**, *41*, 414–436.

Els, C.; McGill, W. J.; *Plast Rub Compos Pro* **1994**, *21*, 115–123.

Fan, X.; Ruan, J.; Chen, Q.; Chen, J.; Zhou, Z.; Zou, J. *J. Macromol. Sci. Part B* **2011**, *50*, 493–502.

Favis, B. D. *J. Appl. Polym. Sci.* **1990**, *39*, 285–300.

Favis, B. D. *Polymer* **1994**, *35*, 1552–1555.

Feng, C.; Li, Y.; Yang, D.; Hu, J.; Zhang, X.; Huang, X. *Chem. Soc. Rev.* **2011**, *40*, 1282–1295.

Feng, X.; East, A. J.; Hammond, W. B.; Zhang, Y.; Jaffe, M. *Polym Adv. Technol.* **2011**, *22*, 139–150.

Fetters, L. J.; Lohse, D. J.; Richter, D.; Witten, T. A.; Zirkel, A. *Macromolecules* **1994**, *27*, 4639–4647.

Focarete, M. L.; Scandola, M.; Dobrzynski, P.; Kowalczuk, M. *Macromolecules* **2002**, *35*, 8472–8477.

Fornof, A. R.; Onah, E; Ghosh, S.; Frazier, C. E.; Sohn, S.; Wilkes, G. L.; Long, T. E. *J. Appl. Polym. Sci.* **2006**, *102*, 6790-697.

Fotiadou, A. D.; Zografos, A. L. *Org. Lett.* **2011**, *13*, 4592–4595.

Fournier, D.; Hoogenboom, R., Schubert, U. S. *Chem. Soc. Rev.* **2007**, *36*, 1369–1380.

Frank, H.; Campanella, L.; Dondi, F.; Mehlich, J.; Leitner, E.; Rossi, G.; Ioset, K. N.; Bringman, G. *Angew. Che. Int. Ed.* **2011**, *50*, 8482–8490.

Friebe, L.; Nuyken, O.; Obrecht, W. *Adv. Polym. Sci.* **2006**, *204*, 1 – 154.

Friedrich, K. *Adv. Polym. Sci.* **1983**, *52*, 225–274.

Gacal, B.; Durmaz, H.; Tasdelen, M. A.; Hizal, G.; Tunca, U.; Yagci, Y.; Demiral, A. L. *Macromolecules* **2006**, *39*, 5330–5336.

Gandini, A. *Macromolecules* **2008**, *41*, 9491–9504.

Gao, H.; Wang, Y. N.; Fan, Y.G.; Ma, J. B. *J. Control Release* **2005**, *107*, 158-173.

Gao, Y.; Kong, L.; Zhang, L.; Gong, Y.; Chen, G.; Zhao, N.; Zhang, X. *Eur. Polym. J.* **2006**, *42*, 764–775.

Gardner, H. W. *Free Radical Bio Med* **1989**, *7*, 65-86.

Garratt, S.; Carr, A. G.; Langstein, G.; Bochmann, M. *Macromolecules* **2003**, *36*, 4276–4287.

Gauthier, D.; Lindhardt, A. T.; Olsen, E. P. K.; Overgaard, J.; Skrydstrup, T. *J. Am. Chem. Soc.* **2010**, *132*, 7998–8009.

Gauthier, M. A.; Gibson, M. I.; Klok, H.-A. *Angew. Chem. Int. Ed.* **2009**, *48*, 48–58.

Gauthier, M.; Lin, W.-Y.; Teertstra, S. J.; Tzoganakis, C. *Polymer* **2010**, *51*, 3123–3129.

Gaylord, N. G.; Tomono, T.; Mandal, B. M. *J. Polym. Sci. Polym. Chem.* **1976**, *14*, 1283–1285.

Gent, A. N. *J. Mater. Sci.* **1980**, *15*, 2884–2888.

Georges, M. K.; Hamer, G. K.; Listigovers, N. A. *Macromolecules* **1998**, *31*, 9087–9087.

Germack, D. S.; Harrisson, S.; Brown, G. O.; Wooley, K. L. *J. Polym. Sci. Part A* **2006**, *44*, 5218–5228.

Germack, D. S.; Wooley, K. L. *J. Polym. Sci. Part A* **2007**, *45*, 4100–4108.ermack, D. S.; Wooley, K. L. *Macromol. Chem. Phys.* **2007**, *208*, 2481–2491.

Gramlich, W. M.; Hillmyer, M. A. *Polym. Chem.* **2011**, *2*, 2062–2067.

Gramlich, W. M.; Robertson, M. L.; Hillmyer, M. A. *Macromolecules* **2010**, *43*, 2313–2321.

Greene, A. C.; Grubbs, R. B. *J. Polym. Sci. Part A* **2009**, *47*, 6342–6352.

Grijpma, D. W.; Joziasse, C. A. P.; Pennings, A. J. *Makromol. Chem. Rapid. Commun.* **1993**, *14*, 155–161.

Grijpma, D. W.; Nijenhuis, A. J.; van Wijk , P. G. T.; Pennings, A. J. *Polym. Bull.* **1992**, *29*, 571–578.

Grijpma, D. W.; Penning, J. P.; Pennings, A. J. *Colloid Polym. Sci.* **1994**, *272*, 1068–1081.

Grijpma, D. W.; Van Hofslot, R. D. A.; Supèr, H.; Nijenhuis, A. J.; Pennings, A. J. *Polym. Eng. Sci.* **1994**, *34*, 1674–1684.

Grubbs, R. B.; Wegrzyn, J. K.; Xia, Q. *Chem. Commun.* **2005**, 80–82.

Gruber, P. R.; Hall, E. S.; Kolstad, J. J.; Iwen, M. L.; Benson, R. D.; Borchardt, R. L.

Hadjichristidis, N.; Roovers, J. *J. Polym. Sci. Polym Phys. Ed.* **1978**, *16*, 851–858.

Hallensleben, M. L.; Schmidt, H. R.; Schuster, R. H. *Angew. Makromol. Chem.* **1995**, *227*, 87–99.

Hallman, P. S.; McGarvey, B. R.; Wilkinson, G. *J. Chem. Soc. A.* **1968**, 3143–3150.

Haq, M.; Burgueño, R.; Hohanty, A. K.; Misra, M. *Comp. Sci. Tech.* **2008**, *68*, 3344 – 3351.

Harada, M.; Iida, K.; Okamoto, K.; Hayashi, H.; Hirano, K. *Polym. Eng. Sci.* **2008**, *48*, 1359-1368.

Harada, M.; Ohya, T.; Iida, K.; Hayashi, H.; Hirano, K.; Fukuda, H. *J. Appl. Polym. Sci.* **2007**, *106*, 1813–1820.

Hashima, K.; Nishitsuji, S.; Inoue, T. *Polymer* **2010**, *51*, 3934–3939.

Hassouna, F.; Raquez, J.-M.; Addiego, F.; Dubois, P.; Toniazzo, V.; Ruch, D. *Eur. Polym. J.* **2011**, *47*, 2134–2144.

Haynes, D.; Naskar, A. K.; Singh, A.; Yang, C.-C.; Burg, K. J.; Drews, M.; Harrison, G.; Smith, D. W. Jr. *Macromolecules* **2007**, *40*, 9354–9360.

Heath, W. H.; Palmieri, F.; Adams, J. R.; Long, B. K.; Chute, J.; Holcombe, T. W.; Zieren, S.; Truitt, M. J.; White, J. L.; Willson, C. G. *Macromolecules* **2008**, *41*, 719-726.

Hengstler, J. G.; Foth, H.; Gebel, T.; Kramer, P.-J.; Lilienblum, W.; Schweinfurth, H.; Völkel, W.; Wollin, K.-M.; Gundert-Remy, U. *Cr. Rev. Toxicol.* **2011**, *41*, 263–291.

Hiemenz, P. C.; Lodge, T. P. Chapter 12: Glass Transition. *Polymer Chemistry*, Second Edition; Taylor & Francis Group: Boca Raton, FL 2007.

Hillmyer, M. A.; Bates, F. S. *Macromolecules* **1996**, *29*, 6994–7002.

Hiran, B.; Singh, D. *J. Chem. Pharm. Res.* **2011**, *3*, 840–847.

Ho, C.-H.; Wang, C.-H.; Lee, Y.-D. *Polymer* **2008**, *49*, 3902–3910.

Hong, S. C. *Elastom. Comp.* **2009**, *44*, 55–62.

Horii, N.; Arato, S.; Narayan, B.; Hosokawa, M.; Sashima, T.; Miyashita, K. *J. Amer. Oil Chem. Soc.* **2007**, *84*, 749–754.

Hraus, W.; van de Lee, H.-M. *Tetrahedron Lett.* **1972**, *51*, 5225-5226.

Hshieh, F.-Y.; Hirsh, D. B.; Beeson, H. D. *Fire Mater.* **2003**, *27*, 9–17.

Hudson, S. D.; Jamieson, A. M. In *Polymer Blends*; Paul, D. R.; Bucknall, C. B.,Eds.; Volume 1; Wiley: New York, 2000; pp 461-495.

Huneault, M. A.; Li, H. *Polymer* **2007**, *48*, 270–280.

Iannace, S.; Ambrosio, L.; Huang, S. J.; Nicolais, L. *J. Appl. Polym. Sci.* **1994**, *54*, 1525–1536.

Inglis, A. J.; Barner-Kowollik, C. *Macromol. Rapid Commun.* **2010**, *31*, 1247–1266.

Inglis, A. J.; Nebhani, L.; Altintas, O.; Schmidt, F. G.; Barner-Kowollik, C. *Macromolecules* **2010**, *43*, 5515–5520.

Iovu, M. C.; Craley, R.; Jeffries-El, M.; Krankowski, A. B.; Zhang, R.; Kowalewski, T.; McCullough, R. D. *Macromolecules* **2007**, *40*, 4733–4735.

Ishida, S.; Nagasaki, R.; Chino, K.; Dong, T.; Inoue, Y. *J. Appl. Polym. Sci.* **2009**, *113*, 558–566.

Ishizu, K.; Hosokawa, T. *Polym. Int.* **2001**, *50*, 1186–1192.

Jakubowski, W.; Juhari, A.; Best, A.; Koyov, K.; Pakula, T.; Matyjaszewski, K. *Polymer* **2008**, *49*, 1567–1578.

Jayawardena, S.; Reyx, D.; Durand, D.; Pinazzi, C. P. *Makromol. Chem.* **1984**, *185*, 2089–2097.

Jerome, R. In *Macromolecular Engineering*; Matyjaszewski, K.; Gnanou, Y.; Leibler, L.; Eds.; 3; Wiley-VHC: Weinheim; p 1753-1782.

Jin, H.-J.; Chin, I.-J.; Kim, M.-N.; Kim, S.-H.; Yoon, J.-S. *Eur. Polym. J.* **2000**, *36*, 165–169.

Jing, F.; Hillmyer, M. A. *J. Am. Chem. Soc.* **2008**, *130*, 13826–13827.

Jitchum, V.; Perrier, S. *Macromolecules* **2007**, *40*, 1408–1412.

Kaita, S.; Doi, Y.; Kaneko, K.; Horiuchi, A. C.; Wakatsuki, Y. *Macromolecules* **2004**, *37*, 5860–5862.

Kanzawa, T.; Tokumistu, K. *J. Appl. Polym. Sci.* **2011**, *121*, 2908–2918.

Kawahara, S.; Kakubo, T.; Sakdapipanich, J. T.; Isono, Y.; Tanaka, Y. *Polymer* **2000**, *41*, 7483–7488.

Ke, T.; Sun, X. *J. Appl. Polym. Sci.* **2003**, *89*, 1203 - 1210.

Kiesewetter, M. K.; Shin, E. J.; Hedrick, J. L.; Waymouth, R. M. *Macromolecules* **2010**, *43*, 2093–2107.

Kikkawa, Y.; Suzuki, T.; Tsuge, T.; Kanesata, M. Doi, Y.; Abe, H. *Biomacromolecules*, **2006**, *7*, 1921–1928.

Kim, M. W.; Hong, S. M.; Lee, D.; Park, K.; Kang, T. J.; Youn, J. R. *Adv. Compos. Mater.* **2010**, *19*, 331–348.

Kim, Y. F.; Choi, C. N.; Kim, Y. D.; Lee, K. Y.; Lee, M. S. *Fiber Polym.* **2004**, *5*, 270–274.

Kim, Y. H.; Pandya, A. *Macromolecules* **1991**, *24*, 6505–6511.

Kopecek, J.; Ulbrich, K.; Vacik, J. Method for producing new biologically tolerated polymers. Canadian Patent 1045296. December 26, 1978.

Kow, C.; Morton, L.; Fetters, L. J.; Hadjichristidis, N. *Macromolecules* **1982**, *55*, 245–252.

Kramer, E. J. *Adv. Polym. Sci.* **1983**, *52*, 1–56.

Krompiec, J.; Sunwiński, J.; Majewski, J.; Grobelny, J. *Polish J. Appl. Chem.* **1998**, *42*, 43–48.

Krompiec, S.; Krompiec, M.; R. Penczek, R.; Ignasiak, H. *Coord. Chem. Rev.* **2008**, *252*, 1819–1841.

Krompiec, S.; Kuźnik, N.; Krompiec, M.; Penczek, R.; Mrzigod, J.; Tórz, A. *J. Mol. Catal. A-Chem.* **2006**, *253*, 132–146.

Krompiec, S.; Penczek, R.; Krompiec, M.; Pluta, T.; Ignasiak, H.; Kita, A.; Michalik, S.; Matlengiewicz, M.; Filapek, M. *Curr. Org. Chem.* **2009**, *13*, 896–913.

Kumar, K. R.; Penciu, A.; Drewitt, M. J.; Baird, M. C. *J. Organomet. Chem.* **2004**, *689*, 2900–2904.

Kuźnik, N.; Krompiec, S. *Coord. Chem. Rev.* **2007**, *251*, 222–233.

Kuźnik, N.; Krompiec, S.; Bieg, T.; Baj, S.; Skutil, K.; Chrobok, A. *J. Organomet. Chem.* **2003**, *665*, 167–175.

Lai, J. T.; Filla, D.; Shea, R. *Macromolecules* **2002**, *35*, 6754–6756.

Larock, R. C.; Dong, X.; Chung, S.; Reddy, C. K.; Ehlers, L. E. *J. Amer Oil Chem. Soc.* **2001**, *78*, 447–453.

Leadprathom, J.; Suttiruengwong, S.; Threepopnatkul, P.; Seadan, M. *J. Met. Mater. Min.* **2010**, *20*, 87–90.

Lee, K. M.; Han, C. D. *Macromolecules* **2002**, *35*, 760–769.

Lehrle, R. S.; Willis, S. L. *Polymer* **1997**, *38*, 5937–5946.

Leigh, W. J.; Mitchell, D. S. *J. Am. Chem. Soc.* **1988**, *110*, 1311–1313.

Lepers, J.; Favis, B. D. *AICHE J.* **1999**, *45*, 885-895.

Li, X.; Nishiura, M.; Hu, L.; Mori, K.; Hou, Z. *J. Am. Chem. Soc.* **2009**, *131*, 13870–13882.

Li, Y.; Shimizu, H. *Eur. Polym. J.* **2009**, *45*, 738–746.

Linos, A.; Reichelt, R.; Keller, U.; Steinbüchel, A. *FEMS Microbiol. Lett.* **2000**, *185*, 155–161.

Linos, A.; Steinbüchel, A. Biodegradation of Natural and Synthetic Rubbers. In *Polyisoprenoids*; Koyama, T.; Steinbüchel, A.; Eds.; Biopolymers, Vol. 2; John Wiley and Sons: New York, 2001; pp 321–360.

Lishanski, I. S.; Tsitokhtsev, V. A. *J. Polym. Sci. Part C* **1968**, *22*, 277–287.

Liu, D.; Cui, D. *Dalton Trans.* **2011**, *40*, 7755–7761.

Liu, H.; Chen, F.; Liu, B.; Estep, G. Zhang, J. *Macromolecules* **2010**, *43*, 6058–6066.

Liu, H.; Song, W.; Chen, F.; Gou, L.; Zhang, J. *Macromolecules* **2011**, *44*, 1513–1522.

Liu, X.; Li, K.; Feng, X.; Cao, Y. *J. Macromol. Sci. A* **2009**, *46*, 937-942.

Liu, Y.; Wang, L.; He, Y.; Fan, Z.; Li, S. *Polym. Int.* **2010**, *59*, 1616 - 1621.

Liu, Z. H.; Zhang, X. D.; Zhu, X. G.; Li, R. K. Y.; Qi, Z. N.; Wang, F. S.; Choy, C. L. *Polymer* **1998**, *39*, 5019-5025.

Lohmeijer, B. G. G.; Pratt. R. C.; Leibfarth, F.; Logan, J. W.; Long, D. A.; Dove, A. P.; Nederberg, F.; Choi, J.; Wade, C.; Waymouth, R. M.; Hedrick, J. L. *Macromolecules* **2006**, *39*, 8574–8583.

Lokaj, J.; Bílá, J. *Acta Polym.* **1992**, *43*, 54–57.

Lokaj, J.; Pivcová, H.; Krabák, F. *Macromol. Mater. Eng.* **1986**, *144*, 207–218.

Lowe, A. B. *Polym. Chem.* **2010**, *1*, 17–36.

Lu, J.; Qiu, Z.; Yang, W. *Polymer* **2007**, *48*, 4196–4204.

Luckachan, G. E.; Pillai, C. K. S. *J. Polym. Environ.* **2011**, *19*, 637–676.

Luettmer-Strathmann, J. *J. Chem. Phys.* **2005**, *123*, 014910.

Lui, H.; Zhang, J. *J. Polym. Sci. Part B* **2011**, *49*, 1051–1083.

Lybarger, H. M. Isoprene. *Kirk-Othmer Encyclopedia of Chemical Technology*; John Wiley & Sons Inc., 2011.

M. B. Smith, and J. March, *March's Advanced Organic Chemistry*, 5th Ed., John Wiley and Sons, New York, 2001, pp. 1062–1075.

Ma, J.; Cheon, H.-S.; Kishi, Y. *Org. Lett.* **2007**, *9*, 319–322.

Macosko, C. W.; Guegan, P.; Khandpur, A. K.; Nakayama, A.; Marechal, P.; Inoue, T. *Macromolecules* **1996**, *29*, 5590-5598.

Magaraphan, R.; Skularriya, R.; Kohjiya, S. *J. Appl. Polym. Sci.* **2007**, *105*, 1914–1921.

Malmberg, S. M.; Parent, J. S.; Pratt, D. A.; Whitney, R. A. *Macromolecules* **2010**, *43*, 8456–8461.

Masuda, T.; Tang, B.-Z.; Tanaka, A.; Higashimura, T. *Macromolecules* **1986**, *19*, 1459–1464.

Masutani, K.; Kawabata, S.; Aoki, T.; Kimura, Y. *Polym. Int.* **2010**, *59*, 1526-1530.

Mathers, R. T. *J. Polym. Sci. Part A* [Online early access] **2011**, DOI: 10.1002/pola. 24939. Published online Sep 12, 2011. http://onlinelibrary.wiley.com/doi/10.1002/pola. 24939/pdf (accessed Oct 24, 2011).

McGrath, M. P.; Sall, E. D.; Tremont, S. J. *Chem. Rev.* **1995**, *95*, 381–398.

McLean, J. K.; Guillen-Castellanos, S. A.; Parent, J. S.; Whitney, R. A.; Resendes, R. *Eur. Polym. J.* **2007**, *43*, 4619–4627.

Mecking, S. *Angew. Chem. Int. Ed.* **2004**, *43*, 1078–1085.

Meier, M. A. R.; Metzger, J. O.; Schubert, U. S. *Chem. Soc. Rev.* **2007**, *36*, 1788-1802..

Michinobu, T.; Bito, M.; Tanimura, M.; Katayama, Y.; Masai, E.; Nakamura, M.; Otsuka, Y.; Ohara, S.; Shigehara, K. *Polym. J.* **2009**, *41*, 843–848.

Minoura, Y.; Ikeda, H. *J. Appl. Polym. Sci.* **1971**, *15*, 2219–2236.

Miura, Y.; Miyake, K. *J. Polym. Sci. Part A* **2005**, *43*, 6153–6165.

Miyauchi, K.; Saito, K. *Bunseki Kagaku* **2006**, *55*, 547–554.

Mok, M. M.; Masser, K. A.; Runt, J.; Torkelson, J. M. *Macromolecules* **2010**, *43*, 5740–5748.

Moriguchi, N.; Tsugaru, T.; Amiya, S. *J. Mol. Struct.* **2001**, *562*, 205–213.

Mun, G. A.; Nurkeeva, Z. S.; Dergunov, S. A.; Nam, I. K.; Maimakov, T. P.; Shaikhutdinov, E. M.; Lee, S. C.; Park, K. *React. Funct. Polym.* **2008**, *68*, 389–395.

Na, Y.; Yong, H.; Shuai, X.; Kikkawa, Y.; Doi, Y.; Inoue, Y. *Biomacromolecules* **2002**, *3*, 1179–1186.

Nakason, C.; Saiwaree, S.; Tatun, S.; Kaesaman, A. *Polym. Test.* **2006**, *25*, 656–667.

Nanu, I.; Andrei, C. *J. Polym. Sci. Polym. Chem.* **1974**, *12*, 231–240.

Nashawi, I. S.; Malallah, A.; Al-Bisharah, M. *Energy Fuels* **2010**, *24*, 1788–1800.

Nath, D. C. D.; Shiono, T.; Ikeda, T. *J. Polym. Sci. Part A* **2002**, *40*, 3086–3092.

Ndoni, S.; Papadakis, C. M.; Bates, F. S.; Almdal, K. *Rev. Sci. Instrum.* **1995**, *66*, 1090–1095.

Neoh, S. B.; Hashim, A. S. *J. Appl. Polym. Sci.* **2004**, *93*, 1660–1665.

Ng, S. C.; Chee, K. K. *Polymer* **1993**, *34*, 3870–3872.

Nijenhuis, A. J.; Grijpma, D. W.; Pennings, A. J. *Macromolecules* **1992**, *25*, 6419-6424.

Noda, I.; Satkowski, M. M.; Dowrey, A. E.; Marcott, C. *Macromol. Biosci.* **2004**, *4*, 269–275.

Noolandi, J.; Hong, K. M. *Macromolecules* **1982**, *15*, 482–492.

Noolandi, J.; Hong, K. M. *Macromolecules* **1984**, *17*, 1531–1537.

Okada, M. *Prog. Polym. Sci.* **2002**, *27*, 87–133.

Orozco, V. H.; Brostow, W.; Chonkaew, W.; López, B. L. *Macromol. Symp.* **2009**, *277*, 69–80.

Owen, E. D.; Al-Moh'd, H. S. M. *Polymer* **1997**, *38*, 3533–3538.

Oyama, H. T. *Polymer* **2009**, *50*, 747–751.

Palit, S. R. *J. Phys. Chem.* **1947**, *51*, 837–857.

Pan, J.; Wang, Y.; Qin, S.; Zhang, B.; Luo, Y. *J. Biomed. Mater. Res., Part B: Appl. Biomater.* **2005**, *74B*, 476–480.

Pan, P.; Zhu, B.; Inoue, Y. *Macromolecules* **2007**, *40*, 9664-9671.

Park, D.; Weinman, C. J.; Finlay, J. A.; Fletcher, B. R.; Paik, M. Y.; Sundaram, H. S.; Dimitriou, M. D.; Sohn, K. E.; Callow, M. E.; Callow, J. A.; Handlin, D. L.; Willis, C. L.; Fisher, D. A.; Kramer, E. J.; Ober, C. K. *Langmuir* **2010**, *26*, 9772–9781.

Perera, M. C. S.; Elix, J. A.; Bradbury, J. H. *J. Polym. Sci. Part A* **1988**, *26*, 637–651.

Perkins, W. G. *Poly. Eng. Sci.* **1999**, *39*, 2445

Perrin, L.; Bonnet, F.; Chenal, T.; Visseaux, M.; Maron, L. *Chem. Eur. J.* **2010**, *16*, 11376–11385.

Pinazzi, C.; Brosse, J. C.; Pleurdeau, A.; Reyx, D. *Appl. Polym. Symp.* **1975**, *26*, 73–98.

Pitet, L. M.; Hillmyer, M. A. *Macromolecules* **2009**, *42*, 3674–3680.

Pounder, R. J.; Standford, M. J.; Brooks, P.; Richards, S. P.; Dove, A. P. *Chem. Commun.* **2008**, 5158-5160.

Pukanszky, B.; Belina, K. Tensile Properties, Creep, and Stress Relaxation. In *Polymer Characterization Techniques and Their Application to Blends*; Simor, G. P., Ed.; Oxford University Press: Oxford, 2003; pp 263–283.

Puskas, J. E.; Gautriaud, E.; Deffieux, A.; Kennedy, J. P. *Prog. Polym. Sci.* **2006**, *31*, 533–548.

Quinebèche, S.; Navarro, C.; Gnanou, Y.; Fontanille, M. *Polymer* **2009**, *50*, 1351–1357.

Rabagliati, F. M.; Muñoz, L. A.; Quijada, R. *Polym. Bull.* **2011**, *67*, 1425–1434.

Ragauskas, A. J; Williams, C. K; Davison, B. H; Britovsek, G.; Cairney, J.; Eckert, C. A; Frederick W. J. Jr; Hallett, J. P.; Leak, D. J.; Liotta, C. L.; Mielenz, J. R.; Murphy, R.; Templer, R.; Tschaplinski, T. *Science* **2006**, *311*, 484–489.

Ricci, G.; Zetta, L.; Alberti, E.; Motta, T.; Canetti, M.; Bertini, F. *J. Polym. Sci. Part A* **2007**, *45*, 4635–4646.

Riley, R. G.; Silverstein, R. M.; Katzenellenbogen, J. A.; Lenox, R. S. *J. Org. Chem.* **1974**, *39*, 1957–1958.

Rios, L. M.; Jones, P. R.; Moore, C.; Narayan, U. V. *J. Environ. Monitor.* **2010**, *12*, 2226–2236.

Robertson, M. L.; Chang, K.; Gramlich, W. M.; Hillmyer, M. A. *Macromolecules* **2010**, *43*, 1807-1814.

Robertson, M. L.; Paxton, J. M.; Hillmyer, M. A. *ACS Appl. Mater. Interfaces* **2011**, *3*, 3402–3410.

Rodrigues, A.-S.; Kirillov, E.; Vuillemin, B.; Razavi, A.; Carpentier, J.-F. *Polymer* **2008**, *49*, 2039–2045.

Rose, K.; Steinbüchel, A. *Appl. Environ. Microb.* **2005**, *71*, 2803–2812.

Rose, M.; Palkovits, R. *Macromol. Rapid Commun.* **2011**, *32*, 1299–1311.

Saelao, J.; Phinyocheep, P. *J. Appl. Polym. Sci.* **2005**, *95*, 28–38.

Safa, K. D.; Nasirtabrizi, M. H.; Tofangdarzadeh, S. *Iran. Polym. J.* **2008**, *17*, 39–47.

Salvini, A.; Piacenti, F.; Frediani, P.; Devescovi, A.; Caporali, M. *J. Organomet.Chem.* **2001**, *625*, 255–267.

Sarazin, P.; Li, G.; Orts, W. J.; Favis, B. D. *Polymer* **2008**, *49*, 599–609.

Satake, Y.; Nishikawa, T.; Hiramatsu, T.; Araki, H.; Isobe, M. *Synthesis* **2010**, *12*, 1992–1998.

Sauer, J. A.; Chen. C. C. *Adv. Polym. Sci.* **1983**, *52*, 169–224.

Schmidt, B. *Eur. J. Org. Chem.* **2004**, *2004*,1865–1880.

Schmidt, S. C.; Hillmyer, M. A. *Macromolecules* **1999**, *32*, 4794–4801.

Schnecko, H. W. Rubber Recycling. In *Polyisoprenoids*; Koyama, T.; Steinbüchel, A.; Eds.; Biopolymers, Vol. 2; John Wiley and Sons: New York, 2001; pp 395–409.

Schreck, K. M.; Hillmyer, M. A. *J. Biotechnol.* **2007**, *132*, 287–295.

Schulz, D. N.; Turner, S. R.; Golub, M. A. *Rubber Chem. Technol.* **1982**, *55*, 809–859.

Scott, C. E.; Joung, S. K. *Polym. Eng. Sci.* **1996,** *36*,1666-1674.

Scott, C. E.; Macosko, C. W. *Polymer* **1995**, *36*, 461–470.

Selman, C. M.; Uraneck, C. A. Preparation of functional polymers. U.S. Patent 3993853. November 23, 1976.

Semba, T.; Kitagawa, K.; Ishiaku, U. S.; Hamada, H. *J. Appl. Polym. Sci.* **2006**, *101*, 1816–1825.

Semba, T.; Kitagawa, K.; Ishiaku, U. S.; Kotaki, M.; Hamada, H. *J. Appl. Polym. Sci.* **2007**, *103*, 1066–1074.

Senyek, M. Polyisoprene. *Kirk-Othmer Encyclopedia of Chemical Technology*; John Wiley & Sons Inc., 2011.

Shamsipur, M.; Hemmateenejad, B.; Akhond, M. *J. Solution Chem.* **2003**, *32*, 819–829.

Shibata, M.; Inoue, Y.; Miyoshi, M. *Polymer* **2006**, *47*, 3557–3564.

Shih, C. K.; Tynan, D. G.; Denelsbeck, D. A. *Polym. Sci. Eng.* **1991**, *31*, 1670–1673.

Shull, K. R.; Kramer, E. J. *Macromolecules* **1990**, *23*, 4769–4779.

Siadat, B.; Lenz, R. W. *J. Polym. Sci.: Polym. Chem. Ed.* **1980**, *18*, 3273–3287.

Singh, G.; Bhunia, H.; Rajor, A.; Choudhary, V. *Polym. Bull.* **2011**, *66*, 939–953.

Singh, G.; Bhunia, H.; Rajor, A.; Jana, R. N.; Choudhary, V. *J. Appl. Polym. Sci.* **2010**, *118*, 496–502.

Sinnwell, S.; Inglis, A. J.; Stenzel, M. H.; Barner-Kowollik, C. Block, Stars, and Combs: Complex Macromolecular Architecture Polymers via Click Chemistry. In *Click Chemistry for Biotechnology and Materials Science*; ed. J. Lahann, John Wiley and Sons, Ltd, United Kingdom, 2009, pp. 89–117.

Smith, M. B.; March, J. *March's Advanced Organic Chemistry, 6th Ed.*; Wiley: New York, 2007; p 1103–1105.

Smith, P. B.; Payne, G. F. The Emergence of Renewable and Sustainable Polymers. In *Renewable and Sustainable Polymers* [Online]; Payne, G. F.; Smith, P. B. Eds.; ACS Symposium Series; American Chemical Society: Washington, D. C., 2011; pp 1–10. http://pubs.acs.org/doi/abs/10.1021/bk-2011-1063.ch001 (accessed Oct 24, 2011).

Sodergard, A.; Nasman, H. *Polym. Degrad. Stab.* **1994**, *46*, 25-30.

Soutif, J.-C.; Brosse, J.-C. *Makromol. Chem.* **1984**, *185*, 839–846.

Stanford, M. J.; Dove, A. P. *Macromolecules* **2009**, *42*, 141-147.

Stanford, M. J.; Pflughaupt, R. L.; Dove, A. P. *Macromolecules* **2010**, *43*, 6538-6541.

Stoclet, G.; Seguela, R.; Lefebvre, J.-M. *Polymer* **2011**, *52*, 1417–1425.

Su, Z.; Li, Q.; Liu, Y.; Hu, G.-H.; Wu, C. *Eur. Polym. J.* **2009**, *45*, 2428–2433.

Subramaniam, N.; Monteiro, M. J.; Taylor, J. R.; Simpson-Gomes, A.; Gilbert, R. G. *Macromol. Symp.* **2000**, *152*, 43–53.

Sumerlin, B. S.; Vogt, A. P. *Macromolecules* **2010**, *43*, 1–13.

Sun, S.; Zhang, M.; Zhang, H.; Zhang, X. *J. Appl. Polym. Sci.* [Online early access]. DOI 10.1002/app.34111. Published Online: Jul 6, 2011. http://onlinelibrary.wiley.com /doi/10.1002/app.34111/pdf (accessed Oct 29, 2011).

Sundararaj, U.; Macosko, C. W. *Macromolecules* **1995**, *28*, 2647–2657.

Swanson, C. L.; Buchanan, R. A.; Otey, F. H. *J. Appl. Polym. Sci.* **1979**, *23*, 743–748.

Switek, K. A.; Bates, F. S.; Hillmyer, M. A. *Macromolecules* **2004**, *37*, 6355-6361.

Takagi, U.; Yasuda, R.; Yamaoka, M.; Yamane, T. *J. Appl. Polym. Sci.* **2004**, *93*, 2363–2369.

Takayama, T.; Todo, M. *J. Mater. Sci.* **2006**, *41*, 4989–4992.

Takayama, T.; Todo, M.; Tsuji, H.; Arakawa, K. *J. Mater. Sci.* **2006**, *41*, 6501-6504.

Thakur, M. *Macromolecules* **1988**, *21***,** 661–664.

Thakur, M.; Swamy, R.; Titus, J. *Macromolecules* **2004**, *37*, 2677–2678.

Theryo, G.; Jing, F.; Pitet, L. M.; Hillmyer, M. A. *Macromolecules* **2010**, *43*, 7394–7397.

Thomas, A. F. *J. Am. Chem. Soc.* **1969**, *91*, 3281–3289.

Trementozzi, Q. A.; Gebura, S. E.; Locke, F. J. Blends of styrene-acrylonitrile resins with graft copolymers of diene rubber substrate and hydroxylic polymer superstrate. U.S. Patent 3488405. January 6, 1970.

Tripathy, A. R.; Morin, J. E.; Williams, D. E.; Eyles, S. J.; Farris, R. J. *Macromolecules* **2002**, *35*, 4616–4627.

Tse, C. K. W.; Penciu, A.; McInenly, P. J.; Kumar, K. R.; Drewitt, M. J.; Baird, M. C. *Eur. Polym. J.* **2004**, *40*, 2653–2657.

Valente, A.; Zinck, P.; Mortreux, A.; Visseaux, M. *J. Polym. Sci. Part A* **2011**, *49*, 1615–1620.

van Beilen, J. B.; Poirier, Y. *Plant J.* **2008**, *54*, 684–701.

Vannaladsaysy, V.; Todo, M.; Takayama, T.; Jaafar, M.; Ahmad, Z.; Pasomsouk, K. *J. Mater. Sci.* **2009**, *44*, 3006–3009.

Vennestrøm, P. N. R.; Osmundsen, C. M.; Christensen, C. H.; Taarning, E. *Angew. Chem. Int. Ed.* [Online early access] **2011**, DOI: 10.1002/anie.201102117. Published Online: Oct 5, 2011. http://onlinelibrary.wiley.com/doi/10.1002/anie.201102117/pdf (accessed Oct 24, 2011).

Vierle, M.; Zhang, Y.; Santos, A. M.; Köhler, K.; Haeßner, C.; Herdtweck, E.; Bohnenpoll, M.; Nuyken, O.; Kühn, F. E. *Chem. Eur. J.* **2004**, *10*, 6323–6332.

Vilaplana, F.; Strömberg, E.; Karlsson, S. *Polym. Degrad. Stabil.* **2010**, *95*, 2147–2161.

Vilay, V.; Mariatti, M.; Ahmad, Z.; Pasomsouk, K.; Todo, M. *J. Appl. Polym. Sci.* **2009**, *114*, 1784–1792.

Vink, E. T. H.; Davies, S.; Kolstad, J. J. *Ind. Biotechnol.* **2010**, *6*, 212–224.

Visconte, L. L. Y.; Andrade, C. T.; Azuma, C. *Polym. Adv. Technol.* **1993**, *4*, 490–495.

Wakamatsu, H.; Nishida, M.; Adachi, N.; Mori, M. *J. Org. Chem.* **2000**, *65*, 3966–3970.

Wang, G.; Fan, X.; Huang, J. *J. Polym. Sci. Part A* **2010**, *48*, 3797–3806.

Wang, L.; Ma, W.; Gross, R. A.; McCarthy, S. P. *Polym. Degrad. Stabil.* **1998**, *59*, 161–168.

Wang, R.; Wang, S.; Zhang, Y.; Wan, C.; Ma, P. *Polym. Eng. Sci.* **2009**, *49*, 26–33.

Wang, Y.; Hillmyer, M. A. *J. Polym. Sci. Part A* **2001**, *39*, 2755–2766.

Weiman, C. J.; Finaly, J. A.; Park, D.; Paik, M. Y.; Krishnan, S.; Sundaram, H. S.; Dimitriou, M.; Sohn, K. E.; Callow, M. E.; Callow, J. A.; Handlin, D. L.; Willis, C. L.; Kramer, E. J.; Ober, C. K. *Langmuir* **2009**, *25*, 12266–12274.

Weisz, P. B. *Phys. Today* **2004**, *57*, 47–52.

Whited, G. M.; Feher, F. J.; Benko, D. A.; Cervin, M. A.; Chotani, G. K.; McAuliffe, J. C.; LaDuca, R. L.; Ben-Shosha, E. A.; Sanford, K. J. *Ind. Biotechnol.* **2010**, *6*, 152–163.

Widmaier, J. M.; Meyer, G. C. *Macromolecules* **1981**, *14*, 450–452.

Williams, C. K.; Hillmyer, M. A. *Polym. Rev.* **2008**, 48, 1–10.

Witzke, D.R.; Narayan, R.; Kolstad, J. J. *Macromolecules* **1997**, *30*, 7075-7085.

Wong, C. L. H.; Kim, J.; Torkelson, J. M. *J. Polym. Sci. Part B* **2007**, *45*, 2842–2849.

Wu, S. *J. Appl. Polym. Sci.* **1988**, *35*, 549–561.

Wu, S. *Polym. Eng. Sci.* **1987**, *27*, 335-343.

Wu, S. *Polymer* **1985**, *26*, 1855–1863.

Xenidou, M.; Beyer, F. L.; Hadjichristidis, N.; Gido, S. P.; Tan, N. B. *Macromolecules* **1998**, *31*, 7659-7667.

Xie, K.; Li, W.; Zhao, W. *Energy* **2010**, *35*, 4349–4355.

Xu, N.; Du, F.-S.; Li, Z.-C. *J. Polym. Sci Part A: Polym. Chem.* **2007**, *45*, 1889-1898.

Yagci, Y.; Mishra, M. K. The Fundamentals. In *Handbook of Vinyl Polymers*, 2nd ed.; Mishra, M. K.; Yagci, Y., Eds.; Taylor & Francis Group, LLC: Boca Raton, FL, 2009.

Yang, Q.; Hirata, M.; Lu, D.; Nakajima, H.; Kimura, Y. *Biomacromolecules***2011**, *12*, 354–358.

Yeh, J.-T.; Tsou, C.-H.; Lu, W.; Li, Y.-M.; Xiao, H. W.; Huang, C.-Y.; Chen, K.-N.; Wu, C.-S.; Chai, W.-L. *J. Polym. Sci. Part B* **2010**, *48*, 913–920.

Yoon, J.-S.; Lee, W.-S.; Kim. K.-S.; Chin, I.-J.; Kim, M.-N.; Kim, C. *Eur. Polym. J.* **2000**, *36*, 435–442.

Yu, G.-Q.; Thakur, M. *J. Polym. Sci., Part B: Polym. Phys.* **1994**, *32*, 2099–2104.

Yu, L.; Petinakis, E.; Dean, K.; Liu, H.; Yuan, Q. *J. Appl. Polym. Sci.* **2011**, *119*, 2189–2195.

Yue, C. J.; Liu, Y.; He, R. *J. Mol. Catal. A: Chem.* **2006**, *259*, 17–23.

Zhang, C.; Man, C.; Pan, Y.; Wang, W.; Jiang, L.; Dan, Y. *Polym. Int.* **2011**, *60*, 1548–1555.

Zhang, H.; Luo, Y.; Hou, Z. *Macromolecules* **2008**, *41*, 1064–1066.

Zhang, J.; Guan, L.; Su, Y.; Qi, R.; Ye, D.; Yu, J.; Huang, S. *J. Appl. Polym. Sci.* [Online early access]. DOI: 10.1002/app.34951. Published Online: Sep 1, 2011. http://onlinelibrary.wiley.com/doi/10.1002/app.34951/pdf (accessed Oct 28, 2011).

Zhang, J.; Jiang, L.; Zhu, L.; Jane, J.-I.; Mungura, P. *Biomacromolecules* **2006**, *7*, 1551–1561.

Zhang, L. Structure-Property Relationship of Polyurethane Flexible Foam Made from Natural Oil Polyols. Ph.D. Thesis, University of Minnesota, September 2008.

Zhang, L.; Xiong, C.; Deng, X. *Polymer* **1996**, *37*, 235–241.

Zhang, N.; Wang, Q.; Ren, J.; Wang, L. *J. Mater. Sci.* **2009**, *44*, 250–256.

Zhang, Z.; Cui, D.; Wang, B.; Liu, B.; Yang, Y. *Struct. Bond* **2010**, *137*, 49 – 108.

Zhu, J.; Ganton, M. D.; Kerr, M. A.; Workentin, M. S. *J. Am. Chem. Soc.* **2007**, *129*, 4904-4905.

Zhu, J.; Lines, B. M.; Ganton, M. D.; Kerr, M. A.; Workentin, M. S. *J. Org. Chem.* **2008**, *73*, 1099-1105.

Zhu, Y.; Burgaz, E.; Gido, S. P.; Staudinger, U.; Weidisch, R.; Uhrig, D.; Mays, J. W. *Macromolecules* **2006**, *39*, 4428–4436.

Appendix A

Reactions of Polyisoprene and End-functionalized Polylactide

This appendix discusses the investigation of melt blends of *N*-2-hydroxylethylmaleimide (HEMI) and HEMI end-functionalized poly(L-lactide) (HEMI-PLLA) with polyisoprene (PI). We found that melt blends of HEMI and HEMI-PLLA did not react with PI, instead they reacted with themselves to create insoluble or high molecular weight products. Peroxides were added to the blends in an effort to graft HEMI-PLLA to PI and HEMI and HEMI-PLLA reacted with themselves instead of reacting with PI. Preparatory gel permeation chromatography (prep-GPC) proved to be an invaluable technique to characterize the reaction products and elucidate the composition of high molecular weight products. Perhaps the most interesting result was that insoluble crosslinked networks of PLLA could be formed by heating HEMI-PLLA with peroxides at 190 °C.

A.1 Introduction

In Chapter 2, we demonstrated that *N*-2-hydroxyethylmaleimide terminated poly(L-lactide) (HEMI-PLLA) underwent a Diels–Alder reaction with conjugated soybean oil. Previous to these successful experiments, we investigated the ability of HEMI and HEMI-PLLA to react with polyisoprene (PI) through both the ene reaction and free radical grafting. The aim was to synthesize reactive blends of HEMI-PLLA and PI that would form compatibilizer while blending, much like those synthesized in Chapter 2. The following introduction discusses the rationale for investigating such reactions.

PI, NR, and other unsaturated polymers are known to react with maleic anhydride (MA) through both the ene and free radical reactions in a process called maleation.[1] For the ene reaction to occur, the temperature of the system needs to be around 200 °C or higher – near to the PLLA melt blending temperature (190 °).[2] At the elevated temperatures in melt blends, radical dehydrogenation occurs, giving conjugated dienes that can undergo Diels–Alder reactions with MA as well.[3] These reactions result in MA being grafted off the main polymer backbone which then can be reacted further to give graft polymers.[4,5,6,7] The MA functionalization and subsequent reaction with it is a two step process to graft copolymers and compatibilizers – we targeted the synthesis of compatibilizers in one step.

To accomplish the one step compatibilization reaction, PLLA was end-functionalized with a maleimide which is similar to MA. Maleimides will undergo ene reactions with small molecules at elevated temperatures, suggesting that a maleimide functionalized PLLA may do the same to PI.[8,9] As discussed in Chapter 2, HEMI can be used to initiate the ring opening polymerization of lactide to give HEMI-PLLA. This end-functionalized polylactide contains the maleimide functionality that could possibly undergo the ene or radical reactions at elevated temperatures.

We investigated melt blends of HEMI and HEMI-PLLA with PI. Blends of HEMI-PLLA and PI gave a small amount of products that had a higher molecular weight than the starting materials. To increase the rate of high molecular weight product generation, peroxides were investigated as blending partners to increase the rate of coupling of the two polymers. Ultimately, it was found that HEMI-PLLA does not react

with PI significantly. Instead, HEMI-PLLA reacts with itself and in the presence of peroxides can even form an insoluble gel, perhaps the most notable result. The tool that was the most useful to determine the composition of the high molecular weight products was preparatory gel permeation chromatography (prep-GPC).

A.2 Experimental Details

A.2.1 Materials and General Methods

All chemicals were purchased from Aldrich and used without further purification unless otherwise stated. L-lactide (Purac) was purified through recrystallization in ethyl acetate and then dried under vacuum at room temperature. Dry toluene (HPLC grade) was purified by passing it through a home built solvent purification system with activated alumina column and a supported copper catalyst. *N*-2-hydroxyethylmaleimide (HEMI) and HEMI initiated poly(L-lactide) (HEMI-PLLA) were synthesized using the procedures outlined in Chapter 2. PI was synthesized through anionic polymerization, following a similar procedure to that in Chapter 3.[10,11,12]

Proton nuclear magnetic resonance (^{1}H NMR) spectroscopy was performed on a Varian Inova 500 MHz spectrometer in CDCl$_3$ unless otherwise noted. Size exclusion chromatography (SEC) was performed on an Agilent 1100 high-pressure liquid chromatograph at 35 °C equipped with a PLgel (Varian) 5 μm guard column followed by three PLgel columns with varying pore sizes with HPLC grade chloroform as the mobile phase. Molecular weights and polydispersity index (PDI) were measured by a Hewlett-Packard P1047A refractometer calibrated with polystyrene standards (Polymer Laboratories). Fourier transform − infrared (FT-IR) spectroscopy was performed on a Magna-IR Spectrometer 550 (Nicolet) with N$_2$ purge.

A.2.2 Melt blends of HEMI/Maleic anhydride and PI

HEMI and maleic anhydride (MA) were first ground to a fine powder using a mortar and pestle. Either powdered HEMI or MA was added to PI (6.6 kg/mol) in a small round bottom flask that was sealed with a septum. Nitrogen was delivered by a needle while the products were heated at 190 °C for 10 minutes. The relative amounts of HEMI

or MA to PI were varied to explore the reactivity of the blends. The blends were characterized by ^{1}H NMR and FT-IR spectroscopy.

A.2.3 Melt blends of HEMI-PLLA and PI (test tube)

HEMI-PLLA and PI were co-dissolved in minimal CH_2Cl_2 in a small test tube to create a homogenous mixture. The solution then was dried by pulling vacuum at room temperature. If peroxides were to be added for the reaction, they were added after the polymer mixture was dried. The dried polymers in test tube were placed in an oil bath at 190 °C and were stirred for the desired time with an overhead mixer. After the reaction, the sample tube was cooled in a water bath. The products were analyzed by SEC and ^{1}H NMR spectroscopy.

A.2.4 Melt blends of HEMI-PLLA and PI (DACA mixer)

Larger scale melt blends of PI and HEMI-PLLA were synthesized in a 4 g scale batch melt mixer (DACA) at 190 °C and 100 rpm screw speed. PI was added to the hot mixer via glass syringe with subsequent HEMI-PLLA addition over a period of 5 minutes. If used, peroxides were added by a glass pipette after the HEMI-PLLA. After all components were added to the mixer, the blend timer would start and the materials would be blended for the desired time period.

A.2.5 Soxhlet extraction of blends

The sample was placed in an extraction thimble and was extracted with refluxing cyclohexane (CHX) for 48 h in a Soxhlet extraction apparatus. After extraction, the thimble and remaining material was dried under vacuum and the CHX fraction was concentrated by rotary evaporation. The thimble with the CHX insoluble fraction was extracted with refluxing CH_2Cl_2 for 48 h in a Soxhlet extraction apparatus. The thimble was dried under vacuum and the CH_2Cl_2 collected fraction was concentrated by roto-evaporation. The soluble fractions were characterized by ^{1}H NMR spectroscopy and SEC.

A.2.6 Preparatory gel permeation chromatography fractionation of blends

Preparatory gel permeation chromatography (prep-GPC) was performed on select blends of HEMI-PLLA and PI to fractionate the high molecular weight reaction products from the two homopolymers. Samples were run on the same Agilent system discussed previously, but with a 6 mL/min flow rate of $CHCl_3$ as the mobile phase passing through a preparatory scale guard column (PLgel Prep Guard, Agilent) and two preparatory columns (PLgel 10 μm Mixed-D, Agilent). Samples were dissolved in $CHCl_3$ at 40–80 mg/mL concentration and their passage through the system was monitored by a UV-vis detector recording at the 254 nm wavelength. Two or more runs of each blend were separated by taking fractions each minute as the polymer passed through the detector. The fractions of different runs at the same elution volume were combined and concentrated by rotary evaporation. The solvent was blown off with N_2 and the sample was dried under vacuum. The recovered products were analyzed by ^{1}H NMR spectroscopy and analytical SEC.

A.2.7 Flash column chromatography fractionation of blends

Flash column chromatography was run with silica gel (60–200 mesh, Mallinckrodt) as the stationary phase and a 2:1 hexanes:CH_2Cl_2 mixture as the mobile phase. The blend (250 mg) was dissolved in the solvent mixture and sonication was used to break up the larger pieces of insoluble material. Fractions were collected in test tubes and spotted using thin layer chromatography with a potassium permanganate stain. Fractions were combined, concentrated by roto-evaporation, and analyzed by ^{1}H NMR spectroscopy.

A.3 Results and Discussion

A.3.1 Melt blends of PI with either HEMI or MA

To investigate the potential of HEMI-PLLA reacting with PI, we investigated the ability of small molecule analogs (HEMI and MA) to react with PI in small scale melt blends at 190 °C. HEMI and MA were mixed with PI (M_n = 6.6 kg/mol) and heated to 190 °C for 10 min (Table A.1). Through ^{1}H NMR spectroscopic analysis of the vinyl protons of the small molecule (R), the conversions of R were found to be high (85–90%) in only 10 minutes of heating, suggesting that a reaction occurred. Further evidence of R

reacting was the appearance of new peaks in the ^{1}H NMR spectra of the reaction products (Figure A.1). The presence of peaks in the 3.0–2.5 ppm region is consistent with the formation of HEMI and MA grafting products to PI.[13,14,15]

Table A.1. Composition of conversion of MA and HEMI melt reaction with PI (6.6 kg/mol) at 190 °C for 10 min.

R[a]	[R]/[C=C][b]	Conversion[c]
MA	0.14	85%
HEMI	0.07	93%
HEMI	0.03	99%

[a]Small molecule heated with PI. [b]Molar ratio of R to the carbon-carbon double bonds in PI. [c]Conversion of R calculated from ^{1}H NMR spectrum of product using the peaks that correspond to the vinyl protons present in R.
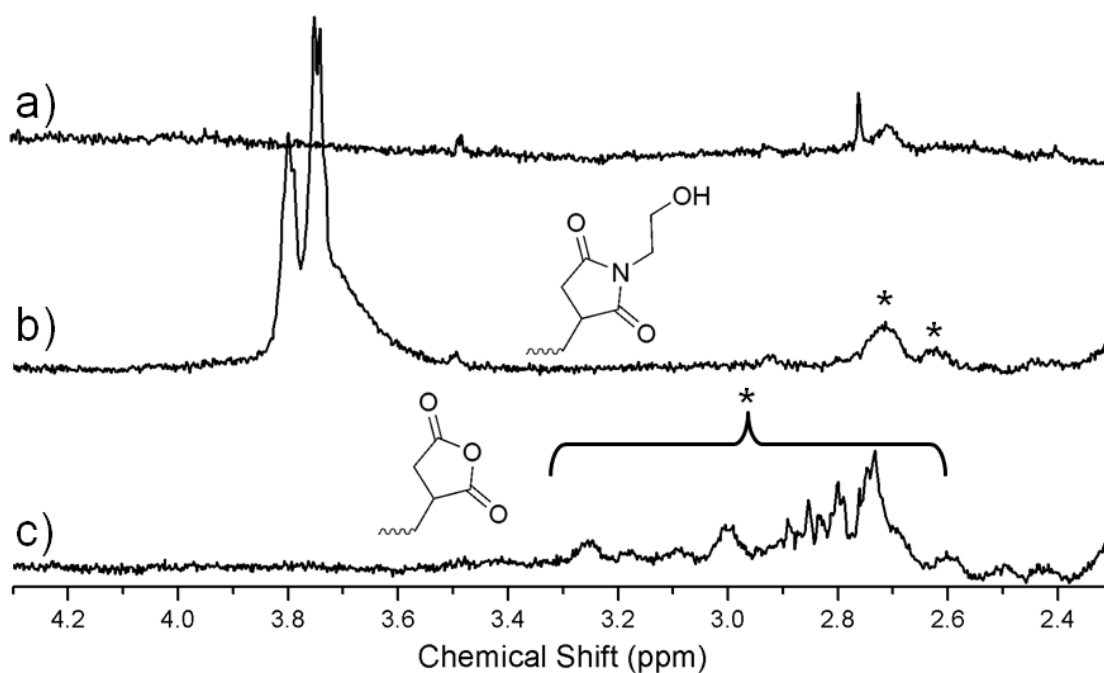
Figure A.1. ^{1}H NMR spectra of (a) PI (6.6 kg/mol), (b) 0.07 [R]/[C=C] melt blend of HEMI and PI, and (c) melt blend of MA and PI (500 MHz, CDCl₃). The possible grafted chemical structures are given. All blends were run at 190 °C for 10 min. Asterisks (*) indicate the peaks that are consistent with MA and HEMI reacting with the PI chain.

The peaks in the 3.0–2.5 ppm region may also be indicative of homopolymerization of maleimides.[16] The product of the HEMI heating with PI typically contained material that was insoluble in the ^{1}H NMR solvent (CDCl$_3$), which may have been HEMI homopolymer. Further evidence of HEMI become insoluble through polymerization is that the ^{1}H NMR spectrum of the heating product (Figure A.1b) has broad peaks that belong to the four methylene protons of HEMI. The peak broadness suggests that these protons are not fully soluble in CDCl$_3$ – consistent with the insoluble product observed visually. Conversely, the MA reacted product is completely soluble, which suggests that MA did successfully graft to PI. Consequently, these small molecule reactions do not confirm or deny the ability of HEMI to graft to PI through either reaction mechanism.

A.3.2 Melt blends of HEMI-PLLA and PI

With the potential grafting of HEMI to PI demonstrated, reactive blending investigations moved to melt blends of HEMI-PLLA and PI. A variety of polymers with different molecular weights were used in the blends (Table A.2). Both PI samples (PI-7 and PI-33) were synthesized by anionic polymerization (see Chapter 3), while the HEMI-PLLA samples were synthesized using the procedure discussed in Chapter 2. PLLA-49 was provided by Toyota.

Table A.2. PI and PLLA polymers used in melt blends

Sample[a]	M_n (kg/mol)[b]	PDI[c]
PI-1	1	1.11
PI-7	7	1.05
PI-33	33	1.03
HEMI-PLLA-1	1	1.11
HEMI-PLLA-2	2	1.08
HEMI-PLLA-18	18	1.27
PLLA-49	49	1.85

[a]Sample code has form aaa-## where aaa is the polymer type and ## is the M_n of the polymer. [b]Calculated from ^{1}H NMR spectroscopy end group analysis. [c]Calculated from SEC with polystyrene standards.

Synthesis of the melt blends occurred at two scales – small scale in a test tube heated in an oil bath and large scale in the DACA melt mixer. Blends were synthesized with a number of different HEMI-PLLA and PI polymers to investigate the formation of higher molecular weight products in systems with different molecular weights (Table A.3). All melt blends had a fraction of their HEMI-PLLA undergo a reaction as indicated by a decrease in the intensity of the HEMI-PLLA vinyl proton peak in ^{1}H NMR spectroscopy. Interestingly, the HEMI end group conversion for the blend synthesized in the DACA mixer was significantly higher than that of a blend with a similar [C=C]/[HEMI] synthesized in a test tube. The increased reactivity may be due to the DACA mixer already hot when adding materials to it as opposed to the test tube samples that start off cold and are heated by the oil bath over time. Under these starting conditions and the same residence times, the materials blended in the DACA mixer would be at 190 °C for longer that the small scale blends, leading to the higher conversion observed.

Table A.3. Reaction conditions and HEMI conversion of melt blend between HEMI-PLLA and PI.

PI used	HEMI-PLLA Used	Mixing Protocol[a]	[C=C]/[HEMI][b]	Mixing Time (min)	HEMI Conversion[c]
PI-1	HEMI-PLLA-2	Small	28	10	12%
PI-7	HEMI-PLLA-18	Small	880	30	24%
PI-33	HEMI-PLLA-1	Small	13	30	13%
PI-33	HEMI-PLLA-18	DACA	860	40	54%

[a]Mixing protocol used for blend – either small scale blend in test tube or blend in DACA mixer, both at 190 °C. [b]Ratio of the carbon-carbon double bonds in PI to the HEMI end groups of HEMI-PLLA. [c]Conversion of HEMI end groups determined by ^{1}H NMR spectroscopy.

Though consumption of the HEMI end group was observed in ^{1}H NMR spectroscopy, peaks associated with HEMI-PLLA grafting to PI were not observed. GPC analysis was used to determine if grafting occurred. Indications of a reaction were seen in the SEC elution curves of the products (Figure A.2 and Figure A.3) as a new shoulder was present that corresponds to high molecular weight products (HMWP). The heated

homopolymer SEC traces did not differ greatly from their originals (Figure A.2 and Figure A.3). Consequently, the HMWP observed in the blends are likely due to some reaction. The other two blends in Table A.3 had similar phenomena in their SEC elution curves.
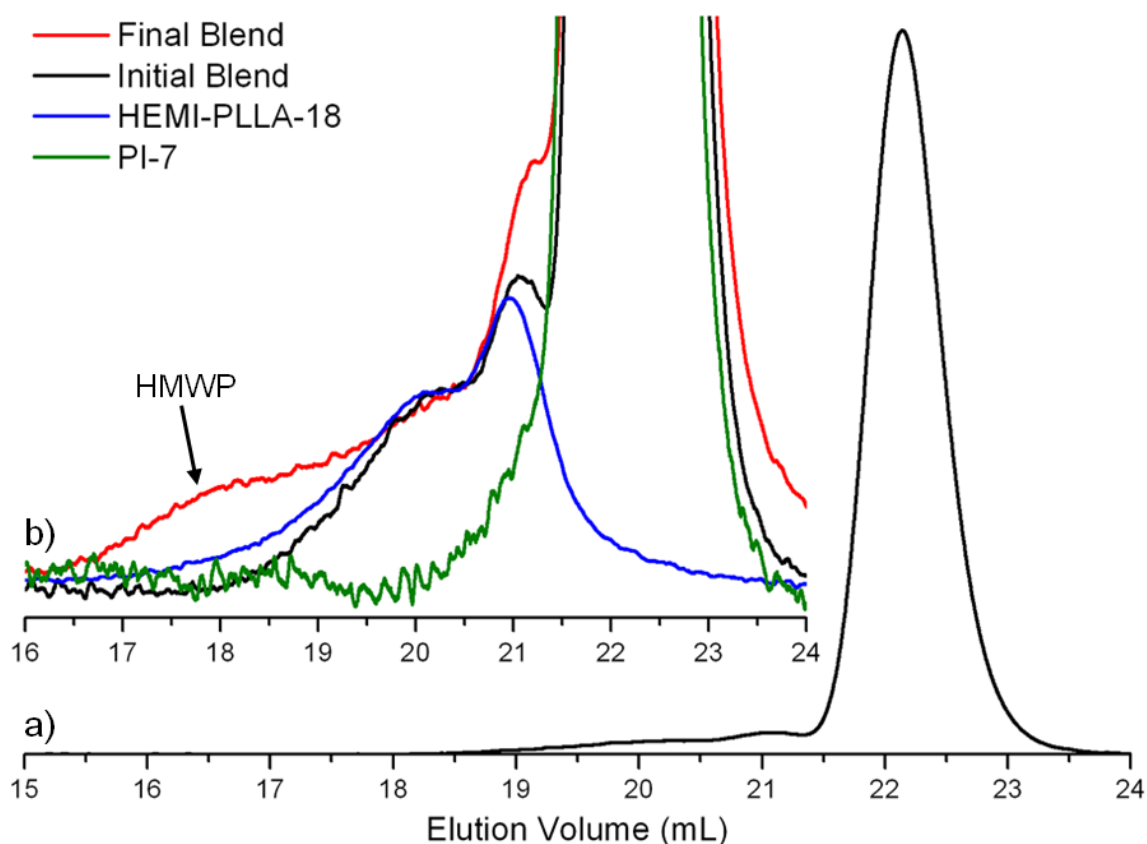
Figure A.2. SEC elution curves of HEMI-PLLA-18 and PI-7. The curves are the (a) initial blend of polymers and (b) zoomed in overlay of initial blend (black), final blend after heating for 30 min (red), HEMI-PLLA-18 (blue), and PI-7 (green). Traces for HEMI-PLLA-18 and PI-17 are of the respective polymers after heating at 190 °C for 30 min. Traces of the individual polymers were scaled to fit their relative intensities in the blend. High molecular weight products (HMWP) are indicated by the arrow.
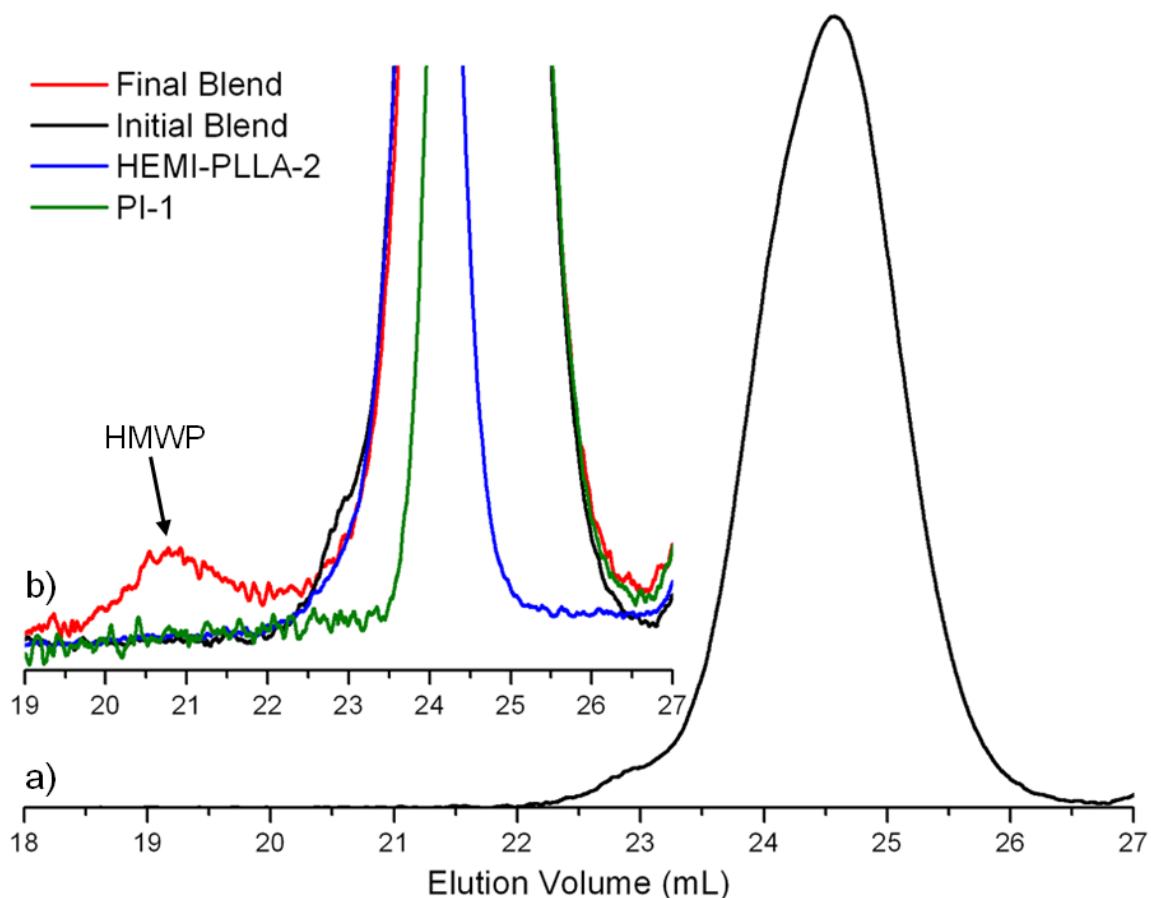
Figure A.3. SEC elution curves of HEMI-PLLA-2 and PI-1. The curves are the (a) initial blend of polymers and (b) zoomed in overlay of initial blend (black), final blend after heating for 30 min (red), HEMI-PLLA-2 (blue), and PI-1 (green). Traces for HEMI-PLLA-2 and PI-1 are of the respective polymers after heating at 190 °C for 10 min. Traces of the individual polymers were scaled to fit their relative intensities in the blend. High molecular weight products (HMWP) are indicated by the arrow.

To determine the composition of the HMWP, they were fractionated from initial homopolymers by prep-GPC. Figure A.4 gives a representative HMWP fraction obtained from prep-GPC on the PI-7 and HEMI-PLLA-18 blend. As demonstrated in Figure A.4, the fraction taken predominately consists of the HMWP. To determine the composition of the prep-GPC fraction, it was analyzed by ^{1}H NMR spectroscopy (Figure A.5). Both reacted HEMI-PLLA and PI are present in the HMWP as indicated by the peaks at 5.2 and 2.0 ppm, respectively. The peak associated with the vinyl protons of the HEMI end group (6.7 ppm) is not present in the spectrum, suggesting that all the end groups of

HEMI-PLLA in the HMWP have reacted. If HEMI-PLLA had reacted with PI (one to one reaction) to form the HMWP, 29 mol % of the polymer repeat units would belong to PI. In the fractionated product, only 0.7 mol % of the repeat units are from PI. The results suggest that either HEMI-PLLA reacts with itself or many HEMI-PLLA chains react with one PI polymer chain to form the HMWP. Both mechanisms mentioned above must require the presence of PI since HMWP are not observed when each homopolymer is heated alone. Perhaps, thermal decomposition of PI produces radicals that initiate the self reaction of HEMI-PLLA. Such a mechanism can explain the presence a small amount of PI compared to reacted HEMI-PLLA. Nevertheless, the thermal coupling of HEMI-PLLA and PI was inefficient so other methods were explored.

Figure A.4. SEC elution curves of blends of HEMI-PLLA-18 and PI-7 before (black) and after (red) heating at 190 °C for 30 min. Also shown is the SEC elution curve of the prep-GPC fraction of the HMWP (blue).
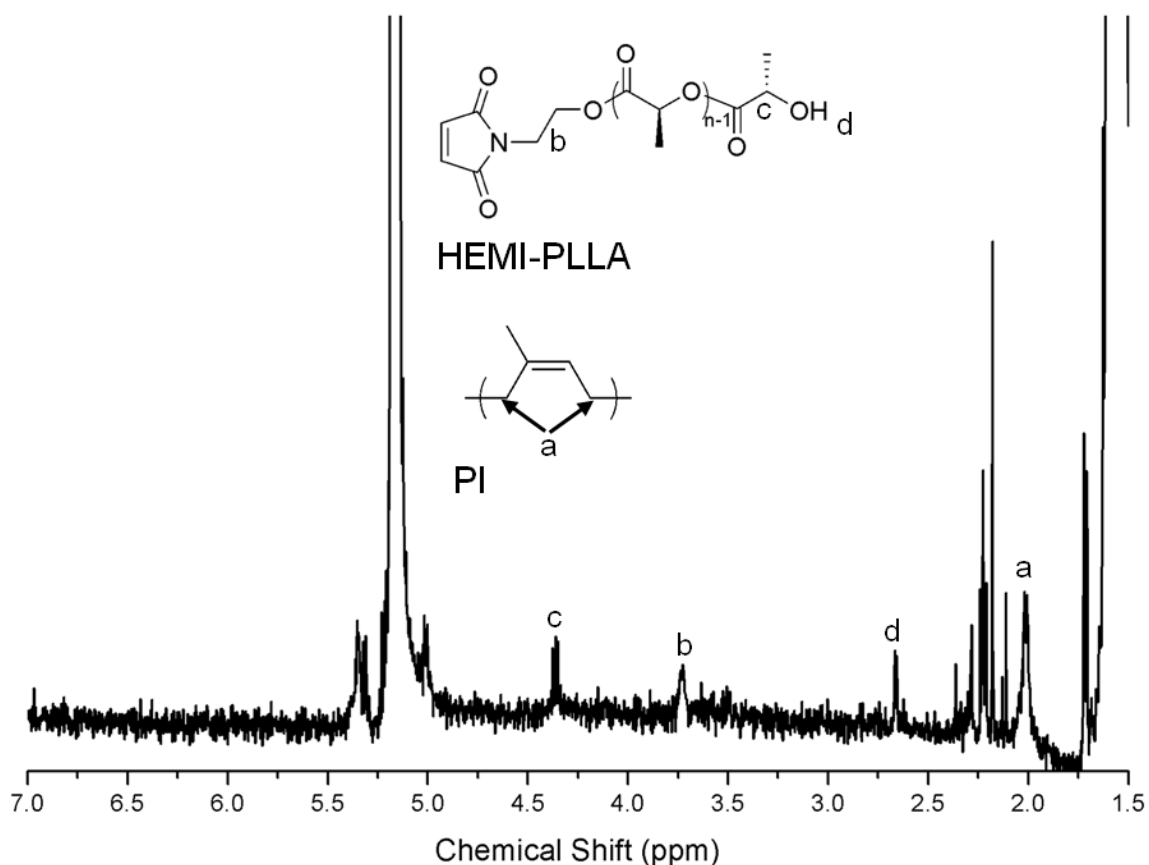
Figure A.5. ^{1}H NMR spectrum of prep-GPC fraction taken from HEMI-PLLA-18 and PI-7 blend (500 MHz, CDCl$_3$). Peaks associated with both HEMI-PLLA and PI are present in the spectrum as labeled.

A.3.3 Ternary melt blends of HEMI-PLLA, PI, and peroxides

In an effort to increase the reactivity of HEMI-PLLA towards PI, radical generating peroxides were mixed into melt blends of HEMI-PLLA and PI. The peroxides investigated (Table A.4) were chosen to give a range of decomposition rates at 190 °C as indicated by their 6 min half life (t$_{1/2}$) temperature. The ternary blends (Table A.5) were processed in either the small scale or in the DACA mixer for 10 min. Compared to similar blends of HEMI-PLLA and PI, the ternary blends with peroxide tended to have an increased conversion of HEMI end-groups. Interestingly, the ternary blends of HEMI-PLLA and PI also led to products with an insoluble gel fraction (Table A.5). The

increased HEMI end-group reaction rate in the ternary blends is due to the radicals generated by the decomposition of the peroxide that then react with HEMI group.

Table A.4. The structures and temperatures for 6 min half life ($t_{1/2}$) of the peroxides used in melt blends of HEMI-PLLA and PI.[17]
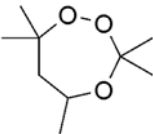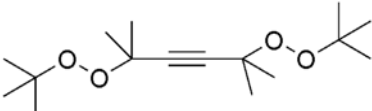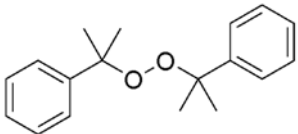
Peroxide	Structure	6 min $t_{1/2}$ temperature (°C)
Trigonox 311		206
Trigonox 145		182
Dicumyl peroxide		162

Table A.5. Composition and conversion of HEMI end group in HEMI-PLLA/PI blends with peroxides at 190 °C for 10 min.

PI	HEMI-PLLA	Mixing Protocol[a]	[C=C]/[HEMI][b]	Peroxide	Wt % Peroxide	HEMI Conversion[c]
PI-1	HEMI-PLLA-2	Small	31	Trigonox 311	5	90%
PI-7	HEMI-PLLA-18	Small	810	Trigonox 311	5	66%
PI-7	HEMI-PLLA-18	Small	810	Trigonox 145	5	Gel[d]
PI-7	HEMI-PLLA-18	Small	850	Dicumyl peroxide	0.1	84%
PI-33	HEMI-PLLA-18	DACA	760	Trigonox 311	5	100%
PI-33	HEMI-PLLA-18	DACA	1200	Trigonox 145	1	100%

[a]Mixing protocol used for blend – either small scale blend in test tube or blend in DACA mixer, both at 190 °C. [b]Ratio of the carbon-carbon double bonds in PI to the HEMI end groups of HEMI-PLLA. [c]Conversion of HEMI end groups determined by ^{1}H NMR spectroscopy. [d]Product had a noticeable gel fraction and subsequently an accurate ^{1}H NMR spectrum could not be obtained.

All blends of HEMI-PLLA and PI with peroxides resulted in products that contained HMWP as indicated by SEC. A representative example of the generation of HMWP is the blend of HEMI-PLLA-18 and PI-7 with 5 wt % Trigonox 311 (Figure A.6) as a new peak in the chromatogram appears an elution volume lower than that of the

starting material. To ascertain the origin of the HMWP in the blends, HEMI-PLLA-18 was heated with 5 wt % Trigonox 311 for 10 min at 190 °C. The SEC trace of the HEMI-PLLA-18 control is given in Figure A.6 (blue) and it follows very closely the trace of the HMWP in the HEMI-PLLA/PI blend, suggesting that the HMWP formed in the blend are due to HEMI-PLLA-18 reacting with itself instead of with PI.
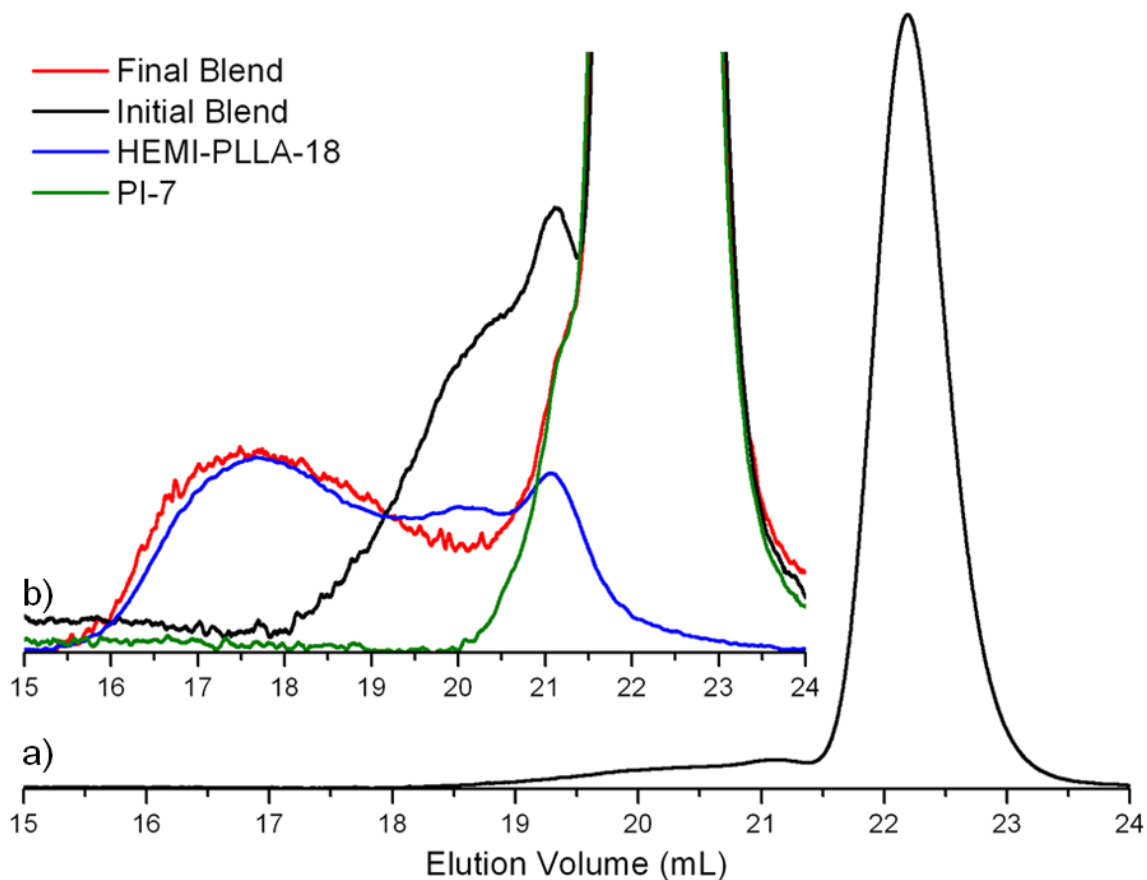
Figure A.6. SEC elution curves of HEMI-PLLA-18 and PI-7 heated with Trigonox 311 at 190 °C for 10 min. The curves are the (a) initial blend of polymers and (b) zoomed in overlay of initial blend (black), final blend after heating for 10 min (red), HEMI-PLLA-18 (blue), and PI-7 (green). Traces for HEMI-PLLA-18 and PI-17 are of the respective polymers after heating with 5 wt% Trigonox 311 at 190 °C for 10 min. Traces of the individual polymers were scaled to fit their relative intensities in the blend.

The HMWP of the HEMI-PLLA-18 and PI-7 blend with Trigonox 311 was analyzed by fractionating with prep-GPC. The SEC traces displayed in Figure A.7 show that a prep-GPC fraction was obtained containing only the HMWP of the final blend. Analysis of the fraction by ^{1}H NMR spectroscopy (Figure A.8) found that only 0.1 mol % of the polymer repeat units in the sample is PI when the expected value is 29 mol %. The lack of PI in the HMWP along with the fact that the SEC trace of HEMI-PLLA-18 blended with peroxides closely matches the HMWP trace of the HEMI-PLLA/PI/peroxide blend, indicates that HEMI-PLLA preferentially reacts with itself in the presence of peroxides.
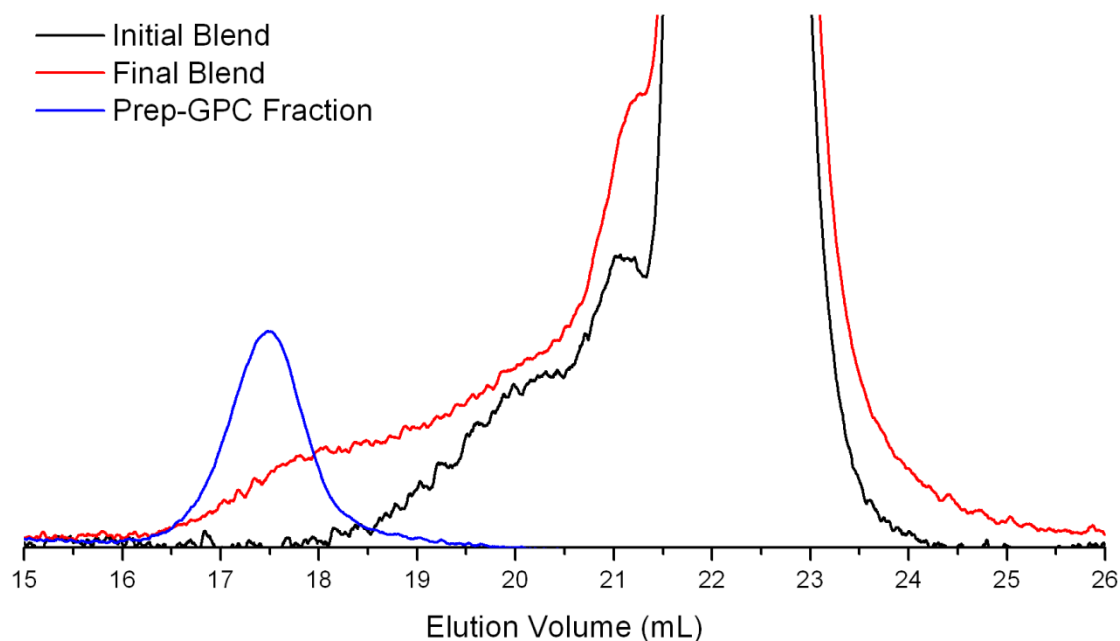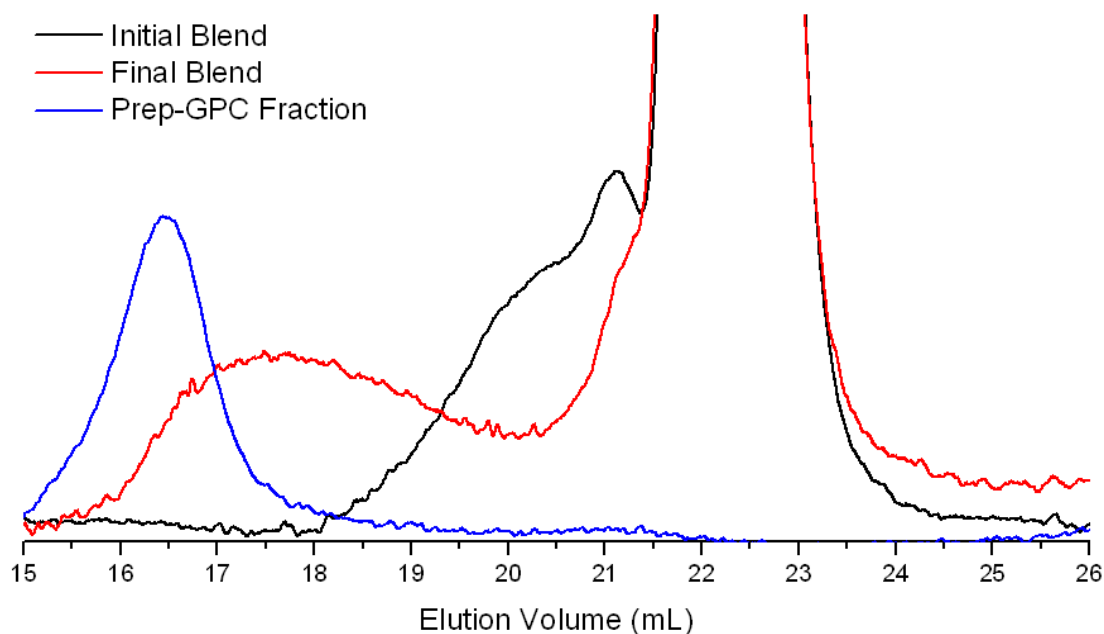

Figure A.7. SEC elution curves of blends of HEMI-PLLA-18 and PI-7 before (black) and after (red) heating at 190 °C for 10 min with 5 wt % Trigonox 311. Also shown is the SEC elution curve of the prep-GPC fraction of the HMWP (blue).
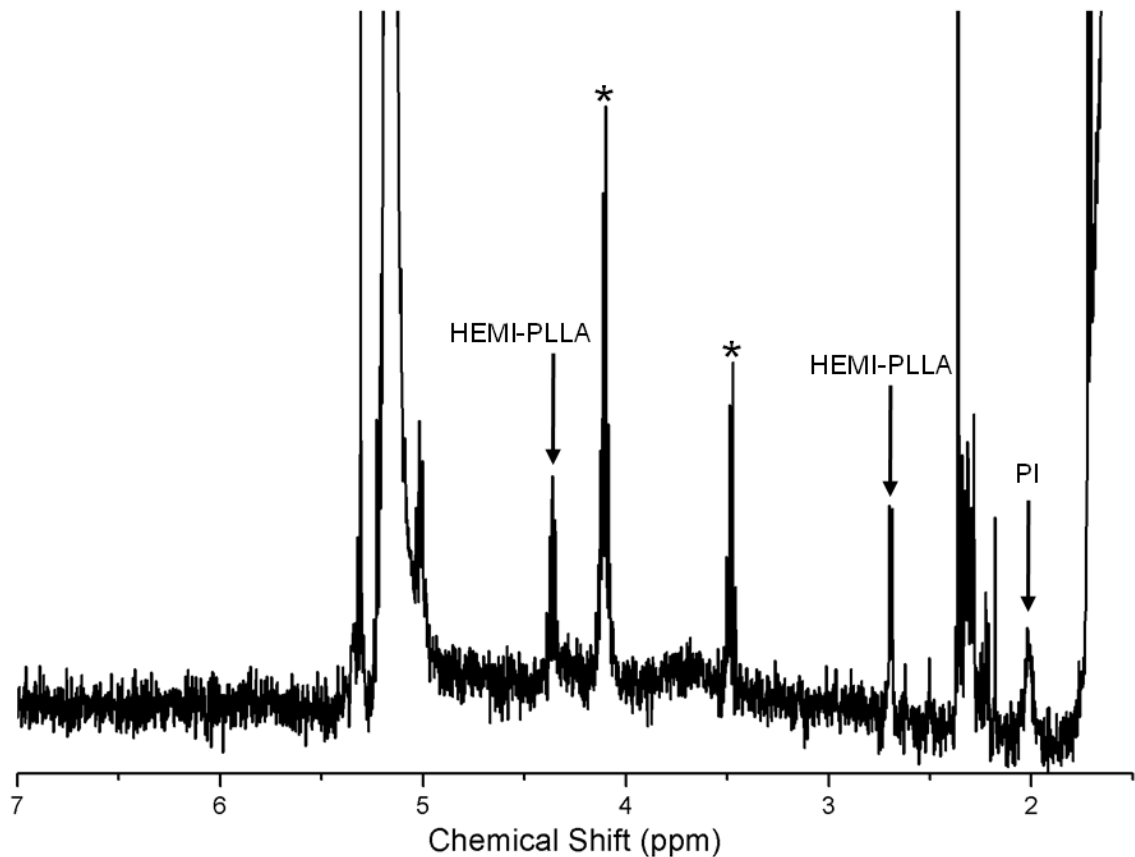
Figure A.8. ^{1}H NMR spectrum of HWMP prep-GPC fraction for HEMI-PLLA-18 and PI-7 blend with Trigonox 311. Peaks are assigned that belong to bother HEMI-PLLA and PI. See Figure A.5 for detailed structure assignments. Asterisks indicate impurities from fractionation process.

A.3.4 Melt reaction of HEMI-PLLA and peroxides

The reaction between HEMI-PLLA and peroxide was investigated in an effort to determine the mechanism by which HEMI-PLLA couples. Blends of HEMI-PLLA-18 and the peroxides were investigated at 190 °C for 10 min (Table A.6). The weight percent of peroxide added was chosen in an effort to minimize the formation of an insoluble gel. Interestingly, with only 0.1 wt % dicumyl peroxide, HEMI-PLLA was still able to form a partial gel. All blends of peroxide and HEMI-PLLA consumed significantly more of the HEMI end-group than the control of HEMI-PLLA heated alone under the same conditions. The exact mechanism for coupling is unclear. Analysis of the ^{1}H NMR

spectra of the reacted samples indicates that the peaks associated with the HEMI end-group decrease in relative intensity while the peaks associated with the PLLA end group do not change, suggesting that the only end-group involved in the reaction is HEMI.

Table A.6. Reaction compositions of HEMI-PLLA-18 blended with peroxides at 190 °C for 10 min.

Peroxide Added	Wt % Peroxide	Conversion of HEMI[a]
None		8%
Trigonox 311	5%	66%
Trigonox 145	1%	55%
Dicumyl peroxide	0.1%	Gel[b]

[a]Determined by ^{1}H NMR spectroscopy. [b]The dicumyl peroxide blend gelled significantly so the total conversion of HEMI end-group could not be determined.

SEC analysis of the soluble products of the reactions in Table A.6 confirms that HEMI-PLLA chains coupled as HMWP formed (Figure A.9). Control blends of PLLA (without a HEMI end-group) using the same peroxides and concentrations as the HEMI-PLLA blends did not generate HMWP (Figure A.10). The HEMI end-group is responsible for the self coupling reaction.
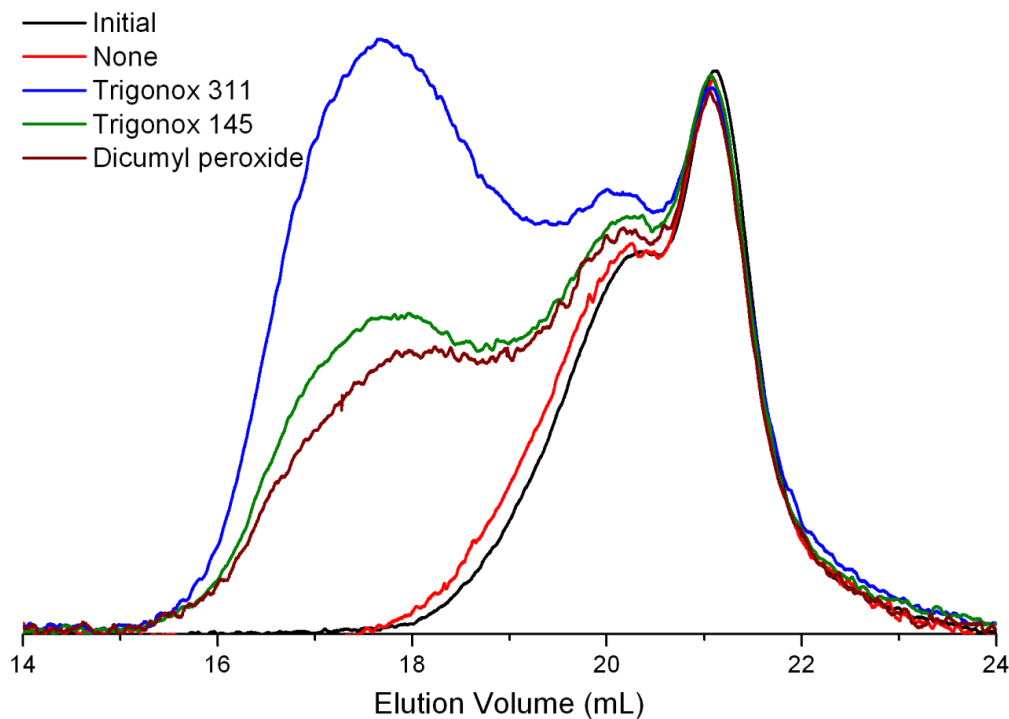
Figure A.9. SEC elution curves for HEMI-PLLA-18 heated with the specified peroxide for 10 min at 190 °C. See Table A.6 for amounts of peroxide used.
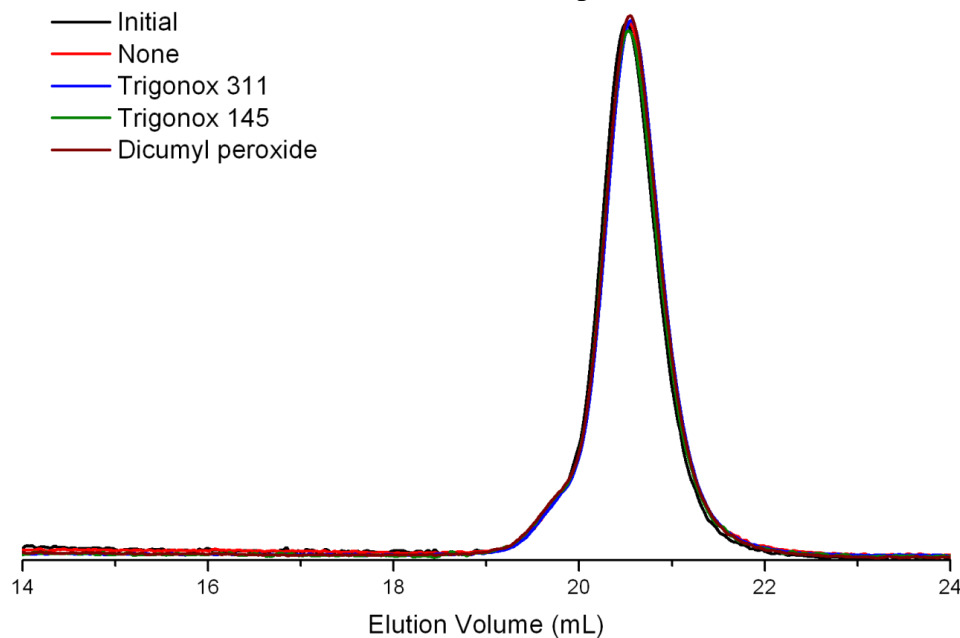
Figure A.10. SEC elution curves for PLLA heated with peroxides for 10 min at 190 °C. Amount of peroxide added is equivalent to that added for corresponding HEMI-PLLA-18 blends (Table A.6).

Since the reaction only occurs at the HEMI end-group, two possible reaction mechanisms exist for the self reaction of HEMI-PLLA: radical polymerization of the HEMI end-group and hydrogen abstraction of the methine proton of PLLA with subsequent reaction with the HEMI end-group (Figure A.11). Both reaction processes are possible as it is known that methine hydrogen extraction from PLLA can lead to the addition of the HEMI analog maleic anhydride and that maleimides can oligomerize through a radical mechanism.[16,18,19] Likely, both reactions occur in the blends, as they both would produce crosslinked material. We suspect that these two reaction mechanisms also occur when HEMI-PLLA is heated without peroxides. Understandably, the reaction rate would be slower without the addition of peroxides as the required initiating radicals only are formed through thermal decomposition process.
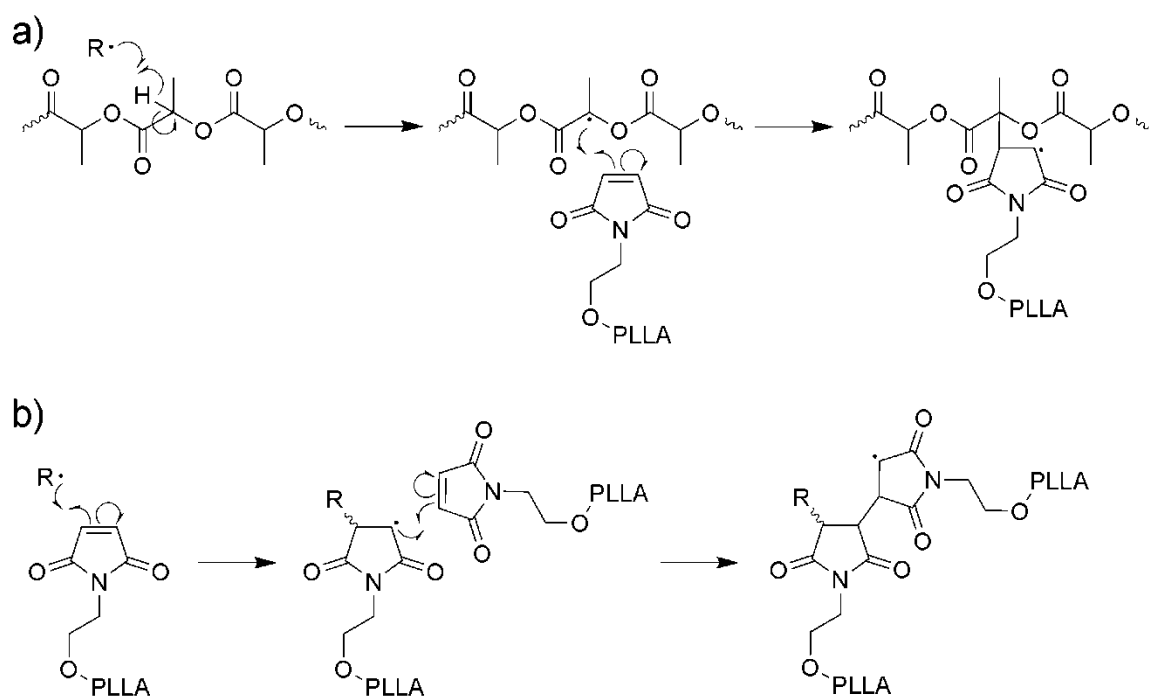
Figure A.11. Possible reaction schemes of HEMI-PLLA reacting with itself. The HEMI-PLLA self reaction can occur by either (a) hydrogen abstraction from PLLA and the subsequent radical reaction with the HEMI end-group or (b) the radical polymerization of the HEMI end-groups.

A.3.5 Evaluation of separation methods to characterize reactive blends

Prep-GPC proved to be a valuable tool when characterizing the HMWP formed in blends of PI and HEMI-PLLA. Other methods to characterize the HMWP were employed with varying degrees of success. We will discuss these other methods to show why we chose prep-GPC over the other methods to analyze the HMWP.

A HEMI-PLLA-18/PI-33 blend was extracted with cyclohexane (CHX), a selective solvent for PI. The CHX phase contained pure PI while the insoluble phase once dissolved in methylene chloride (CH_2Cl_2) contained both PLLA and PI. Interestingly, the HEMI end-group appeared to have been removed from PLLA as free HEMI was observed in the ^{1}H NMR spectrum, while HEMI-PLLA was not observed, suggesting that HEMI may have been hydrolyzed from the PLLA chain during the extraction process. The SEC elution curve of each fraction (Figure A.12) followed the same span in elution volumes as the original blend, confirming that PI was not completely removed from the PLLA fraction. Possibly, an extraction longer than 48 h may have removed all PI, but the apparent hydrolysis of HEMI off PLLA is worrisome. Prep-GPC was the better option since we did not have to worry about the hydrolysis of HEMI and the incomplete removal of PI.
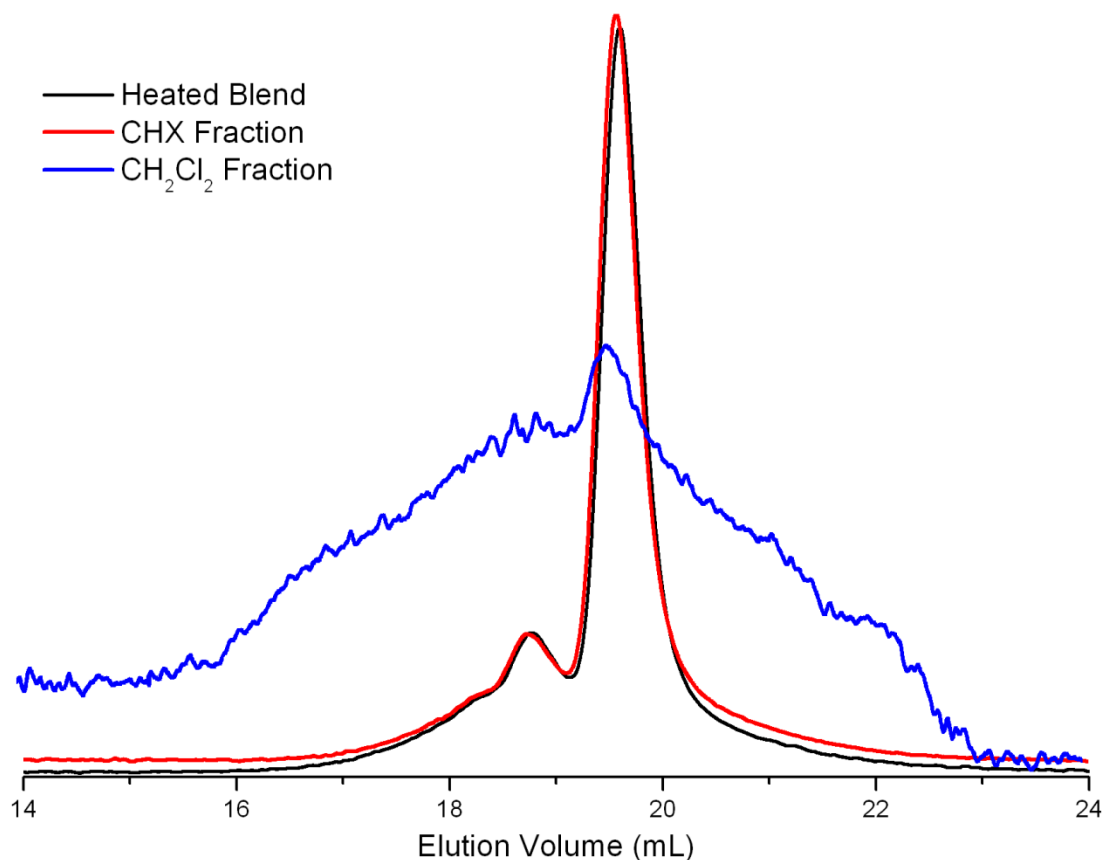
Figure A.12. SEC elution curves of HEMI-PLLA-18/PI-33 original heated blend (black), fraction collected by CHX extraction (red), and remaining fraction collected by CH_2Cl_2 (blue).

Another method investigated to analyze the HMWP for blends of HEMI-PLLA and PI was separation by column chromatography with a silica gel stationary phase. The blend investigated was of HEMI-PLLA-2 and PI-1 that had been heated for 10 min. A mixed solvent system of 2:1 hexanes:CH_2Cl_2 was employed to separate the polymers on the column. PI moved more on the column (R_f = 0.75) than HEMI-PLLA (R_f = 0) as it tended to stick to the silica gel. Thin layer chromatography (TLC) of the blend indicated that a streak of material, presumably reaction products, extended from the initial point to about R_f = 0.45. By taking small fractions as the column ran, the PI was separated from the supposed reaction products. Analysis of the reaction products by ^{1}H NMR spectroscopy signifies that all the material that moved down the column was PI and its

reaction products – no PLLA was collected off the column. Upon washing the column with CH_2Cl_2, the collected fraction contained a majority of HEMI-PLLA and some PI. The SEC elution curve of the CH_2Cl_2 washed fraction follows closely that of HEMI-PLLA, confirming that a majority of the material was in fact HEMI-PLLA (Figure A.13). The CH_2Cl_2 washed fraction also had the characteristic HMWP peak observed in the reaction, demonstrating that the HMWP could not be separated from the homopolymer using flash column chromatography. Prep-GPC was run on the CH_2Cl_2 fraction and we found that the HMWP, like in the previously discussed experiments, was primarily products of the HEMI-PLLA self reaction.
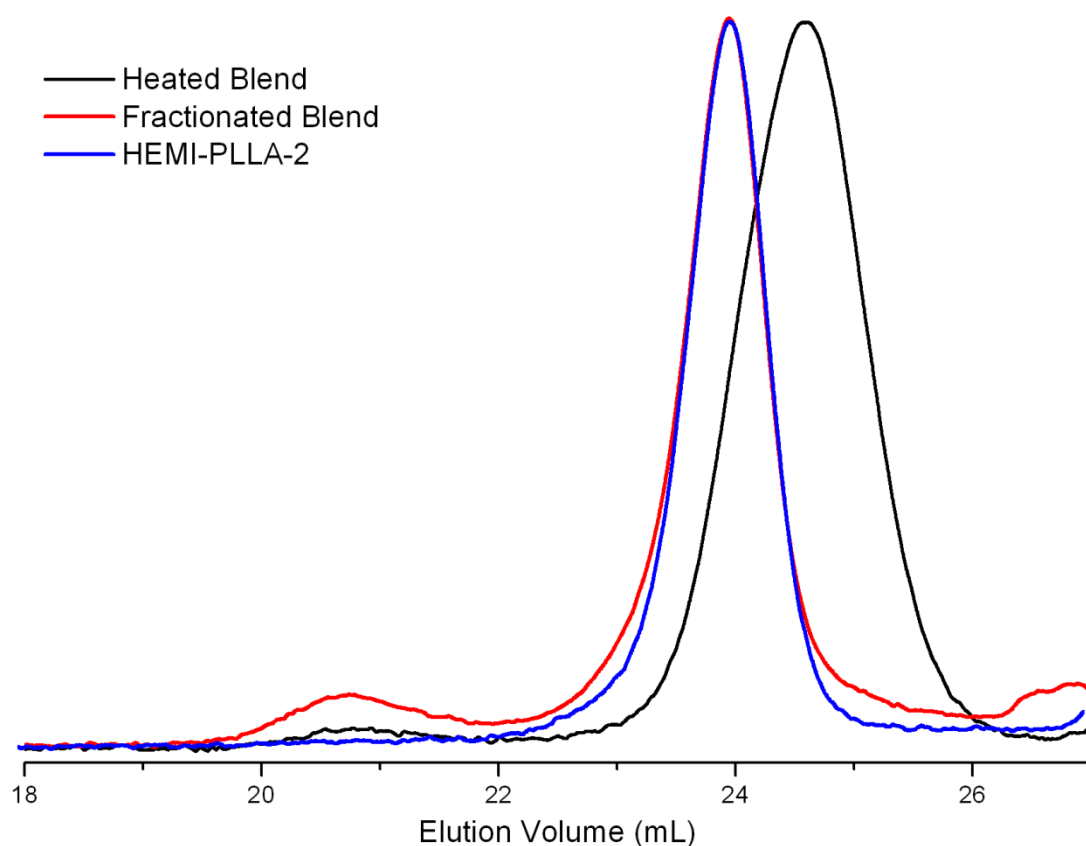
Figure A.13. SEC elution curves of HEMI-PLLA-2/PI-1 heated blend (black), fraction collected by column chromatography (red), and original HEMI-PLLA-2 (blue).

A.4 Conclusions

HEMI and HEMI-PLLA when heated with PI at 190 °C do not react with PI through an ene or radical mechanism. Instead, HEMI and HEMI-PLLA react with themselves. Addition of peroxides to the blends of HEMI-PLLA and PI has very similar results to heating alone . The strongest evidence that HEMI-PLLA reacts with itself was from the collection of HMWP using prep-GPC – the HMWP were primary composed of PLLA. This self reaction of HEMI-PLLA in the presence of peroxides could be used to produce crosslinked networks to give a renewable thermoset.

A.5 References

[1] Burlett, D. J.; Lindt, J. T. *Rubber Chem. Technol.***1993**, *66*, 411–434.

[2] Smith, M. B.; March, J. *March's Advanced Organic Chemistry, 6th Ed.*; Wiley: New York, 2007; p 1103–1105.

[3] Tripathy, A. R.; Morin, J. E.; Williams, D. E.; Eyles, S. J.; Farris, R. J. *Macromolecules* **2002**, *35*, 4616–4627.

[4] Els, C.; McGill, W. J.; *Plast Rub Compos Pro* **1994**, *21*, 115–123.

[5] Magaraphan, R.; Skularriya, R.; Kohjiya, S. *J. Appl. Polym. Sci.* **2007**, *105*, 1914–1921.

[6] Carone, E. Jr; Kopcak, U.; Goncalves, M. C.; Nunes, S. P. *Polymer* **2000**, *41*, 5929–5935.

[7] Nakason, C.; Saiwaree, S.; Tatun, S.; Kaesaman, A. *Polym. Test.* **2006**, *25*, 656–667.

[8] Leigh, W. J.; Mitchell, D. S. *J. Am. Chem. Soc.* **1988**, *110*, 1311–1313.

[9] Binger, P.; Freund, A.; Wdemann, P. *Tetrahedron* **1989**, *45*, 2887–2894.

[10] Ndoni, S.; Papadakis, C. M.; Bates, F. S.; Almdal, K. *Rev. Sci. Instrum.* **1995**, *66*, 1090–1095.

[11] Hillmyer, M. A.; Bates, F. S. *Macromolecules* **1996**, *29*, 6994–7002.

[12] Schmidt, S. C.; Hillmyer, M. A. *Macromolecules* **1999**, *32*, 4794–4801.

[13] Chino, K.; Ashura, M. *Macromolecules* **2001**, *34*, 9201–9204.

[14] Miyauchi, K.; Saito, K. *Bunseki Kagaku* **2006**, *55*, 547–554.

[15] Binger, P.; Freund, A.; Wedemann, P. *Tetrahedron* **1989**, *45*, 2887–2894.

[16] Hiran, B.; Singh, D. *J. Chem. Pharm. Res.* **2011**, *3*, 840–847.

[17] *Crosslinking Peroxides and Polymer Additives*; BTB Communication 2154 [Online]; Akzo Nobel Polymer Chemicals: Chicago, IL, June, 2006.

[18] Carlson, D.; Nie, L.; Narayan, R.; Dubois, P. *J. Appl. Polym. Sci.* **1999**, *72*, 477–485.

[19] Pan, J.; Wang, Y.; Qin, S.; Zhang, B.; Luo, Y. *J. Biomed. Mater. Res., Part B: Appl. Biomater.* **2005**, *74B*, 476–480.

Appendix B

Reactions of End-functionalized Polylactide with Soybean Oil Derivatives

This appendix discusses blends of *N*-2-hydroxyethylmaleimide end-functionalized poly(L-lactide) (HEMI-PLLA) with soybean oil (SO) and its derivatives. Blends of HEMI-PLLA and SO with peroxides in the melt resulted in HEMI-PLLA forming a gel. Similar reactions in solution polymerized SO and isomerized double bonds in SO, but HEMI-PLLA and SO did not couple. Solution blends HEMI-PLLA and CS with peroxides gave HEMI-PLLA/CS coupled products and polymerized CS (polyCS) as well as the apparent polymerization of CS off the HEMI-PLLA/CS coupled product. CS was polymerized by heating in air and then blended with HEMI-PLLA. Melt blends of HEMI-PLLA reacted with the unreacted CS but not the polyCS. All the polyCS was incorporated into the melt blends, yielding materials with mechanical properties similar to blends of HEMI-PLLA and CS.

B.1 Introduction

Appendix A discussed how the attempted melt coupling of *N*-2-hydroxyethylmaleimide terminated poly(L-lactide) (HEMI-PLLA) and polyisoprene (PI) did not form HEMI-PLLA grafts off PI. In Chapter 2 we addressed the shortcomings of the HEMI-PLLA/PI melt blends by blending HEMI-PLLA with the more reactive conjugated soybean oil (CS), coupling HEMI-PLLA and CS through a Diels–Alder reaction mechanism. Though the HEMI-PLLA/CS blends give tough polylactide, limits exist in their synthesis – the requirement to synthesize CS and the maximum CS that can be incorporated into the blend (9 wt %). To address these two limitations, we investigated that ability of HEMI-PLLA to couple with soybean oil (SO) and methods to incorporate additional CS into the melt blend.

Previous work in our group demonstrated that polymerized SO (polySO) can be incorporated into melt blends of PLLA up to 15 wt %.[1] Following this result, we investigated the polymerization of CS both before blending with HEMI-PLLA and during the coupling of HEMI-PLLA. Polymerizing CS, while coupling CS and HEMI-PLLA in solution, lead to HEMI-PLLA reacting with CS and the polymerization of CS. Also with these blends we observed the possible CS polymerization off the HEMI-PLLA/CS product. Polymerization of the CS before reacting with CS resulted in complete incorporation of the polyCS (16 wt %) into the blend, but no improvement in mechanical properties were realized.

B.2 Experimental Details

B.2.1 Materials and General Methods

All chemicals were purchased from Aldrich and used without further purification unless otherwise stated. Trigonox 311 was purchased from Akzo-Nobel and used without further purification. HEMI-PLLA and CS were synthesized following the procedures discussed in Chapter 2. Soybean oil (SO) (Wesson) was purchased from a local grocery store and stored in a freezer prior to use. Toluene was dried on a home built solvent purification system by passing it through columns of activated alumina and a supported copper catalyst.

Proton nuclear magnetic resonance (^{1}H NMR) spectroscopy was performed on a Varian Inova 500 MHz spectrometer in CDCl$_3$ unless otherwise noted. Size exclusion chromatography (SEC) was performed on an Agilent 1100 high-pressure liquid chromatograph at 35 °C equipped with a PLgel (Varian) 5 μm guard column followed by three PLgel columns with varying pore sizes with HPLC grade chloroform as the mobile phase. Molecular weights and polydispersity index (PDI) were measured by a Hewlett-Packard P1047A refractometer calibrated with polystyrene standards (Polymer Laboratories).

B.2.2 Small scale melt blends

The desired amounts of HEMI-PLLA and SO were placed in small test tubes with a magnetic stir bar and heated in an oil bath set at 190 °C. A septum sealed the top of each tube through which a needle constantly fed N$_2$ to the system. The HEMI-PLLA and SO were compounded for 5 min prior to adding the peroxide by syringe. After peroxide addition, the blends were mixed for 1 h and then quenched by cooling the test tube in a 4 °C refrigerator. Control blends of HEMI-PLLA or SO alone with peroxides were synthesized using the same method. The blends were analyzed by ^{1}H NMR spectroscopy and SEC.

B.2.3 Small scale solution blends

HEMI-PLLA and CS or polyCS were massed into a 10 round bottom flask (350–400 mg total mass) with a magnetic stir bar. Solvent (3 mL) was then added to the materials – benzene for blends at 80 °C and dry toluene for blends at 100 °C – followed by the desired peroxide. Note: materials did not completely go into solution until heated. A condenser was placed on top of the flask which was placed in an oil bath set at the desired temperature. After the desired reaction time, the flask was removed to cool and the solvent was blown off with N$_2$. The product was dissolved in CH$_2$Cl$_2$ for sampling. The products were analyzed by ^{1}H NMR spectroscopy and SEC.

B.2.4 Thermal polymerization of CS

The desired mass of CS was placed in a round bottom flask (50 mL) open to air. The flask was placed in an oil bath at 190 °C to heat for the desired time period after which the flask was removed from the oil bath to cool. The product was analyzed by ^{1}H NMR spectroscopy and SEC.

B.2.5 Melt blends in DACA mixer

All larger scale blends (4 g) were made in a twin screw batch mixer (DACA Instruments) at 190 °C and 100 RPM screw speed. Prior to mixing, HEMI-PLLA was dried overnight at 60 °C to remove moisture. To the 190 °C mixer, the matrix polymer was added first and allowed to mix for 5 min prior to the addition of polyCS, allowing for complete melting of the polymer. PolyCS was added drop wise to the mixer at the desired ratio (total blend mass of 4 g) over 1 min of mixing. After the polymer and polyCS were compounded for 10 minutes, the blend was collected from the mixer. The blends were cooled in liquid nitrogen upon being removed from the mixer and were stored in a -20 °C freezer until the samples could be further processed.

B.2.6 Preparatory gel permeation chromatography fractionation of blends

Preparatory gel permeation chromatography (prep-GPC) was performed on select blends of HEMI-PLLA and PI to fractionate the high molecular weight reaction products from the two homopolymers. Samples were run on the same Agilent system discussed previously with a 6 mL/min flow rate of $CHCl_3$ as the mobile phase passing through a guard column (PLgel Prep Guard, Agilent) and two preparatory columns (PLgel 10 μm Mixed-D, Agilent). Samples were dissolved in $CHCl_3$ at 40–80 mg/mL concentration and their passage through the system was monitored by the UV-vis detector recording at the 254 nm wavelength. Two or more runs of each blend were separated by taking fractions each minute as the polymer passed through the detector. The fractions of different runs for the same time off the column were combined and concentrated by rotoevaporation. The solvent was blown off with N_2 and the sample was dried under vacuum. The recovered products were analyzed by ^{1}H NMR spectroscopy and analytical SEC.

B.2.7 Melt blend mechanical analysis

Blends were analyzed by SEC and ^{1}H NMR spectroscopy. In addition, the blends were compression molded at 190 °C into "dog bone" tensile bars (gap dimensions, 15 mm by 3 mm by 0.4 mm) and cooled to room temperature in the press. It should be noted that though the bar dimensions do not follow any testing standard, literature values for the mechanical properties of PLLA were obtained.[2] A minimum of 3 bars were tested for each blend on a Rheometrics Instruments MINIMAT tensile tester at a cross head speed of 10 mm/min.

Scanning electron microscopy images for particle analysis were taken on a JEOL 6500 microscope. Samples were taken from the middle section of a piece of extrudate from the mixer. Prior to imaging, the surface of each sample was polished by cryo-microtomy (Reichert Ultracut S) with a glass knife at -120 °C to provide a smooth surface for image analysis. The microtomed surfaces were coated with 5-10 nm of Pt via sputtering and imaged at a 5.0 kV acceleration voltage. Microtomy of the samples resulted in the CS being pulled from the matrix, creating dark holes that were used for particle analysis.

B.3 Results and Discussion

B.3.1 Blends of HEMI-PLLA and SO with peroxides

Blends of HEMI-PLLA with soybean oil (SO) and its derivatives were investigated to see if conjugation was required for coupling. A variety of HEMI-PLLA molecules (Table B.1) were used in the blends with 20 wt % HEMI-PLLA given in Table B.2. Two peroxides were investigated – dicumyl peroxide (DCP) and Trigonox 311 heated at 150 °C and 190 °C, respectively. All blends after mixing for 1 h gave materials with gel fractions and consequently the sol fractions were extracted in CH_2Cl_2 for ^{1}H NMR spectroscopic analysis.

Table B.1. HEMI-PLLA used in blends of SO and its derivatives.

HEMI-PLLA	M_n[a] (kg/mol)	PDI[b]
HEMI-PLLA-1	1.1	1.24
HEMI-PLLA-20	20	1.05
HEMI-PLLA-27	27	1.25
HEMI-PLLA-67	67	1.24

[a]Number average molecular weight, determined by ^{1}H NMR spectroscopy. [b]Found from SEC with polystyrene standards.

Table B.2. Melt blends of HEMI-PLLA (20 wt %) and SO with peroxides for 1 h.

HEMI-PLLA	Peroxide[a]	[SO]/ [HEMI][b]	% wt. peroxide (%)	X_{BA}[c] (%)	% wt. PLLA in sol[d] (%)
HEMI-PLLA-1	DCP	4.4	17	47	5
HEMI-PLLA-1	DCP	4.4	9	27	6
HEMI-PLLA-20	DCP	92	10	20	21
HEMI-PLLA-1	Trigonox 311	4.4	9	2	15
HEMI-PLLA-1	Trigonox 311	4.6	17	2	14

[a]DCP = dicumyl peroxide, DCP blends were run at 150 °C and Trigonox 311 blends were run at 190 °C. [b]Ratio of SO molecules (M_n = 872 g/mol) to HEMI end-groups. [c]Conversion of bis-allylic protons in SO, calculated from ^{1}H NMR spectroscopy. [d]All samples had a significant gel fraction, % wt. PLLA was calculated from ^{1}H NMR spectra of the sol fractions.

The conversion of the bis-allylic protons in SO (X_{BA}) was used as a metric to measure the degree that SO reacted (Table B.2) as the bis-allylic protons should be the most reactive in SO.[3,4,5] In blends with DCP, a significant fraction of the SO reacted as X_{BA} was greater than 20% for all DCP blends. Conversely, the Trigonox 311 blends had considerably less of the SO react as evidenced by low X_{BA} values. At their respective blend temperatures, the half lives ($t_{1/2}$) of DCP and Trigonox 311 are 19 and 25 min respectively.[6] The difference in $t_{1/2}$ could possibly result in the different behaviors observed in the X_{BA} values.

The wt % of PLLA in the sol fraction was used to infer the composition of the gel fraction (Table B.2). HEMI-PLLA-1/SO blends with DCP lost significant HEMI-PLLA to the gel fraction, suggesting that the gel was comprised of crosslinked HEMI-PLLA. The HEMI-PLLA-20/DCP blend sol fraction had the same composition as the initial blend, suggesting that the gel fraction may contain HEMI-PLLA and SO at the same composition as in the initial blend. The HEMI-PLLA-1 blends with Trigonox 311 retained more of the HEMI-PLLA in the sol fraction as compared to the HEMI-PLLA-1/DCP blends, which may be due to the different $t_{1/2}$ value of the peroxides at their respective blend temperatures.

The sol fractions of the HEMI-PLLA/DCP blends were also characterized by SEC. Control blends of SO and DCP at 9 and 17 wt % DCP were synthesized to compare to the blends of HEMI-PLLA/SO/DCP. The SEC elution curve of the blend of HEMI-PLLA-1/SO with 17 wt % DCP (Figure B.1) indicates the formation of high molecular weight products (HMWP) as product eluted at volumes lower than the original material. Comparison of the ternary blend to the control blend of SO with 17 wt % DCP (polySO-17), indicates that most of the HMWP are due SO polymerizing as both traces follow each other closely. The HMWP of the ternary blend does extend to lower elution volumes than the polySO-17 which may be due to a reaction of HEMI-PLLA-1 with itself or SO. Similar results are observed with the HEMI-PLLA-20/SO blend with 10 wt % DCP (Figure B.2) as HMWP are observed at elution volumes less than both the HEMI-PLLA-20 and SO controls.
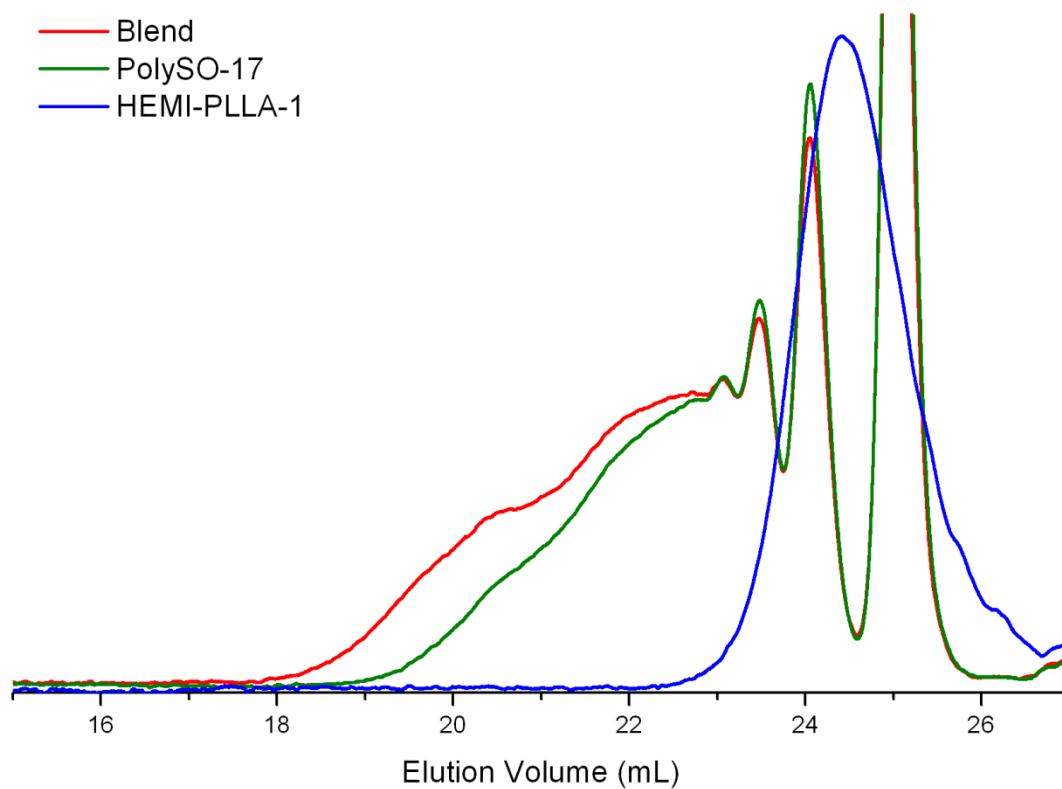
Figure B.1. SEC elution curve of HEMI-PLLA-1 blend with SO and DCP (17 wt%). SEC elution curves for HEMI-PLLA-1/SO/DCP blend (red), SO/DCP (polySO-17, 17 wt% DCP) blend (green), and original HEMI-PLLA-1 (blue). SO/DCP blend was synthesized following the HEMI-PLLA-1/SO/DCP blend protocols.
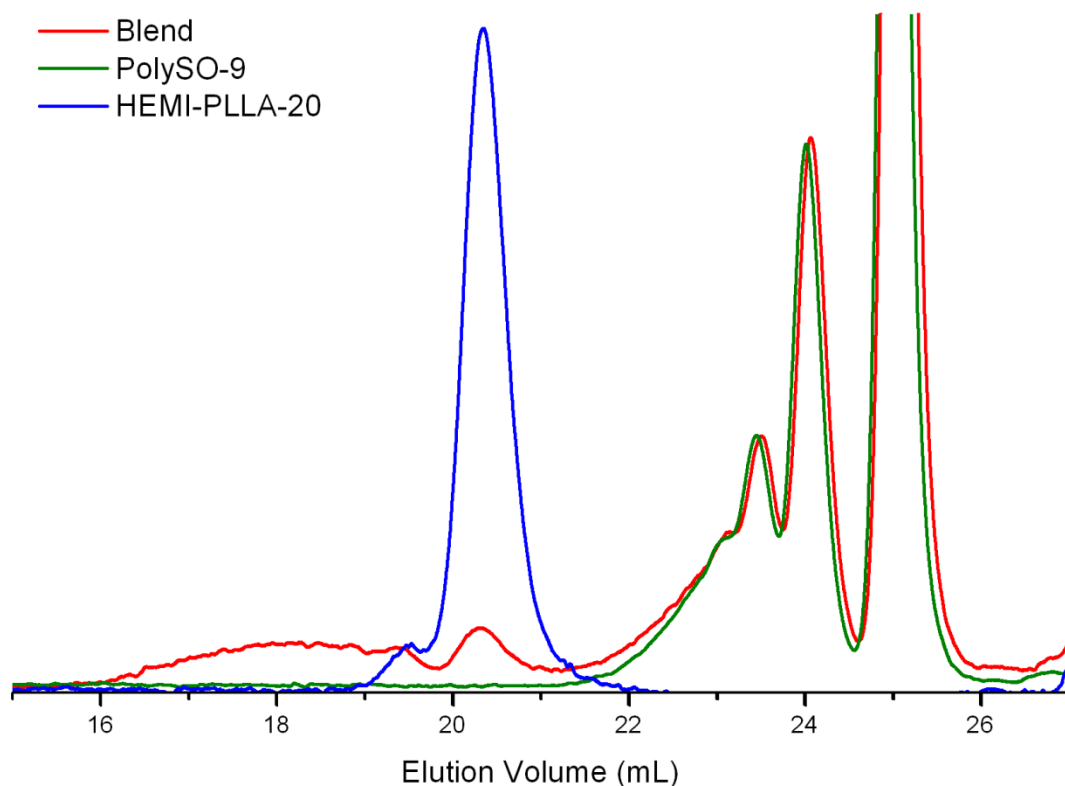
Figure B.2. SEC elution curve of HEMI-PLLA-20 blend with SO and DCP (9 wt%). SEC elution curves for HEMI-PLLA-20/SO/DCP blend (red), SO/DCP (polySO-9, 9 wt% DCP) blend (green), and original HEMI-PLLA-20 (blue). SO/DCP blend was synthesized following the HEMI-PLLA-20/SO/DCP blend protocols.

The ^{1}H NMR spectrum of the sol fraction of the blends with DCP (Figure B.3) had peaks in the 6.4–5.5 ppm region that are consistent with conjugated diene protons. These peaks are not present in the original SO spectrum, indicating that they are formed due to the reaction with DCP. Radical reactions with SO are known to undergo hydrogen abstraction of a bis-allylic hydrogen and subsequent rearrangement to give a conjugated diene as depicted in Figure B.3.[4,7] The formation of conjugated dienes is known to prelude the polymerization of SO, but the conjugated dienes could also react with HEMI-PLLA to form the HMWP seen.[8] However, peaks consistent with HEMI-PLLA undergoing a Diels–Alder reaction with the conjugated diene were not observed. Likely, HEMI-PLLA reacts with itself instead of reacting with the available conjugated dienes.
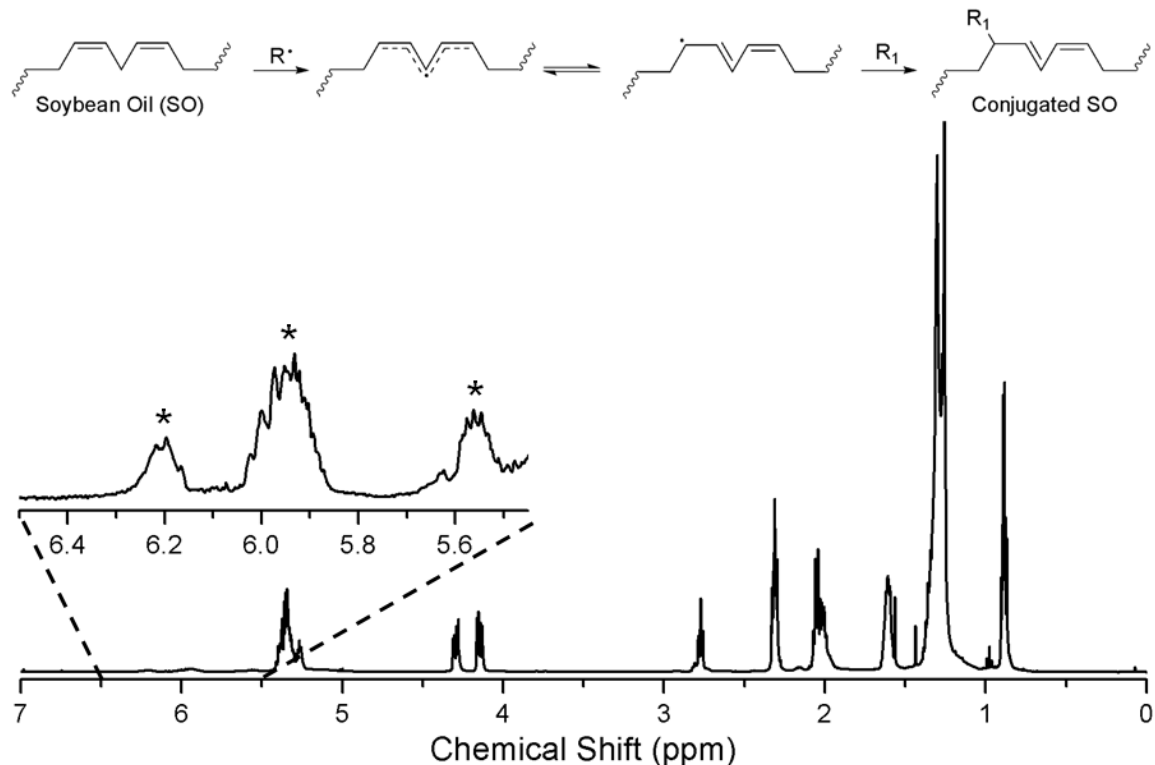
Figure B.3. ^{1}H NMR spectrum of SO heated with DCP and radical conjugation reaction scheme. Abstraction of a hydrogen from SO allows for the isomerization and subsequent conjugation of SO. Asterisks indicate peaks in ^{1}H NMR spectrum associated with the conjugated olefinic protons. See Figure 2.7 for detailed SO peak assignments.

B.3.2 Blends of HEMI-PLLA and CS with peroxides

With the melt blends discussed in Chapter 2, a limiting condition was the amount of CS that could be incorporated into the blend due to the differences in viscosity between molten PLLA and CS at 190 °C. We hypothesized that by including more rubbery minor phase (polyCS) into the HEMI-PLLA, the mechanical properties possibly could improve. To this end, we investigated the ability of HEMI-PLLA to couple with CS while simultaneously polymerizing CS via a free radical mechanism.

One set of reaction conditions investigated was the solution blend of HEMI-PLLA and CS in benzene with benzoyl peroxide (BP) as the radical generating species (Table B.3). Blends were heated for 18 h at 80 °C with varying concentrations of BP and two different HEMI-PLLA polymers. Evidence of reaction was observed by ^{1}H NMR

spectroscopy, allowing for the calculation of the conversions of the HEMI end group (X_{HEMI}), the *E,Z* isomers of CS (X_{EZ}), and the *E,E* isomers of CS (X_{EE}). A control blend of HEMI-PLLA-1 and CS heated without BP resulted in high X_{HEMI} and X_{EE} values, consistent with the Diels–Alder coupling discussed in Chapter 2. Upon addition of BP to the HEMI-PLLA-1/CS blend, X_{HEMI}, X_{EE}, and X_{EZ} increased compared to the control, suggesting that additional reactions occurred. Most notably were the X_{EZ} values increasing from 8% to 100%. Presumably the observed increased conversions were due to BP initiated reactions.

Table B.3. Composition and conversion of HEMI-PLLA blends with CS and BP at 80 °C.

HEMI-PLLA	[CS]/[HEMI]	wt % BP (%)	X_{HEMI}[a] (%)	X_{EZ}[b] (%)	X_{EE}[c] (%)
HEMI-PLLA-1	0.9	0	83	8	94
HEMI-PLLA-1	0.9	10	80	100	100
HEMI-PLLA-1	0.9	17	99	100	100
HEMI-PLLA-27	88	9	8	85	86
HEMI-PLLA-27	86	17	18	89	90

[a]Conversion of HEMI end-groups of HEMI-PLLA, found from ^{1}H NMR spectroscopy. [b]Conversion of *E,Z* isomers of CS, found by ^{1}H NMR spectroscopy. [c]Conversion of *E,E* isomers of CS, found by ^{1}H NMR spectroscopy.

Interestingly, the X_{HEMI} values for the HEMI-PLLA-27/CS blends were significantly lower that the HEMI-PLLA-1 blends (Table B.3), while the CS conversion values were similar to those for the HEMI-PLLA-1 blends. The different X_{HEMI} behavior suggests that the Diels–Alder reaction rate in the HEMI-PLLA-27 blends was slower than that of the HEMI-PLLA-1 blends. The slower reaction was probably due to the lower concentration of HEMI end groups in the HEMI-PLLA-27 blends and the competition with the radical polymerization reaction of CS. Since the Diels–Alder coupling reaction was significantly slowed in the HEMI-PLLA-27 blends, the majority of the CS diene conversion is due to polymerization reactions.

SEC elution curves of the HEMI-PLLA-27/CS blends without BP (Figure B.4) do not differ greatly from a mixture of HEMI-PLLA-27 and CS blended with BP, suggesting

that CS polymerizes and does not couple significantly with HEMI-PLLA-27. Conversely, SEC elution curves of the HEMI-PLLA-1/CS reaction products (Figure B.5) confirm the formation of HMWP due to coupling of HEMI-PLLA-1 and CS as the traces shift to lower elution volume compared to both the HEMI-PLLA and CS control blends with BP. Interestingly, the trace for the HEMI-PLLA-1/CS blend with 10 wt % BP starts at a lower elution volume than the HEMI-PLLA-1/CS blend without BP. The increase in the HMWP weight indicates that additional reactions occur − the HEMI-PLLA-1/CS blend with 17 wt % BP gives similar results. Two types of reactions could have occurred: radical polymerization of CS off CS coupled to HEMI-PLLA (PLLA-CS) and the radical coupling of PLLA-CS.
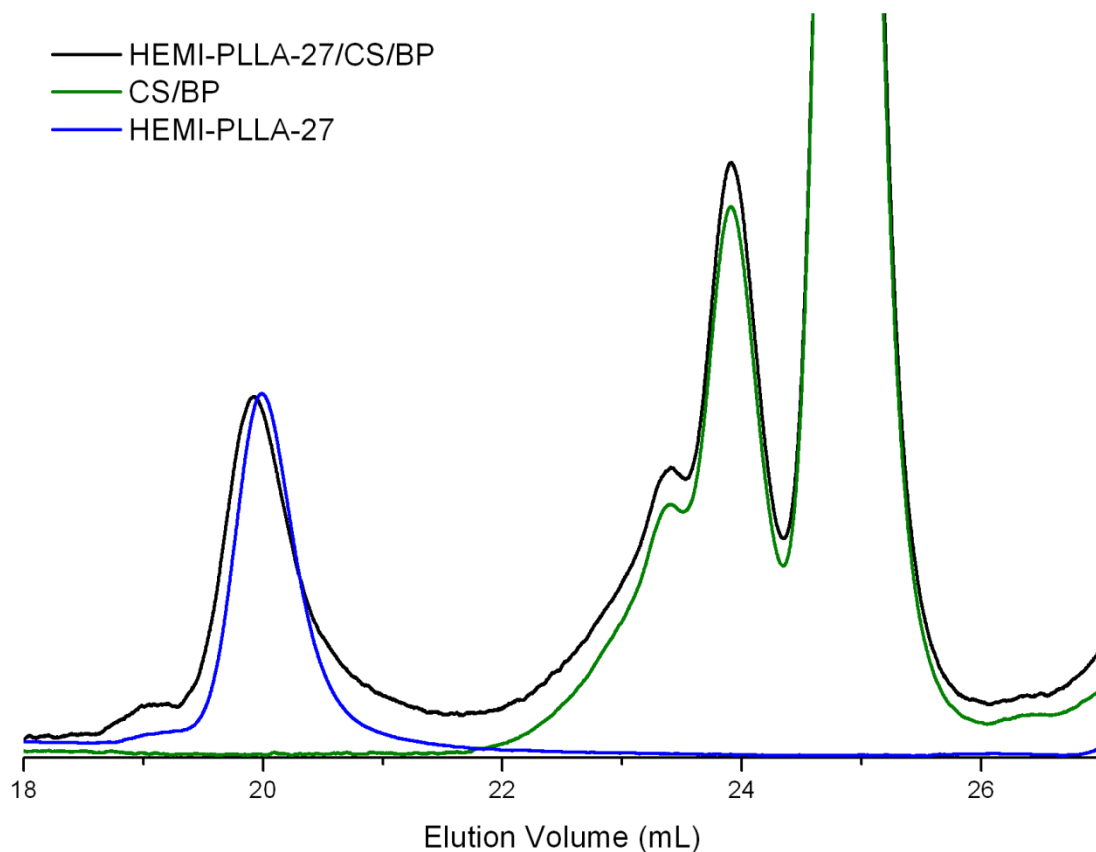
Figure B.4. SEC elution curves of HEMI-PLLA-27 blends with CS and 9 wt % BP at 80 °C in benzene. Elution curve of HEMI-PLLA-27/CS/BP blend (black) is compared against a CS/BP blend (green, 10 wt% BP), and the original HEMI-PLLA-27 (blue).
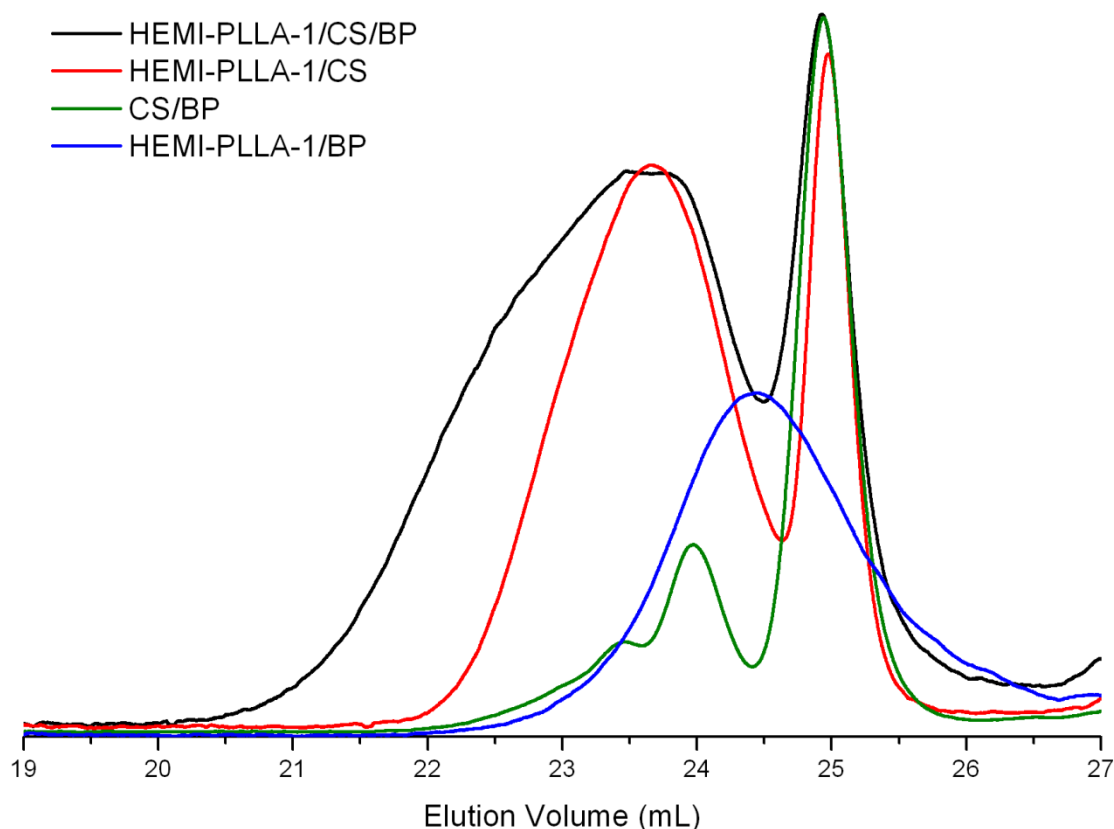
Figure B.5. SEC elution curves of HEMI-PLLA-1 blends with CS and BP (10 wt% BP) at 80 °C in benzene. Elution curve of HEMI-PLLA-1/CS/BP blend (black) is compared against a HEMI-PLLA-1/CS blend without BP (red), a CS/BP blend (green, 10 wt% BP), and a HEMI-PLLA-1/BP blend (blue, 10 wt% BP).

We used prep-GPC to analyze the HMWP formed in the HEMI-PLLA-1/CS/BP blends by fractionating the HMWP from the lower molecular weight material (Figure B.6). ^{1}H NMR spectroscopic analysis of the fraction shown in Figure B.6 indicated that the ratio of CS to PLLA increased by a factor of 2.4 as compared to the original composition fed to the reactor. The increase is consistent with CS polymerizing off HEMI-PLLA as the free CS was excluded from the fraction. If instead the PLLA-CS coupled to each other to form the HMWP, the ratio of CS to HEMI-PLLA would be less than the original composition fed to the reactor. Since the prep-GPC fraction does include the region that contains polyCS, some of the CS present in the fraction may be of the polyCS form instead of coupled to PLLA.
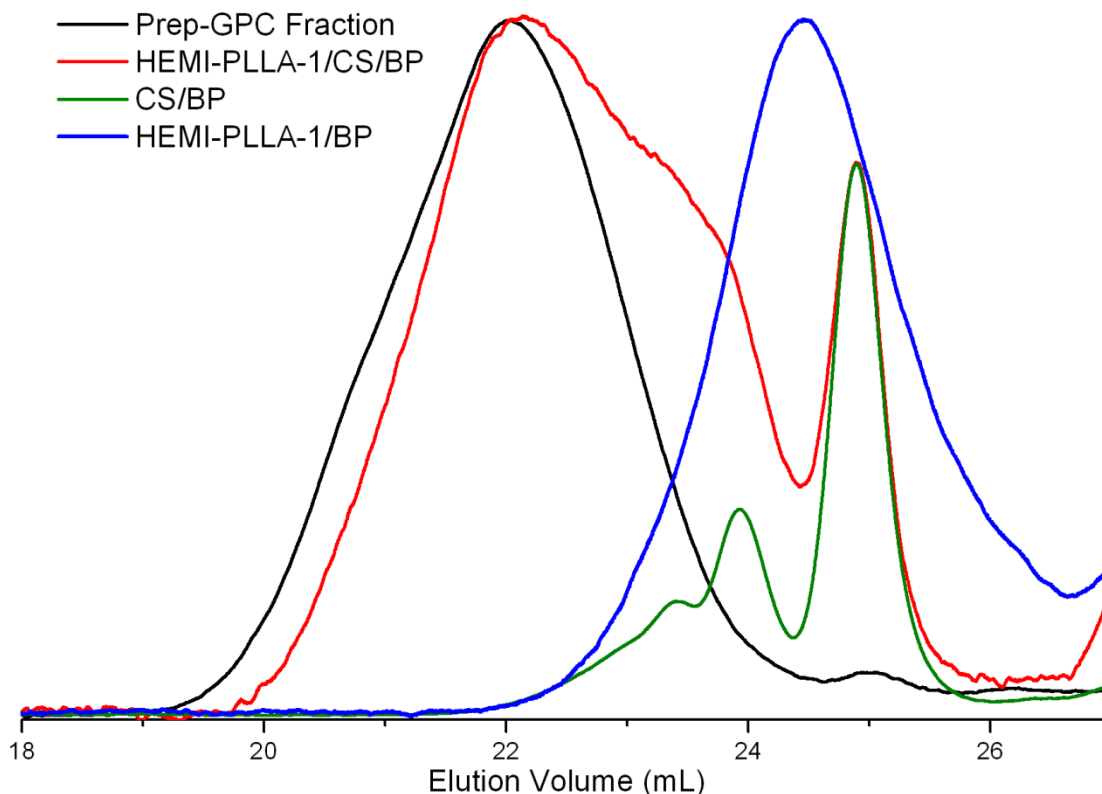
Figure B.6. SEC elution curve of prep-GPC fraction of HEMI-PLLA-1/CS/BP blend (17 wt% BP). Prep-GPC fraction elution curve (black) is give as well as original HEMI-PLLA-1/CS/BP (17 wt% BP) blend (red), CS/BP (green, 17 wt% BP), and HEMI-PLLA-1/BP (blue, 17 wt% BP) elution curves for comparison.

In an attempt to recreate the simultaneous polymerization and coupling of CS to HEMI-PLLA in the melt, we synthesized a 15 wt % CS and HEMI-PLLA-67 blend with Trigonox 311 as the peroxide initiator in the DACA mixer. Blends with 1 and 3 wt % Trigonox were mixed at 190 °C for 20 min and generated materials with significant gel fractions, likely due to HEMI-PLLA reacting with itself through a radical reaction mechanism. These results differ from the solution reactions as soluble compound were formed in the solution blends. Likely, the HEMI-PLLA self-coupling competes with the HEMI-PLLA-CS coupling reaction in both systems. In the melt blending scenario, the HEMI-PLLA self-coupling is the faster reaction. In solution, the HEMI-PLLA self-coupling is slow enough that CS can react with HEMI-PLLA and polymerize off it.

B.3.3 Polymerization of CS

CS was polymerized thermally in a round bottom flask open to air at 190 °C to give polyCS (Table B.4). The M_w of the polyCS obtained by this process appears to be dependent upon the free surface of the oil in contact with the air as seen in previous literature.[1] Using the same size round bottom flask, the CS polymerizes to two different molecular weights depending on the amount of CS added to the flask. The smaller mass of CS gives a larger free surface area to volume of CS ratio and consequently more O_2 is available to polymerize the material, leading to the higher M_w observed (7.3 versus 2.5 kg/mol). In all polyCS, a significant fraction of the conjugated dienes reacted as evidenced by the high values of X_{EE}. SEC elution curves of the polyCS products (Figure B.7) indicate that single CS molecules remain as demonstrated by the continued presence of the CS peak at 25 min while HMWP form from polyCS.

Table B.4. Synthesis parameters and molecular weights of polymerized CS (polyCS).

Sample[a]	Mass of CS[b] (g)	Reaction Time (h)	X_{EE}[c] (%)	M_w[d] (kg/mol)	PDI[d]
polyCS-7.3	0.5	3	91	7.3	3.06
polyCS-2.5	1.5	3	49	2.5	1.48
polyCS-3.0	1.5	4	55	3.0	1.62
polyCS-17	1.1	5	90	17	5.4

[a]Sample code is polyCS-## where ## is the weight average molecular weight (M_w) of the polyCS. [b]Mass of CS polymerized in a 50 mL round bottom flask (Note: polyCS-3.0 was polymerized in a 25 mL round bottom flask.). [c]Found from ^{1}H NMR spectroscopy, X_{EZ} was similar to X_{EE} for all blends. [d]Determined from SEC with polystyrene standards.
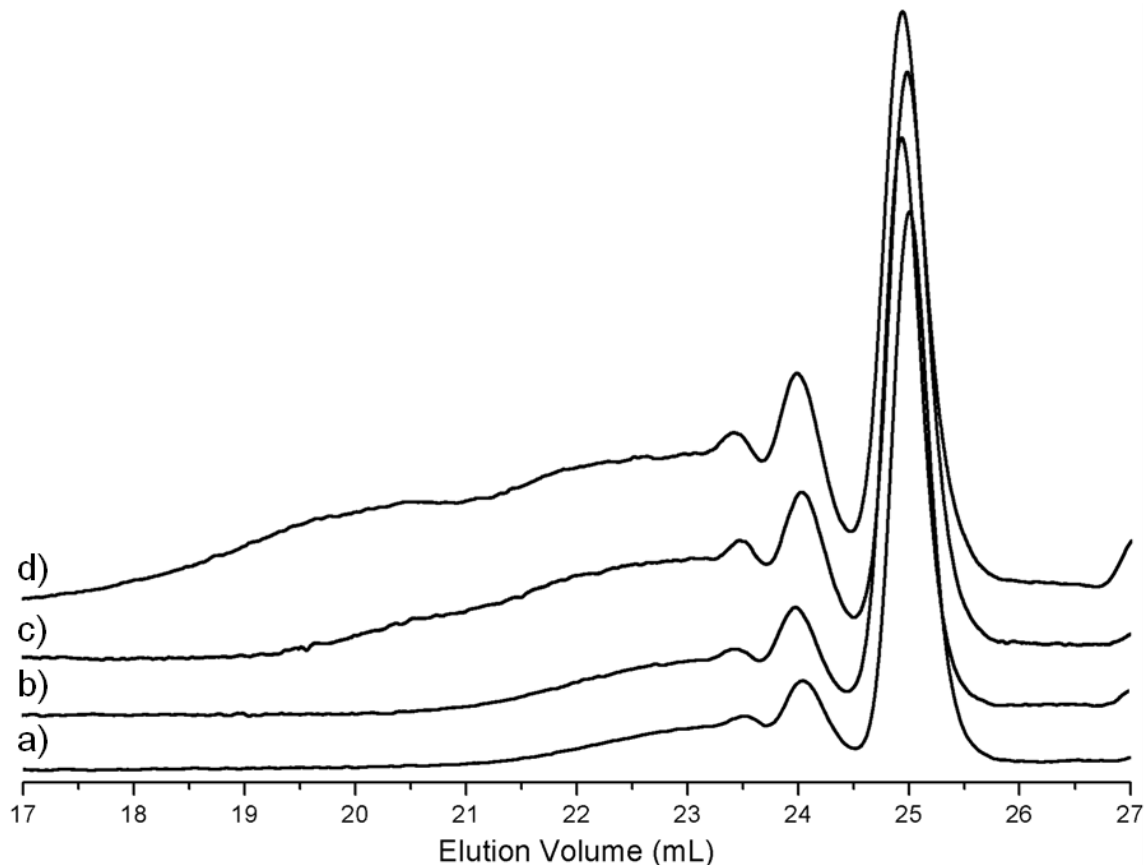
Figure B.7. SEC elution curves of (a) polyCS-2.5, (b) polyCS-3.0, (c) polyCS-7.3, and (d) polyCS-17.

^{1}H NMR spectroscopic analysis of the polyCS confirm the reaction of CS (Figure B.8) as the intensity of the peaks associated with the conjugated dienes decreases relative to the other peaks belonging to CS while new peaks form. Tentative peak assignments are given that belong to two possible products: the Diels–Alder adduct of two conjugated fatty acids and the oxygen radical reaction product. Both products have been observed in the polymerization of SO, where conjugated dienes form during the heating process.[4,8] Of note, peaks at chemical shifts corresponding to conjugated dienes still exist, indicating the possibility that HEMI-PLLA could react with these polyCS products. Whether the conjugated dienes are present on the polyCS or only the unreacted CS is unclear from the data obtained.
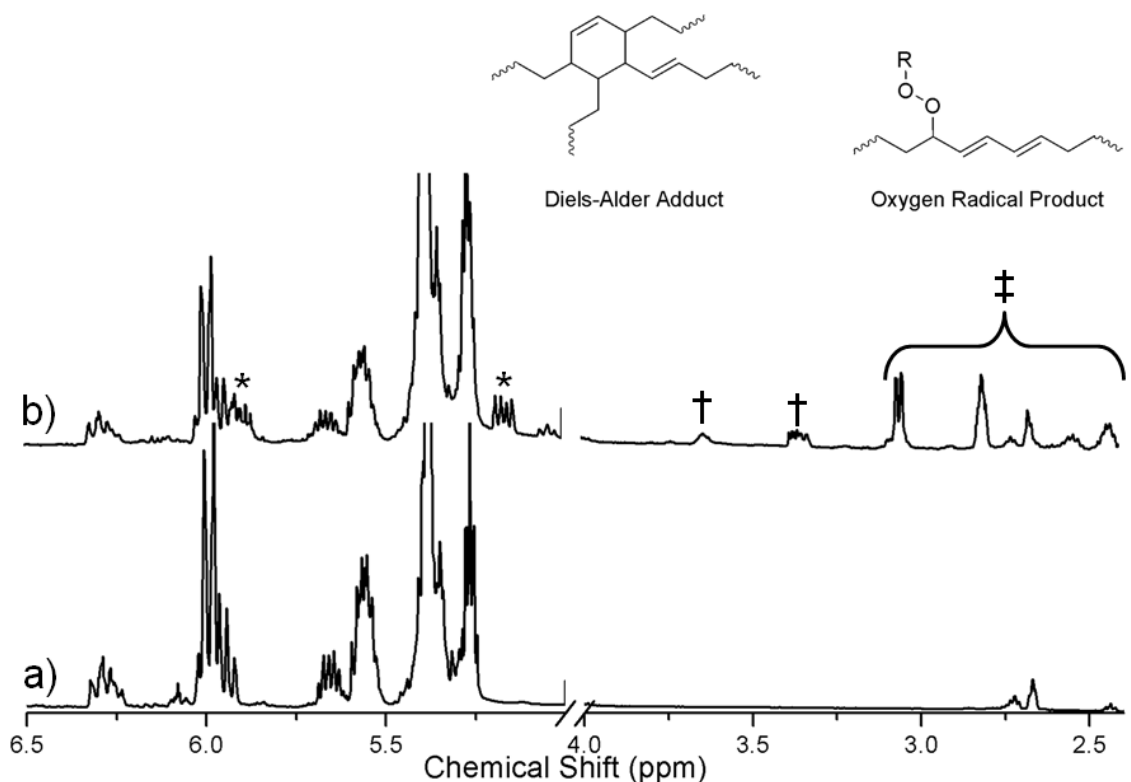
Figure B.8. ^{1}H NMR spectra of (a) CS and (b) polyCS-3.0 and structures of the probable major reaction products. Peaks are assigned as (*) vinyl protons, (†) oxygen adjacent protons, and (‡) allylic protons of the two major types of products – Diels–Alder adducts and oxygen radical products.

B.3.4 Blends of HEMI-PLLA and polyCS

The polyCS discussed above (Table B.4) were blended with various HEMI-PLLAs under several reaction conditions (Table B.5). Two of the blends were synthesized by heating overnight in a solution of toluene, resulting in high conversions of the remaining *E,E* isomers in the polyCS (X_{CS}). The X_{HEMI} values follow closely those expected for HEMI-PLLA reacting with the remaining *E,E* isomers at the ratios given in Table B.5. SEC analysis of the solution blends (not shown) is consistent with HEMI-PLLA reacting with monomeric CS and not the polyCS. All the conjugated dienes appear to be consumed on the polyCS during its synthesis.

Table B.5. Composition and conversion of HEMI-PLLA/polyCS blends.

HEMI-PLLA-1	polyCS	Solvent[a]	[C=C-C=C]/ [HEMI][b]	X_{CS}[c] (%)	X_{HEMI}[d] (%)
HEMI-PLLA-1	polyCS-3.0	Toluene	0.7	89	60
HEMI-PLLA-27	polyCS-7.3	Toluene	0.2	100	26
HEMI-PLLA-67	polyCS-17	None	1.6	33	17

[a]Reactions performed in toluene were run at 100 °C overnight (ca. 18 h), while reactions performed in bulk were run at 190 °C for 10 min. [b]Ratio of *E,E* conjugated dienes in polyCS to HEMI end groups. [c]Conversion of the *E,E* conjugated dienes in polyCS, determined by ^{1}H NMR spectroscopy. [d]Conversion of HEMI end groups, determined by ^{1}H NMR spectroscopy.

     A melt blend of HEMI-PLLA-67 and polyCS-17 was synthesized in the DACA mixer at 190 °C for 10 min of compounding. Both the *E,E* isomers and HEMI end groups reacted as confirmed by ^{1}H NMR spectroscopy, suggesting that either polyCS or CS reacted to form compatibilizers. The SEC trace of the blend (Figure B.9) compared to the original HEMI-PLLA-67 shows an increase in the molecular weight of the blend, consistent with a coupling reaction and formation of compatibilizer. However, the HMWP production of the HEMI-PLLA-67/polyCS-17 blend is less than that of the HEMI-PLLA-67/CS blend. Notably, the shoulder at 18 min in the HEMI-PLLA-67/CS blend is less pronounced in the HEMI-PLLA-67/polyCS-17 blend. With fewer reactive CS molecules in the polyCS, HMWP formation is reduced. Compatibilizer formed in the HEMI-PLLA-67/polyCS-17 blend, but it is from HEMI-PLLA-67 and the remaining CS coupling and not HEMI-PLLA-67 and polyCS-17 coupling.
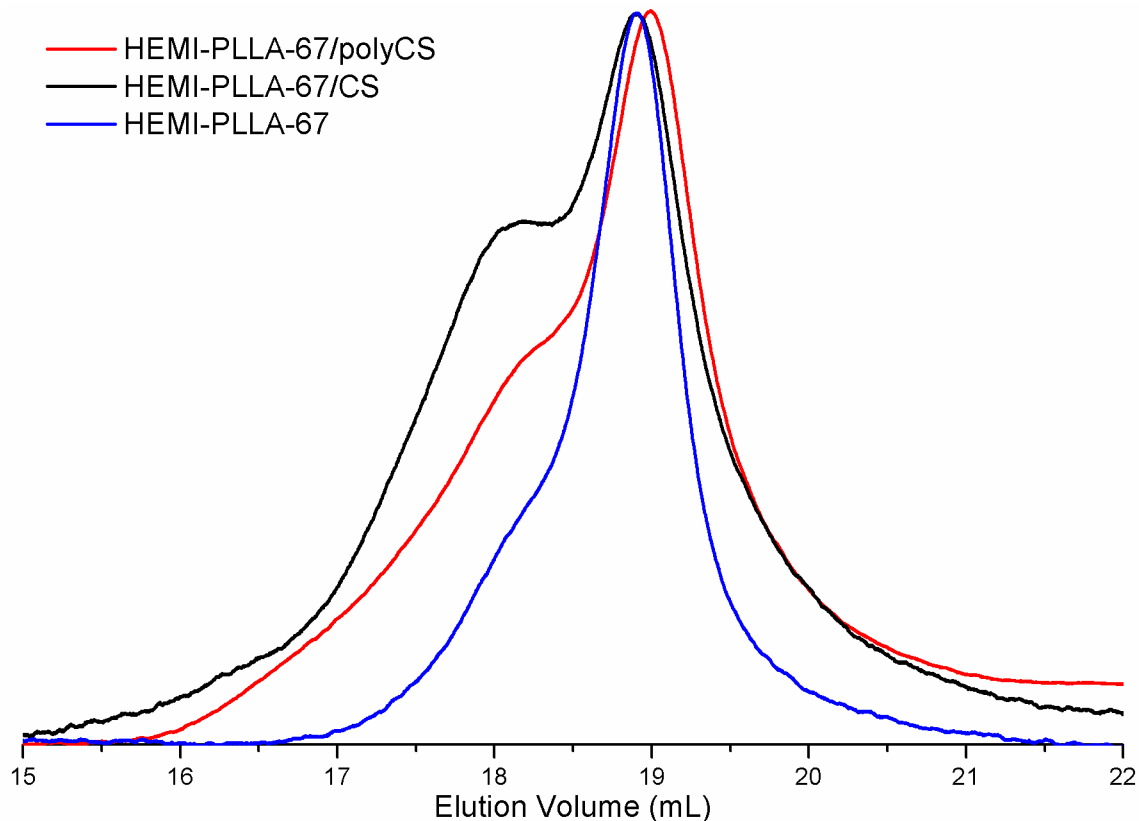
Figure B.9. SEC elution curves of HEMI-PLLA-67 blend with 15 wt % polyCS-17 (red), HEMI-PLLA-67 blend with 15 wt % CS (black), and HEMI-PLLA-67. Blends were synthesized in DACA mixer at 190 °C.

Though polyCS and HEMI-PLLA do not react – polymerization of CS consumes the reactive conjugated dienes – compatibilizer still forms. As discussed in Chapter 2, the formation of a HEMI-PLLA/CS compatibilizer leads to a compatibilized blend that can give mechanical properties superior to those of a binary blend. To determine whether the compatibilized HEMI-PLLA/polyCS blend improve mechanical properties, we mechanically tested the blended material (Table B.6). As mentioned earlier, one of the goals with polymerizing CS is to incorporate more CS into the blend. ^{1}H NMR spectroscopic analysis of the material confirmed that all the polyCS incorporates into the blend (16 wt %) as compared to similar blends with CS (7 wt %). The mechanical properties of the material (Table B.6), however, are not that different from both the reactive HEMI-PLLA-67/CS blend and the unreactive PLLA-49/CS blend as the

variation in the tensile sample was large. With the incorporation of additional rubbery component, the only significant change in mechanical properties is a decrease in the modulus of the material as compared to the CS blends.

Table B.6. Physical properties and composition of selected melt blends of HEMI-PLLA/PLLA and 15 wt % CS/polyCS.

Matrix Polymer	Minor Phase	W_{CS}[a] (%)	E[b] (GPa)	σ_b[c] (MPa)	ε_b[d] (%)
HEMI-PLLA-67	CS	7	2.4 ± 0.4	35 ± 1	48 ± 37
HEMI-PLLA-67	polyCS-17	16	1.6 ± 0.2	28 ± 1	33 ± 32
PLLA-49[e]	CS	9	2.4 ± 0.4	28 ± 4	22 ± 7

[a]Weight percent of CS or polyCS in final blend, determined by ^{1}H NMR spectroscopy. [b]Elastic modulus. [c]Stress at break. [d]Elongation at break. [e]PLLA-49 is PLLA (M_n = 49 kg/mol, PDI = 1.85) without a HEMI end group.

A representative scanning electron microscopy (SEM) image of the HEMI-PLLA/polyCS blend (Figure B.10) compared to the representative images of HEMI-PLLA/CS blends qualitatively suggests that the minor phase particle diameter of the blend is similar to that of the HEMI-PLLA/CS blend and less than that of the unreactive PLLA/CS blend. With the apparent similar droplet diameters, we would expect comparable mechanical properties as discussed in Chapter 2. The reduction of droplet diameter as compared to the unreacted blend would be expected with the formation of compatibilizer as it reduces the interfacial tension.[9,10] The increased viscosity of polyCS compared to that of CS at 190 °C could also explain the decrease in droplet diameter since the smallest diameters can be obtained when the viscosity of the minor phase matches that of the matrix phase.[1,11]
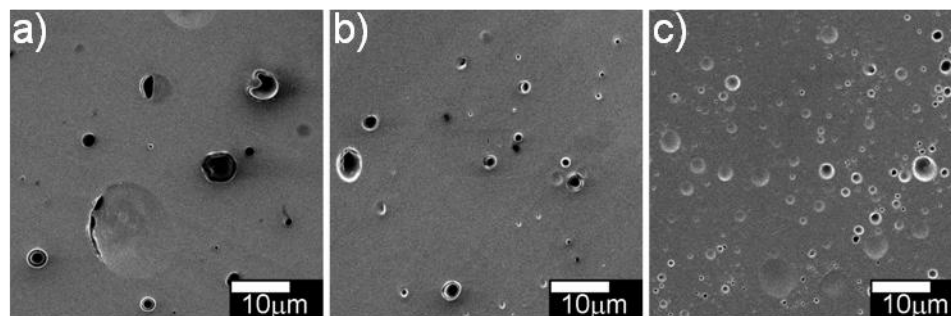
Figure B.10. Representative SEM images of (a) PLLA-49/CS, (b) HEMI-PLLA-67/CS, and (c) HEMI-PLLA-67/polyCS-17 blends with 15 wt % of the minor component.

B.4 Conclusions

Melt blends of HEMI-PLLA and SO with the addition of peroxides led to HEMI-PLLA crosslinking with itself and SO homopolymerizing. Possibly, a small amount of HEMI-PLLA could react with SO once it has been isomerized to give conjugated double bonds through a radical process. Solution blends of HEMI-PLLA and CS with BP gave products consistent with HEMI-PLLA and CS coupling through a Diels–Alder reaction followed by either CS polymerizing off PLLA-CS or PLLA-CS coupling with each other. Unfortunately, blending HEMI-PLLA and CS with peroxides in the melt resulted in significantly crosslinked HEMI-PLLA and polyCS. PolyCS was synthesized before blending by heating CS in air at 190 °C, resulting in a product with an increased molecular weight and decreased content of reactive conjugated dienes. In blends of HEMI-PLLA and polyCS the HEMI-PLLA reacted with the remaining monomeric CS in the polyCS, while being unreactive towards the polyCS. In a melt blend of HEMI-PLLA-67 and polyCS-17, all the polyCS was incorporated into the matrix, but the material properties did not improve compared to similar reactive blends with only CS. The particle diameter of the HEMI-PLLA/polyCS blend decreased compared to the unreactive PLLA/CS blend due to compatibilizer formation and the higher viscosity of polyCS. No further improvement in mechanical properties was observed, presumably due to the particle diameter being similar to that of the HEMI-PLLA/CS blend – above the optimal particle diameter.

B.5 References

[1] Robertson, M. L.; Chang, K.; Gramlich, W. M.; Hillmyer, M. A. *Macromolecules* **2010**, *43*, 1807-1814.

[2] Auras, R.; Harte, B.; Seke, S. *Macromol. Biosci.* **2004**, *4*, 835-864.

[3] Meier, M. A. R.; Metzger, J. O.; Schubert, U. S. *Chem. Soc. Rev.* **2007**, *36*, 1788-1802.

[4] Gardner, H. W. *Free Radical Bio Med* **1989**, *7*, 65-86.

[5] Asadauskas, S.; Erhan, S. Z. *J. Am. Oil Chem. Soc.* **2001**, *78*, 1029-1035.

[6] Values calculated from data in *Crosslinking Peroxides and Polymer Additives*; BTB Communication 2154 [Online]; Akzo Nobel Polymer Chemicals: Chicago, IL, June, 2006 and assuming Arrhenius relationship.

[7] Fornof, A. R.; Onah, E; Ghosh, S.; Frazier, C. E.; Sohn, S.; Wilkes, G. L.; Long, T. E. *J. Appl. Polym. Sci.* **2006**, *102*, 6790-697.

[8] Adams, H. E.; Powers, P. O. *J. Appl. Phys.* **1946**, *17*, 325-337.

[9] Macosko, C. W.; Guegan, P.; Khandpur, A. K.; Nakayama, A.; Marechal, P.; Inoue, T. *Macromolecules* **1996**, *29*, 5590-5598.

[10] Lepers, J.; Favis, B. D. *AICHE J.* **1999**, *45*, 885-895.

[11] Wu, S. *Polym. Eng. Sci.* **1987**, *27*, 335-343.

Appendix C

Other Methods to Conjugate

Polyisoprene

This appendix describes the preliminary attempts at conjugation of polyisoprene using iodine. The heating of polyisoprene with iodine led to a small amount of conjugated dienes along the polymer backbone. Charge-transfer complexes between iodine and polyisoprene were predominately formed which were unstable at ambient temperatures and subsequent reaction conditions. The instability and lack of control led us to focus on the research described in Chapter 3.

C.1 Introduction

As mentioned in Chapter 3, reports exist of polyisoprene (PI) being conjugated through a reaction with molecular iodine (I_2).[1,2,3] I_2 is believed to add across the carbon-carbon double bond to form di-iodated functionality. Subsequent elimination reactions, where two equivalents of hydrogen iodide are removed, give a conjugated diene system in place of the isolated diene. The literature reports of iodated PI (IPI) target conducting polymers. Consequently, the goals of the reports were to synthesize highly conjugated materials while for post-polymerization functionalization less conjugation is required. For our purposes, we targeted incomplete conjugation of the polymer chain, necessitating that less I_2 reacts with PI. The following appendix outlines our attempts at conjugating PI with I_2. The IPI synthesized contained conjugated dienes and appeared to undergo Diels–Alder reactions with *N*-2-hydroxyethylmaleimide terminated poly(L-lactide) (HEMI-PLLA) in solution. Unfortunately, the IPI polymers synthesized were highly unstable and hampered their implementation in post-polymerization functionalization schemes.

C.2 Experimental Details

C.2.1 General materials and methods

All chemicals were purchased from Aldrich and used without further purification unless otherwise noted. HPLC grade toluene was dried on a home built solvent column by passing it over an activated alumina column and a supported copper catalyst. HPLC grade CH_2Cl_2 was dried on an MBraun solvent purification system. HEMI-PLLA was synthesized following the procedure in Chapter 2. PI was synthesized following the anionic polymerization procedure used in Chapter 3.

^{1}H NMR spectroscopy was performed on a Varian Inova 500 MHz spectrometer in $CDCl_3$ (Cambridge) using the residual $CHCl_3$ peak as reference. Size exclusion chromatography was performed on an Agilent 1100 high-pressure liquid chromatograph at 35 °C equipped with a PLgel (Varian) 5 μm guard column followed by three PLgel columns with varying pore sizes with HPLC grade chloroform as the mobile phase. Molecular weights and polydispersity index (PDI) were measured by a Hewlett-Packard P1047A refractometer calibrated with polystyrene standards (Polymer Laboratories).

C.2.2 Iodation of PI

PI (200 mg) and I_2 (16.6 mg) were dissolved in dry toluene (4 mL) and the solution was placed in a 10 mL air-free flask. The solution was degassed by three freeze-pump-thaw cycles and the flask was backfilled with argon. The flask was placed in a 60 °C oil bath and heated for 21 h. After heating, the mixture was allowed to cool, was precipitated in 10 volume excess methanol, and the product (IPI) was dried under vacuum at room temperature over several days, giving a green-black viscous product (yield = 59%).

C.2.3 Reaction of IPI and HEMI-PLLA

IPI (50 mg) and HEMI-PLLA (100 mg) were dissolved in dry toluene (3 mL) in a 10 mL round bottom flask that was fitted with a condenser. The solution was refluxed at 110 °C for 17 h. The reaction was quenched by cooling the mixture and the cooled solution was dried by pulling vacuum overnight at room temperature. Product analyzed by SEC and ^{1}H NMR spectroscopy.

C.2.4 IPI purification

Addition of 1,8-Diazabicyclo[5.4.0]undec-7-ene (DBU)

IPI (800 mg) and DBU (310 µL) were dissolved in benzene (24 mL) and refluxed at 85 °C for 17 h. A brown precipitate formed and upon cooling it was filtered off. The soluble components were precipitated in 10 volume excess methanol and dried over night under vacuum at room temperature to give a brown polymer.

Addition of dioxane to remove charge-transfer complexes

A portion of the raw iodation reaction solution (5 mL) and dioxane (55 µL) were mixed and allowed to stir at room temperature for two days. The solution color transformed from yellow-green to having a slight yellow tint. The solution was precipitated in 10 volume excess methanol to give a product that was near colorless (slight yellow color), but gelled at ambient conditions and could not be analyzed.

C.2.5 Bromination of PI and attempted elimination

PI (1 g) was dissolved in 100 mL of a 90/10 CH_2Cl_2/THF solvent mixture at 0 °C. The solution was degassed by sparging N_2 for 30 min. The Br_2 was added as a solution of Br_2 in CH_2Cl_2 with a concentration of 0.1 mL Br_2/1 mL CH_2Cl_2 (190 µL). The mixture was allowed to stir for 1.3 h at which point it was washed twice with a concentrated Na_2SO_3/water solution. The red solution was precipitated in 10 volume excess methanol to yield a yellow rubbery material. The material was collected and dried under vacuum at room temperature overnight. The dried product was subjected to an attempted elimination with DBU – the description follows. Brominated PI (200 mg) and DBU (176 µL) were dissolved in benzene (6 mL) and the solution was degassed by sparging N_2. The solution was refluxed at 85 °C for 1 h and a red solid precipitated out over the course of the reaction. Upon cooling, the solids were filtered off and the solution was precipitated in 10 volume excess methanol. The product was collected and dried.

C.2.6 TiCl₄ conjugation attempt of PI

In a N_2 dry box, PI (400 mg) was dissolved in dry toluene (40 mL) in a 75 mL pressure vessel. $TiCl_4$ (43 µL) was added by syringe to the solution which became yellow upon addition. The flask was sealed and removed from the dry box to stir overnight (18 h) at room temperature. The contents of the flask were precipitated in 10 volume excess methanol and allowed to dry overnight under vacuum at room temperature.

C.3 Results and Discussion

C.3.1 Iodation of PI

Two PI samples with molecular weights of 1 kg/mol (PI-1) and 33 kg/mol (PI-33) were synthesized using anionic polymerization and used as the starting materials for iodation. The PI polymers were iodated at a 45 to 1 ratio of carbon-carbon double bonds (C=C) to I_2 ($[C=C]:[I_2] = 45$) for 21 h at 60 °C under air free conditions. Decreasing the $[C=C]:[I_2]$ (increasing I_2 content) from 45 to 15 under the same reaction conditions, gave polymers that gelled quickly under ambient conditions. Lowering the I_2 content used during the iodation ($[C=C]:[I_2] = 90$, 24 h, 60 °C) gave materials with undetectable levels

of conjugation. These unsuccessful conjugation attempts led us to focus on the iodation reactions at $[C=C]:[I_2] = 45$.

Reaction of PI-1 with I_2 at $[C=C]:[I_2]$ equal to 45 gave IPI (IPI-1) with conjugated double bonds. The presence of conjugated dienes in IPI-1 was confirmed by analysis of the ^{1}H NMR spectrum of the collected material (Figure C.1a and c) as peaks are present that are consistent with protons in conjugated systems. In the spectrum of the original PI-1, none of these peaks are present (6.2 and 5.8 ppm), indicating that they are a result of the reaction of PI-1 and I_2. The conjugated isomer was identified by the ^{1}H NMR spectrum to be the E1 isomer (see Figure C.1 for structure and Chapter 3 for naming convention). Using the peak belonging to the methyl end groups of PI-1 as an internal standard, the conversion of C=C bonds was estimated to be 40% with only 1.9% of the original bonds were conjugated. Consequently, conversion of 38% of the original C=C bonds is unaccounted for. Similarly, the ^{1}H NMR spectrum of IPI-33 synthesized under the same conditions as IPI-1 had peaks at chemical shifts consistent with protons in conjugated diene systems (Figure C.2a). These peaks were less defined and consequently difficult to attribute a specific conjugated isomer and calculate a total conversion.
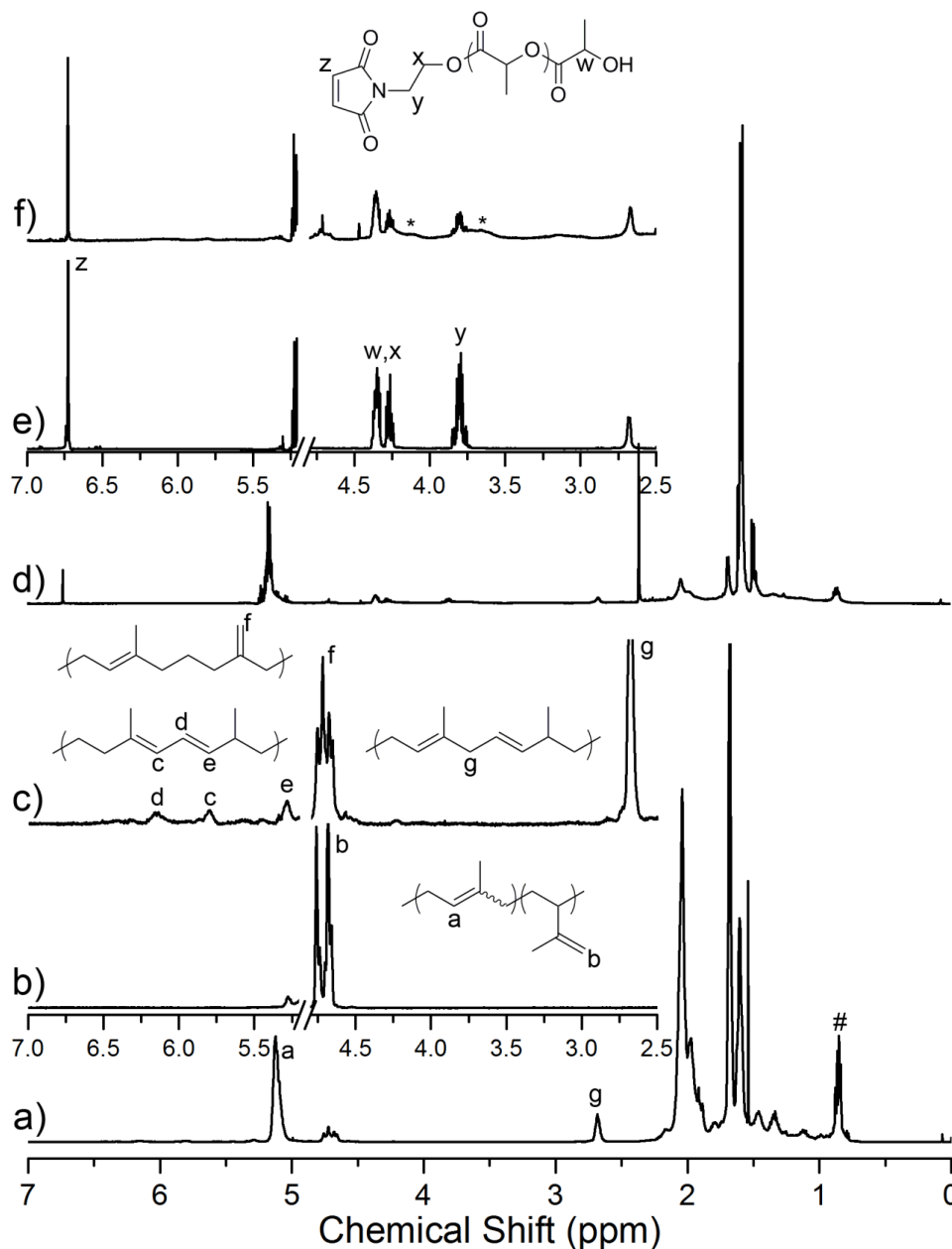
Figure C.1. ^{1}H NMR spectra and peak assignments of (a) IPI-1 and (d) reaction of IPI-1 with HEMI-PLLA-1 as well as expanded spectra for (b) PI-1, (c) IPI-1, (e) HEMI-PLLA-1, and (f) reaction products of HEMI-PLLA-1 and IPI-1. The # symbol indicates the methyl end-groups of PI used as an internal standard for conversion calculations. The asterisks (*) denote broad peaks that belong to HEMI-PLLA reaction products. Through the iodation of PI, peaks are generated that are consistent with protons in conjugated double bonds. Iodation was performed at [C=C]:[I$_2$] = 45 and 65 °C for 21 h.
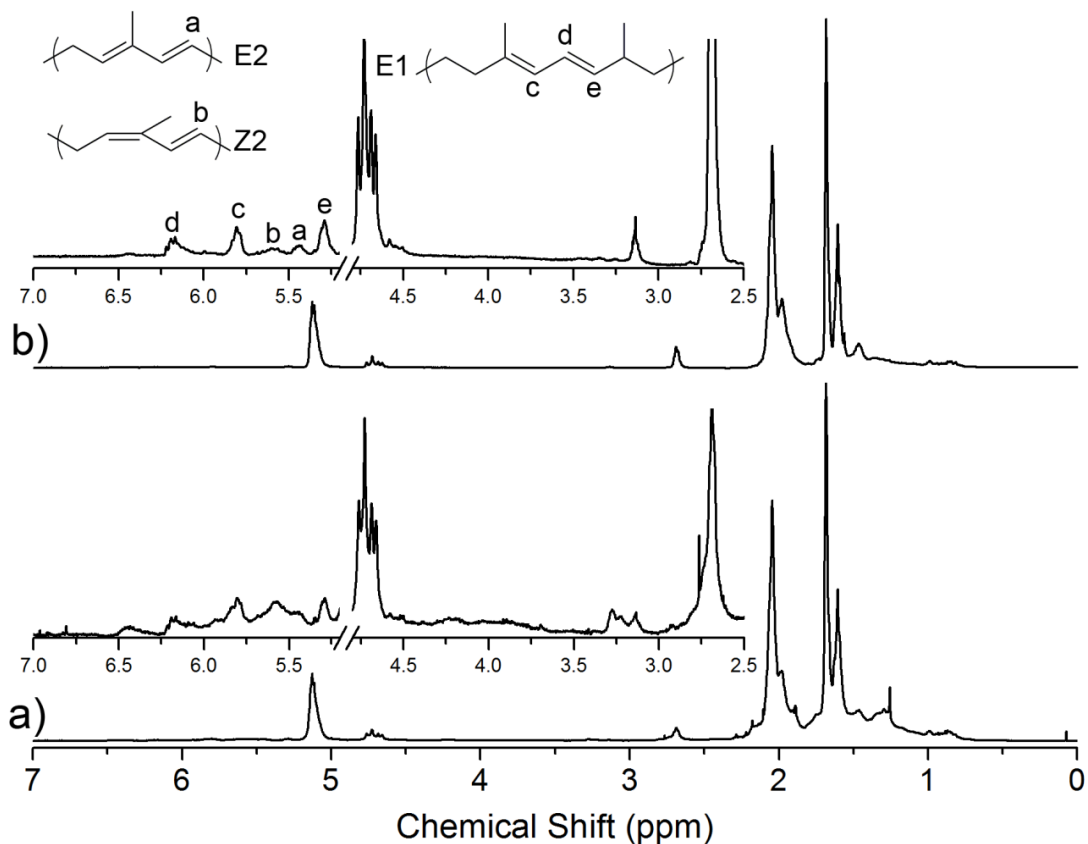
Figure C.2. ^{1}H NMR spectra with peak assignments for (a) IPI-33 as synthesized and (b) IPI-33 purified by reaction with DBU. In the IPI-33 spectrum (a) the broad peaks in the 6.5–5.2 ppm region are consistent with protons in conjugated systems. In the DBU purified IPI-33 spectrum (b) distinct peaks are present in the 6.5–5.2 ppm region that are consistent with the three conjugated diene isomers given. The reaction of IPI-33 with DBU removes some of the I$_2$-PI charge-transfer complexes.

In addition to the peaks associated with protons in conjugated systems, two other new peaks were observed in the spectra of IPI at 4.7 and 2.7 ppm that were not present in the original PI. The peaks are tentatively assigned to protons belonging to pendent vinyl groups (4.7 ppm) and bis-allylic protons (2.7 ppm). Roughly, 10 mol % of the carbon-carbon double bonds are now in a bis-allylic system. Interestingly, no peaks are seen at chemical shifts consistent with protons adjacent to carbon-iodine bonds (4.5–3.0 ppm) in IPI-1 (Figure C.1c), suggesting that no iodine is covalently bound to PI. In the IPI-33 spectrum (Figure C.2a), some peaks do exist at the expected chemical shifts of protons adjacent to bound iodine, indicating that some iodine does bind to PI.

The SEC distribution of IPI-1 is similar to that of the parent PI-1 (Figure C.3). Consequently, the number average molecular weight (M_n) calculated by SEC is the same for PI-1 and IPI-1 (1.6 kg/mol) and the polydispersity index (PDI) of IPI-1 is slightly higher (1.11 versus 1.10) than that of PI-1. The similarities in SEC traces of IPI-1 and PI-1 indicate that minimal degradation or coupling occurred during the iodation process. Iodation of PI-33 led to significant degradation and coupling. The PDI and M_n of PI-33 were 62 kg/mol and 1.04, initially. After iodation, IPI-33 had a M_n of 37 kg/mol and a PDI of 2.67. The iodation process appears to degrade higher molecular weight polymers.
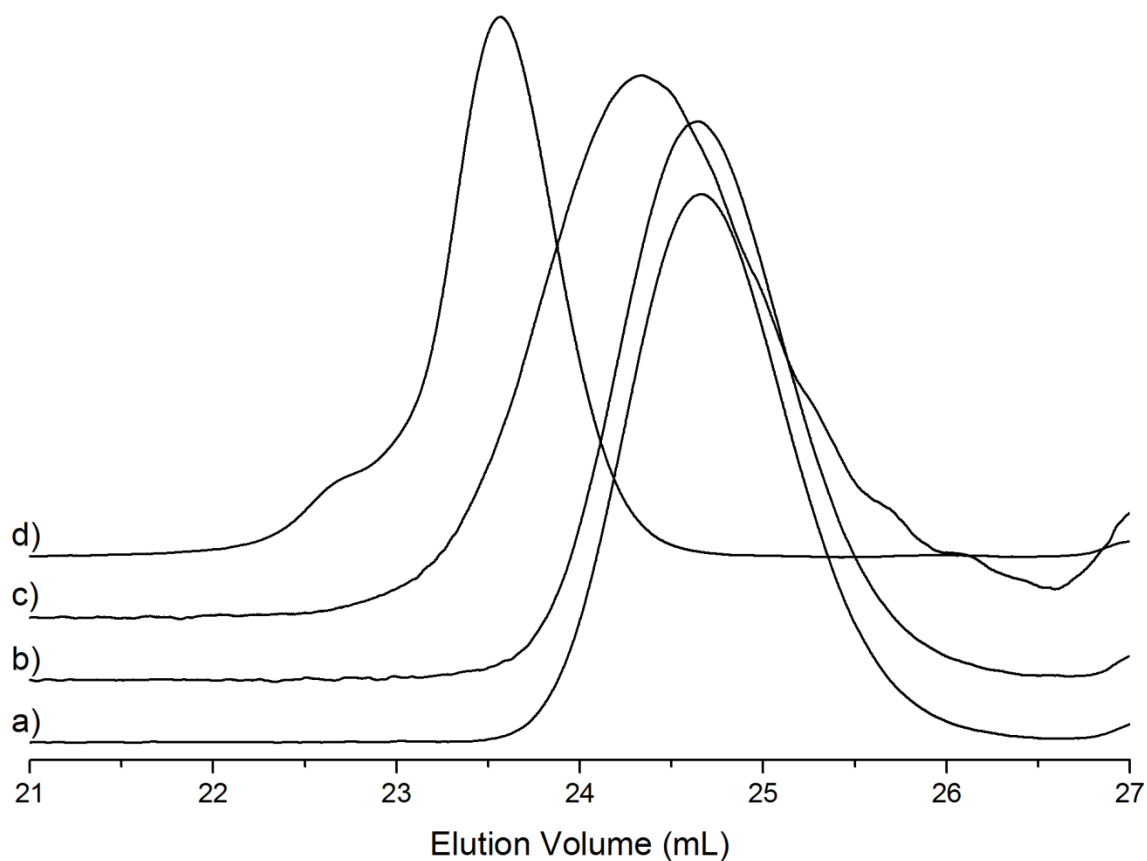
Figure C.3. SEC elution curves of (a) PI, (b) iodated PI, (c) HEMI-PLLA, and (d) reaction product of HEMI-PLLA and iodated PI. The iodation of the 1 kg/mol PI gave a product with a distribution similar to the starting PI. Iodations of higher molecular weight PI (33 kg/mol) gave iodated products that degraded and crosslinked. The reaction of iodated PI and HEMI-PLLA (1 kg/mol) for 17 h at 110 °C gave a product with a SEC distribution shifted to a lower elution volume, indicating an increase in molecular weight.

The exact mechanism for the conjugation in IPI is unclear. The reported mechanisms of PI conjugation through reaction with iodine (Figure C.4a) conclude that I_2 adds across the carbon-carbon double bond to give the diiodated species.[1,2,3] Subsequent elimination of HI gives conjugated dienes. If this reaction pathway is correct, a significant concentration of carbon-iodine bonds should be seen in the ^{1}H NMR spectrum. No evidence of carbon-iodine bonds is present in the ^{1}H NMR spectrum of IPI-1 (Figure C.1a) and minimal evidence is present in the spectrum of IPI-33 (Figure C.2a). Additionally, under the reported mechanism a majority of the conjugated dienes would be E2 and Z2 conjugated diene isomers. The conjugated diene isomers of the IPI synthesized are primarily E1. The iodation/elimination mechanism likely is not correct under the conditions investigated in our study. Another mechanism has been proposed where the I_2 forms charge-transfer complexes with the double bonds of PI (Figure C.4b).[4,5,6] The charge-transfer complexes can lead to the formation of radical cations along the polymer backbone. The radical species could undergo isomerization leading to double bond migration and conjugated dienes. The radical mechanism would result in bis-allylic species as intermediates which are observed in ^{1}H NMR spectra of the IPI product. Additionally, the E1 conjugated diene isomer could be the primary isomer formed under the radical-cation mechanism. The IPI products have a green to black color, confirming the presence of charge-transfer complexes.
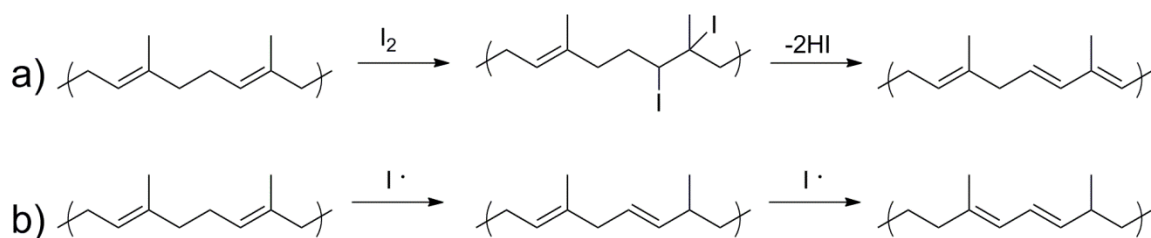
Figure C.4. Reaction schemes for the reaction of iodine with PI to give conjugated dienes following mechanisms of (a) iodation of double bond with subsequent elimination or (b) iodine radical isomerization of double bonds to conjugated diene systems. The iodine radical mechanism (b) can progress through charge-transfer complexes of iodine and PI creating radical cation species.

The charge-transfer complexes were unstable and led to cross-linking of the IPI at ambient conditions. Additionally, the IPI-33 degraded when heated to 110 °C likely as a

result of these unstable charge-transfer complexes. A couple methods were investigated to remove the charge-transfer complexes. Dioxane forms a charge-transfer complex with I_2 so it was added to a solution of IPI-33 in an effort to remove the complexed I_2 from IPI-33.[7] After mixing, the IPI-33 underwent a color change from green-black to clear, but became significantly crosslinked. In a separate reaction, DBU, a strong base, was added to promote possible elimination of HI from the IPI-33 system and give additional conjugated dienes. Upon addition of DBU and subsequent heating (85 °C for 17 h), a solid precipitate formed and the color of the IPI-33 had become brown. The 6.5–5.2 ppm region of the ^{1}H NMR spectrum of the product (Figure C.2b) more clearly showed that the IPI-33 was conjugated. The improved clarity may be due to the removal of charge-transfer complexes, giving clearly defined conjugated systems. In addition to E1 conjugated dienes (1.7 mol % of C=C bonds), a small amount of E2 and Z2 isomers were present (0.7 mol % of C=C bonds). Unfortunately, the SEC trace of the DBU reacted IPI-33 still broadened significantly when heated at 110 °C for 17 h (PDI went from 1.70 to 7.35) indicating degradation and coupling.

C.3.2 Reactions with HEMI-PLLA

IPI-1 was heated with a 1 kg/mol HEMI-PLLA (HEMI-PLLA-1) in a toluene at 110 °C for 17 h. The SEC elution curve of the reaction product (Figure C.3d) shifted to lower elution volume as compared to the two starting materials, consistent with the coupling of IPI-1 and HEMI-PLLA-1. The M_n of the reaction product was greater than that of the HEMI-PLLA-1 and IPI-1 combined. The SEC M_n values of the reaction product, HEMI-PLLA-1, and IPI-1 were 3.9, 1.2, and 1.8 kg/mol, respectively. The ^{1}H NMR spectra of the reaction product (Figure C.1d and f) no longer has peaks in the 6.5-5.2 ppm region confirming that the IPI-1 reacted and the conjugated double bonds are no longer present. The decrease of the relative intensities of peaks in the ^{1}H NMR spectra that correspond with the end-group protons in HEMI-PLLA is consistent with the reaction of HEMI-PLLA (71% conversion). Broad peaks appear in the ^{1}H NMR spectrum of the product (marked by asterisks) that are also consistent with HEMI-PLLA reacting, but are not clear enough to determine the reaction products. IPI-33 degrades when heated

with HEMI-PLLA at 110 °C as indicated by a decrease in M_n (33 to 2 kg/mol) and there was no evidence of a reaction with HEMI-PLLA – HEMI-PLLA peak did not shift to lower elution volume.

C.3.3 Other conjugation attempts

Following a reported PI conjugation, $TiCl_4$ was stirred for 18 h (solution of toluene) at room temperature.[8] The solution became yellow, but no color was present in the collected polymer. Analysis of the ^{1}H NMR spectrum of the product did not find any peaks consistent with protons in conjugated systems. A small peak was present at 2.69 ppm in the ^{1}H NMR spectrum, consistent with the presence of bis-allylic systems (1 mol % of all C=C), indicating that an isomerization process may occur. A longer reaction time and higher $TiCl_4$ concentration could possibly lead to conjugated dienes through such an isomerization mechanism.

The bromination with Br_2 and subsequent elimination with a strong base was investigated to synthesize conjugated dienes.[9,10] The Br_2 was added to a solution of PI in methylene chloride at a ratio of C=C to Br_2 of 20 to 1 at 0 °C for 1.3 h. The collected polymer had a yellow color and peaks in its ^{1}H NMR spectrum (4.5–3.0 ppm) consistent with slight bromination of PI (approximately 1 mol %). Treatment of the brominated PI with dioxane removed the color, suggesting that the color was a result of a bromine charge-transfer complex with PI. Heating the brominated with DBU did not result in elimination reactions that produced conjugated dienes. Likely, most of the Br_2 formed charge-transfer complexes with PI instead of adding across the C=C, similar to I_2, and consequently was not able to undergo elimination reactions to give conjugated dienes.

C.4 Conclusions

Iodation of PI can produce PI with conjugated dienes that appear to undergo reactions with HEMI-PLLA. The exact mechanisms behind both reactions are unclear. IPI contains significant charge-transfer complexes that lead to degradation of the polymer at ambient temperatures or when heated. Bromination of PI with subsequent elimination did not give conjugated dienes, likely due to the formation of charge-transfer complexes.

Halogenation of PI and subsequent eliminations were shown not to be a reliable and stable means to produce conjugated PI.

C.5 References

[1] Dai, L.; Mau, A. W. H.; Griesser, H. J.; Winkler, D. A. *Macromolecules* **1994**, *27*, 6728–6735.

[2] Dai, L.; White, J. W. *Polymer* **1991**, *32*, 2120–2127.

[3] Owen, E. D.; Al-Moh'd, H. S. M. *Polymer* **1997**, *38*, 3533–3538.

[4] Thakur, M. *Macromolecules* **1988**, *21*, 661–664.

[5] Thakur, M.; Swamy, R.; Titus, J. *Macromolecules* **2004**, *37*, 2677–2678.

[6] Ayres, R. L.; Michejda, C. J.; Rack, E. P. *J. Am. Chem. Soc.* **1971**, *93*, 1389–1394.

[7] Shamsipur, M.; Hemmateenejad, B.; Akhond, M. *J. Solution Chem.* **2003**, *32*, 819–829.

[8] Dai, L.; Mau, A. W. H. *Synthetic Met.* **1997**, *86*, 1893–1894.

[9] Buzdugan, E.; Ghioca, P.; Badea, E. G.; Serban, S. *Eur. Polym. J.* **1997**, *33*, 1713–1716.

[10] Malmberg, S. M.; Parent, J. S.; Pratt, D. A.; Whitney, R. A. *Macromolecules* **2010**, *43*, 8456–8461.

Appendix D

2-Hydroxyethyl methacrylate/isoprene Copolymers

In this appendix, we discuss the reversible addition-fragmentation transfer (RAFT) copolymerization of isoprene and 2-ethylhydroxy methacrylate (HEMA) at 125 °C in a large scale pressure reactor. As mentioned in Chapter 4, the reaction system is complex due to the Diels–Alder side reactions of HEMA and isoprene competing with the copolymerization. Isoprene dimerizes to form limonene through a Diels–Alder mechanism at a rate similar to the copolymerization. The side reaction of HEMA and isoprene affects the copolymerization kinetics and distribution of HEMA along the polymer chain, creating a gradient copolymer P(I-co-HEMA) with the initiating end with high concentration of HEMA and the terminus with no HEMA. Ultimately, the P(I-co-HEMA) contains hydroxyl functionality that was utilized to initiate the ring opening polymerization of D,L-lactide to produce P(I-co-HEMA)-g-PLA graft copolymers.

D.1 Introduction

The reversible RAFT controlled radical copolymerization of HEMA and isoprene was investigated on a larger scale than the experiments in Chapter 4. Copolymers with hydroxyl content higher than 3 mol % and molecular weights greater than 10 kg/mol were synthesized. The same Diels–Alder reaction between HEMA and isoprene (Chapter 4) occurred on the large scale polymerizations, leading to gradient copolymers. In spite of these side reactions, a gradient copolymer of isoprene and HEMA (P(I-co-HEMA)) was produced containing pendent hydroxyl groups able to undergo reactions. The polylactide graft copolymers using P(I-co-HEMA) as a macroinitiator are discussed in Appendix E.

D.2 Experimental Details

D.2.1 General Materials and Methods

All chemicals were purchased from Sigma-Aldrich and used without further purification unless otherwise noted. HPLC grade toluene was dried on a home built solvent system by passing it over an activated alumina column and a supported copper catalyst. HPLC grade CH_2Cl_2 was dried on an MBraun solvent purification system. The monomer 2-hydroxyethyl methacrylate (HEMA) was purified by vacuum distillation (67 mtorr, 34 °C) prior to polymerization. D,L-lactide (Purac) was recrystallized from ethyl acetate and stored under nitrogen prior to use. The RAFT CTA (2-(((dodecylthio)carbonothioyl) thio)-2-methylpropanoic acid) was synthesized following a previously reported procedure.[1]

^{1}H NMR spectroscopy was performed on a Varian Inova 500 MHz spectrometer in $CDCl_3$ (Cambridge) using the residual $CHCl_3$ peak as reference. Size exclusion chromatography was performed on an Agilent 1100 high-pressure liquid chromatograph at 35 °C equipped with a PLgel (Varian) 5 μm guard column followed by three PLgel columns with varying pore sizes with HPLC grade chloroform as the mobile phase. Molecular weights and polydispersity index (PDI) were measured by a Hewlett-Packard P1047A refractometer calibrated with either polystyrene (Polymer Laboratories) or polyisoprene (Scientific Polymer Products Inc.) standards. Differential scanning calorimetry (DSC) was performed on a TA Instruments Discovery Series instrument with

the P(I-co-HEMA) samples cycled between -85 and 200 °C with two heating and one cooling cycle. Glass transition temperatures were measured from the second heating ramp.

D.2.2 Large scale HEMA and isoprene copolymerizations

Isoprene was purified by first degassing it by 3 freeze-pump-thaw cycles in a 500 mL purification flask. A majority of the isoprene was then vacuum transferred to another degassed and tared 500 mL purification flask. Given the mass of isoprene collected, the desired quantities of TBP and RAFT CTA were dissolved in HEMA and transferred by syringe to a 250 mL purification flask. The solution was degassed by 2 freeze-pump-thaw cycles and left frozen in liquid N_2. All the purified isoprene was vacuum transferred to the flask with the HEMA solution. The flask was warmed up slowly in an ice bath, allowed to stir to give a homogenous solution, backfilled with 3 psig argon, and sealed so that the solution could be transferred to the reactor. The reactor used was a homebuilt system made of stainless steel with a maximum capacity of 125 mL. The reactor was able to be sealed gas tight by a flange system with a PTFE gasket. The top flange had a port for monomer addition and another to degas the system along with a thermocouple connected to a controller that regulated the reaction temperature using a resistive heater. A pressure gauge was equipped to the reactor so that the reaction pressure could be monitored. Prior to adding the reaction solution, the reactor was degassed by three cycles of evacuation/backfill with 3 psig argon. Through the addition port, the solution in the purification flask was transferred by gravity through an Ultra-Torr connection to the evacuated reaction vessel. The resistive heater was turned on and the system was allowed to heat to 125 °C (typically 20 min), starting the reaction time. The pressure of the reactor could be monitored by the pressure gauge with the initial pressures around 140 psig for pure isoprene. The pressure of the reactor would decrease due isoprene forming products with a lower vapor pressure at 125 °C. Once the reaction ran for the desired time, the heater was turned off and the system was allowed to cool to room temperature to stop the polymerization. The solution was removed from the reactor, diluted in CH_2Cl_2, suction filtered to remove solids, and precipitated three times in 10 times volume excess MeOH

from CH_2Cl_2. Raw solutions were taken before dilution and precipitation. After the final precipitation, the product was dissolved in CH_2Cl_2 and 0.5 wt % butylatedhydroxytoluene was added as a radical inhibitor. The solution was concentrated with blowing N_2 and further dried under vacuum at 50 °C for 4 days to yield a sticky yellow polymer. From the ^{1}H NMR spectra the three regioisomers for polyisoprene were observed at the following average mole fractions: 89.8 % 1,4-isoprene of which 30% are the *cis* and 70% are the *trans* isomers; 4.4% 1,2-isoprene; and 5.8% 3,4-isoprene. ^{1}H NMR spectrum chemical shifts for a general P(I-co-HEMA) copolymer (500 MHz, $CDCl_3$) δ 5.76 (br m, 1,2 isomer -C*H*=CH$_2$), 5.12 (br, 1,4 isomer –C*H*=C-), 5.0 – 4.8 (br m, 1,2 isomer – CH=C*H*$_2$), 4.8 – 4.6 (br m, 3,4 isomer -C=C*H*$_2$), 4.20 (br m, OCO-C*H*$_2$-CH$_2$-O), 4.03 (m, end group =CH-C*H*$_2$-S), 3.82 (br, OCO-CH$_2$-C*H*$_2$-O), 3.35 (m, end group S-C*H*$_2$-CH$_2$), 2.2 – 1.8 (br, allylic protons), 1.68 (br, *cis*-1,4 –C*H*$_3$), 1.60 (br, *trans*-1,4 –C*H*$_3$), 0.94 (br, HEMA and 1,2 PI –C*H*$_3$).

D.2.3 Characterization of Diels–Alder adducts

To collect the Diels–Alder adduct between HEMA and isoprene from the raw polymerization solution, the MeOH soluble fraction after the first precipitation of the raw solution was concentrated by rotary evaporation to give a slightly yellow liquid that was analyzed by ^{1}H NMR spectroscopy. ^{1}H NMR spectroscopic chemical shifts of Diels–Alder adduct of isoprene and HEMA (500 MHz, $CDCl_3$) δ 5.32 (br, -C=C*H*-), 4.20 (br m, OCO-C*H*$_2$-CH$_2$-O), 3.78 (t, J = 4.4 Hz, OCO-CH$_2$-C*H*$_2$-O), 1.64 & 1.62 (s, different peaks for different regioisomers -CH=C-C*H*$_3$), and 1.20 & 1.19 (s, different peaks for different regioisomers -C-C*H*$_3$).

D.2.4 Calculation of conversions

Since isoprene is highly volatile special steps were taken to infer the conversions of it to the various reaction products. To calculate the conversion of each monomer to polymer, we assumed that every polymer chain contained a RAFT CTA and knowing the initial ratios of monomers to the RAFT CTA were able infer the amount of monomer (HEMA and isoprene) incorporated into the polymer. It should be noted that some error may exist with this assumption as not all polymer chains may contain the RAFT CTA,

but previous works have accepted the practice.[2,3] Samples of the raw polymerization solutions immediately removed from the reaction vessel were analyzed by ^{1}H NMR spectroscopy to determine the total conversion of both isoprene and HEMA into their respective products. The total HEMA conversion to the Diels–Alder adduct and polymer was found by comparing the integrations of the peaks at 4.20 and 3.78 ppm (reaction products) with that of the nearby monomer peaks. With the total HEMA conversion known, the conversion of HEMA to polymer was subtracted from the total HEMA conversion to give the conversion of HEMA to the Diels–Alder adduct. From the raw solution, the ratio of limonene integration to HEMA (all forms) integration was found and multiplied by the ratio of HEMA to isoprene in the feed to calculate the conversion of isoprene to limonene. The overall conversion of isoprene was found by adding the conversions to limonene, polymer, and the isoprene/HEMA Diels–Alder product.

D.3 Results and Discussion

D.3.1 Kinetics of large scale copolymerization

The RAFT copolymerization of isoprene and HEMA was performed in the bulk at 125 °C, targeting the P(I-co-HEMA) molecule outlined in Figure D.1. HEMA was added as the minor component with isoprene acting as both monomer and solvent. In all the investigated isoprene/HEMA compositions (0–20 mol % HEMA), both HEMA and the CTA were completely miscible in isoprene. The CTA used was 2-((((dodecylthio)carbonothioyl)thio)-2-methylpropanoic acid (RAFT CTA) and tert-butyl peroxide (TBP) was the radical generating species, added at a 0.2:1 ratio to the RAFT CTA. Polymerizations were performed in a large scale (125 mL) stainless steel pressure reactor equipped with a pressure gauge. As the reactor is a sealed system, aliquots could not be taken during the polymerization. Consequently, all the data presented in this appendix are from the quenched reaction solutions. All time dependent data are from separate reactions with the same initial conditions and quenched at the desired time point.
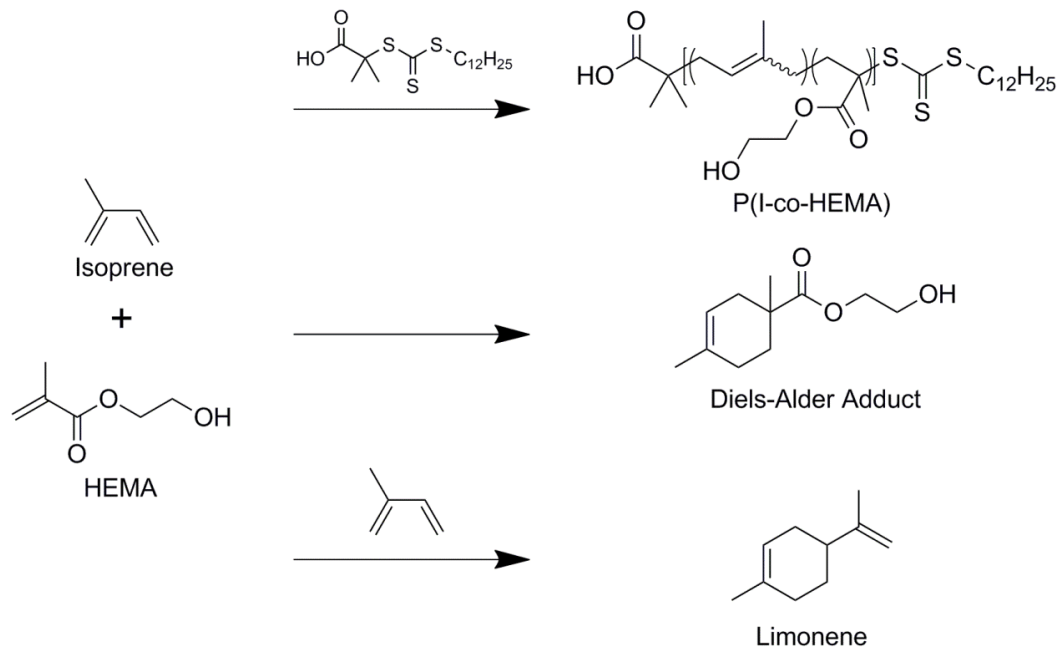
Figure D.1. Reaction schemes of the three reactions that occur during a RAFT copolymerization of HEMA and isoprene at 125 °C with TBP as the radical generating species. Isoprene and HEMA copolymerize to form the polymer P(I-co-HEMA) or undergo a Diels–Alder reaction to form their Diels–Alder adduct. Isoprene also dimerizes to form limonene. Both the Diels–Alder adduct and limonene can form their respective regioisomers not pictured.

As discussed in Chapter 4, isoprene dimerizes during the RAFT homopolymerizations and copolymerizations. The conversion of isoprene to limonene, to polymer, and to HEMA Diels–Alder adducts was monitored for a series of copolymerizations with [M]:[CTA] = 1735, 3.7 mol % HEMA, and different completion times at 125 °C in the pressure reactor (Figure D.2). As indicated by Figure D.2, at the time points investigated isoprene dimerizes to limonene at nearly the same rate as isoprene is polymerized. The conversion of isoprene to limonene in the small scale copolymerization in Chapter 4 and the large scale copolymerization are similar 7 and 10 % at 4 h, respectively, showing that scale up does not significantly affect the dimerization kinetics. Interestingly, the polymerization rates are also similar with 11 and 10% isoprene conversion for [M]:[CTA] equal to 190 and 1735, respectively. The large scale copolymerization ([M]:[CTA] = 1735) would be expected to be slower as the [M]:[CTA] ratio is nearly ten times that of the small scale ([M]:[CTA] = 190) copolymerization in Chapter 4.
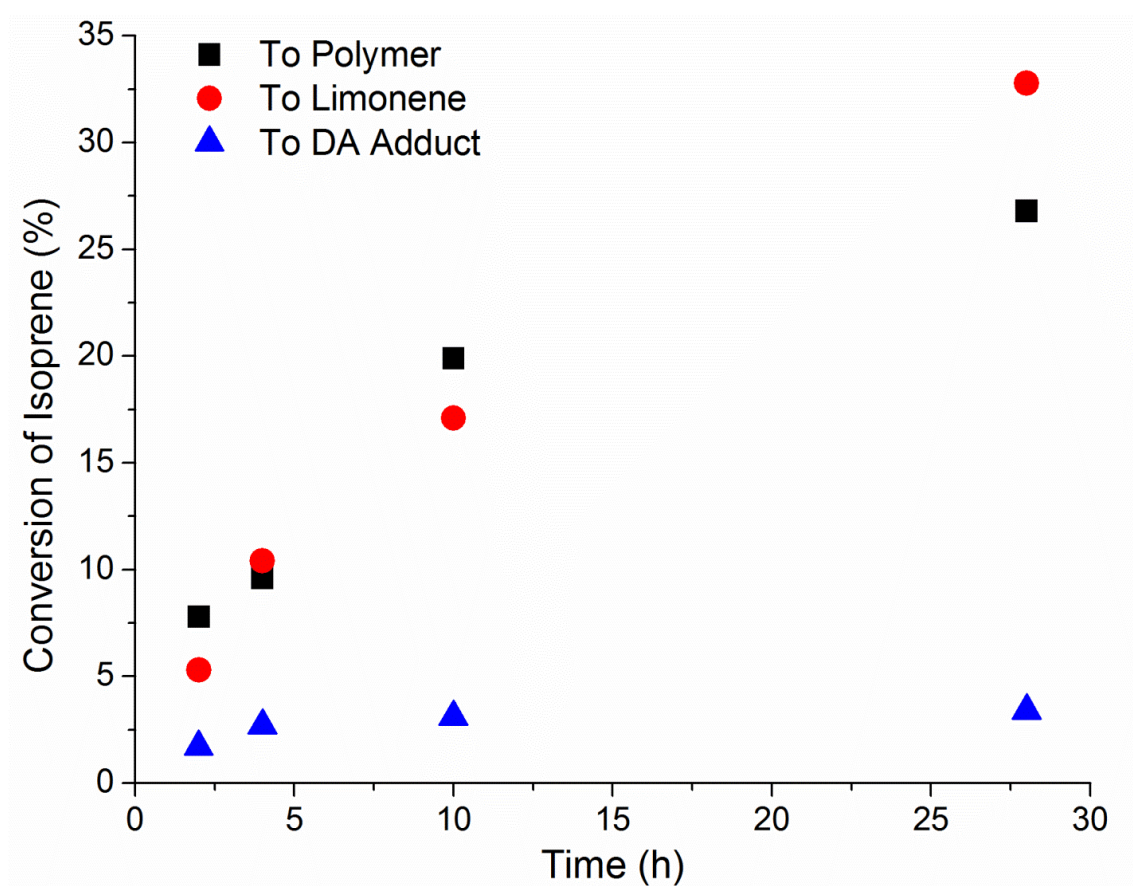
Figure D.2. Conversion of isoprene to its three products over time for the P(I-co-HEMA) RAFT copolymerization at 125 °C. The [M]:[CTA] = 1735 and HEMA was 3.7 mol % of the feed. The conversion of isoprene to the desired polymer product is similar to that of the conversion of isoprene to the side product limonene over the course of the reaction. Such results demonstrate that the limonene side reaction can significantly change the overall concentration of isoprene and consequently change the polymerization kinetics.

Isoprene and HEMA react through a Diels–Alder mechanism to produce an isoprene/HEMA Diels–Alder adduct (Figure D.1). Evidence of the Diels–Alder reaction between isoprene and HEMA is present in the ^{1}H NMR spectrum of the raw reaction solution as peaks consistent with such a product are present.[4] In polymerizations where nearly all the HEMA reacted, the Diels–Alder adduct can be collected by concentrating the soluble fraction from the precipitation of the raw reaction solution into methanol. The ^{1}H NMR spectrum of the methanol soluble products (Figure D.3) are consistent with that of Diels–Alder adduct of isoprene and HEMA.
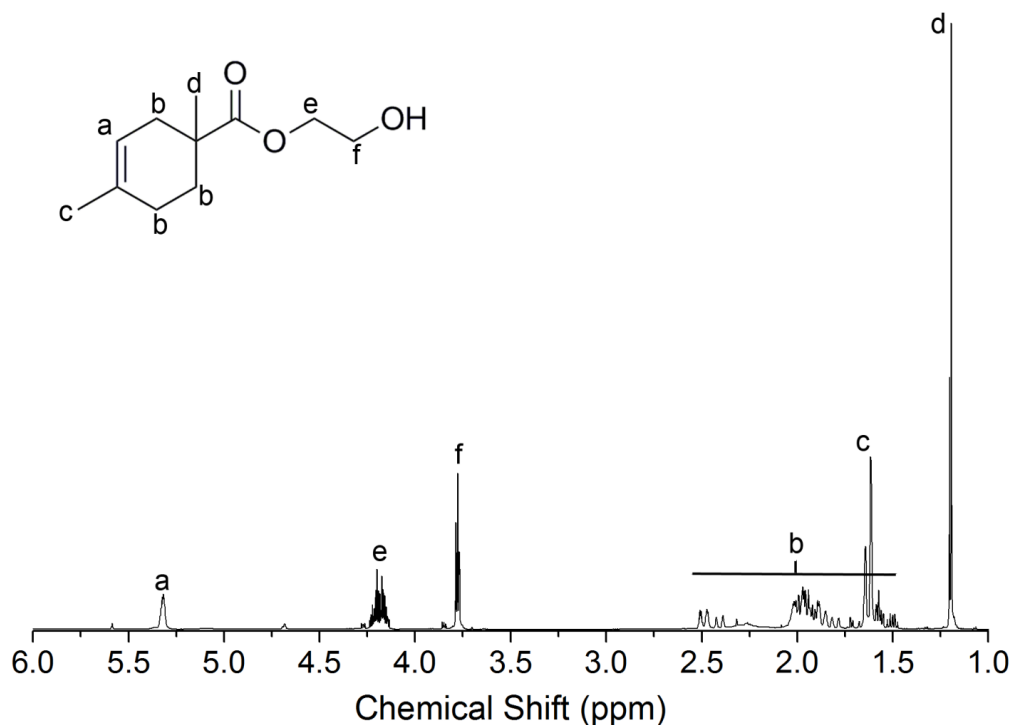
Figure D.3. ^{1}H NMR spectrum of the Diels–Alder adduct between isoprene and HEMA. The structure of one the possible regioisomers is given with peak assignments. The two peaks at 1.64 and 1.62 ppm are consistent with the formation of both possible regioisomers.

As discussed in Chapter 4, the side reactions affect the composition of the copolymer during the polymerization on the large scale. In Figure D.4, the ratio of isoprene to HEMA in the polymer increases as monomer is consumed. Early on in the polymerization (before 25% isoprene conversion) the polymer composition is rich in HEMA as compared to the feed composition. As the reaction proceeds, both isoprene and HEMA are consumed, but with HEMA being consumed faster due to the Diels–Alder side reaction. Consequently, the ratio of isoprene to HEMA incorporated into the polymer goes up as later on in the reaction nearly all the HEMA has been consumed by the side reaction (77% HEMA to adduct at 63% isoprene conversion). At the end of the polymerization, only isoprene is added to the growing polymer chain and a gradient copolymer has been formed.
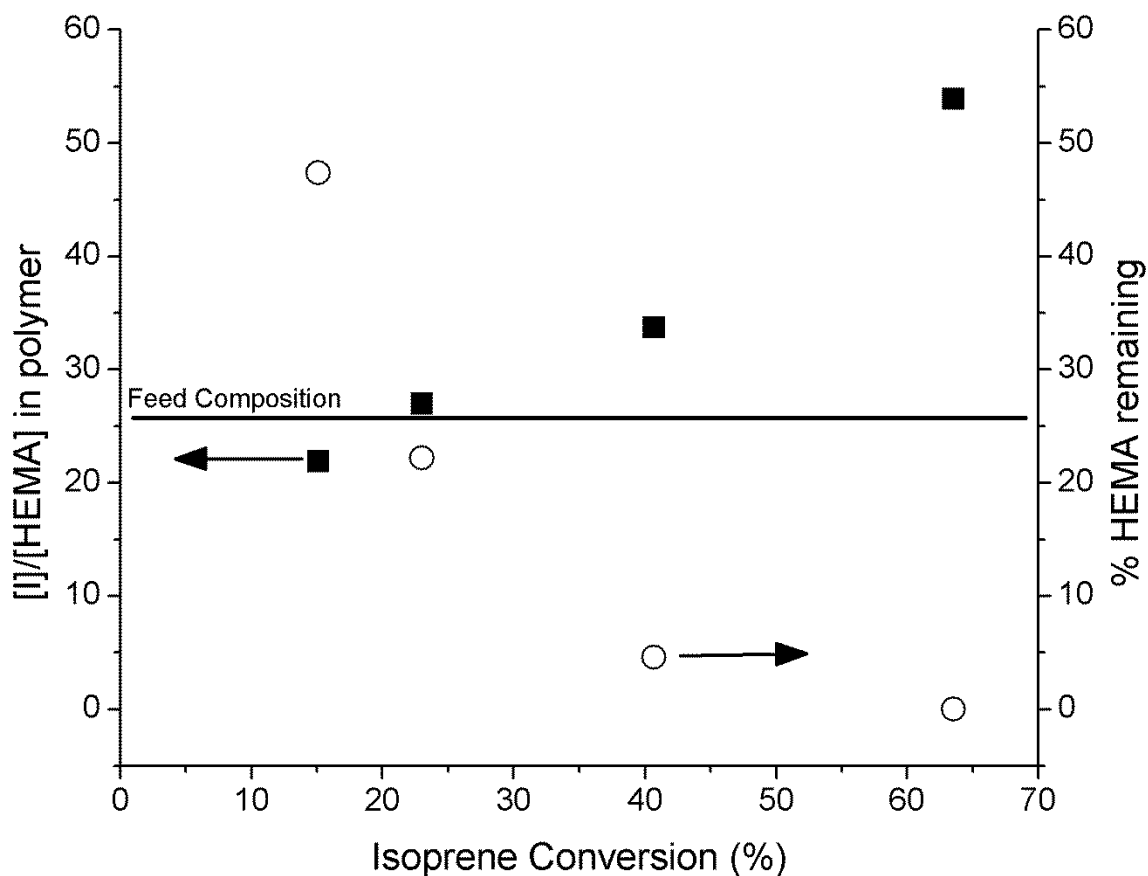
Figure D.4. The ratio of isoprene to HEMA ([I]/[HEMA]) incorporated into the polymer (left axis) and percent of the original HEMA remaining the in the reaction mixture (right axis) as functions of isoprene conversion for a copolymerization at 125 °C with [M]:[CTA] = 1735. The solid line denotes the initial ratio of isoprene to HEMA in the feed (25.7). The [I]/[HEMA] increases as both isoprene and HEMA are consumed which indicates that the isoprene/HEMA Diels–Alder reaction affects the incorporation of HEMA into the polymer.

To limit the rate of HEMA/isoprene Diels–Alder adduct formation relative to the rate of polymerization, the polymerization temperature was lowered. Polymerizations were conducted at 65 and 85 °C using AIBN as the radical initiator with the same [M]:[CTA] ratio and HEMA loading used for the 125 °C polymerizations discussed previously (1735 and 3.7 mol %, respectively). AIBN replaced TBP as the radical generating species in the lower temperature polymerizations to keep the number of propagating radicals similar to the polymerization at 125 °C. The 10 h half life

temperatures for AIBN and TBP are 65 and 120 °C, respectively.[5] The lower temperature reactions (65 and 85 °C) polymerized to a lesser extent than the 125 °C polymerization (10% versus 60% isoprene conversion) at 28 h. The polymerization rates decreased significantly at the lower temperatures. With the lower temperatures more of the reacted isoprene and HEMA were incorporated into polymer instead of side products (Figure D.5). Unfortunately, the amount of HEMA converted into side products was still a majority of all HEMA reacted at all temperatures investigated.
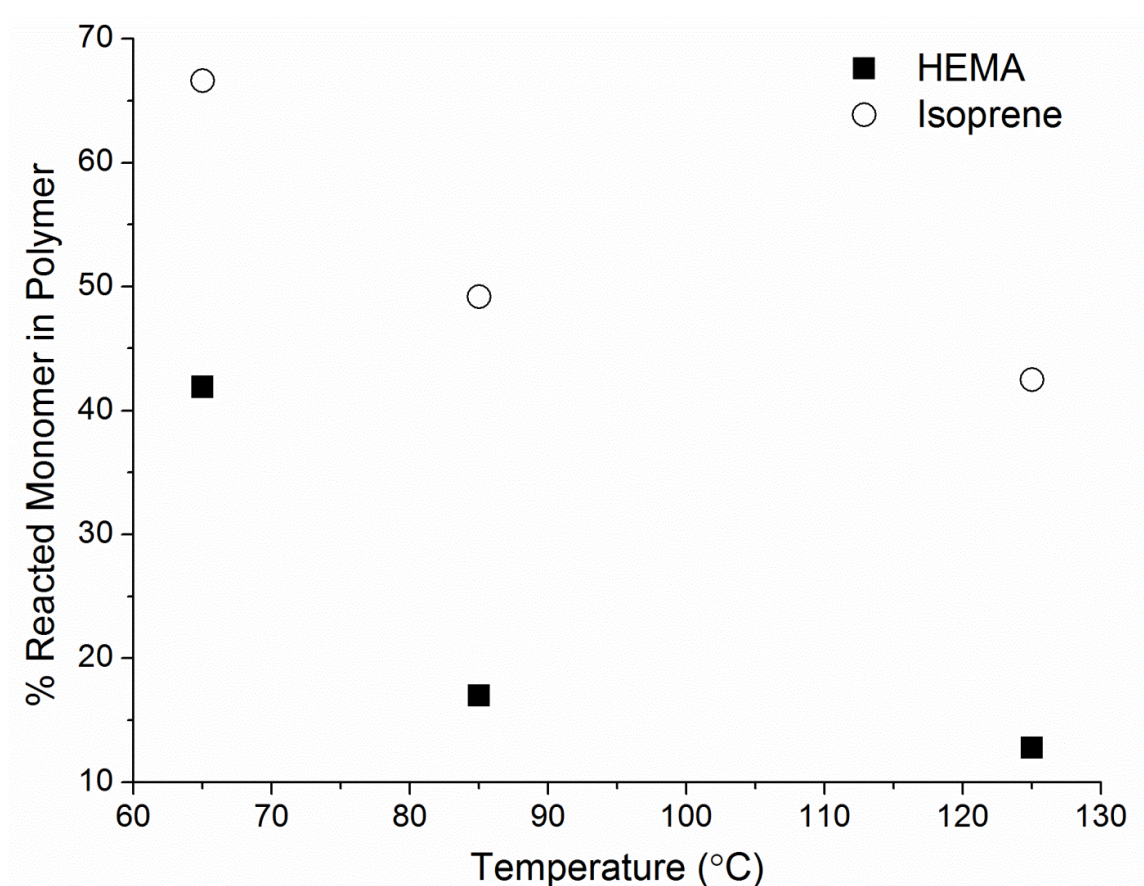
Figure D.5 The percentage of total monomer reacted that is incorporated into polymer for different RAFT polymerization temperatures. In all polymerizations, a majority of the HEMA was converted into Diels–Alder adduct instead of polymeric material. Polymerizations run at 65 and 85 °C were initiated with AIBN and those run at 125 °C were initiated with TBP (the temperatures for a 10 h half life of AIBN and TBP are 65 and 120 °C respectively). All reactions were run for 28 h with the monomer conversions at 65 and 85 °C being significantly less than those at 125 °C (e.g. 10 mol % isoprene versus 60 mol %). The [M]:[CTA] = 1735 and the feed concentration of HEMA was 3.7 mol %.

Even though the isoprene/HEMA RAFT copolymerization is a complex system where side reactions consume HEMA and isoprene, a variety of PI polymers containing hydroxyl groups can be synthesized with some degree of control. By varying [M]:[CTA], the polymerization time, and initial loading of HEMA, P(I-co-HEMA) copolymers were synthesized with different number average molecular weights (M_n) and HEMA mol % (F_H) (Table D.1). The resulting copolymers have monomodal distributions and PDI values narrower than those for a traditional free radical polymerization, similar to the RAFT homopolymerization of isoprene.[3,6] The M_n values calculated by ^{1}H NMR spectroscopic end group analysis of the RAFT CTA mostly agreed with those found by SEC calibrated with PI standards (Table D.1), suggesting that a majority of the P(I-co-HEMA) copolymers contain the RAFT CTA.

Table D.1. Selected P(I-co-HEMA) polymers synthesized by RAFT polymerization at 125 °C.

Sample Code[a]	[M]:[CTA][b]	Reaction Time (h)	f_H[c] (%)	F_H[d] (%)	M_n NMR[e] (kg/mol)	M_n SEC[f] (kg/mol)	PDI[f]
IH(23-0)	1850	22	0		23	20	1.46
IH(42-11.9)	1850	22	19	11.9	42	30	1.52
IH(27-1.9)	1730	28	3.7	1.9	27	22	1.44
IH(26-2.6)	1730	22	4.8	2.6	26	20	1.40
IH(24-1.4)	1550	22	3.2	1.4	24	21	1.52
IH(11-4.0)	540	15	7.4	4.0	11	10	1.39

[a]Sample designation where IH = P(I-co-HEMA) copolymer and IH(##-$$) where ## is the M_n measured by [1]H NMR spectroscopy and $$ is the mol % of HEMA incorporated into the polymer. [b]The molar ratio of all monomers (isoprene and HEMA) to the RAFT CTA. [c]Mol % of feed that is HEMA. [d]Mol % of copolymer that is HEMA. [e]M_n calculated from ^{1}H NMR end group analysis. [f]Found from SEC calibrated with PI standards.

At a set reaction time and feed composition of HEMA, the M_n values achievable by varying the [M]:[CTA] fall on a linear line that passes through the origin (Figure D.6). Interestingly, at a set polymerization time and HEMA composition, the conversions of each monomer to polymer appear to be constant regardless of the [M]:[CTA]. Such a

result suggests that the reaction kinetics are invariant of the CTA concentration. Changes in HEMA feed composition affect the rate of polymerization with higher mole fractions of HEMA leading to faster polymerizations. Varying the feed composition allows for the amount of HEMA incorporated into the polymer to be varied in spite of the Diels–Alder side reactions (Figure D.7). As shown in Figure D.7, the polymers typically contain less HEMA than fed. With the competing Diels–Alder reaction affecting the F_H and the HEMA feed content affecting the rate of polymerization, targeting both M_n and F_H a priori is challenging.
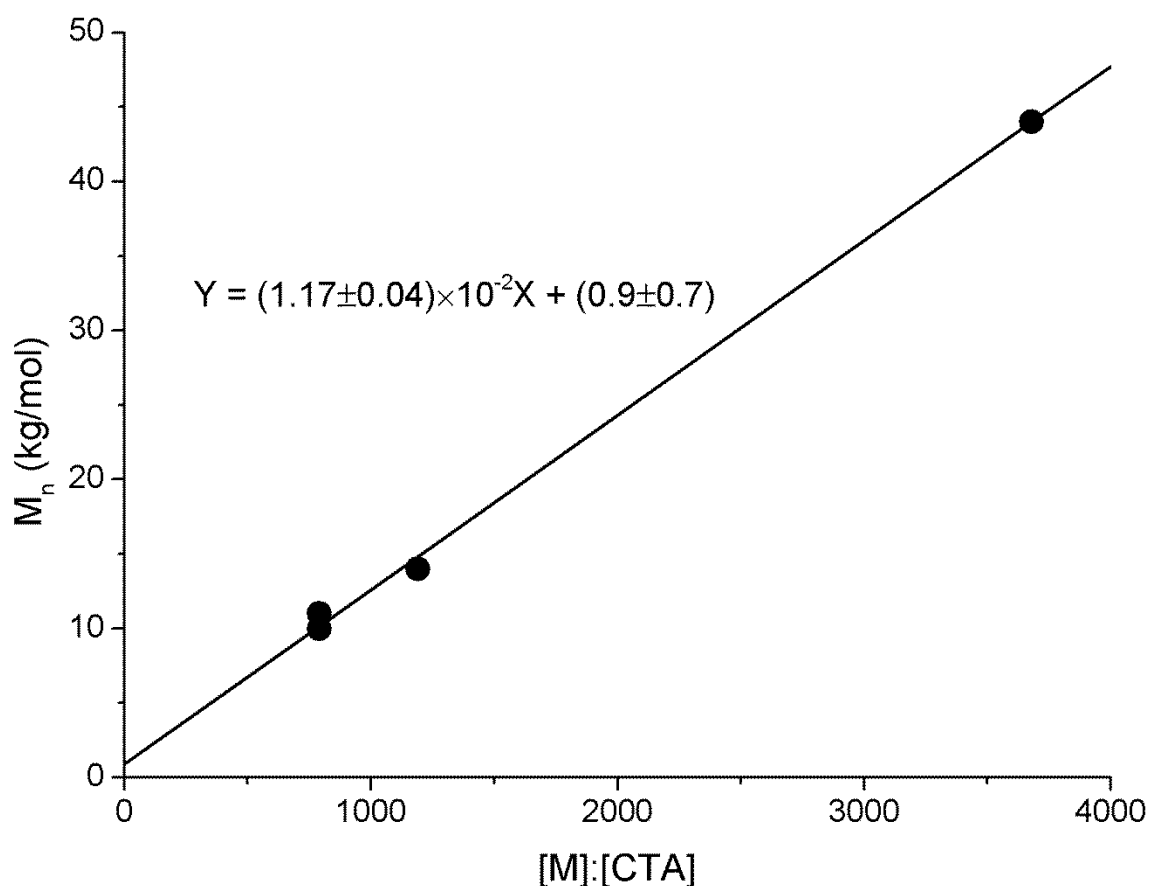
Figure D.6. Calculated SEC M_n as a function of the ratio total monomer concentration to RAFT CTA concentration ([M]:[CTA]). The best fit line of the data using least squares method and its equation are given. The linear relationship of M_n to [M]:[CTA] is characteristic of a controlled polymerization. All data are after 14 h of reaction at 125 °C with 5 mol % of HEMA in the feed. Conversions of isoprene to polymer for all points varied between 13 and 14 mol % while the conversions of HEMA to polymer were between 8 and 11 mol %.
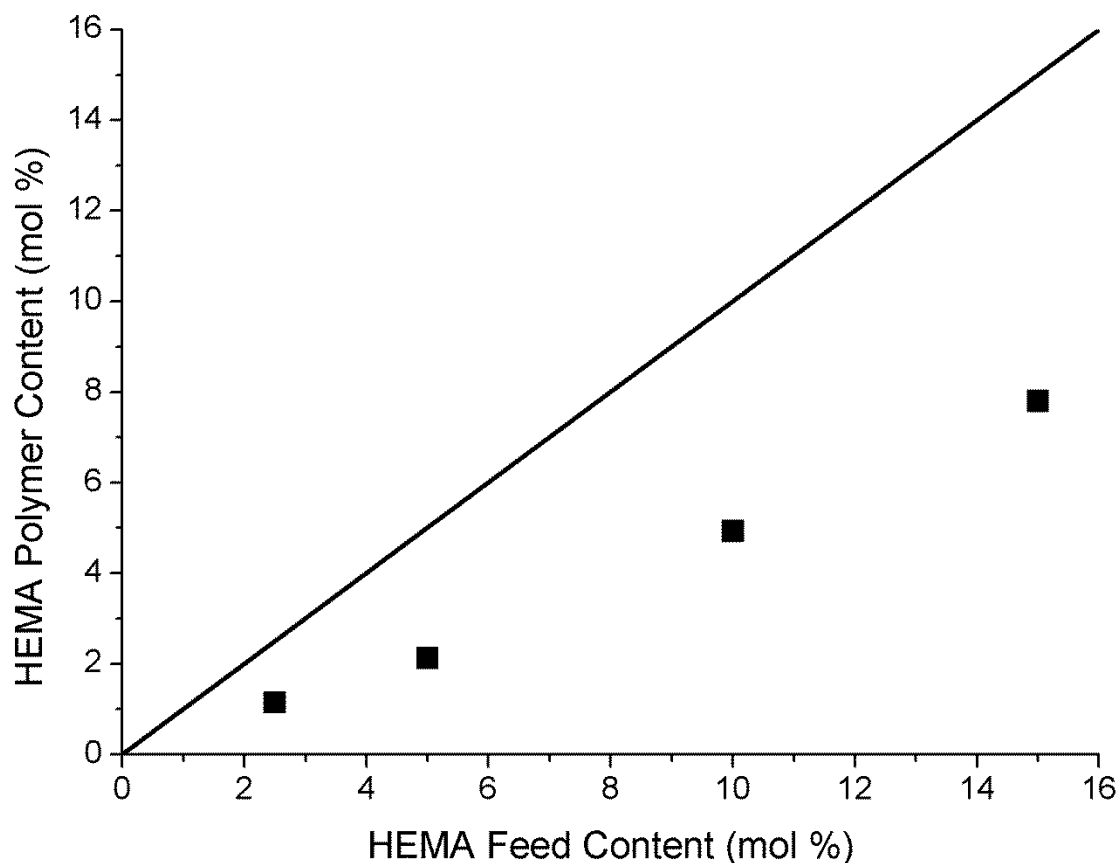
Figure D.7. Mole fraction of HEMA in polymer as a function of the HEMA mol % in the feed solution for 790 [M]:[CTA] and 22 h reaction time at 125 °C. The solid line denotes where the polymer and feed HEMA content would be equal. All reactions had isoprene conversions between 29 and 37 mol % and between 13 and 18 mol % of the fed HEMA polymerized.

D.3.2 Thermal properties of copolymers

The glass transition temperatures (T_g) of copolymers typical exist between those of the two respective homopolymers. For the HEMA/isoprene copolymers, PI is a low T_g (between -70 and -60 °C),[7,8] rubbery material while polyHEMA is a high T_g (98 °C),[9] glassy material. As expected, as more HEMA is incorporated into the P(I-co-HEMA) copolymer the T_g of the copolymer goes up (Figure D.8). Plotting the copolymer T_g as a function of the HEMA wt % in the polymer further demonstrates the increase in T_g with additional HEMA (Figure D.9). In Figure D.9, the Fox equation[10] is plotted assuming the

found T_g of IH(23-0) (-64.6 °C) is the T_g of pure PI. Using this pure PI T_g, the theoretical T_g values for the copolymers are below those observed. If the Fox equation is fit to the copolymer data to find the T_g of pure PI, the trend is linear and the calculated value is -60.2 ± 0.3 °C. The cause of the discrepancy is unclear.
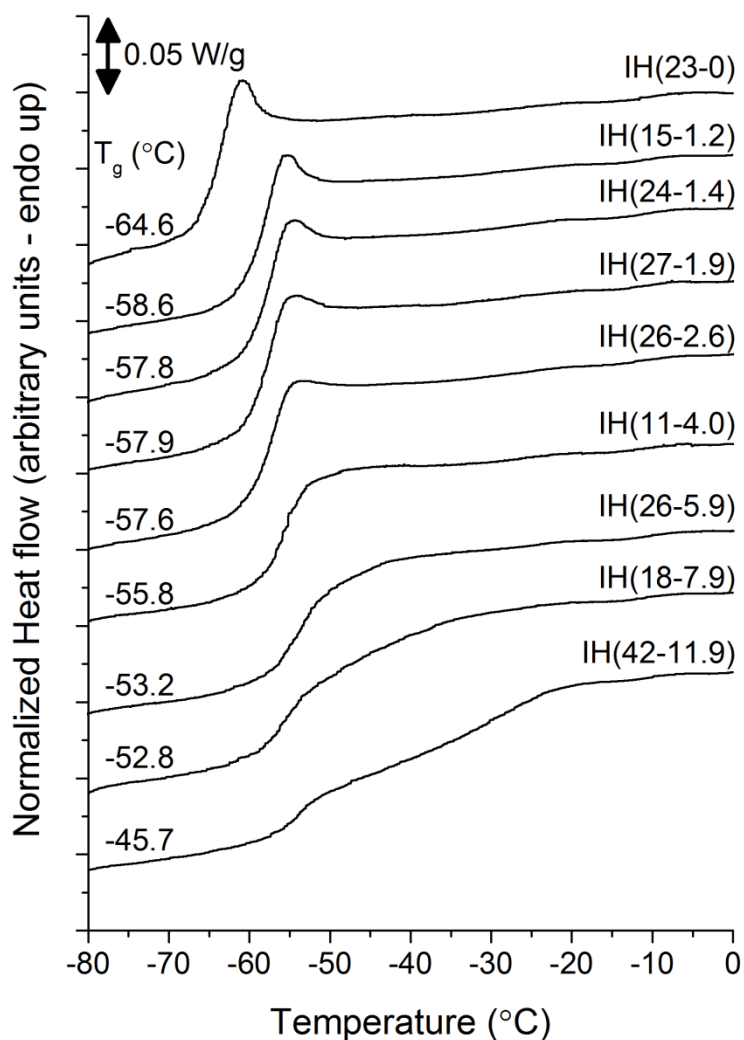
Figure D.8. DSC thermograms of the P(I-co-HEMA) copolymers outlined in Table 1. The HEMA content of the polymer increases down the figure. As the HEMA content goes up, the T_g transition occurs over a larger temperature range, consistent with the formation of a gradient copolymer.
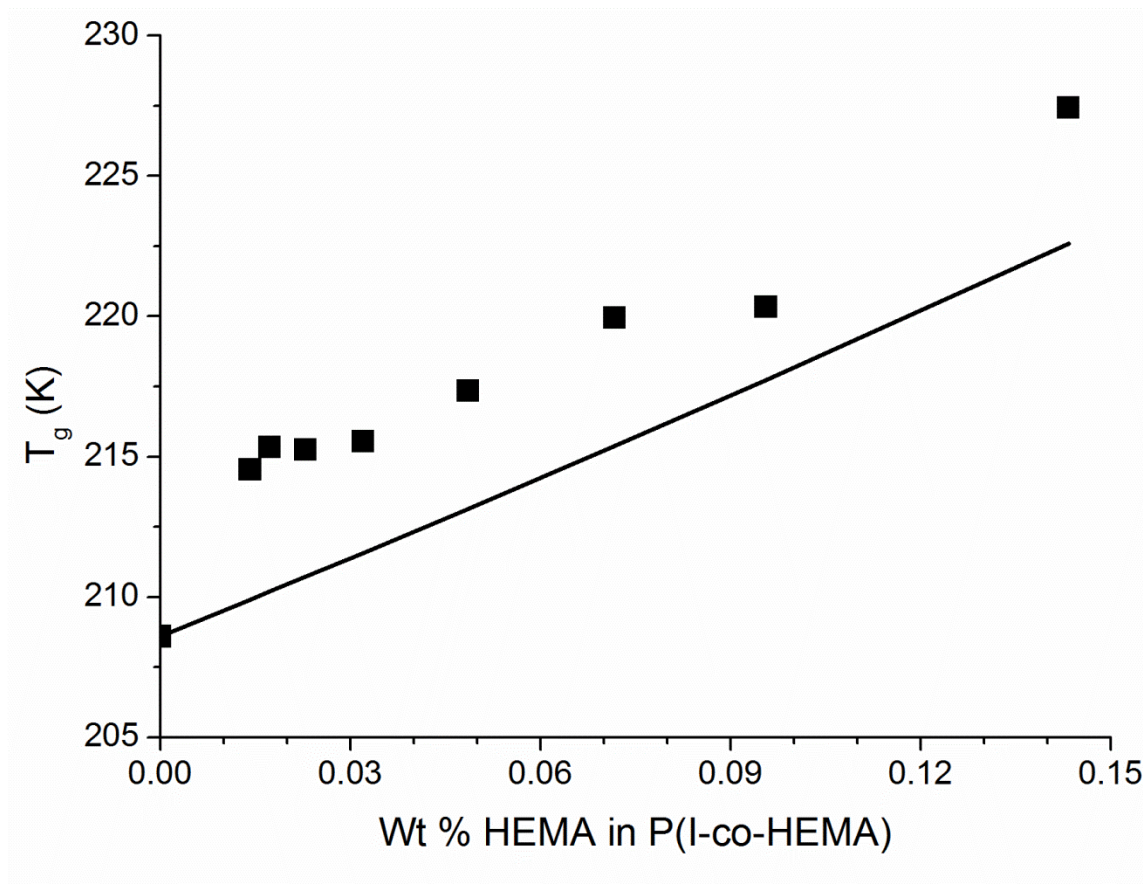
Figure D.9. T_g values of P(I-co-HEMA) polymers as a function of the wt % HEMA present in the copolymer. As the amount of HEMA in the copolymers increases the T_g values do as well. The solid line is the calculated Fox equation, using T_g = -64.6 °C for pure PI and T_g = 98.4 °C for pure polyHEMA.

Polymers with less than 2 mol % HEMA incorporated still have sharp glass transitions (Figure D.8), as indicated by the breadth of the transition. As the HEMA content goes up, the breadth of the glass transition increases. Interestingly, the onset of the glass transition is nearly the same for all the copolymers regardless of the HEMA content (ca. -60 °C), but the conclusion of the transition appears to shift to higher temperatures with increasing HEMA content. The IH(42-11.9) polymer even appears to have two glass transitions over the broad transient. The broadening of the glass transition is consistent with the gradient copolymer architecture of the P(I-co-HEMA) found from the copolymerization kinetics.[11,12,13,14] Since the monomer composition is gradient

throughout the copolymer chain, local regions can have higher concentrations of HEMA than what was fed. Additionally, there are regions of PI homopolymer. Thus, the glass transitions would span from the areas of the polymer with highest concentration of HEMA (initiating end) to the end of the polymer with no HEMA, giving the broad glass transition.

D.4 Conclusions

HEMA and isoprene can be copolymerized successfully on a large scale, yielding gradient copolymers. Despite the side reactions, a range of molecular weights and HEMA content can be achieved by varying the [M]:[CTA] and amount of HEMA fed. At all temperatures investigated, the Diels–Alder reaction between HEMA and isoprene is faster than polymerization. The glass transitions of the copolymers are consistent with gradient copolymers. Even with the complex nature of the copolymerization, hydroxyl functionalized PI was synthesized, providing a macroinitiator for graft polymerization and other complex or functional polymers.

D.5 References

[1] Lai, J. T.; Filla, D.; Shea, R. *Macromolecules* **2002**, *35*, 6754–6756.

[2] Grubbs, R. B.; Wegrzyn, J. K.; Xia, Q. *Chem. Commun.* **2005**, 80–82.

[3] Jitchum, V.; Perrier, S. *Macromolecules* **2007**, *40*, 1408–1412.

[4] Hraus, W.; van de Lee, H.-M. *Tetrahedron Lett.* **1972**, *51*, 5225-5226.

[5] *Crosslinking Peroxides and Polymer Additives*; BTB Communication 2154 [Online]; Akzo Nobel Polymer Chemicals: Chicago, IL, June, 2006

[6] Germack, D. S.; Wooley, K. L. *J. Polym. Sci. Part A* **2007**, *45*, 4100–4108.

[7] Kow, C.; Morton, L.; Fetters, L. J.; Hadjichristidis, N. *Macromolecules* **1982**, *55*, 245–252.

[8] Widmaier, J. M.; Meyer, G. C. *Macromolecules* **1981**, *14*, 450–452.

[9] Al-Issa, M. A.; Davis, T. P.; Huglin, M. B.; Yip, D. C. F. *Polymer* **1985**, *26*, 1869–1874.

[10] Hiemenz, P. C.; Lodge, T. P. Chapter 12: Glass Transition. *Polymer Chemistry*, Second Edition; Taylor & Francis Group: Boca Raton, FL 2007; pp 494.

[11] Mok, M. M.; Masser, K. A.; Runt, J.; Torkelson, J. M. *Macromolecules* **2010**, *43*, 5740–5748.

[12] Jakubowski, W.; Juhari, A.; Best, A.; Koyov, K.; Pakula, T.; Matyjaszewski, K. *Polymer* **2008**, *49*, 1567–1578.

[13] Beginn, U. *Colloid Polym. Sci.* **2008**, *286*, 1465–1474.

[14] Wong, C. L. H.; Kim, J.; Torkelson, J. M. *J. Polym. Sci. Part B* **2007**, *45*, 2842–2849.

Appendix E

Characterization of Polyisoprene-g-Polylactide

In this appendix, we investigate the morphological and mechanical properties of the polyisoprene/polylactide graft polymers (PI-g-PLA). The PI-g-PLA polymers investigated were synthesized using polyisoprene macroinitiators from Chapters 3 and 4 and Appendix D. The PI-g-PLA materials with 95 wt % PLA content were confirmed by small angle x-ray scattering and transmission electron microscopy to be microphase separated. The tensile properties of the PI-g-PLA were significantly improved over polylactide homopolymer, but the elongations to break obtained were generally less than 30%.

E.1 Introduction

As discussed in Chapter 1, poly(D,L-lactide) graft copolymers with a rubbery backbone can be very tough materials. Polyisoprene (PI) is rubbery and can be produced from renewable materials, making it a desirable material for a PLA graft copolymer backbone. In Chapters 3 and 4 and Appendix D, PI with pendent hydroxyl groups were synthesized that can serve as macroinitiators for D,L-lactide polymerization. Using the work of Theryo et al.[1] as a guide, we synthesized PI/polylactide graft polymers (PI-g-PLA) with 95 wt % PLA, using the various macroinitiators created. Three macroinitiators were investigated: conjugated polyisoprene with pendent hydroxyl groups (CPI-g-HEMI), a controlled radical copolymer of 2-hydroxyethyl methacrylate and isoprene (P(I-co-HEMA), and a emulsion polymerized copolymer of methylenebut-3-en-1-ol and isoprene (P(I-co-IOH)). The specifics of the copolymerizations can be found in Chapter 4 and Appendix D for P(I-co-IOH) and P(I-co-HEMA), respectively. The mechanical properties of the PI-g-PLA were characterized through tensile testing. Morphology of the phase separated materials was characterized by both small angle x-ray scattering (SAXS) and transmission electron microscopy (TEM). Generally, the graft copolymers were not found to be highly tough materials.

E.2 Experimental Details

E.2.1 General materials and methods

All chemicals were purchased from Aldrich and used without further purification unless otherwise noted. N-2-hydroxyethylmaleimide was synthesized by a previously published procedure.[2] D,L-lactide (Purac) was purified by recrystallization in ethyl acetate and then dried under vacuum at room temperature. HPLC grade CH_2Cl_2 was dried on an MBraun solvent purification system. P(I-co-HEMA), P(I-co-IOH), and CPI were synthesized following the procedures outlined in Appendix D, Chapter 4, and Chapter 3, respectively.

^{1}H NMR spectroscopy was performed on a Varian Inova 500 MHz spectrometer in $CDCl_3$ (Cambridge) using the residual $CHCl_3$ peak as reference. Size exclusion chromatography was performed on an Agilent 1100 high-pressure liquid chromatograph

at 35 °C equipped with a PLgel (Varian) 5 μm guard column followed by three PLgel columns with varying pore sizes with HPLC grade chloroform as the mobile phase. Molecular weights and polydispersity index (PDI) were measured by a Hewlett-Packard P1047A refractometer calibrated with polystyrene standards (Polymer Laboratories). Transmission electron microscopy (TEM) was performed on a FEI Tecnai Spirit BioTWIN at an operating voltage of 80 keV. Samples for TEM were microtomed at 25 °C on a Leica EM UC6 Ultramicrotome to a thickness of approximately 70 nm and stained with OsO_4 vapor (4 wt % aqueous solution) for 20-30 minutes prior to imaging.

E.2.2 Functionalization of CPI with HEMI

Under N_2 atmosphere in a glove box, CPI (CPI-17, 250 mg) and dry toluene (7.5 mL) were combined in a 75 mL thick walled pressure vessel. HEMI was added as a stock solution (25 mg HEMI/1 mL CH_2Cl_2) in dry methylene chloride to give the desired number of grafts per chain in the final product. The sealed vessel was removed from the glovebox and placed in a 110 °C oil bath to heat for 16 h. The cooled vessel was transferred back to the glove box for graft copolymer synthesis.

E.2.3 PI-g-PLA synthesis from P(I-co-HEMA), P(I-co-IOH), and CPI-g-HEMI.

1,5,7-triazabicyclo[4.4.0]dec-5-ene (TBD) D,L-lactide polymerization

In the glove box, the macroinitiator (500 mg), D,L-lactide (9.5 g) and dry methylene chloride (40 mL) were added to the vessel to give 19:1 mass ratio of lactide to macroinitiator. To start the polymerization, 920 μL of a TBD stock solution (10 mg TBD/1 mL CH_2Cl_2) at a 1000:1 lactide to TBD ratio was added to the vessel. Upon addition of the TBD catalyst, the vessel was sealed and removed from the glove box to stir in an ice bath for 1 h (CPI-g-HEMI) or at room temperature for 30 min (P(I-co-HEMA) and P(I-co-IOH)). To quench the reaction, 10 molar excess of benzoic acid dissolved in minimal CH_2Cl_2 was added to the solution. The viscous solution was diluted with CH_2Cl_2, precipitated in 10 volume excess MeOH, redissolved in CH_2Cl_2, and precipitated in 10 volume excess hexanes. The collected product was then dried overnight under vacuum. Conversions of lactide were all around 98% for all TBD polymerizations. *Tin octoate (Sn(Oct)₂) catalyzed D,L-lactide polymerization* In the glove box, P(I-co-

HEMA) (1 g) was dissolved in dry toluene (140 mL) in a pressure vessel. $Sn(Oct)_2$ was added as a stock solution in toluene (50 mg/5 mL) to the reaction mixture (1.9 mL stock solution). D,L-lactide (19 g) was then added to vessel which was removed from the glove box and set in a 100 °C oil bath for 19 h to polymerize. The reaction was quenched by cooling to room temperature and with subsequent dilution with CH_2Cl_2. The polymer was precipitated twice from CH_2Cl_2 into 10 volume excess hexanes and dried under vacuum. See respective chapters for ^{1}H NMR spectroscopic assignments.

E.2.4 PLA homopolymer synthesis

Homopolymer PLA materials with M_n values close to the PLA arm M_n in PI-*g*-PLA were synthesized to compare mechanical properties. Briefly, in the N_2 dry box D,L-lactide (5 g) was dissolved in CH_2Cl_2 (42 mL) in a pressure vessel. Benzyl alcohol was added as an initiator at volumes required to give the targeted M_n at complete conversion. TBD (5 mg) was added as a stock solution in CH_2Cl_2. Upon addition of the TBD, the reaction vessel was sealed, removed from the dry box, and allowed to stir at room temperature for 20 min. A 10 molar excess of benzoic acid was added as a solution in minimal CH_2Cl_2 to quench the polymerization. Solutions were precipitated in 10 fold volumetric excess of MeOH after which the solid product was collected and set to dry under vacuum at room temperature.

E.2.5 SAXS analysis of CPI-g-PLA

Room temperature synchrotron small-angle X-ray scattering (SAXS) was carried out at the Advanced Photon Source (APS) at Argonne National Laboratories at the Sector 5-ID-D beamline maintained by the Dow-Northwestern-Dupont Collaborative Access Team (DND-CAT) with a source that produces x-rays with a wavelength of 0.84 Å. Scattering intensity was monitored by a Mar 165 mm diameter CCD detector with a resolution of 2048 × 2048. The two-dimensional scattering patterns were integrated azimuthally, giving one-dimensional scattering profiles. In each scattering profile, the lowest spatial frequency (q) peak was designated as q* – the principle scattering peak. From the q* value, the domain spacing (d) of each sample was calculated using d =

$2\pi/q^*$. To estimate the hard sphere radius (R_{HS}) of the PI domains, the higher q-value inflections and broad peaks were fit by eye to the hard sphere scattering form factor:

$$I = A\left[\frac{3}{x^3}(\sin x - x \cos x)\right]^2$$

where A is a arbitrary constant, I is the scattering intensity, and $x = qR_{HS}$.

E.2.6 Differential scanning calorimetry (DSC) analysis of CPI-g-HEMI graft polymers

DSC was performed on a TA Instruments Discovery Series instrument on CPI-g-HEMI graft polymers. Samples were stored in a -20 °C freezer prior to any aging protocol. "Un-aged" samples were set to run on the DSC instrument the day that they were removed from the freezer. "Aged" samples were left at room temperature for 2 d prior to running on the DSC instrument. Samples were cooled to -80 °C and heated to 210 °C at 10 °C/min for two cycles. The initial heating cycle from -80 to 210 °C was used for the analysis.

E.2.7 Sample preparation and mechanical testing of CPI-g-PLA

Approximately 4 g of graft copolymer were dissolved in CH_2Cl_2 (100 mL) along with 0.5 wt % BHT. The resulting solution was filtered through a coarse pore size frit filter to remove particulates and poured into a Teflon lined crystallization dish. The solution was covered and allowed to dry in air for $2 - 3$ days. The films were removed from the Teflon and placed in a vacuum oven to dry at 60 °C for 4 days. Between drying and pressing the films were stored in a 4 °C fridge. The films were pressed into 0.5 mm plaques at 150 °C (3 min initial melt, 2 min press) and subsequently rectangular bars of the approximate dimensions 25 mm by 6 mm were cut from the plaques. The bars were then laid over a tensile bar mold (dog bone shape, 25 mm length with 3 mm width in the gap and 6 mm at the grip) and pressed at 150 °C (3 min initial melt, 2 min press). Tensile bars were removed from the mold and the flashing was removed carefully with a sharp razor. The bars were aged 2 days prior to tensile testing either in at room temperature (23 °C) in the dark or in a fridge (4 °C). A minimum of 3 bars were tested for each blend on a Rheometrics Instruments MINIMAT tensile tester at a cross head speed of 10 mm/min.

The bars were tested with a 13 mm gap length (grip to grip), 0.5 mm thickness, and 3 mm minimum width in the gap.

E.3 Results and Discussion

E.3.1 Synthesis of PI-g-PLA

The three different types of macroinitiators used for PI-g-PLA synthesis were slightly different. All the CPI-g-HEMI macroinitiators were synthesized from the same parent CPI (25 kg/mol, PDI = 1.08) that was functionalized with varying numbers HEMI groups prior to graft polymerization. By changing the number of HEMI groups off the CPI, macroinitiators were synthesized with different number of pendent hydroxyl group and consequently the macroinitiators had different values for the average molecular weight between grafts (M_E). The calculation of M_E assumes equal spacing of the hydroxyl groups along the polymer chain. The hydroxyl groups are assumed to be randomly spaced along the CPI-g-HEMI macroinitiator because the distribution of conjugated dienes and consequently reacted HEMI group appear to be random. The M_E for the P(I-co-HEMA) and P(I-co-IOH) was controlled by the amount of each hydroxyl monomer incorporated into the copolymer during polymerization. As discussed in Chapter 4 and Appendix D, the hydroxyl groups are not dispersed randomly along the polymer chain for the copolymers. The controlled radical polymerized P(I-co-HEMA) has a majority of the hydroxyl groups at the initiating end of the copolymer, but is still relatively narrow in distribution (27 kg/mol, PDI = 1.42). The emulsion copolymerized P(I-co-IOH) has a broad distribution of polymers with varying amounts of hydroxyls throughout the polymer, possibly concentrated more towards the terminating end of polymer (74 kg/mol (SEC), PDI = 6.35). Though the materials differ significantly, generally the macroinitiators have similar M_E and M_n values (Table E.1).

Table E.1. Properties of PI-g-PLA polymers synthesized using CPI-g-HEMI, P(I-co-HEMA), and P(I-co-IOH) macroinitiators.

Sample[a]	M_E[b] (kg/mol)	M_G[c] (kg/mol)	M_n[d] (kg/mol)	PDI[d]	d[e] (nm)	R_{HS}[f] (nm)
CPI-g-HEMI-5.2	5.2	97	260	1.98	46.8	10.2
CPI-g-HEMI-4.7	4.7	84	370	1.70	33.1	7.6
CPI-g-HEMI-2.9	2.9	60	470	1.49	28.8	6.8
CPI-g-HEMI-2.8	2.8	53	480	1.26	27.5	6.7
CPI-g-HEMI-1.3	1.3	25	450	1.15	18.4	4.1
P(I-co-HEMA)-3.8	3.8	70	313	1.94	34.1	8.8
P(I-co-HEMA)-3.6[g]	3.6	52	309	1.67	27.2	8.0
P(I-co-IOH)-2.7[h]	2.7	26	332	5.89	33.0	NA

[a]Sample code @@@-### where @@@ indicates the macroinitiator used and ### indicates the average molecular weight between grafts. M_n of the macroinitiators CPI-g-HEMI, P(I-co-HEMA, and P(I-co-IOH) are 25, 27, and 74 (SEC) kg/mol, respectively. [b]Number average molecular weight between grafts. [c]Number average molecular weight of PLA arms off macroinitiator, found by ^{1}H NMR spectroscopy. [d]Number average molecular weight of graft copolymer, found by SEC calibrated with polystyrene standards. [e]Domain spacing calculated from small angle x-ray scattering (SAXS). [f]Radius of PI domains calculated from SAXS assuming hard sphere form factor (see Experimental Details). [g]Lactide polymerized with $Sn(Oct)_2$ [h]Significant homopolymer was present in P(I-co-IOH)-2.7, resulting in the calculated M_G being less than the theoretical M_G (55 kg/mol). No inflection points were observed so a R_{HS} could not be estimated.

Each macroinitiator was used to synthesize PLA graft copolymers containing 95 wt % PLA. All D,L-lactide polymerizations, except for P(I-co-HEMA)-3.6, were catalyzed with TBD. The P(I-co-HEMA)-3.6 graft copolymer was synthesized using $Sn(Oct)_2$ as the catalyst. General trends can be observed in the data due to the set concentration of PLA. As the number of PLA grafts increases the number average molecular weight of the PLA grafts (M_G) decreases because of the reduction in the ratio of monomer to initiator (Table E.1). For the CPI macroinitiators, with an increase in grafting points, the molecular weight between grafts (M_E) decreases for the set molecular weight of the macroinitiator. The changing M_G and M_E values result in a wide range of

polymer structures, from CPI-g-HEMI-5.2 having long PLA arms spaced far apart to CPI-g-HEMI-1.3 having short arms spaced closely together.

For the CPI macroinitiators, as M_E and M_G increase, the peaks of CPI-*g*-PLA SEC elution curves (Figure E.1) shift to lower elution volume and broaden. Ideally, with the set 95 wt % PLA composition all graft copolymers should have the same overall M_n by SEC and one may expect that their SEC elution curves should lie at the same elution volume. However, SEC separates materials based on their hydrodynamic radius not their M_n so a change in elution curve position indicates a change in the hydrodynamic radius value.[3] The increase in elution curve peak suggests that longer PLA arms give larger hydrodynamic radii.
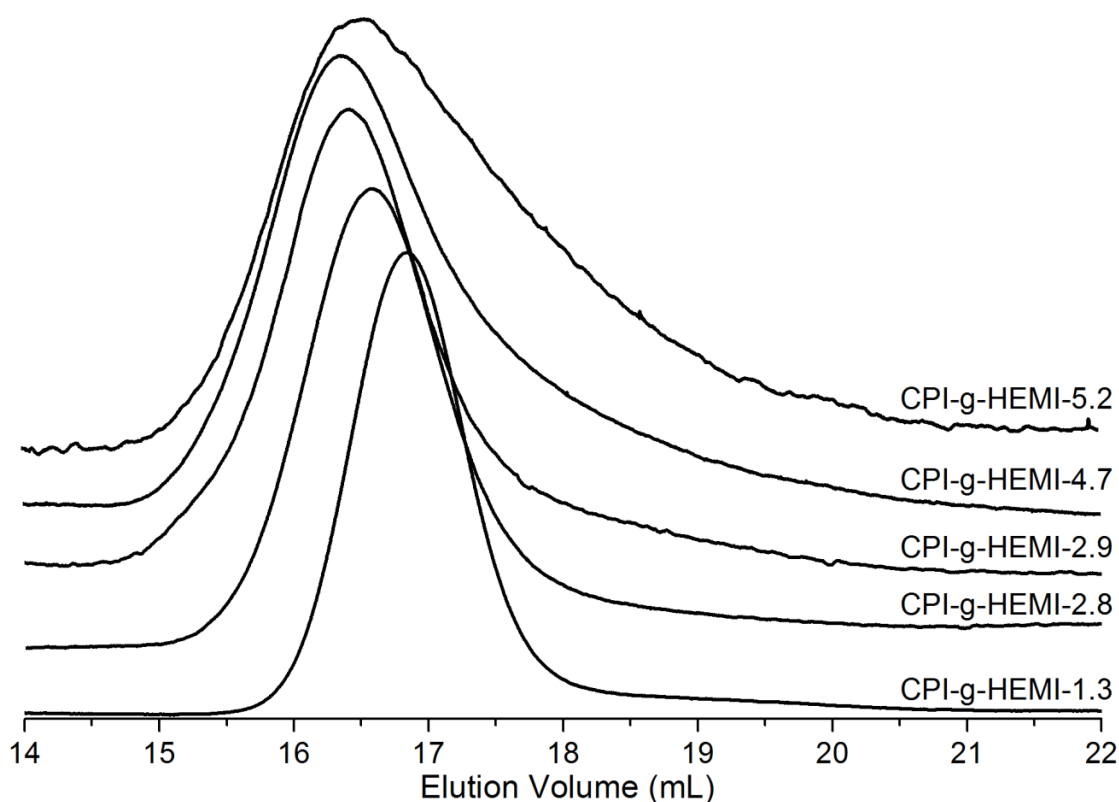

Figure E.1. SEC elution curves of CPI-*g*-HEMI PLA graft polymers. The number after CPI-g-HEMI is the M_E (average molecular weight between grafts) of the macroinitiator in kg/mol. As the number of grafting points along the backbone decreases, the SEC elution curve peaks shift to lower elution volume and broaden. The broadening likely is due to PLA homopolymer contamination.

The broadening of the CPI-*g*-PLA distributions can be quantified by the SEC determined PDI values (Table E.1). Generally, as the target M_G increases the distribution broadens towards the right of main peak, resulting in lower molecular weight material accounting for more of the polymers in the sample. The SEC calculated M_n (Table E.1) reduces with number of grafts to reflect this increase in low molecular weight material. The origin of the low molecular weight material is unclear, though PLA homopolymer formed from advantageous initiator in the monomer is one possibility. The concentration of initiators decreases with a decrease in the number of grafting points, resulting in the fraction of any advantageous initiator present in the lactide monomer to go up. Consequently, homopolymer PLA initiated by the advantageous initiators becomes a significant fraction of all polymers present and observable in the SEC elution curves. Another possible origin of the low molecular weight material is unreacted macroinitiator, but the ^{1}H NMR spectra of the products suggests that all the macroinitiator reacts to give graft copolymer. Additionally, the broadening of the SEC elution curves may be due to increased transesterification for the graft copolymers synthesized with fewer growing chains – transesterification leads to broader PLA distribution.

The PLA graft copolymers synthesized from copolymer macroinitiators (P(I-co-HEMA) and P(I-co-IOH)) were similar to the CPI-g-HEMI initiated copolymers in terms of the M_E and M_G. P(I-co-HEMA)-3.6 and P(I-co-IOH)-2.7 had significant PLA homopolymer contamination as indicated by the low molecular weight shoulders in the SEC traces (Figure E.2). The ^{1}H NMR spectroscopy end-group analysis measured M_G of P(I-co-IOH)-2.7 was half of the expected value due to the homopolymer PLA formed – PLA homopolymer and graft polymer peaks overlap. Likely, the graft copolymer has an M_G value near the theoretical (55 kg/mol) with low molecular weight PLA homopolymer. P(I-co-HEMA)-3.8 had a broad PDI either due to some PLA homopolymer or a broad distribution of the PLA arm molecular weights.
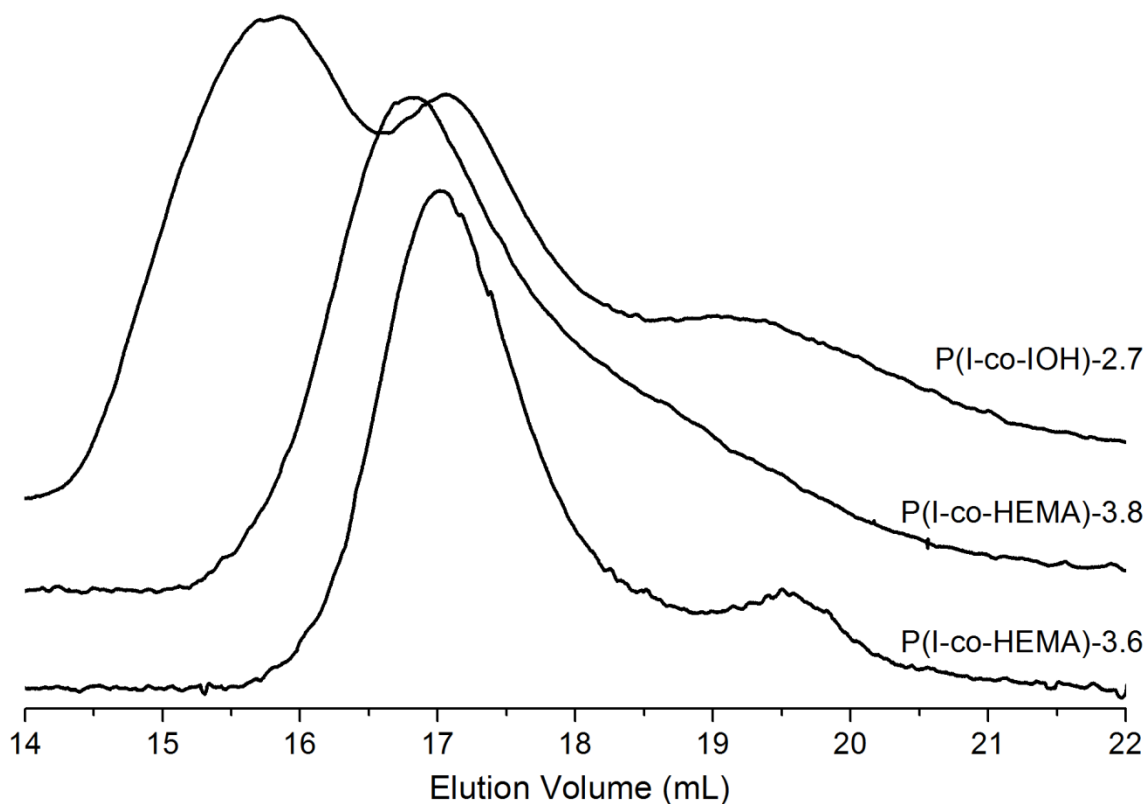
Figure E.2. SEC elution curves of PI-g-PLA synthesized off P(I-co-IOH) and P(I-co-HEMA) macroinitiators. Low molecular weight peaks (19–20 mL) in the chromatograms are indicative of homopolymer formation.

E.3.2 SAXS analysis of PI-g-PLA

The microstructures of the PI-*g*-PLAs were characterized by the SAXS line at Argonne National labs. Scattering profiles (Figure E.3) of each graft copolymer have a broad peak at low-q corresponding to the principle scattering peak (q*), demonstrating that the graft copolymers are phase separated at room temperature. Broad peaks occur at higher q-values, but do not correspond to known Bragg reflections. Previous 95 wt % PLA graft copolymer SAXS profiles have given one broad peak corresponding to a poorly ordered spherical microstructure of rubbery particles.[1] The broad q* in the PI-*g*-PLA SAXS profiles likely are due to a similar disordered spherical microstructure, while the higher q-value reflections are due to the spherical form factor of the PI domains. Such

form factor scattering at high q-values in addition to the structure factor scattering at low q-values has been observed in both graft copolymers as well as concentrated (3 wt % and higher) micelle solutions.[4,5]

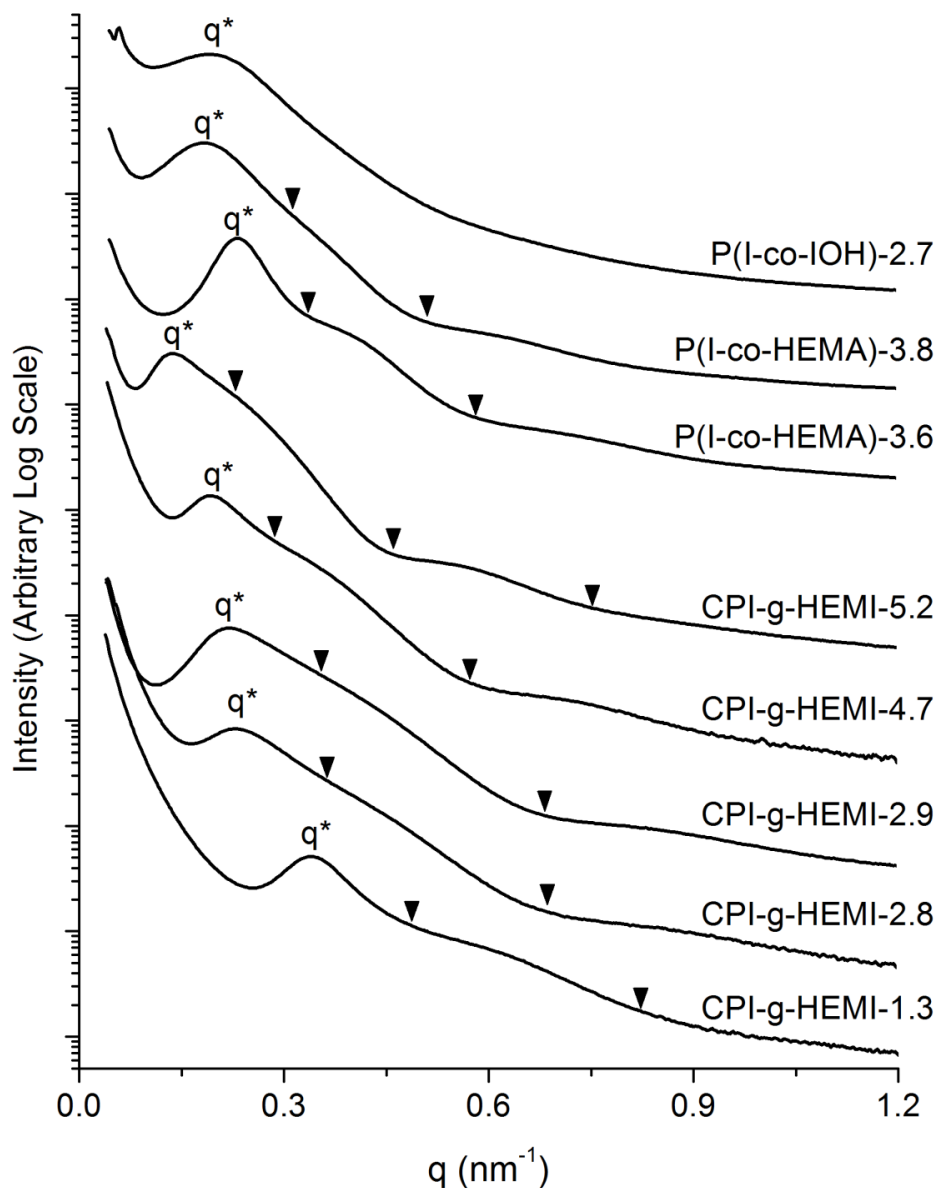Figure E.3. Integrated, one-dimensional SAXS patterns at room temperature of the PI-*g*-PLA polymers. The principle scattering peak (q*) is labeled in each profile corresponding to the structure factor of disordered spheres. Inflection points for the hard sphere form factor a labeled as solid triangles. Profiles are plotted on an arbitrary log scale and have been translated vertically to improve clarity.

The domain spacing for each PI-*g*-PLA was calculated from their respective q* (Table E.1) value. Generally, the domain spacing increases with M_G (number of grafts decrease) due to the longer PLA arms separating the PI domains. A hard sphere form factor fits the inflection points and peaks of each scattering profile (Figure E.3) to a close approximation (see Figure E.4 for example), allowing for the estimation of the hard sphere radius of the PI spheres (R_{HS}) in the PLA matrix (Table E.1). The R_{HS} rises correspondingly with the M_G, suggesting that the number of PI-*g*-PLA molecules that aggregate to form the PI spheres increases with M_G to give the larger particles. The larger R_{HS} values are consistent with the observed domain spacing because at a set volume of each component (set weight fraction), an increase in particle radius (volume) results in less particles, corresponding to further distance between particles.
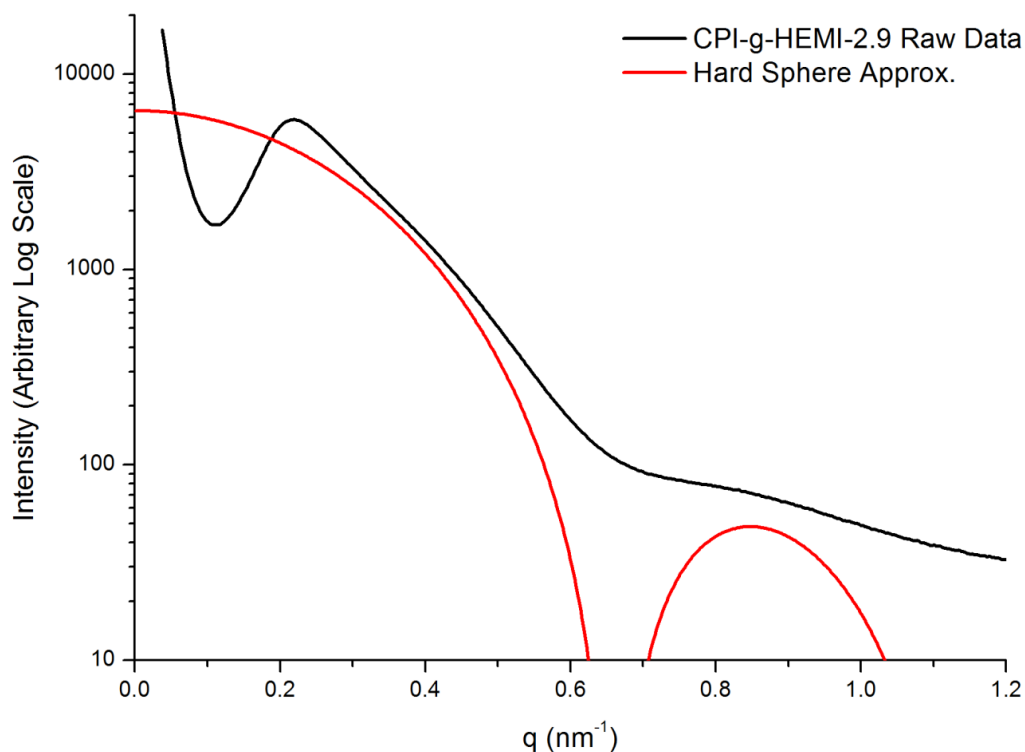

Figure E.4 One-dimensional SAXS profile of CPI-g-HEMI-2.9 and its corresponding hard sphere approximation fit for the form factor found from the high-q scattering data. The hard sphere approximation was fit to all PI-g-PLA SAXS profiles to estimate the diameter of the PI spheres in the PLA matrix. See Experimental Data for detailed process to calculate the fit.

Interestingly, the R_{HS} values of the P(I-co-HEMA) polymers are greater than those CPI-g-HEMI polymers with similar M_G and M_E values. The result may be due to the differing architectures of the P(I-co-HEMA) and CPI-g-HEMI graft copolymers. CPI-g-HEMI is more comb-like (random distribution) so the distance between grafts is close to M_E; therefore, the maximum molecular weight of PI that could extend into the sphere would be $M_E/2$ on average. Consequently, the maximum radius of the sphere would be the fully extended chain of $M_E/2$ equivalent length. P(I-co-HEMA) is a gradient copolymer so the graft copolymers would be more bottle brush-like and the distance between grafts would likely be less than M_E. However, since the graft points are all at the initiating end of the polymer, a free end of the macroinitiator exists at the terminus. The length of this terminal PI chain would be greater than M_E on average; therefore, the maximum radius of the PI sphere would be the fully extended chain of a radius greater than M_E on average.

The phase separation, domain spacing, and rubbery sphere size are supported by representative TEM images of the PI-g-PLA polymers (Figure E.5). In all samples, the OsO_4 stained PI phase is separate from the PLA matrix phase, confirming phase separation. The TEM micrographs of CPI-g-HEMI graft polymers shown across the top of Figure E.5 correspond to increasing M_E (increasing M_G) going left to right. As the SAXS indicated, in the CPI-g-HEMI TEM images the q* and R_{HS} increase as M_E goes up, qualitatively. P(I-co-HEMA)-3.8 and P(I-co-IOH)-2.7 have microstructures that qualitatively compare to the values found by SAXS. These TEM images of PI-g-PLA are compared to a representative TEM image of poly(cyclooctadiene-co-norbornene methanol)-g-PLA (PCN-3.3) with M_E equal to 3.3 kg/mol.[1] The PI-g-PLA images are similar phase separated as compared to the PCN-3.3 though there may be some difference in the fine structure of the PCN domains as compared to the PI domains. The PI domains in all the samples appear to be mostly discrete structures while the PCN-3.3 sample has more elongated structures.
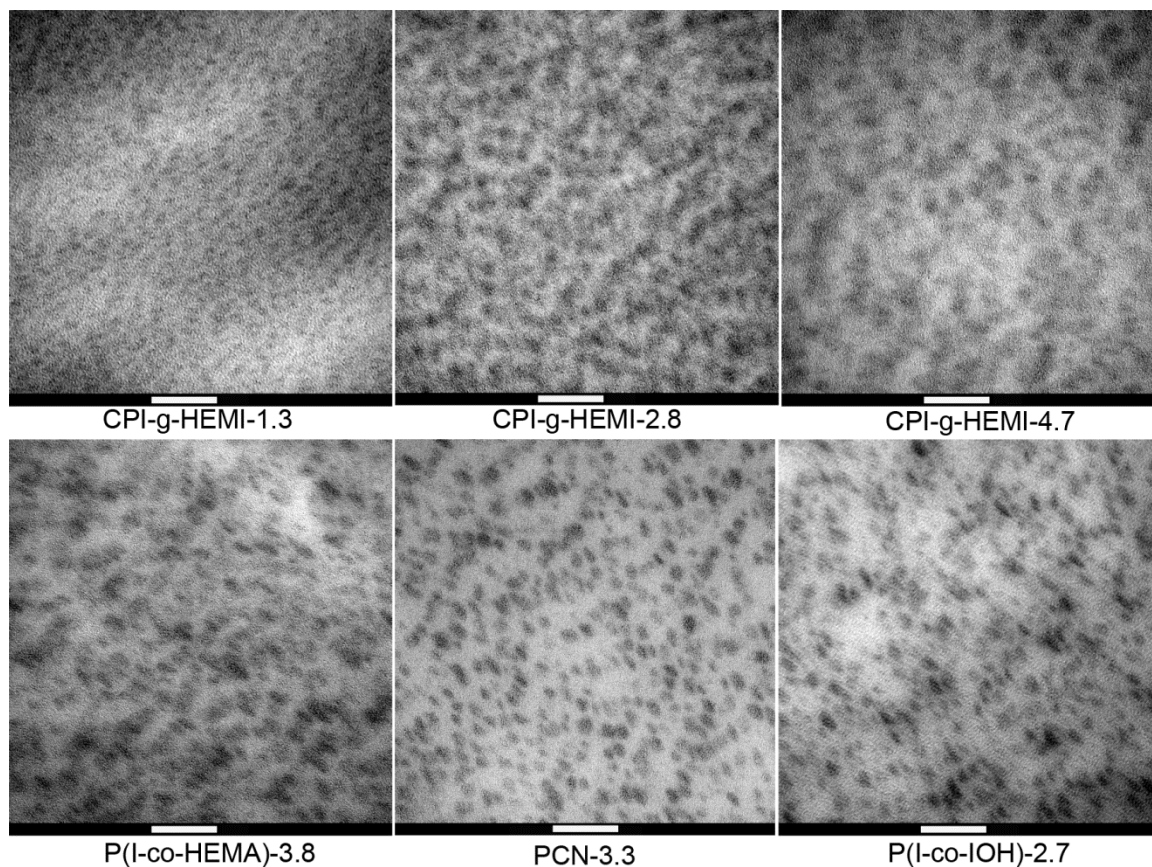
Figure E.5. Representative TEM images of PLA graft copolymers. Scale bar is 50 μm. The dark regions are the rubbery domains stained with OsO$_4$. Included with PI-g-PLA micrographs is a TEM image of the poly(cyclooctadiene-co-norbornene methanol)-g-PLA (PCN-3.3) with a M$_E$ value of 3.3 kg/mol from the work of Theryo et al. as a comparison.[1] The PCN-3.3 image has been scaled to match the same scale as the PI-g-PLA images. All images are courtesy of Grayce Theryo.

E.3.3 Mechanical testing of PI-g-PLA

The mechanical properties of select PI-*g*-PLAs were investigated by tensile testing. The CPI-g-HEMI samples were aged at both room temperature (23 °C) and in a refrigerator (4 °C) (Table E.2). The P(I-co-HEMA) and P(I-co-IOH) graft copolymers were all aged at room temperature. After aging at 4 °C for 2 days, the elongation to break (ε_b) values of both CPI-g-HEMI-4.7 and CPI-g-HEMI-2.8 were over 20 times greater than that of a PLA homopolymer (PLA-55) with a M$_n$ similar to the M$_G$ of the polymers. When the same polymers are aged at room temperature for two days prior to testing, the

increase in ε_b is significantly less – only 2–4 times that of PLA-55. The ε_b values of CPI-g-HEMI-1.3, PLA-55, and PLA-24 do not vary with aging temperature (T_A). The cause of the ε_b variation with T_A is unclear. SEC elution curves of the polymer before and after aging do not show signs of polymer degradation – the two SEC elution curves overlap. ^{1}H NMR spectroscopic analysis of the polymer after aging gives no indication that a chemical change occurred. Aging time and temperature have been reported to affect the mechanical properties of PLLA, but the control PLAs tested do not show any such variation, suggesting that both aging protocols used were sufficient to age PLA for mechanical testing.[6]

Table E.2. Tensile properties of PI-*g*-PLA polymers and representative PLA homopolymers aged at different temperatures prior to testing. PLA-25 and PLA-55 are PLA homopolymers with M_n values of 25 and 55 kg/mol, respectively. Error presented is one standard deviation.

Sample	$T_A{}^a$ (°C)	E^b (GPa)	$\sigma_b{}^c$ (MPa)	$\varepsilon_b{}^d$ (%)
CPI-g-HEMI-4.7	4	1.7 ± 0.2	39 ± 4	240 ± 30
	23	1.9 ± 0.1	44 ± 7	40 ± 30
CPI-g-HEMI-2.8	4	1.8 ± 0.1	40 ± 9	220 ± 70
	23	1.9 ± 0.2	44 ± 3	20 ± 10
CPI-g-HEMI-1.3	4	1.8 ± 0.2	43 ± 4	17 ± 4
	23	1.8 ± 0.3	47 ± 4	19 ± 3
PLA-24	4	2.5 ± 0.1	57 ± 2	7 ± 1
	23	2.3 ± 0.2	56 ± 2	6 ± 1
PLA-55	4	2.3 ± 0.1	57 ± 3	9 ± 2
	23	2.4 ± 0.1	57 ± 3	9 ± 2
P(I-co-HEMA)-3.8	23	1.7 ± 0.4	46 ± 3	17 ± 4
P(I-co-HEMA)-3.6	23	1.8 ± 0.4	41 ± 3	27 ± 6
P(I-co-IOH)-2.7	23	1.5 ± 0.2	46 ± 3	15 ± 2

[a]Aging temperature that samples were aged at for two days prior to testing. [b]Modulus calculated from initial slope of stress-strain curve. [c]Stress at break. [d]Elongation at break.

Samples were taken from CPI-g-PLA tensile bar plaques for DSC analysis to look for signs of sample aging. Prior to sampling, the plaques were kept in a -20 °C to limit any aging from storage. One set of samples for each polymer was taken directly from the plaque once it left the freezer to give an "un-aged" polymer that was then immediately analyzed by DSC. Another sample of polymer was left out in air at room temperature (23 °C) for 2 days prior to analysis by DSC to give an "aged" material. Comparison of the initial heating curves (Figure E.6) for both the un-aged and aged samples shows differences around the glass transition of PLA. The enthalpy overshoot of the aged samples for both the homopolymers and graft copolymers is greater than for the un-aged samples. Also, the glass transition is significantly sharper in the aged samples than in the un-aged samples. The sharper glass transition and larger enthalpy overshoot suggest that the polymers do age to some degree when sitting at room temperature.[6] Unfortunately, the results do not confirm an origin for the difference in mechanical properties between the samples stored at 4 °C and 23 °C, though they do suggest that the physical aging is the root in the variation.
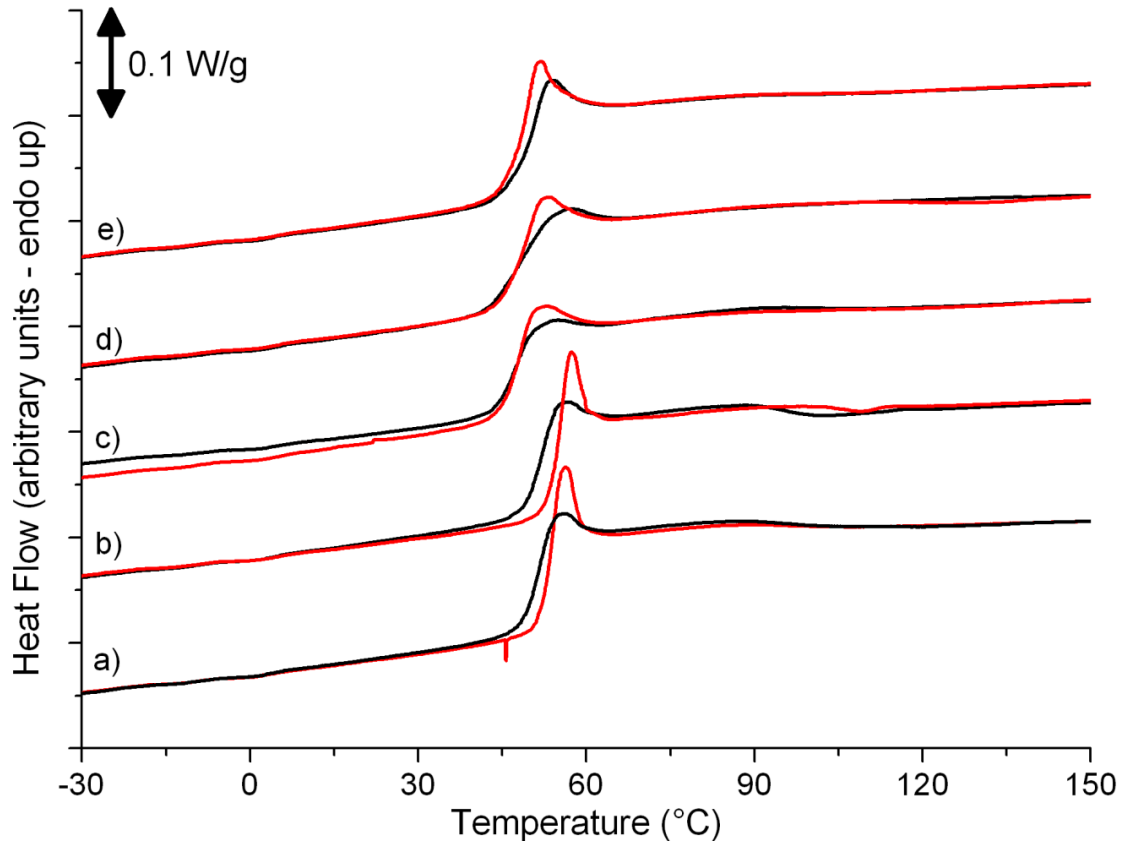
Figure E.6. Normalized DSC thermographs for the initial heating curve of (a) PLA-24, (b) PLA-55, (c) CPI-g-HEMI-1.3, (d) CPI-g-HEMI-2.8, and (e) CPI-g-HEMI-4.7 un-aged (black) and aged (red) for 2 days at room temperature. Enthalpy overshoot at the glass transition increased upon aging for all polymers tested.

The room temperature aged P(I-co-HEMA) and P(I-co-IOH) graft copolymers gave similar ε_b values as compared to the room temperature aged CPI-g-HEMI materials (Table E.2). All room temperature aged graft copolymers had statistically significant increases in toughness over the PLA homopolymers, but they also had significant decreases in the elastic modulus and stress at break (σ_b). The decrease in modulus, or softening of the polymer, as compared to the homopolymer PLA is due to the inclusion of the low modulus PI into the matrix. Essentially, the properties of two polymers mix to some extent. The increase in ε_b likely is due to this softening and not a result of any rubber toughening mechanism as the ability to toughen was invariant of the rubber domain diameter.

Interestingly, the chemical (M_G, M_E, PLA wt %, and overall M_n) and morphological properties (q*) of the PI-g-PLA are similar to the tough PCN-3.3 (q* = 32 nm, M_G = 57 kg/mol, overall M_n = 300 kg/mol), but the PCN-3.3 is extremely tough (ε_b = 240 ± 40%) and the PI-g-PLA materials are not. Perhaps the slight differences in the observed morphology account for the disparaging mechanical properties. The biggest differences between the two materials are the composition of the rubbery domain and the distribution of grafts along the polymer chain. PCN has a lower T_g than PI (-80 versus -60 °C) and some crystallinity – PI is amorphous. The PCN may also have a more random distribution of M_E values than the PI macroinitiators investigated. The exact cause of the different mechanical properties is unclear.

E.4 Conclusions

Hydroxyl functionalized PI can be used as a macroinitiator to produce PI-g-PLA materials which contain 95 wt % PLA. At the set PLA content the lengths of the PLA arms can be controlled by chaining the number of initiation points off the macroinitiator. The PI and PLA polymers phase separate at the high PLA content as confirmed by SAXS and TEM. The domain spacing of the polymers could be controlled by the length of the PLA arms. When aged at room temperature prior to mechanical testing, all PI-g-PLA materials had slightly improved elongation to break (2-fold increase) as compared to PLA homopolymers. Aging CPI-g-HEMI graft polymers at 4 °C prior to testing could give highly tough materials. The difference in the mechanical behaviors due to aging temperature may be caused by the graft copolymers aging slower at 4 °C. The cause of the poor performance of the PI-g-PLA polymers as compared to PCN-g-PLA is unclear.

E.5 Reference

[1] Theryo, G.; Jing, F.; Pitet, L. M.; Hillmyer, M. A. *Macromolecules* **2010**, *43*, 7394–7397.

[2] Gramlich, W. M.; Robertson, M. L.; Hillmyer, M. A. *Macromolecules* **2010**, *43*, 2313–2321.

[3] Hiemenz, P. C.; Lodge, T. P. Chapter 12: Glass Transition. *Polymer Chemistry*, Second Edition; Taylor & Francis Group: Boca Raton, 2007; pp 361-362.

[4] Choi, S.-H.; Bates, F. S.; Lodge, T. P. *J. Phys. Chem. B* **2009**, *113*, 13840-13848.

[5] Xenidou, M.; Beyer, F. L.; Hadjichristidis, N.; Gido, S. P.; Tan, N. B. *Macromolecules* **1998**, *31*, 7659-7667.

[6] Pan, P.; Zhu, B.; Inoue, Y. *Macromolecules* **2007**, *40*, 9664-9671.